A *Drosophila* model to understand lung disease related regulatory imbalances

Dissertation

Zur Erlangung des Doktorgrades

der Mathemathisch-Naturwissenschaftlichen Fakultät

der Christian-Albrechts-Universität zu Kiel

vorgelegt von

Xiao Niu

Erstgutachter: Prof. Dr. Thomas Roeder
Zweitgutachter: Prof. Dr. Holger Heine

Tag der Disputation: 02.07.2020

Table and contents

Summary

JAK/STAT and WNT-Yki/Sd signalling systems are evolutionary highly conserved and are found in almost all metazoan organisms. They play critical roles in maintaining cell homoeostasis and functionality, while being relevant for differentiation of many tissues. In the lung, accumulating evidence has shown that deregulation of the two signalling pathway is causally linked to a number of different, mostly chronic lung diseases such as COPD or asthma. To understand the underlying molecular framework that translates this dysregulated signalling into pathogenic states, I used the fruit fly *Drosophila* as a model, because the corresponding pathways are present in highly simplified versions.

In the first part, I was able to show that a balanced JAK/STAT signalling is necessary to ensure the normal functionality of the airway system (trachea) of *Drosophila*. I found that JAK/STAT signalling is necessary to prevent apoptosis in the larval airway system and that this signalling pathway is recruited in all airway epithelial cells. Stressful stimuli such as cigarette smoke evoked a strong and regionalized activation of the pathway that was most likely been driven by the concurrently induced pathway ligand Upd2. To understand the effect of chronic JAK/STAT activation, which has been associated with chronic lung diseases, I ectopically activated this pathway in the larval trachea. This intervention caused larval or pupal death and induced massive structural changes in airway epithelial cells. The changes comprise epithelial thickening combined with a narrowing of the air-conducting space and a disruption of the tracheal epicuticular structure. Transcriptomic studies revealed that vesicle-mediated transport processes are highly impaired leading to mislocated junctional proteins. In this study, I also investigated the effects of deregulated JAK/STAT signalling on the progenitor cells in three distinct regions. Considering the different response of the three regions to up-regulated JAK/STAT signalling or/and FGF/FGFR signalling, I supposed the cells in the three regions to be distinct cell types. Interestingly, although the JAK/STAT signalling is induced in these proliferating regions, up-regulating this signalling interfered with cell proliferation. Taken together, in this part, I could show that JAK/STAT signalling is essential in fully functional airway epithelium and that its chronic activation induces massive structural changes that strongly interfere with normal cell- and therewith organ functionality.

In the second part, I focused on the WNT-Yki/Sd signalling pathway. Here I could show stressful

stimuli such as cigarette smoke can evoke regionalized activation of the pathway as well that GFP tagged Yki translocated into the nucleus upon the heavy smoke. To understand the effect of chronic activation of WNT-Yki/Sd signalling pathway, which possibly disturb the repair in response to cigarette induced injury, I ectopically activated this pathway in the larval trachea as well. Here, I could show that the expression of the constitutively active form of the components in the signalling pathway contributed to a similar phenotype. This phenotype occurs in a specific stage during trachea remodelling which relies on the cell spatial differences in shape, structure and function. Transcriptomic studies revealed the intrinsic changes within the affected cells. One additional feature is an induced expression of Wnts corresponding to the noncanonical WNT signalling pathway in response to activation of WNT-Yki/Sd signalling pathway. In this part, I was able to show that the noncanonical WNT-Yki/Sd signalling interfered with cell differentiation. This result is reminiscent of the inhibition of cell differentiation during emphysematous destruction provoked by noncanonical WNT signalling and implicates that the inhibition of YAP/TAZ (human homolog) as a potential therapy for emphysema in mammals.

Zusammenfassung

Der JAK/STAT und der WNT-Yki/Sd Signalweg sind evolutionär hochkonserviert und werden in fast allen Metazoen gefunden. Beide Signalwege spielen eine kritische Rolle in der Zellhomöostase, Zellfunktion und in der Zelldifferenzierung und das in einer Vielzahl von Geweben. Eine reihe jüngerer Ergebnisse zeigen, dass eine Fehlregulation der beiden Signalwege in der Lunge mit verschiedenen, meist chronischen Krankheiten wie COPD und Asthma assoziiert werden kann. Um die molekularen Mechanismen zu verstehen, wie aus der Fehlregulation von Signalwegen ein krankheitsverursachendes Stadium erreicht wird, habe ich die Taufliege *Drosophila* als Model verwendet. Beide Signalwege sind in der Fliege in einer vereinfachten Form präsent.

Im ersten Teil der Arbeit konnte ich zeigen, dass eine ausgewogene Aktivität des JAK/STAT Signalwegs nötig ist, um eine normale Funktionalität des Atemwegsystems von *Drosophila* zu sichern. Ich habe herausgefunden, dass der JAK/STAT Signalweg wichtig für die Vermeidung von Apoptose in den larvalen Atemwegszellen ist. Stressstimuli, wie Zigarettenrauch, lösten eine starke regionale Aktivierung des Signalwegs aus, welche höchstwahrscheinlich durch den Signalweg-Liganden Upd2 induziert wurde. Der JAK/STAT Signalweg wird oft mit chronischen Lungenkrankheiten assoziiert. Um zu verstehen welche Effeket diese chronische Aktivierung hat, habe ich diesen Signalweg in den larvalen Tracheen ektopisch aktiviert. Diese Intervention führte zum Tod der Larven oder Puppen und induzierte massive strukturelle Veränderungen der Epithelzellen der Atemwege. Zu diesen Veränderungen gehörten eine Verdickung des Epithels kombiniert mit einer Verengung der Atemwege und einer Zerstörung der extrazellulären Matrix. Eine Trankriptomanalyse zeigte, dass durch Vesikel vermittelte Prozesse stark beeinträchtigt sind und somit zu einer falschen Lokalisation von Zellverbindungsproteinen führen. Außerdem wurde der Effekt einer Fehlregulation des JAK/STAT Signalwegs auf die Tracheenvorläuferzellen in drei verschiedenen Regionen untersucht. Aufgrund der unterschiedlichen Reaktionen auf einen aktivierten JAK/STAT Signalweg und/oder FGF/FGFR Signalweg nehme ich an, dass es sich um unterschiedliche Zelltypen in diesen drei unterschiedlichen Regionen handelt. Obwohl der JAK/STAT Signalweg in diesen proliferierenden Regionen induziert war, kam es interessanterweise zu einer Beeinträchtigung der Proliferation. Zusammenfassend konnte ich zeigen, dass der JAK/STAT Signalweg essenziell für die Funktionalität des Atemwegsepithels ist und eine chronische

Aktivierung massive strukturelle Veränderungen induziert, die die Zell- und damit die Organfunktionalität stark einschränken.

Im zweiten Teil fokussierte ich mich auf den WNT-Yki/Sd Signalweg. Hier konnte ich zeigen, dass Stressstimuli wie Zigarettenrauch sowohl eine regionale Aktivierung des Signalwegs als auch eine Zellkerntranslokation einer GFP-markierten Yki-Variante durch die starke Rauchbelastung hervorrufen. Um den Effekt einer chronischen Aktivierung des WNT/Yki/Sd Signalwegs zu verstehen habe ich diesen ebenfalls in den larvalen Tracheen ektopisch aktiviert. Dies könnte die Reparaturmechanismen, ausgelöst durch zigarettenrauchabhängige Schäden, beinträchtigen. Hier konnte ich zeigen, dass die Expression von konstitutiv aktiven Signalwegkomponenten zu einem ähnlichen Phänotyp führte. Dieser Phänotyp trat in einem bestimmten Stadium während der Tracheenneugestaltung auf, welche räumlichen, strukturellen und funktionellen Zellveränderungen unterliegt. Eine Transkriptomanalyse zeigte intrinsische Veränderungen in den betroffenen Zellen, in denen viele differenzierungs-abhängige Gene während der Entwicklung inhibiert wurden. Eine andere Besonderheit war die induzierte Expression von Wnts, die dem nicht-kanonischen Signalweg zugeordnet werden können, als Antwort auf die Aktivierung des WNT-Yki/Sd Signalwegs. In diesem Teil konnte ich zeigen, dass der nicht-kanonische Wnts/Yki/Sd Signalweg mit der Zelldifferenzierung interferiert. Dieses Ergebnis erinnert an die Inhibierung der Zelldifferenzierung in emphysematischen Veränderungen, ausgelöst durch den nicht-kanonischen WNT Signalweg und schließt eine Inhibierung des YAP/TAZ (humanes Homolog) als potenzielle Therapie für Emphyseme in Säugern ein.

Introduction

1.1 Lung tissue homeostasis and chronic inflammatory lung disease

The lung is the respiratory organ that enables to obtain oxygen from the air and dispose of carbon dioxide produced by the metabolism. This organ is exposed to the environment and therewith comes into direct contact with numerous stressors, including smoking, pollutants, gastro-oesophageal reflux, occupational exposures, and viral or bacterial infections. Especially these infections contribute significantly to the development of lung diseases. To get rid of these external particles and pathogens, different resident and non-resident cell types are required to clean them up, remember them and repair wounded structures.

The lung airway is relatively quiescent compared with other barrier tissues exposed to the external environment having dedicated stem maintaining tissue homeostasis. Upon injury, several types of stem and/or progenitor cells are activated by up-regulation of specific key signals that enable self- renewal and differentiation into multiple cell lineages. These distinct stem cell lineages are critical for tissue regeneration after injury and in the context of chronic lung diseases[1]).

In the trachea and the proximal airways, the epithelium contains multiple cell types (Fig. 1), including multiciliated cells, secretory cells, goblet cells and basal stem/progenitor cells (BSCs)[1]. BSCs act as resident stem cells and they are capable of self- renewal and of producing multiciliated and secretory cells after injury. On the other hand, BSCs are distributed widely in the airway and therefore they are thought to have a pronounced role in maintaining and repairing the airway epithelium[1]. Additionally, secretory cells in mice are able to repopulate the airways following airway damage, however, it is unclear if the secretory cells maintain the characteristics of progenitor in the human airway. Apart from one pseudostratified epithelium, the trachea and airways are underlined with heterogeneous mesenchymal cell types, including cartilage around the trachea, smooth muscle and interstitial fibroblasts. Previous studies showed that these mesenchymal cells have a critical role in regulating the regenerative response of the airway epithelium following airway injuries[2–5]. In addition, in response to severe injuries, glandular myoepithelial cells (MECs) can spread to the luminal surface and give rise to different types of surface airway epithelial cells[6,7]. The proliferation and differentiation processes in the airway epithelium are initiated or prevented by specific key signals and the

underlying mechanisms are under active investigation. FGFs (fibroblast growth factor) and WNT ligands, which show an important role in patterning the airways and promoting mesenchymal cell proliferation and differentiation during respiratory system development[8–10] exhibit their importance in the response to airway injury as well[2,5].

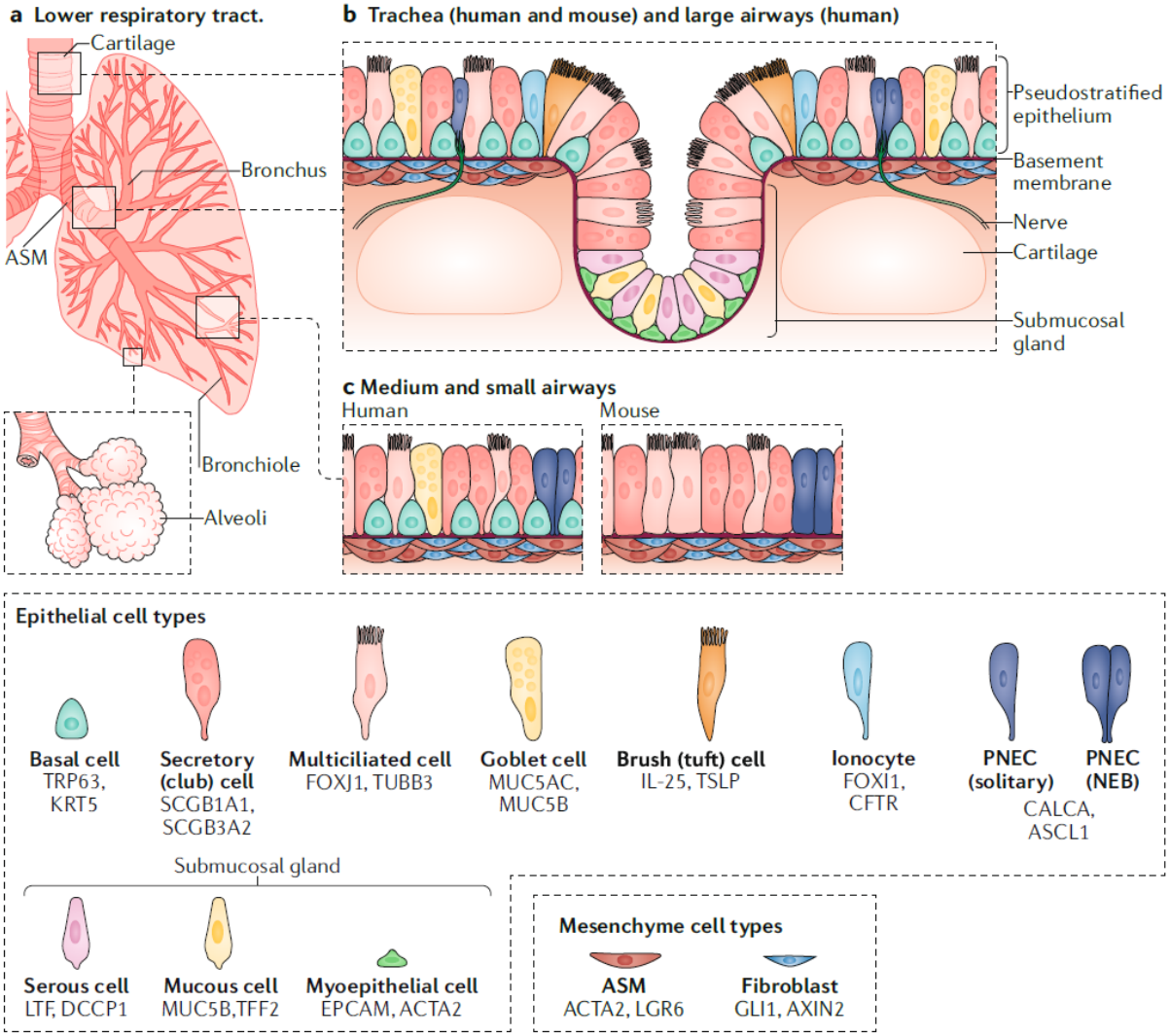

Fig. 1 Cellular composition of airways.[1]
(a) The lower respiratory tract can be divided into the trachea, large airways(bronchus), small airways(bronchiole) and alveoli. (b,c) Cellular composition of respiratory epithelium in the mouse and the human. ASM, airway smooth muscle (Jarod A. Zepp, 2019).

The alveoli are distinct in structure from the airways. The two major epithelial cell types within the alveoli are alveolar type 1 (AT1) and alveolar type 2 (AT2) cells (Fig. 2). AT1 cells stop their proliferation during the first few days after birth[11], whereas the proliferation and differentiation of AT2 cells into new AT2 and AT1 cells was observed in homeostatic situations and after injury[12,13]. In addition to epithelial cells, the lung alveolus contains several

mesenchymal cell types and the endothelial capillary plexus. Previous studies showed that paracrine growth factors such as WNT ligands play decisive roles in the self-renewal and differentiation of AT2 cells. WNT responsiveness wanes before the alveologenesis and is enhanced after the alveologenesis, which indicates a close relationship between the differentiation of AT2 cells and WNT responsiveness[14]. Further studies using the inhibition of this signalling pathway found an aberrant increase in AT1 cells at the expense of AT2 cells[14]. Upon tissue damage, WNT signalling plays a critical role in lung repair as well. In response to injuries in the alveoli, mesenchymal cells increase WNT ligand expression to regulate AT2 self-renewal and differentiation into mature AT2 and AT1 cells[15,16].

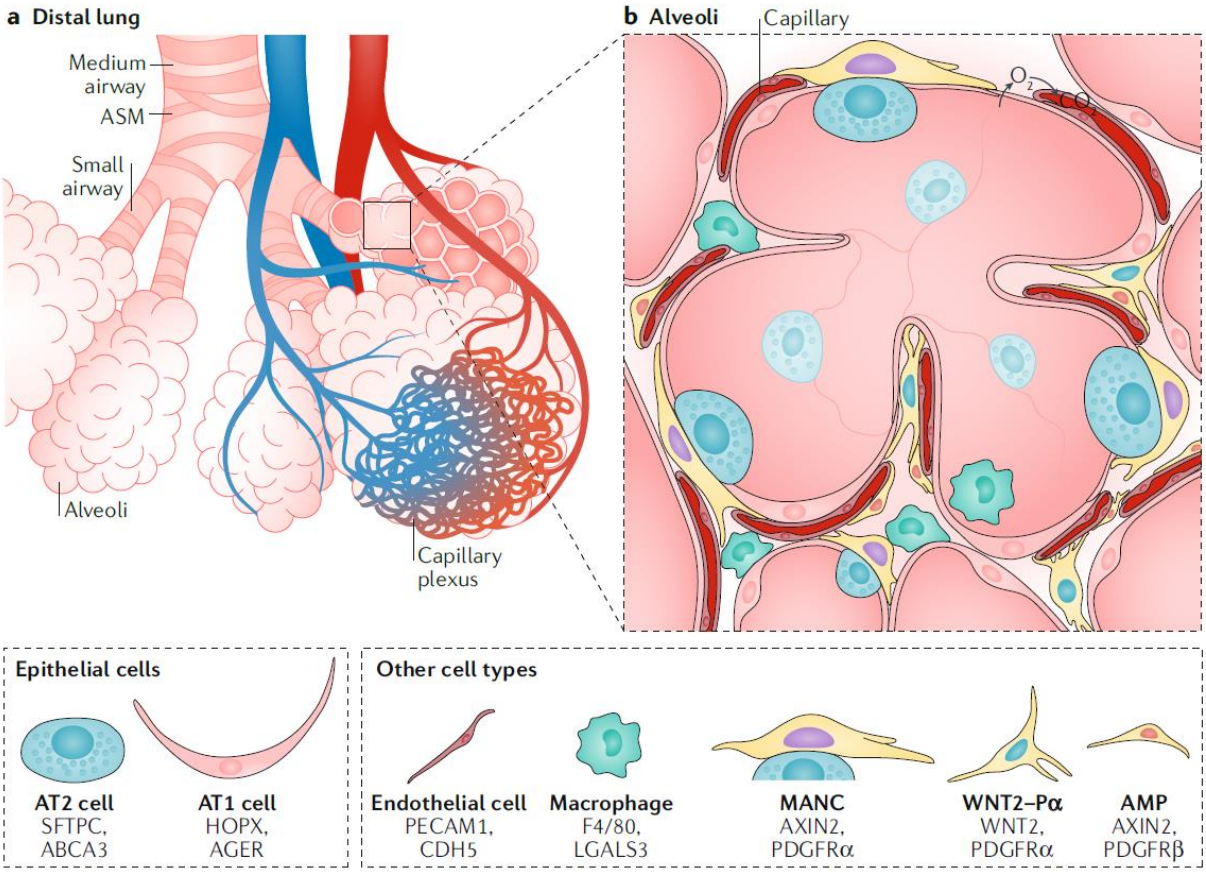

Fig. 2 Cellular composition of alveoli.[1]
(a) The distal regions of the lower respiratory tract consist of alveolar sacs. **(b)** The alveolar wall is composed of alveolar type 1 (AT1) cells and alveolar type 2 (AT2) cells. Interstitial fibroblasts consisting of *Axin2*-positive myogenic precursors (AMPs), *wnt2*-expressing platelet-derived growth factor-α (PDGFRα)-positive cells (WNT2–Pα) and mesenchymal alveolar niche cells (MANCs) make up most of the alveolar mesenchyme. Additionally, there are sentinel immune cells such as alveolar and interstitial macrophages (Jarod A. Zepp, 2019).

The respiratory system capability of countering insults relies on its effective defence system. Defined by the sensitivity and specificity, the defence process is usually divided into two parts, the innate immune system and the adaptive immune system.

Innate immune systems refer to nonspecific defence mechanisms that can act immediately. It includes physical barriers provided by epithelial cells and mucociliary clearance of the airways, which works cooperatively with the monocyte/macrophage system to move deposited particles up the mucociliary escalator. However, this protective barrier could be broken down by exposure to noxious particles, which could initiate an acute inflammatory response. In response to the acute inflammation, the inflammatory cells and proteins would be delivered to the sites and take up or destroy foreign particles.

Another arm of the immune system is the adaptive response composed of highly specialized, systemic cells and processes. Here, mainly B- and T-lymphocytes are operative. In this process, antigens may cross the epithelium through injured sites or are transported by specialised epithelial cells. Then, these antigens are recognized by dendritic cells (DCs) beneath the basement membrane which migrates to the bronchial associated lymphatic tissue (BALT). They process antigen material and present it on their cell surface to T-cells in the lymphoid follicles in the BALT and regional lymph nodes. Since B-cells receive the signals delivered by CD4-positive T-helper lymphocytes, these B-cells would start their proliferation and then migrate to germinal centres where they begin to produce antibodies[17,18]. Apart from the plasma cells capable to produce antibodies, B cells can become memory cells as well. These cells re-enter the circulating blood as the lymph drains into the central venous system and home back to the site of injury. To date, human antibodies can be classified into five isotypes (IgA, IgD, IgE, IgG, and IgM). The expression of each class is inducible by specific signals. Transforming growth factor (TGF-beta) and interleukin 5 (IL-5) can induce the expression of IgA, whereas IL-4 stimulates B-cells to produce IgE. In the defence process, cytokines play an important role in both innate and adaptive responses. On the one hand, they can initiate the innate defence and on the other hand, they orchestrate both the innate and adaptive defences [19]. The relevant cytokines (such as TNF alpha, IL-1beta, macrophage inflammatory protein 1, granulocyte-macrophage colony-stimulating factor (GM-CSF), interleukin 6 (IL-6), and interleukin 8[20,21]) are mainly derived from the epithelial cells (such as IL-1beta and leukaemia inhibitory factor[22–24]) and inflammatory cells recruited to the site of injury. Previous studies showed their multiple roles in the immune response but also in the repair process, which has especially been demonstrated for TGF beta[25,26] and IL-6[27].

Defects in the repair and defence can result in tissue injury and inflammation. Chronic injury and unchecked inflammation are considered to be the main driver of lung diseases, such as

idiopathic pulmonary fibrosis (IPF), asthma, cystic fibrosis (CF), chronic obstructive pulmonary disease (COPD), or acute respiratory distress syndrome (ARDS)[1]. Accumulating evidence identified the important role of deregulated WNT and JAK/STAT signalling pathways in the progress of these chronic lung diseases. However, the effects provoked by them are still not clear.

1.2.1 Chronic obstructive pulmonary disease (COPD)

COPD is a chronic inflammatory lung disease that causes airflow obstruction in the lungs. It is one of the main chronic lung diseases. The Global Burden of Disease Study reported a prevalence of 251 million cases of COPD globally in 2016. Symptoms can limit the patients' ability to do routine activities and even can be a cause of death. Data from the Canadian Chronic Disease Surveillance System (2011-2012) showed all-cause mortality rates were higher among those living with COPD than those without COPD, across all age groups; rate ratios ranged from 4.7 in the 35-39 age group to 1.7 in the 85 and older age group (Figure 3). According to the world health organization (WHO), COPD is one of the top 10 global causes of death, which, combined contribute to more than 50% of the 56.9 million deaths worldwide.

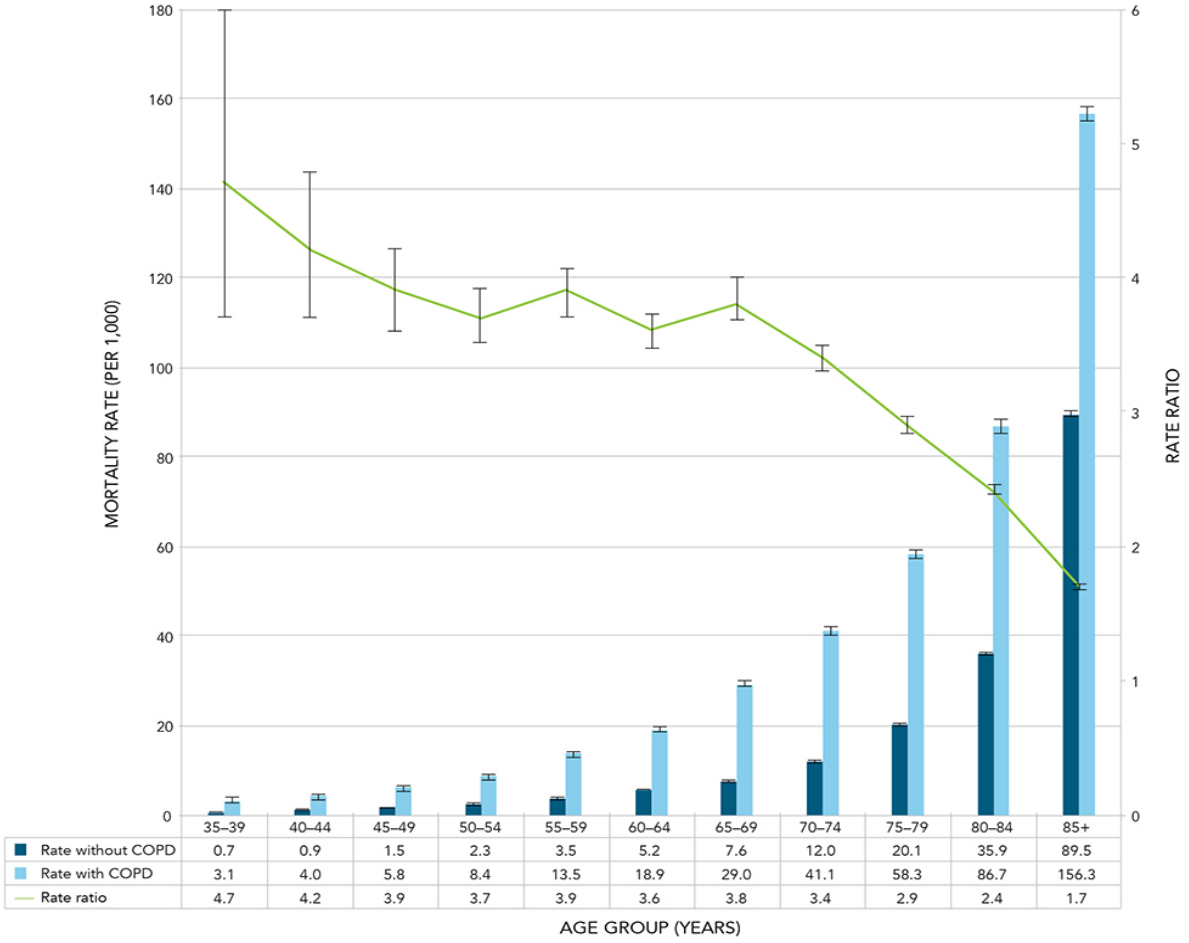

Fig. 3 All-cause mortality rates and rate ratios among Canadians aged 35 years and older with diagnosed COPD compared to those without diagnosed COPD, by age group, Canada, 2011-2012

The pathogenesis of COPD is closely associated with a long-lasting innate and adaptive inflammatory immune response of the lung to a chronic exposure to irritating gases or particulate matter[28]. Cigarette smoking, as a risk factor for a broad range of non-neoplastic pulmonary lesions, can contribute to several kinds of chronic lung diseases, like COPD, pulmonary hypertension, interstitial lung disease, and lung cancer[29,30]. Although genetic determinants, environmental exposures, other lung diseases, and a history of severe childhood respiratory infection have been identified as risk factors for COPD[31], the main cause of COPD is cigarette smoking (including both, active and passive smoking). Cigarette smoking is prevalent worldwide and it has been reported that approximately 1/3 of the adult population smokes tobacco[32]. According to the WHO, about 20 to 30 percent of chronic smokers may develop clinically apparent COPD, and many smokers with long smoking histories may develop reduced lung function. Some smokers develop less common lung conditions. They may be misdiagnosed as having COPD until a more thorough evaluation is performed. One report from Fletcher and colleagues showed that the rate of decline in forced expiratory

volume per second (FEV_1) of most smokers is similar to that for non-smokers, however, for some studies showed susceptibilities to tobacco smoke, with the FEV1 declining rapidly, which can be rescued by smoking cessation[33,34].

COPD develops very slowly and unfortunately, it has no cure yet. No current treatments can affect the overall course of COPD and the current medications focus on symptomatic relief and are used for reducing exacerbation rates. More knowledge of the mechanisms of the fundamental pathogenic mechanisms that underpin disease development may pave the way to cytoprotective and regenerative therapeutics. COPD is defined by the feature of irreversible airflow limitation measured during forced expiration[33,35] caused by either an increase in the resistance of the small conducting airways,[36–38] an increase in lung compliance due to emphysematous lung destruction,[39] or by both. The decline of the forced expiratory volume (FEV1) and its ratio to forced vital capacity (FVC) were used as screening tools for COPD, resembling airflow limitations. The symptoms of COPD reflect the characteristics of obstructive pulmonary function and inflammation reactions, including shortness of breath, wheezing, chest tightness, mucus (sputum) production, cyanosis, frequent respiratory infections. COPD patients often have additional symptoms besides the declined function of the lung in severe disease, such as fatigue, weight loss, and anorexia.

1.2.2 Pathophysiology of obstructed airflow in COPD

COPD is a debilitating lung disease characterized by three major disease types, chronic bronchitis, small airway obstruction, and emphysema[31].

1.2.2.1 Chronic bronchitis

Chronic bronchitis is the inflammation of the epithelium of the central airways where it extends along the gland ducts into the mucus-producing glands[40,41]. The inflammation is associated with increased production of mucus, defective mucociliary clearance, and disruption of the epithelial barrier provided by the innate immune system[42–44]. On the basis of the lung anatomy, enlarged bronchial mucus glands and thicker bronchial walls that mainly involve an increase in connective tissue (fibrosis) were observed in COPD patient[45,46].

Chronic bronchitis is a common pathophysiology in COPD, whereas it cannot explain the subsequent rapid decline in FEV_1 alone[47,48]. The chronic airflow limitation that characterizes

COPD is thought to be mainly caused by a mixture of small airway diseases (e.g., obstructive bronchiolitis) and parenchymal destruction (emphysema)[31].

1.2.2.2 Small airway obstruction

Small airway means the airways with small diameter (less than 2 mm in internal diameter). These airways are spread out between the fourth and 14th generation of airway branching, since the human bronchial tree branches in a non-dichotomous fashion[49]. In fact, the airway obstruction is mainly found in these small airways rather than in the central airways [50–52]. The obstruction in the small conducting airways is involved in the disruption of the epithelial barrier, interference with mucociliary clearance apparatus, infiltration of the airway walls by inflammatory cells, and deposition of connective tissue in the airway wall [28]. Previous observations of the conducting airways of smokers revealed a visible change in these airways compared to non-smokers [53,54]. Another investigation based on the anatomical observation of the lungs from patients at different stages of COPD classified by GOLD showed a relation between the accumulation of inflammatory exudates in the lumen and the severity of COPD[54].

Airway obstruction can be mainly attributed to the pathology in the airway wall and lumen, given the increase of either of these tissues under the epithelium or on the luminal surface will affect the lumen calibre and therewith raise resistance[54]. Apart from the pathology in the airways, destroyed support between the airway tube and the alveoli could be observed in the inflammation process as well. However, direct measurements of peripheral airway resistance implicated a less important role of this destroyed alveolar support for the airway obstruction.

1.2.2.3 Emphysema

Another feature of COPD is emphysema development, which contributes to airflow limitation by decreasing the elastic recoil force available to drive air out of the lung[39]. Principally, emphysema can be divided into three forms: centrilobular emphysema, pan lobular emphysema and cicatricial emphysema. The previous study showed that the centrilobular form of emphysema is closely associated with cigarette smoking[55,56]. The emphysema development is a complex process which is associated with oxidative stress, protease stress, sustained macrophage activation and infiltration of other immune cells leading to a progressive loss of lung tissue[57].

1.3 Close relation between airway obstruction and immune defence responses

Although the mechanisms of COPD pathogenesis is still unclear, previous observations showed its close relation to the chronic innate and adaptive inflammatory immune response[28]. As a major risk factor for the development of COPD, cigarette smoking plays dual roles in regulating immunity by either exacerbation of pathogenic immune responses or attenuation of defensive immunity and affects both cell-mediated and humoral immune responses[58,59].

1.3.1 Innate response

Mucociliary clearance (MCC) is the primary innate defence mechanism of the lung airways. In response to noxious particles produced by cigarette smoke, MCC cooperates with the monocyte/macrophage system to move particles trapped in the mucus out from the airways. In contrast, the interference with MCC could lead to the accumulation of inflammation exudates containing mucin, which obstructs the airways and potentially allows for increased bacterial infections. Increased production and secretion of inflammation exudates is a feature of COPD[60]. Studies in humans and mice have shown that cigarette smoke significantly decreases ciliary beat frequency[61,62] and increases mucus secretion[63]. On the other hand, chronic cigarette smoke can disrupt the tight junctions between epithelial cells[42,44,64], which could initiate an acute inflammatory defence response. Inflammatory cells (e.g. phagocytes) would be recruited and assisted by proteins, they can take up and destroy the particles[65,66]. Several types of cells participate in the process, including eosinophils, polymorphonuclear cells (PMNs), natural killer cells, macrophages, and mast cells. Previous studies showed that extracts from cigarette smoke can activate autophagy and induce apoptosis in alveolar or bronchial epithelial cells and this process relies on the accumulation of MAP1LC3B and LC3B2 (its active form) in a time- and dose-dependent manner in vitro [55]. Further, increases in the LC3B2 protein concentrations in patients with COPD positively correlated with disease severity, suggesting a pathogenetic relevance[67].

1.3.2 Adaptive response

The innate immune response can recognize inhaled pathogens and react to them but it shows almost no memory of previous exposures[68]. By contrast, the adaptive response creates immunological memory after an initial response to a specific antigen, which can make up this deficiency. In this process, antigens inhaled in the airways may either be transported across

the epithelial barrier by M cells or penetrate the epithelium at wounded sites. Then, dendritic cells would take up the antigens and transport them to bronchial associated lymphatic tissue (BALT) or to regional lymph nodes[28]. The increase in BALT always indicates the increase in the lymphocytes. Strikingly, this type of response is rarely found in healthy nonsmokers but is frequently observed in cigarette smokers[69]. The investigation based on the anatomical observation of the lung tissue from patients at all stages of the GOLD classification of COPD exhibited a relation between the BALT abundance and severity of COPD[54].

In the adaptive immune system, lymphocytes affected by smoking mainly include T helper cells (Th1/Th2/Th17), CD4+CD25+ regulatory T cells, CD8+ T cells, B cells and memory T/B lymphocytes while innate immune cells impacted by smoking are mostly DCs, macrophages and NK cells[59]. The increase in some kinds of inflammation cells (e.g. B cells and CD8 lymphocytes) contributes to the decline of FEV1[70–73].

1.3.3 Humoral immune responses and IL-6-JAK/STAT signalling pathway

Cigarette smoking affects humoral immune responses as well. A large network of pulmonary and systemic cytokines is involved in chronic inflammation of smokers. The epithelial cells and inflammatory cells attracted to the site of injury are major sources of these cytokines[23,74–76]. As far as I know, cigarette smoke induces the production of multiple cytokines, including tumour necrosis factor (TNF)-α, interleukins (IL)-1, IL-6, IL-8 and granulocyte-macrophage colony-stimulating factor (GM-CSF)[77–79]. On the other hand, cigarette smoke can also reduce the release of these cytokines such as IL-6, IL-10, IL-1, IL-2, TNF-α, and IFN-γ due to the decreased cell function[58,80,81]. IL-6 (and TNF-α) abundances are tightly regulated and affected by the exposure to smoke, which indicates its presumably decisive position in the progress of COPD. Indeed, accumulating evidence indicates a pathological role for IL-6 in various disease conditions, such as inflammatory, autoimmune, and neoplastic diseases[82] and the therapeutic approach to block the actions of IL-6 by use of a humanized anti-IL-6R antibody has been proven to be therapeutically effective for many kinds of diseases, including rheumatoid arthritis, systemic juvenile idiopathic arthritis and Castleman's disease[83–85]. A previous investigation showed FEV1 significantly improved with roflumilast therapy[86], which can decrease the level of IL-6 in the broncho-alveolar fluid[87]. However, it is still not clear which role the aberrant IL-6 concentration is taking in the initiation and progression of the disease. *In vitro*, IL-6 strongly influences the proliferation and differentiation state of normal human

airway epithelial basal cells and mice experiment proved anti–IL-6R (tocilizumab) to be an efficient inhibitor for epithelial hyperplasia and the development of squamous metaplasia, which was commonly found in the smokers[27].

IL-6 encoded by the IL6 gene belongs to IL-6-type cytokine family. Upon systemic release, IL-6 triggers the Janus kinase–signal transducer of activators of transcription (JAK/STAT) signalling through activation of IL-6 receptor (type I cytokine receptor complex) and gp130 (a transmembrane signal-transducing protein). This signalling pathway plays an important role in inflammation, host defence and tissue injury responses[88,89].

Discovery of the JAK/STAT pathway resulted from a logical progression of empirical findings related to the anti-viral activity of interferons and their ability to rapidly instruct gene expression in human cells[90]. It is now recognized as an evolutionarily conserved signalling pathway and is found in almost all metazoan organisms. JAK and STATs are the key parts in the signalling pathway and their activation always depends on the reaction between ligands and receptors. JAKs bind specifically to intracellular domains of cytokine receptor signalling chains and catalyze ligand-induced phosphorylation of themselves and of intracellular tyrosine residues on the receptor, creating STAT docking sites. Phosphorylation of STATs on activating tyrosine residues leads to STAT homo- and heterodimerization. STAT dimers are rapidly transported from the cytoplasm to the nucleus and are now competent for DNA binding. More than 50 cytokines and growth factors have been identified to be operated by the JAK/STAT signalling pathway[91]. In mammalian cells, there are four JAK proteins (JAK1, JAK2, JAK3, and TYK2) and seven STAT proteins (STAT1, STAT2, STAT3, STAT4, STAT5A, STAT5B, and STAT6). JAK/STAT signalling pathways not only function as a central communication node for the immune system but also play an important role in cell fate decisions. An increase in the activity of the JAK/STAT signalling is always observed in proliferating cells [92] and constitutive activation of JAK2, a fusion of JAK2 with the oligomerization domain of the TEL transcription factor, causes acute lymphoblastic leukaemia[93,94]. Inhibition of this pathway contributes to a reduction of stem cell proliferation and even to cell programmed death[92,95]. Genetic mutations and polymorphisms are functionally relevant to a variety of human diseases, especially for cancer and for immune-related diseases[96]. The clinical relevance of the pathway has been highlighted by new therapeutics that targets JAKs[96]. Recent studies on the signalling pathway reveal the importance of aberrant JAK/STAT signalling in developing COPD and the compounds that target the JAK/STAT signalling are proposed to be useful for the treatment of COPD

patients as well[97,98].

1.4 Close association between airway obstruction and injury response

Previous studies discussed an increased risk of tissue damage through the release of toxic mediators, including proteolytic enzymes and reactive oxygen species during cigarette smoking[99]. One most direct evidence for the CS-induced injuries in the airway epithelium is that the observation of apoptotic T-lymphocytes and airway epithelial cells in ex- and continuing smokers with COPD compared to nonsmoking controls[100]. In addition, the histological appearance of airways from COPD patients shows changes in the structure of the airway epithelium, which contribute to a decline of the epithelial barrier function[54]. At the same time, the histological analyses also show that irreversible airway narrowing is mainly attributed to fibrosis around small airways, whereas the increase in the thickness of the smooth muscle cell layer is not apparent[54]. This indicates the requirement for a more efficient barrier against the inhaled toxic agents or microorganisms (which could be frequently found during exacerbation periods of COPD) due to dysfunction of the epithelium. This process causes changes in the airway structure and is closely associated with pro-angiogenic factors, such as VEGF, TGF-β, FGF, and proteolytic enzymes[101]. Epithelial to mesenchymal transition (EMT), defined as the losing of epithelial character and becoming migratory with an assumed mesenchymal phenotype is key in this process. It has been proven to be activated by cigarette smoke and considered as the possible major pathogenic factor of COPD[102,103]. EMT indicates that the epithelial cells may be reprogramming their metabolism by receiving successive mesenchymal growth related signalling. So which signal is the key in the airway remodelling and reprogramming of the cells is a major research aim since decades. However, this mechanism is not fully understood until now.

Wnt plays a critical role in cell proliferation and differentiation and the corresponding signaling systems could be divided into β-*Catenin* dependent signalling (canonical WNT signalling) and β-*Catenin* independent signalling (noncanonical WNT signalling). Studies focusing on early lung development proved the necessity of canonical WNT signalling in specifying lung progenitors by performing conditional expression or conditional inactivation of β-*Catenin* during the branching morphogenesis[104,105]. In the alveolar AT2 cells in emphysema, there is reduced β-*Catenin* signalling[106] and additional studies pointed to a canonical to noncanonical

WNT signalling shift contributing to emphysema related pathogenesis. Indeed, the studies on the CS induced emphysematous lung destruction revealed CS can inhibit differentiation of AT2 via the inhibition of β-*Catenin* dependent WNT signalling and showed that the noncanonical WNT5a plays a decisive role in the shift[107,108].

In vertebrates, noncanonical WNT signalling is involved in multiple biological processes, including convergent extension movements, planar cell polarity, tissue regeneration, dorsoventral patterning through activation of different signal transduction pathways[109,110]. Among the WNTs (19 in human), WNT5a exhibits its critical role in cell regeneration and differentiation and antagonism of canonical WNT signalling[111–113]. A recent study uncovered a new noncanonical pathway, the WNT-YAP/TAZ signalling axis which consists of WNT-FZD/*ROR*-$G\alpha_{12/13}$-Rho GTPases-Lats1/2 to promote YAP/TAZ activation and TEAD-mediated transcription [114]. YAP/TAZ mediate the biological functions of noncanonical WNT signalling, including antagonism of WNT/β-catenin signalling. The expression of YAP reduces WNT target gene expression[115,116] and the component in the signalling pathway, $G\alpha_{12/13}$ and RhoA, and other activators of YAP/TAZ, SOX2 and LPA were shown to inhibit WNT/β-catenin signalling as well[117,118]. These results pointed to the important role of activation of WNT5a-YAP signalling in the canonical to noncanonical WNT signalling shift. However, it is not clear if the activation of WNT5a-YAP is the key factor in the emphysema pathogenesis. Another report showed that WNT5a may contribute to the differentiation of mesenchymal stem cells into AT2 cells through WNT-JNK or WNT-PKC Signalling[119]. The mechanism of injuries and repair and the effects of aberrant repair during the cigarette smoke are still not clear and more studies are needed.

In mammals, the multiple redundancies in the genome and complex crosstalks among the cells make the disease study at the molecular mechanism hard to decipher. Consequently, a genetically amenable animal model with a simple airway system and conserved function of the genes of interest will give researches great support to understand the onset and pathogenesis of the disease and to find out possible potential therapy.

1.5 *Drosophila melanogaster* as a lung disease model

Taking the advantage of the well-known constitution of the genes and the simple structure of the tissues, researchers choose *Drosophila* as a model organism to investigate the genetic, molecular and cellular processes underlying tubulogenesis and disease progression for

decades. *Drosophila* as a lung disease model has been successfully used to examine the hallmarks of diseases such as asthma, COPD or lung cancer and to investigate the function of disease-related genes and to identify compounds as candidate therapeutics[120–122].

Drosophila trachea form from 10 groups of approximately 40 cells in the embryo stage by a post-mitotic program of morphogenesis. The embryonic development of *Drosophila melanogaster* has been subdivided into 17 stages by Volker Hartenstein and José Campos-Ortega according to the developmental event and the time after fertilization at which they occur. The embryogenesis needs totally about 22hours. Tracheal develops begins at stage 5 (2:10 - 2:50h after fertilization) when segmentally repeating tracheal placodes are formed. The basic pattern of the larval tracheal tree is laid down at stage 13 (around 7:20 - 10:20h after fertilization) when the anteriorly directed dorsal branches of all segments fuse into the dorsal longitudinal tracheal trunks [123]. Finally the main components of the fully developed early larval tracheal tree form at stage 17.

Following cell specification, branching morphogenesis of the tracheal epithelium can be divided into three major phases (first phase, from mid-embryogenesis to the final stages of embryogenesis; the second phase, most time of the larval stages; third phase, most time of pupal stage). In the first phase, fully-functional trachea form that involves the morphogenesis of the entire tracheal tree as well as lumen clearance and gas-filling. In the second phase, the functional tracheal network undergoes further growth, development and remodelling in order to maintain efficient gas flow. One striking feature of tracheal development, the control of tube size, is orchestrated both at the level of diameter (branch expansion) and length (branch elongation) and depends on the structural changes of cells and the apically-secreted extracellular matrix in the absence of cell death and proliferation. Tube size regulation is intimately associated with epithelial lumen morphogenesis and encompasses processes such as the addition of apical membrane by exocytosis occurring in tandem with the removal of luminal products by endocytosis[124–126], oriented cell intercalation[127,128], cell elongation and polarized cell shape changes along the tube axis[129]. Along with adjustments in tubule size, extensive arborizations of fine terminal branches tracheate growing tissues during larval stages [130,131]. In the third phase, extensive remodeling of the entire tracheal network occurs wherein some branches (e.g. posterior part of the trachea) are lost and new branches form to support the developing adult tissues[130,132,133].

1.5.1 Genome structure and genetics of *Drosophila*

Drosophila melanogaster is among the genetically best-known organisms and one of the most widely used eukaryotic models in molecular biology. Its genome is 60% homologous to that of humans and about 75% of the genes responsible for human diseases have homologs in flies [134]. Furthermore, most of the signalling pathways controlling cell growth, apoptosis, proliferation and differentiation in mammals have a conserved function in flies allowing their modulation use to mimic COPD biology in a simple model organism like *Drosophila* [135]. The genome is less redundant than those of mammals. For example, *Drosophila* has a simplified, but well-conserved JAK/STAT signalling pathway. The only diversification of this pathway is seen on the level of the ligands, where three Unpaired ligands are operative, namely Unpaired (Upd), Unpaired 2 (Upd2), and Unpaired 3 (Upd3). The signal by binding to a single common GP130-like receptor, encoded by *domeless* (*dome*)[136,137]. Upon ligand binding, the single JAK tyrosine kinase in *Drosophila*, encoded by *hopscotch* (*hop*), is activated; Hop then activates the single known STAT, STAT92E, which functions as a homodimer[136,138–140].

1.5.2 Simple airways and their conserved developmental processes

With regard to the airway structure, *Drosophila* has a simplistic airway which is only made of a branched tubular network. The primary function of the airway is gas transport and exchange. The secretory functions of the trachea are exemplified by their cuticle secretions. So the functions of the *Drosophila* trachea encompass the vast majority of physiological roles typically fulfilled by far more complex tubular organs in humans or in other mammals[141]. The cellular composition of *Drosophila* trachea is very simple as well, consisting of cells of varying size with distinct cellular-scale morphologies. Compared with the pseudostratified epithelium in the human lung, the tracheal system consists of an interconnected network of monolayered epithelial tubes.

Although the airway structures between humans and *Drosophila* are quite different, studies on the cellular and molecular mechanisms of tube morphogenesis in *Drosophila* and mammals have revealed common mechanisms in the tracheal formation and maturation and they also revealed the conserved role of key pathways in regulating the growth and structuring of tubular networks[142,143]. Growth and patterning need to be tightly coordinated for normal development, and errors can lead to developmental defects and diseases. The understanding of the defects in these key pathways in tube patterning, outgrowth, ramification and

maturation is of clinical relevance, since many factors are evolutionarily conserved and may have similar functions in humans[143]. Previous studies have characterized the morphogenesis of the *Drosophila* spiracular branch (SB) tracheoblasts, which are multipotent progenitors that generate pupal tracheoles (specialized pupal airways)[144], as well as adult tracheal tubes, spiracles, and epidermal cells[145]. SB tracheoblasts are an emerging and attractive model for studying signalling events that control stem cell homeostasis given its growth and patterning are tightly coordinated by the similar critical molecular regulators as observed in the human lung, like BMP, WNT and FGF signalling pathway[1,130,133,142].

1.5.4 The powerful tools for gene expression control and clonal analysis in *Drosophila*

Drosophila is one of the most powerful genetic models. The development of binary expression systems in *Drosophila* has allowed researchers to manipulate gene function in specific cell populations for cell labelling, gene-function analysis or cell-lineage tracing. The first binary expression system that had been introduced was the *GAL4*–upstream activating sequence (*UAS*) for transgene expression[146]. Following the *Gal4*/*UAS* system, various other methods have been developed using alternative expression systems as well as site-specific recombinases to manipulate and label cell populations[147]. Now, the binary expression systems mostly used include *GAL4 -UAS*, LexA- *lexAop* and QF- *QUAS* systems. The *GAL4-UAS* system is the workhorse of *Drosophila* genetics, it consists of two key components, the yeast *GAL4* transcriptional activator expressed in a specific pattern and a transgene under the control of a *UAS* promoter that is largely silent in the absence of *GAL4*[146]. GAL80 repressor of *GAL4* was always used to restrict *UAS* responder expression both spatially and temporally. For temporal control, the temperature sensitive mutant version of GAL80, $GAL80^{ts}$, which is active at 18 °C but does not repress GAL4 at 29 °C or higher temperatures. On the other hand, the technique called flp-out consisting of two components: yeast site-specific recombinase, flipase (Flp) and its recognition target sequence (*FRT*) provides another way in gene expression control, spatially and temporally. Stop signals flanked by *FRT* sites can silence gene expression and can be removed by the expression of Flp to activate gene expression. To date, thousands of *GAL4* lines and more *UAS* lines were generated for the gene overexpression, cell- or tissue-specific genetic mutant rescue, RNA interference screens and other applications. For cell- or tissue-specific genetic mutant rescue, gene overexpression, RNA interference screens and many other applications, and has been extensively used for developmental studies in tissues such as

the central nervous system, eye and muscles.

1.6 Aim

COPD develops in a multistep way, involving multiple detrimental processes, including inflammation, cellular apoptosis, oxidative stress, and abnormal cellular repair[148,149]. Much attention has focused on the general pathogenetic principles in these diseases, whereas the origin and the onset of the disease are not really understood. The onset possibly involves perpetuated reactivation of inflammatory cells[150] or/and microinjuries to the epithelium[151]. Consequently, one major task is to elucidate which effects these highly COPD relevant factors have on the epithelial cells? Major molecular and morphologic changes occur in the airway epithelium during COPD development, and growing evidence suggests that airway epithelial dysfunction is involved in disease initiation and progression[152]. Especially conserved signalling systems that are involved in lung development and in lung repair processes are thought to be highly relevant for disease development, but their exact contribution is still not understood at all. Therefore, the major aim of this study is to the physiological and the pathophysiological significance of these signalling pathways for the development of COPD. Using *Drosophila* as a model, a focus will be made on the JAK/STAT and the WNT signaling pathway of airway epithelial cells. Beside elucidation of their role in maintaining the tissue homoeostasis, the effect of deregulation of these pathways on the airway structure and functionality should be unraveled to allow a better understanding of their role during the different phases of COPD development. Finally, it should be elucidated, if these models can be used to search for new, more targeted therapeutic strategies to fight the disease.

Material and methods

2.1 Devices

Device	Company
Abakytical balance	Kern & Sohn GmbH(Balingen,Germany)
AxioImager	Zeiss (Oberkochen, Germany)
Bead ruptor 24	Omni International(Kennesaq, USA)
Balance (MXX-412)	Denver Instrument GmbH (New York, USA)
Centrifuge (5415D)	Eppendorf (Hamburg,Germany)
Centrifuge (5417R)	Eppendorf (Hamburg,Germany)
Electrophoresis chambers	Biometra GmbH (Göttingen, Germany)
Geldocumentation (Transilluminator)	Heinrich Eimecke GmbH (Kiel, Germany)
Incubators (WB250K,WB120K)	Heinrich Eimecke GmbH (Kiel, Germany)
LabGard (IBS)	INTEGRA Biosciences GbmH(Biebertal,Germany)
Light source (U-RFL-T)	Olympus (Hamberg, Germany)
Magnetic stirrer (RET)	IKA (Staufen,Germany)
Magnetic stirrer (MR3001)	Heidolph (Schwabach, Germany)
pH 340/ION	WTW (Weiheim, Germany)
Power supply (EV245)	ConsortNT (Nürnberg,Germany)
StepOne Real-Time OCR System	Applied Biosystems (Foster City, USA)
Stereo microscope (MZ19F)	Leica Microsystems (Wetzlar,Germany)
Stereo microscope (S6E)	Leica (Wetzlar,Germany)
Stereo microscope (stemi 506)	Zeiss (Oberkochen, Germany)
Stereo microscope, fluorescence (SZX129	Olympus (Hamburg, Germany)
Thermocycler (Labcycler)	SensoQuest GmbH (Göttingen,Germany)
Thermomixer comfort	Eppendorf (Hamburg,Germany)
Pipettes	Eppendorf (Hamburg,Germany)

2.2 *Drosophila* strains

Reporter strains: 10XSTAT-GFP, 10XSTAT92E binding sites driving expression of EGFP [153]

The *Gal4-UAS* system[154] was used to express fluorescent reporters and other proteins in specific tissues and cell types *in vivo*.

Gal4 drivers were: *btl-Gal4*/FM7; *btl-Gal4*, *UAS-GFP* on the 3rd chromosome; *btl-Gal4*, *UAS-GFP* on the 2nd chromosome were obtained from the Leptin group, Heidelberg, Germany. *Btl-Gal4* expresses *GAL4* mainly in tracheal cells under the control of a *btl* enhancer trap, approximately 3kb upstream of the transcriptional start; *upd2-Gal4*, *upd3-Gal4*[121]; *nach-Gal4*, a transgene containing 2 kb of the *nach* promoter region controlling *Gal4* and expressing in

tracheal cells specifically; *cut-Gal4* (BDSC 27327); *fz3-Gal4* (made in the lab)[155].

UAS responder lines were: *UAS-lacZ.nls* (BDSC 3956), *UAS-dome⊿cyt2.1* (*UAS-dome.DN*) obtained from N. Perrimon[156]; *UAS-hop.CA* obtained from N. Perrimon[157]; *UAS*-upd3 constructed in our lab[121]; *UAS-btl*.lambda, a mutant *btl* encodes an FGFR gain of function allele (BDSC 29045); *UAS-Ror1*, *UAS-Ror2*(*Nrk*), *UAS-Ror1.GFP* and *UAS-Ror2.GFP* were constructed in this work, gene sequence of *Ror1* and *Ror2* were cloned into the pBID-*UAS*C plasmid (Addgene, 35200) and the injection into embryos was done by Bestgene, Chino Hills, USA; *UAS-wnt2* (BDSC 6961); *UAS-wnt4* (BDSC 80070); *UAS-wnt5* (BDSC 64299); *UAS-yki.GFP* (BDSC 28815); *UAS-yki.CA* (BDSC 28817); *UAS-Rho1.CA* (BDSC 8144); *UAS-wts.IR* (BDSC 27662); *UAS-cta.CA*, a gift from H. Susumu[158]; *UAS-Gaq.CA* (BDSC 30743), tubP-*Gal80*.ts (BDSC 7018), a transgene that ubiquitously expresses a temperature-sensitive conditional repressor of *GAL4*, was used to limit *UAS* responder expression to specific time periods. Stocks were raised on standard cornmeal-agar medium at 25^{o}C.

2.3 Oligonucleotides and Plasmids

2.3.1 The primers used for polymerase chain reaction as following:

Primer	**Sequence (5’ - 3’)**
*Fz3-Gal4*_F	GGGGTACCGAACGAAAGAGTTGGCAGAGAG
*Fz3-Gal4*_R	ATAAGAATGCGGCCGCGCTTAGTGGGTTTCAGGAGG
qPCR-rpl32_F	AAGCCGTAATGTCGTTTTTG
qPCR-rpl32_R	TGGGCAGTATCCATTGAGTT
qPCR-*vvl*_F	ATCCGTGGATGCAAACCCAT
qPCR-*vvl*_R	TGCGACATCTCCTGCTTGAC
qPCR-*btl*_F	GCCGTCAAGATGGTCAAGGA
qPCR-*btl*_R	CACGATCACCCACAGAGGAC
qPCR-*yorkie*_F	CGCGCACATTGTAGTTCTGC
qPCR-*yorkie*_R	ATCCCCCAGCTCCAGATTCA
qPCR-*wnt2*_F	CCCAACTACTGCGAGCGAA
qPCR-*wnt2*_R	CGTGGTCCTTCGAATGTGCT
qPCR-*wnt4*_F	ATGGTAGCCCCATTCCGTTG
qPCR-*wnt4*_R	TTGGGCAGCAGTACATCGAG
qPCR-*wnt5*_F	CGGGTGAATAGGGCGAGATG

qPCR-*wnt5*_R	CATCAAGAGGGCCTACGCAA
Ror-F	TCACAAGACGCATACCAAACGAACAAAATGAACAAATACTCGGCATTTATAGTC
Ror(with GFP)_R	ACCGAGGCGCCCTTTGGCTTCGAGGCGATCATTTCTGGATTACTGGCCTTAAAG
Ror(without GFP)_R	AAGATCCTCTAGAGGTAC TTACATTTCTGGATTACTGGCCTTAAAG
Nrk-F	GAATCACAAGACGCATACCAAACGAACAAAATGGCTGCCGGGCAATGG
Nrk(with GFP)_R	ACCGAGGCGCCCTTTGGCTTCGAGGCGATGAGCATTGCCTTGCACTCGCTCT
Nrk(without GFP)_R	AAGATCCTCTAGAGGTACCTAGAGCATTGCCTTGCACTCGCTCT
(*Ror* or *Nrk*) GFP_F	CGAAGCCAAAGGGCGCCTCGGTTCGTGCAATGGTGAGCAAGGGCGAG
(*Ror* or *Nrk*) GFP_R	ATAAGCTGCAATAAACAAGTTTCACTTGTACAGCTCGTCCATG

IgG2 linker (CGAAGCCAAAGGGCGCCTCGGTTCGTGCA) were used between interest gene and GFP.

2.3.2 Plasmids

pBID-*UAS*C, addgene 35200 was used to construct *UAS* line; pBPGUw, addgene 17575 was used to construct the *GAL4* lines

2.4 Enzymes and kits

Enzymes and kits	**Company and catalog #**
DNeasy Blood & Tissue Kits	QIAGEN (Cat No. 69504)
PureLink™ RNA Mini Kit	Invitrogen™ (Cat No. 12183025)
Taq DNA Polymerase	Thermo Fisher (Cat No. 10342020)
NucleoSpin Plasmid QuickPure™ Kit	Macherey-Nagel™ (Cat No. 740615.250)
NucleoSpin™ Gel and PCR Clean-up Columns	Macherey-Nagel™ (Cat No. 740609.250S)
PureLink™ HiPure Plasmid Filter Midiprep Kit	Invitrogen™ (Cat No. K210015)
qPCRBIO SyGreen Mix Hi-Rox	PCR Biosystems Ltd(Cat No. PB20.11-50)
SuperScript IV Reverse Transcriptase	Thermo Fisher (Cat No. 18090050)
Q5® High-Fidelity DNA Polymerase	NEW ENGLAND BioLab (Cat No. M0491L)
Gibson Assembly® Master Mix	NEW ENGLAND BioLab (Cat No. E2611)

Gibson assembly allows for successful assembly of multiple DNA fragments, regardless of fragment lengths or end compatibilites in a single-tube isothermal reaction[159,160]. The protocol was provided by NEW ENGLAND BioLabs (Gibson Assembly® Master Mix – Assembly (E2611)). In this study, the reaction volume I used was 10µL.

2.5 Fly food

All the experimental animals were raised in the general *Drosophila* medium at 25°C, except those used in temperature-inducible experiment. For the temperature-inducible experiments, animals were kept in the 18°C to silence the *UAS*-gene expression and then transferred to 29°C to activate the *UAS*-gene expression. The recipes of 500mL general *Drosophila* medium include:

-mL	H_2O
31.25g	Brewer´s yeast
31.25g	Commeal
5g	Agar-agar
10g	Glucose
15g	Molasses
15g	Sugar beat syrup
cooking for 10-15min in the water bath, autoclaving 15-20min, cool down 60°C	
5 mL	Propionic acid (10%)
15 mL	Nipagin (10% in EtOH)

2.6 Analysis of ectopic gene expression

Vvl-FLP/CyO; *btl-moe.mRFP* line(BDSC 64233), *tubP-Gal80.ts* and CoinFLP-*Gal4*, *UAS*-2xEGFP lines (BDSC 58751) were used to construct tracheal mosaics. Ventral veins lacking (*vvl*) was expressed in larval tracheal clones that covered approximately 30% to 80% of the trachea [9]. And coinFLP-*Gal4* generates mosaic tissues composed of clones of which only a subset expresses *Gal4* [12]. The genotype of the flies are *vvl-FLP*, coinFLP-*GAL4*, *UAS*-2x*EGFP*/CyO and *vvl*-FLP, coinFLP-*GAL4*, *UAS*-2x*EGFP*/CyO; *tub-Gal80.ts*.

2.7 Developmental viability

For quantifying the viability of eggs, the eggs were collected overnight and were not physically handled in any way. The number of total eggs, the hatched eggs and the pupa were counted starting from two days after the collection and then viabilities were calculated. For developmental viability analysis of larvae, tub-Gal80*.ts* was used to limit *UAS* responder expression at the larvae stage. Animals were raised at 18^{o}C to keep the *UAS* responder gene silent. Then Larvae at different instar stages were picked out and transferred to new medium at 29^{o}C. In this study, 4 replicates were performed with 30 larvae each. The stage of larvae was determined via the appearance of anterior spiracles.

2.8 Determination of epithelial thicknesses

The trachea of L2 and L3 Larvae were carefully dissected out from the posterior side of the body in PBS. The isolated trachea was immersed in 50% glycerol and digital images were captured within 15mins. L2 Larvae were distinguished from L3 larvae by the appearance of anterior spiracles. The relative ages of L3 larvae were inferred from the size of the animal; older larvae are larger. 30 larvae were used in each group and specimens were analysed by Image J.

2.9 Cigarette smoke and hypoxic exposure

All cigarette smoking exposure experiments were carried out in a smoking chamber, attached to a diaphragm pump. Common research 3R4F cigarettes (CTRP, Kentucky University, Lexington, USA) were used for all experiments. The vials containing animals were capped with a monitoring grid to allow the cigarette smoke to diffuse into the vial. The mortality rate of the wildtype larvae caused by quick smoke and slow smoke controlled via adjustments of the diaphragm pump was measured.

For long-time smoke experiments, L2 larvae were exposed to smoke three times a day for 30 minutes each, on two consecutive days. For strong smoke experiments, L3 larvae were exposed to 2 cigarettes smoke, one time for 45mins, which led to about 35-50% mortality rate of animals. To study the effects of hypoxia on the activity of JAK/STAT signalling pathway, larvae were exposed to long-term hypoxia and short-term hypoxia, separately. For long-term hypoxia experiments, L2 larvae were exposed to 5% oxygen three times a day for 30 minutes each, on two consecutive days. For short-term hypoxia experiments, L3 larvae were exposed to 1% oxygen one time for 5 hours.

2.10 Antibodies and immunohistochemistry

Larvae were dissected by ventral filleting and fixed in 4% paraformaldehyde for 30 minutes. Embryos were staged according to Campos-Ortega and Hartenstein[161] and fixed in 4% formaldehyde for 30 min. Immunostaining followed standard protocols as described[162,163]. GFP signals were amplified by immunostaining with polyclonal rabbit anti-GFP (Sigma, SAB4301138; used at 1:500) primary antibody. 40-1a (DSHB, used at 1:50) was used to detect beta-galactosidase. Coracle protein was detected with DSHB C566.9, a monoclonal mouse anti-

coracle antibody (used at 1:200). Armadillo protein was detected with DSHB N2 7A1, a monoclonal mouse anti-armadillo antibody (used at 1:500). A monoclonal rabbit anti-phospho-Histone H3 (Ser10) (Sigma-Aldrich # 05-1136) was used to stain mitotic cells. A monoclonal rabbit cleaved *Drosophila* Dcp-1 antibody (Cell Signalling # 9578) was used to detect apoptotic cells. Secondary antibodies used were: Cy3-conjugated goat-anti-mouse, Cy3-conjugated goat-anti-rabbit, Alexa488-conjugated goat-anti-mouse (Jackson Immunoresearch), Alexa488-conjugated goat-anti-rabbit (Cell signalling). Tracheal chitin was stained with the 505 star conjugated chitin-binding probe (NEB; 1:300). Nuclei were stained with 4',6-Diamidino-2-Phenylindole, Dihydrochloride (DAPI) (Roth 6843). Ethidium Homodimer III, a cell membrane-impermeant nucleic acid dye was used to visualize necrosis[164].

2.11 Time-lapse microscopy

All images were acquired using a Zeiss AxioImager Z1 fluorescent microscope. Embryos were dechlorinated in 3% sodium hypochlorite and immersed in Halocarbon oil 700 (Sigma Aldrich, 9002-83-9). Then the embryos were imaged after stage 15 when the tracheal tree formed at 3 hours intervals.

2.12 Image analysis

Fluorescent images were acquired with a Zeiss AxioImager Z1 or a Zeiss confocal microscope. The count of cell numbers and quantification of the GFP or RFP intensities were performed using ImageJ.

2.13 RNA isolation, sequencing and analysis

For the gene expression analysis of 3rd instar larvae trachea, larvae were dissected in cold PBS and transferred to RNA Magic (BioBudget, Krefeld, Germany) and processed essentially as described earlier[165] with slight modifications. The tissue was homogenized in a Bead Ruptor 24 (BioLab products, Bebensee, Germany) and the RNA was extracted by using the PureLink RNA Mini Kit (Thermo Fisher, Waltham, MA, USA) for phase separation with the RNA Magic reagent. An additional DNase treatment was performed following the on-column PureLink DNase treatment protocol (Thermo Fisher, Waltham, MA, USA).

HiSeq were performed by Illumina HiSeq 3000/4000 and the sequencing reads were trimmed

for low-quality bases and adapters using the fastq Illumina filter (http://cancan.cshl.edu/labmembers/gordon/fastq_illumina_filter/) and cutadapt (version 1.8.1)[166]. Transcriptomics analysis including gene expression values and differential expression analysis was done using CLC Genomics Workbench. The detailed protocols can be obtained from the CLC Web site (http://www. clcbio.com/products/clc-genomics-workbench). The *D. melanogaster* reference genome (Release 6)[167] was used for mapping in this research.

The transcription factor binding site enrichment and the Gene Ontology enrichment analyses of the differentially expressed genes were carried out using Pscan and Panther, respectively. Date was visualized through the circos software.

Results

3.1.1 JAK/STAT signalling is necessary to maintain epithelial cells homeostasis but long-term upregulation reprograms cell fates

3.1.1.1 JAK/STAT signalling is required for epithelial cells to maintain a homeostatic situation

Previous studies uncovered a strong activation of the JAK/STAT signalling pathway in the trachea during embryogenesis and the importance of this signalling system for organ development[153]. However, the exact pattern of activation is still not clear. In this study, I used the STAT92E-GFP reporter[153] to observe the activation of the JAK/STAT pathway concurrently with *btl*>LacZ.nls[168] to label the trachea specifically. Fig. 4A shows the components of the JAK/STAT signalling pathway in *Drosophila*. Based on the activity of the STAT92E-reporter, a central region in the trachea, mainly belonging to the transverse connective (TC), possesses a stronger activation of the corresponding reporter (Fig.4 B-D).

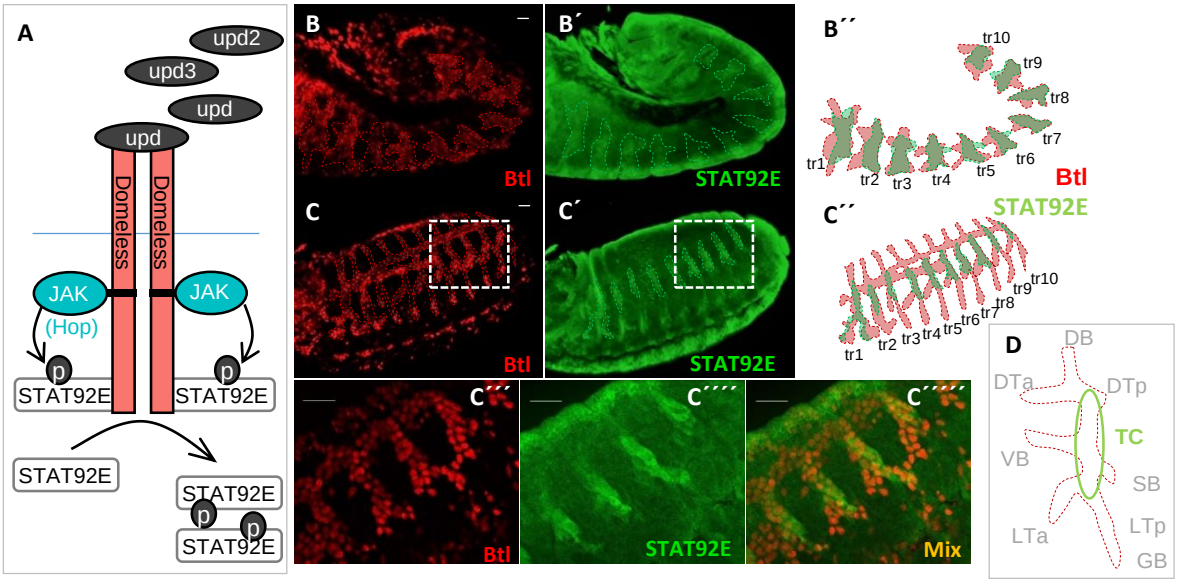

Fig. 4 The pattern of activation of JAK/STAT signalling in the airway of *Drosophila* embryos.

(A) shows a model of JAK/STAT signalling pathway in *Drosophila* comprising all major components. Three ligands (upd, upd2 and upd3) bind to a single receptor, Domeless (Dome), which transmits this information via a single JAK (hopscotch (hop)) to a single STAT transcription factor (STAT92E). (B-D) Fluorescence micrographs of *Btl-Gal4*; 10XSTAT92E-GFP; *UAS*-lacZ.nls embryos. 10XSTAT92E-GFP *in vivo* reporters detect JAK/STAT pathway activation in the *Drosophila* trachea in the embryo. The JAK/STAT signalling pathway is activated in the whole trachea placode (tr). The activation of JAK/STAT pathway in the terminal regions is weaker than that in the central regions before (B) and after fuse of tracheal invaginations of all segments (C). (D) shows the pattern of activation of JAK/STAT signalling in the trachea metamere of embryos. DB, dorsal branch; DTa, dorsal trunk anterior; DTp, dorsal trunk posterior; VB, visceral branch; LTa, lateral trunk anterior; LTp, lateral trunk posterior; and GB, ganglionic branch; SB, spiracular branch. The stronger signal in the central regions mainly belong to TC. * P<0.05, ** P<0.01 by Student's t test. Scale bar: 20um.

To further confirm the importance of the JAK/STAT pathway in the development of the respiratory system of *Drosophila,* I manipulated its activity in the trachea by driving a dominant-negative isoform of Domeless (*dome.DN*) with the *btl-Gal4* driver. Even though some animals grew up to the larval stage, all of them died before the pupal stage (Fig. 5A). Microscopical analysis of these survived larvae showed that the animals lacked an intact dorsal trunk (DT) (Fig. 5B). Time-lapse imaging of the *dome.DN* trachea-specific expressing in the embryo revealed that all tracheal segments were fused at stage 15, however, the DT broke in the following hours (Fig. 5C and 5E). Afterwards, I tested the effects of ectopic activation of the JAK/STAT signalling pathway either by expression of the ligand (*upd3*) of the constitutively active Jak-allele (*hop.CA*) on the tracheal development. The corresponding animals showed premature death at the embryo or larval stage (Fig. 5B). Microscopical analysis of the larvae and embryos showed that the tracheal segment separation occurred in the larvae stage as well (Fig. 5B), but the disconnection of segments was caused by the failure of their fusion at the beginning of the tracheal development (Fig 5D and 5E). Interestingly, compared with the animals that express the ligand *upd3*, most animals expressed *hop.CA* in the trachea have a full tracheal tree, although they all died in the first larval stages as well. This indicated the influence of upregulated JAK/STAT signalling on the development of the trachea after the first tracheal structures had been formed.

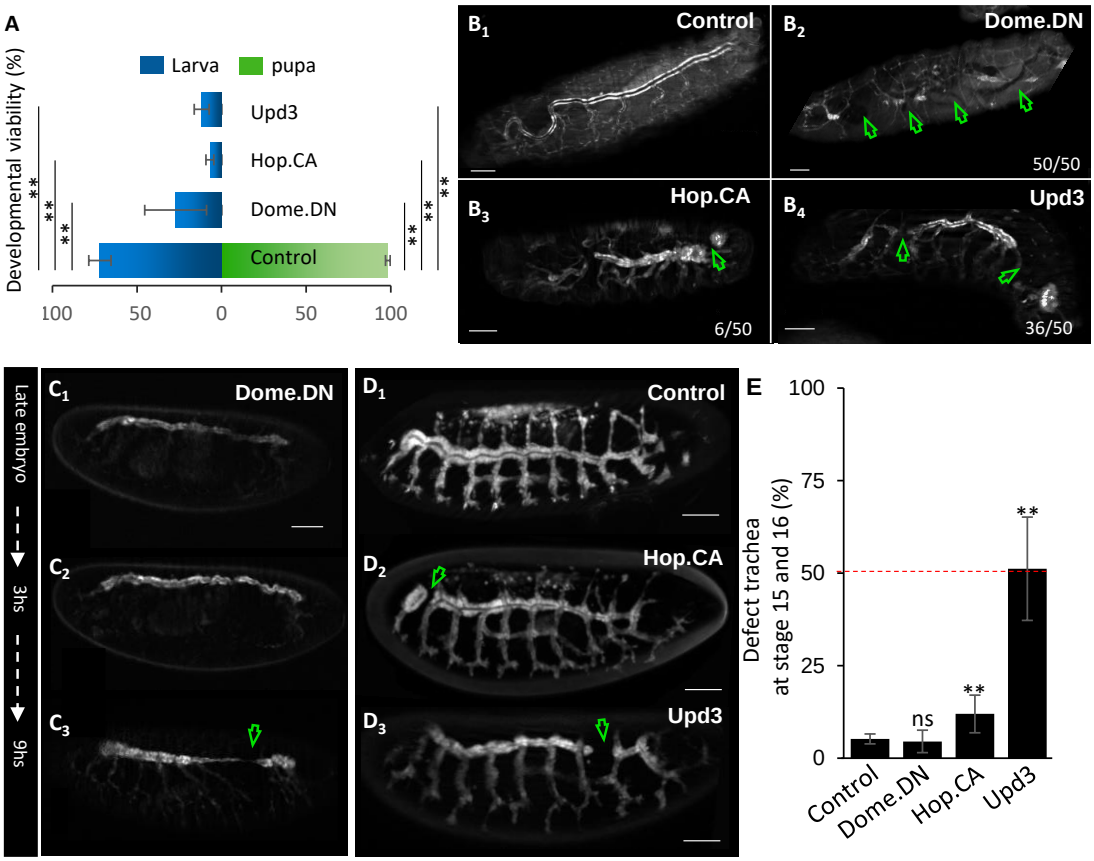

Fig. 5 Effects of JAK/STAT signalling in the airway development in *Drosophila* embryos.
(A) Ectopic blocking or activation of JAK/STAT signalling in the trachea was done by expressing *dome.DN* or *hop.CA* (or upd3) respectively under the control of *btl-Gal4*. The percentage of embryos that hatched and the percentage of larvae that developed into pupae is shown at the left side. (B) Micrographs of surviving larvae. *Btl* driving the expression of upd3 and dome.DN inhibited the formation of an intact tracheal tree. *Btl* driving the expression of *hop.CA* in the trachea showed more intact tracheal trees compared to expressing upd3 and dome.DN in the trachea. X/XX: broken trachea/intact trachea; n=50. (C) Time-lapse imaging the trachea of *btl-Gal4*, *UAS-dome.DN* embryo continuously for 9 hrs after trachea formed. (D-E) Activation of the JAK/STAT pathway in the trachea led to incompleted tracheal development during tracheal morphogenesis. Fluorescence micrographs of *Btl-Gal4*, *UAS-hop.CA* (or *UAS-upd3*) embryos (D) and numbers of the trachea which had no fused tr. (E) Quantification of the numbers of defect tracheal branches in response to the different treatments. ns means no significant, * P<0.05, ** P<0.01 by Student's t test. Scale bar: 50um.

3.1.1.2 JAK/STAT signalling is required for the larval airway system.

To elucidate if JAK/STAT signalling pathway is also operative in a functional airway epithelium, namely in the larval tracheal system, I again used the STAT reporter line. In 3rd instar larvae, STAT signalling is active in all regions of the tracheal system (Fig. 6A), although a reduced activity of JAK/STAT was observed in the posterior zone of the trachea (tr10) where cells are progressively undergoing apoptosis in response to trachea metamorphosis in the following hours (Fig. 6B). However, Some regions like Tr2, SB, and DB, where the cells re-enter into cell

cycle progression at this stage, exhibited much stronger JAK/STAT activity if compared to the quiescent cell area close to them (Fig.6 C-D).

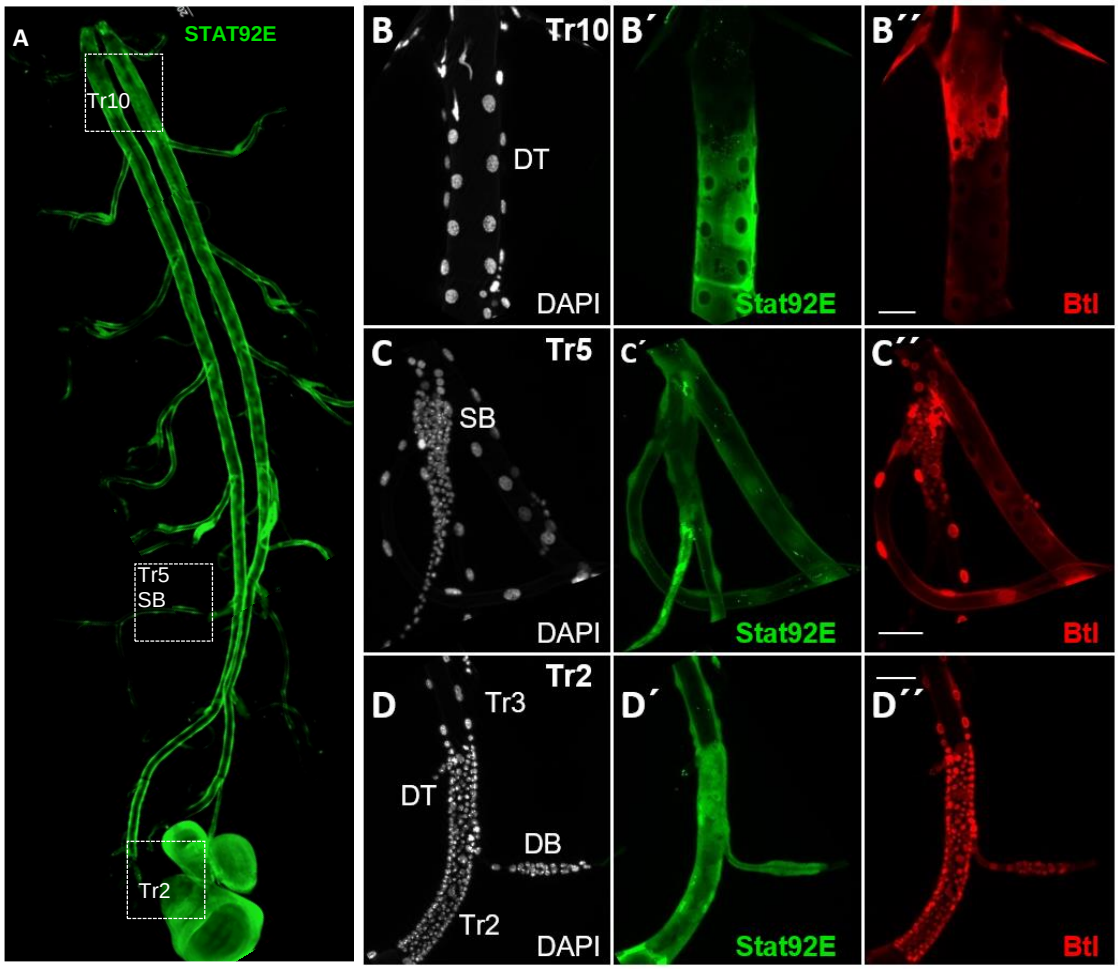

Fig. 6 Activation of the JAK/STAT signalling pathway in the trachea of L3 larva.
(A-D) Fluorescence micrographs of *Btl-Gal4*; 10XSTAT92E-GFP; *UAS-lacZ.nls* larvae. The activation of JAK/STAT signalling was detected by using the 10XSTAT92E-GFP reporter. In general, JAK/STAT signalling was induced in the whole trachea of the larva. Some regions such as tr2, DB (C) and SB (D) where the cell re-enter into cell cycle exhibited stronger JAK/STAT signalling compared to the cell quiescent areas close to them. n=50. Scale bar: 20um.

Reducing JAK/STAT signalling, on the other hand, changed the fate and the morphology of larval airway epithelial cells (Fig. 7A). This inhibition was achieved by ectopic expression of the dominant negative isoform (dome.DN) of the domeless receptor. These cells show a gradual loss of their shape and the induction of apoptotic processes two days after induction of this ectopic expression. This induction of apoptosis could be further demonstrated by the occurrence of Dcp1 positive cells that, at the same time, show other features of apoptotic cells (Fig. 7B-C). This induction of apoptosis was even stronger (and quicker) in stem cells of the

larval tracheal system, where Dcp1 positive cells could be observed at day 1 after induction of the ectopic *dome.DN* expression (Fig. 7E). As already shown, the JAK/STAT pathway is activated in the entire tracheal system. Therefore, I evaluated the expression of the three different Unpaired ligands in the tracheal system. With corresponding enhancer-*Gal4* lines, I was able to show that Unpaired2 ligand is the most important ligand to activate JAK/STAT signalling pathway in the tracheal system (Fig. 8).

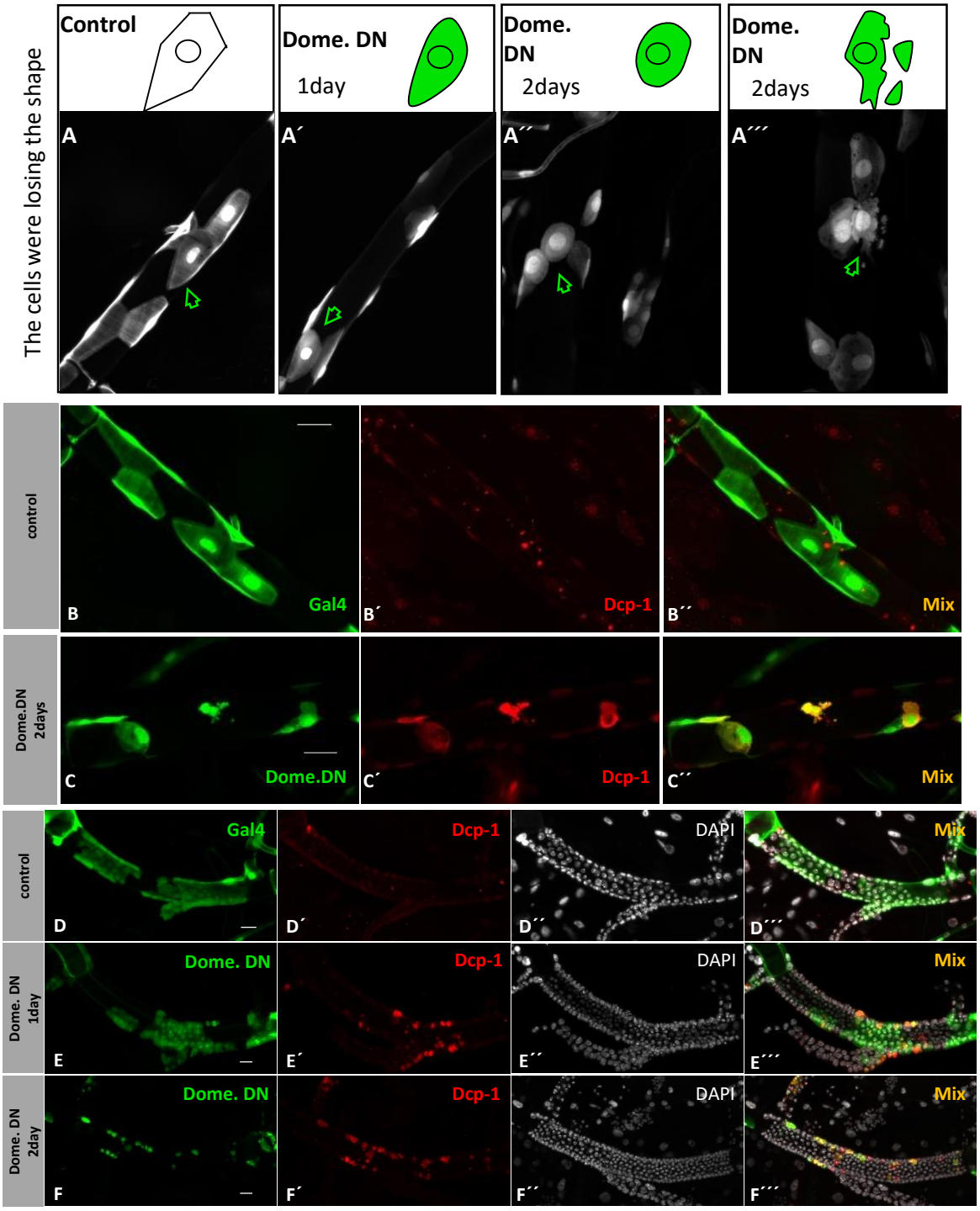

Fig. 7 Inhibition of JAK/STAT signalling pathway induced cell apoptosis.

(A) Fluorescence micrographs of the mutant clones in the trachea of *vvl*-FLP, coin-FLP, *UAS-EGFP, UAS-dome.DN*; *tub-Gal80*^{ts} larva. Negative regulation of JAK/STAT signalling pathway by expressing dome.DN in the trachea led to the loss of cell shape and disintegration afterwards. n=50. (B-C) Fluorescence micrographs of the trachea of *vvl*-FLP, coin-FLP, *UAS-EGFP; tub-Gal80*^{ts} (B) and the trachea of *vvl*-FLP, coin-FLP, *UAS-EGFP, UAS-dome.DN; tub-Gal80*^{ts} larvae (C) stained for cleaved Dcp-1 (red). Modified stem cells (E) could be stained by cleaved Dcp-1 earlier than the mutant somatic cells. Inhibition of JAK/STAT signalling induced blockade of cell division (F). n=50. Scale bar: 20um.

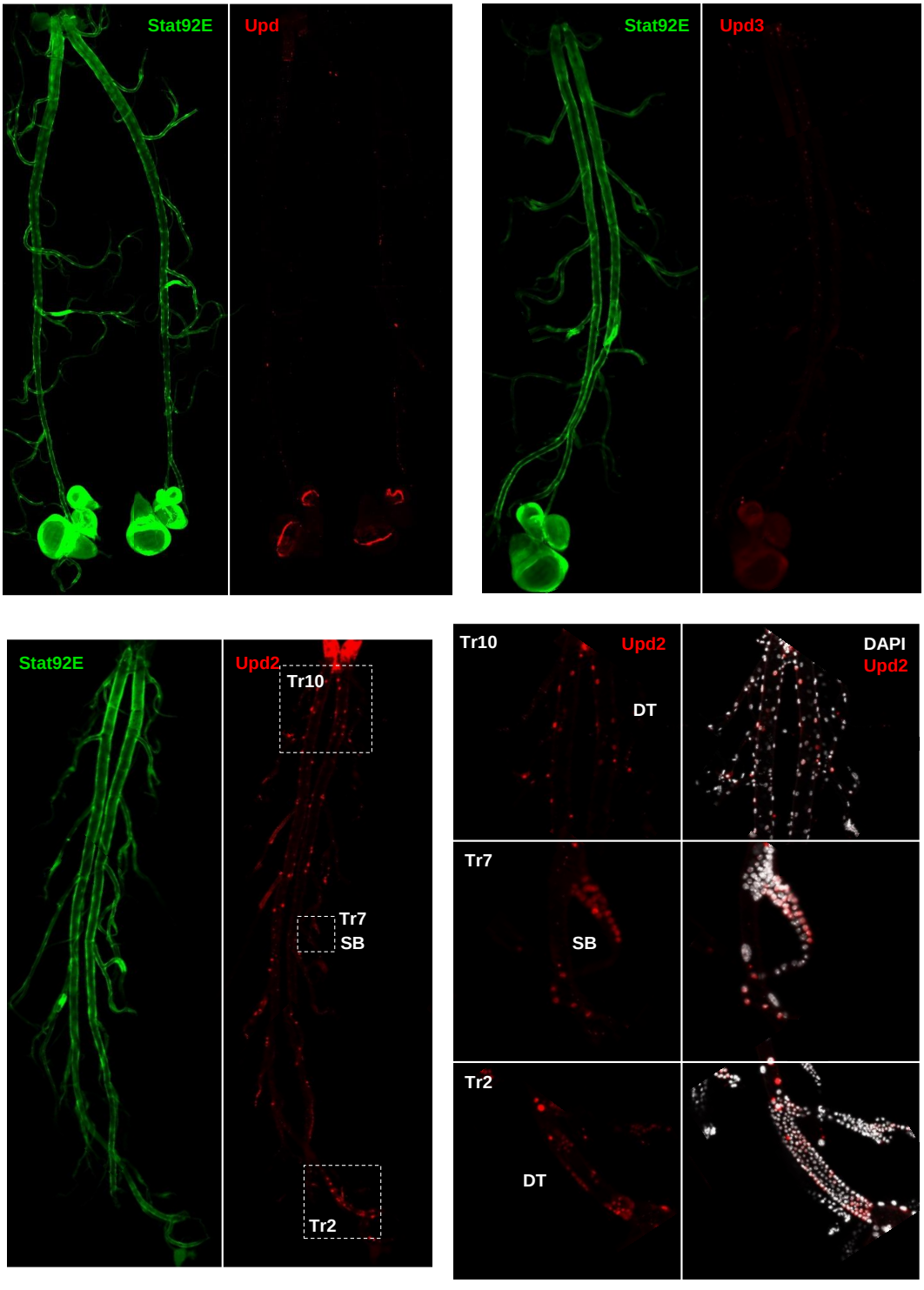

Fig. 8 JAK/STAT signalling is activated in the larval trachea.

(A-C) Fluorescence micrographs of the trachea of ligand(upd, upd2 or upd3)-*Gal4*, *UAS*-lacZ.nls; 10X STAT92E-GFP larvae stained to show ligand expressing cells (anti-ß-galactosidase, red) and JAK/STAT signalling positive cells (anti-GFP, green). Upd2 displayed a higher transcript level in the trachea compared to upd(which showed a strong expression in the other tissue, like the imaginal disc) and upd3 (whose expression in the trachea is weak in the moderate condition but could be induced by CS). (D-F) Fluorescence micrographs of tr2 DT, tr7 SB and tr10 DT of upd2-*Gal4*, *UAS*-lacZ.nls; 10X STAT92E-GFP larva. In the dividing active regions such as tr2 DT and tr7 SB there are stronger JAK/STAT signalling and high intensity of upd2 positive cells compared to their surrounding regions(E-F). n=50:

In order to elucidate if deregulation of JAK/STAT signalling initiated at different time points of the larval development in the tracheal system has deleterious effects on development, I employed the temperature inducible *Gal4*/*Gal80*^{ts} system (Fig. 9A). Firstly, I tested the effects of inhibition of the tracheal JAK/STAT pathway by ectopic expression of the *dome.DN* on survival and the larval structure (Fig. 9B). Ectopic activation was initiated at three different time points during larval development (Fig. 9B). The earlier the expression began, the higher the larval mortality was. It has to be mentioned that none of the larvae survived the pupal stage (Fig. 9C). Ectopic activation of JAK/STAT signalling on the other hand induced with the same experimental design induced lower levels of larval death, both for ectopic expression of the upd3 or the *hop.CA*. In all these cases, no pupa developed into an adult.

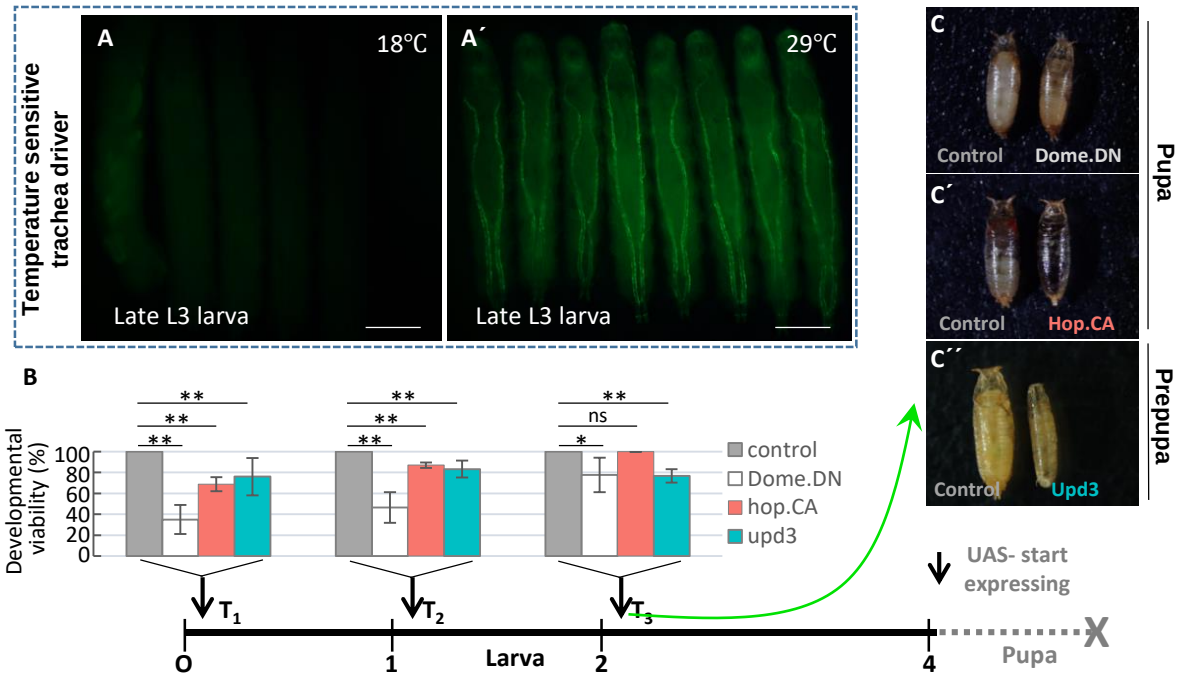

Fig. 9 Ectopic activation of epithelial JAK/STAT signalling promoted cell thickness.
(A) *Btl-Gal4*, *UAS-GFP*; *tub-Gal80*^{ts} (*btl*.ts driver) larvae were reared at 18°C (nonpermissive, A) and 29°C (permissive, A´), respectively. Using the *Gal4*/*UAS* system, comprising the temperature-sensitive repressor Gal80^{ts}, were used to time ectopic gene expression. (B) Developmental viability of larvae with different genotypes (including dome.DN, *hop.CA* and Upd3 expression in the trachea driven by *btl*.ts driver) and different start points of expression (indicated by black arrows). Statistical analysis of survival times is included. (C) In general, none of

these manipulations allowed survival up to adults. Ns means no significant, * P<0.05, ** P<0.01 by Student's t test.

3.1.1.3 Up-regulated JAK/STAT signalling promotes epithelium thickness

Furthermore, I analysed the effects of this intervention on the tracheal structure. Whereas the *dome.DN* overexpression had only minor effects on the tracheal structure, I observed a massive epithelial thickening in response to either *upd3* or *hop.CA* overexpression (Fig. 10A-D). This effect was cell-autonomous as it was observed in experiments using a mosaic expression of *hop.CA* driven by *vvl*-coin. Here, the *hop.CA* expressing cells were much thicker than the non-affected neighbours (Fig.10F). A quantitative evaluation of the epithelial thickness revealed that especially the ectopic expression of *hop.CA* led to massively increased values (Fig. 10E).

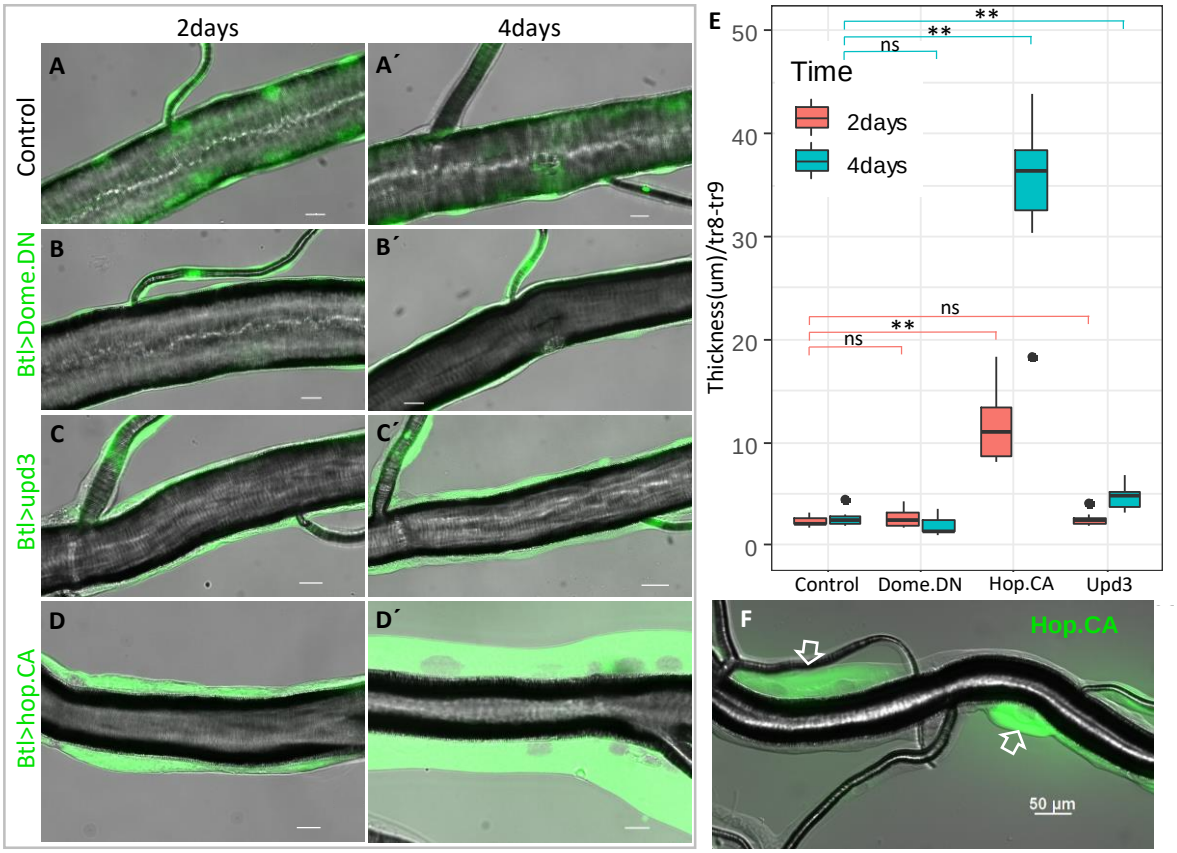

Fig. 10 Ectopic activation of epithelial JAK/STAT signalling induces cell thickening.
(A-D) Micrographs of tr8-tr9 of *btl*.ts driver L3 larvae (A); *btl*.ts driver, *UAS-dome.DN* L3 larvae (B); *btl*.ts driver, *UAS-hop.CA* L3 larvae (C) and *btl*.ts driver, *UAS-upd3* L3 larvae (D) that were raised at 29°C for 2 and 4 days, respectively. (E) Statistical analysis of the epithelial thicknesses in tr8-tr9 of the corresponding larvae. (F) Micrographs of tr8 of *vvl*-FLP, coin-FLP, *UAS-EGFP, UAS-hop.CA* larvae. The thickening of the tracheal epithelium is observed in those cells that express *hop.CA*. Ns means no significant, * P<0.05, ** P<0.01 by Student's t test. Scale bar: 500um in A; 20um in D-G.

To understand the underlying reaction, I analysed the phenotype in more detail. For this, the

lengths of defined areas of the tracheal system, (between Tr8 and Tr9), the length X width product and the cell numbers were quantified (Fig. 11A-B). Despite the manipulation of JAK/STAT signalling in the trachea, the lengths remained almost unaltered, except the reduced length observed after 4 days of the ectopic *dome.DN* expression (Fig. 11B). Consequently, the product of length and thickness mirrored the findings of the measurements of thickness. However, in comparison with the control trachea, the modified tracheal DT tr8-tr9 had similar cell numbers as the matching controls (Fig. 11A). That means that the thickening was caused by an increase in the cell volume but not by an increase in the cell number.

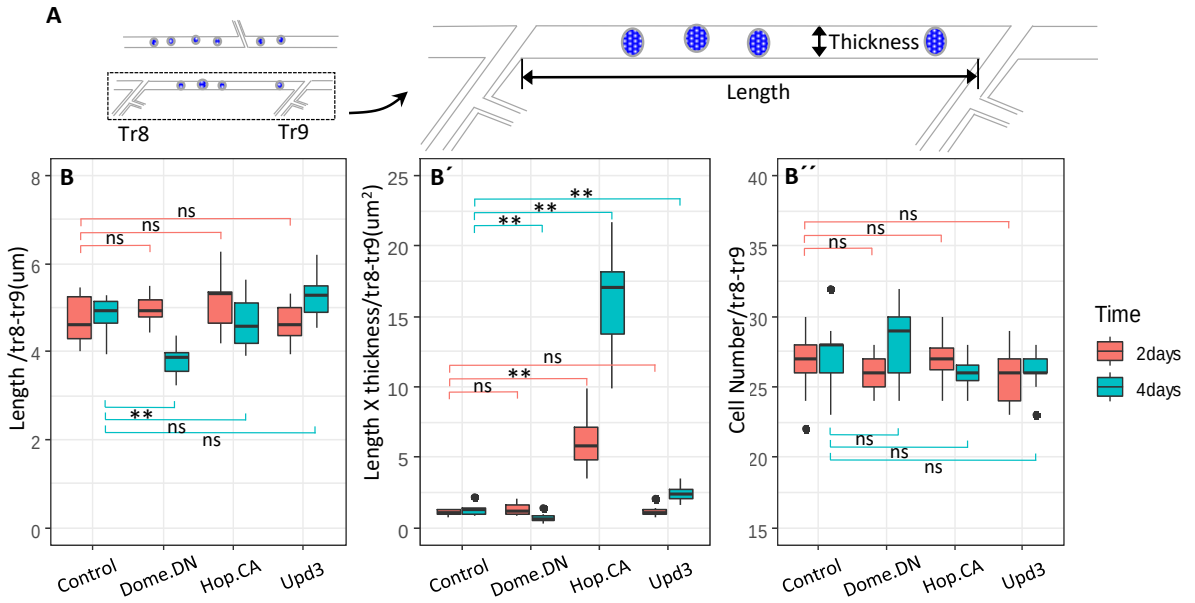

Fig. 11 Changes in epithelial thickness could be attributed to the increase in the cell volume.
(A-B) Illustration and quantification of the length, length X thickness, and the cell number of the tr8-tr9 region of larvae with different types of ectopic manipulation (including *dome.DN*, *hop.CA* and *Upd3* expression in the trachea driven by *btl*.ts driver) for 2 or 4 days, respectively. ns means no significant, * P<0.05, ** P<0.01 by Student's t test.

3.1.1.4 The increase in the thickness of the epithelium is time dependent.

This thickening is not an artefact of the isolation method, it can also be observed in the trachea that had been directly fixed after removal and in those that were isolated in cell culture medium with the same osmolarity as the hemolymph (Fig. 12). In order to quantify the time course of this reaction, I subjected the trachea to different treatment regimens prior to analysis. Apparently, a minimum of two days of ectopic expression is necessary to induce this phenotype (Fig. 13).

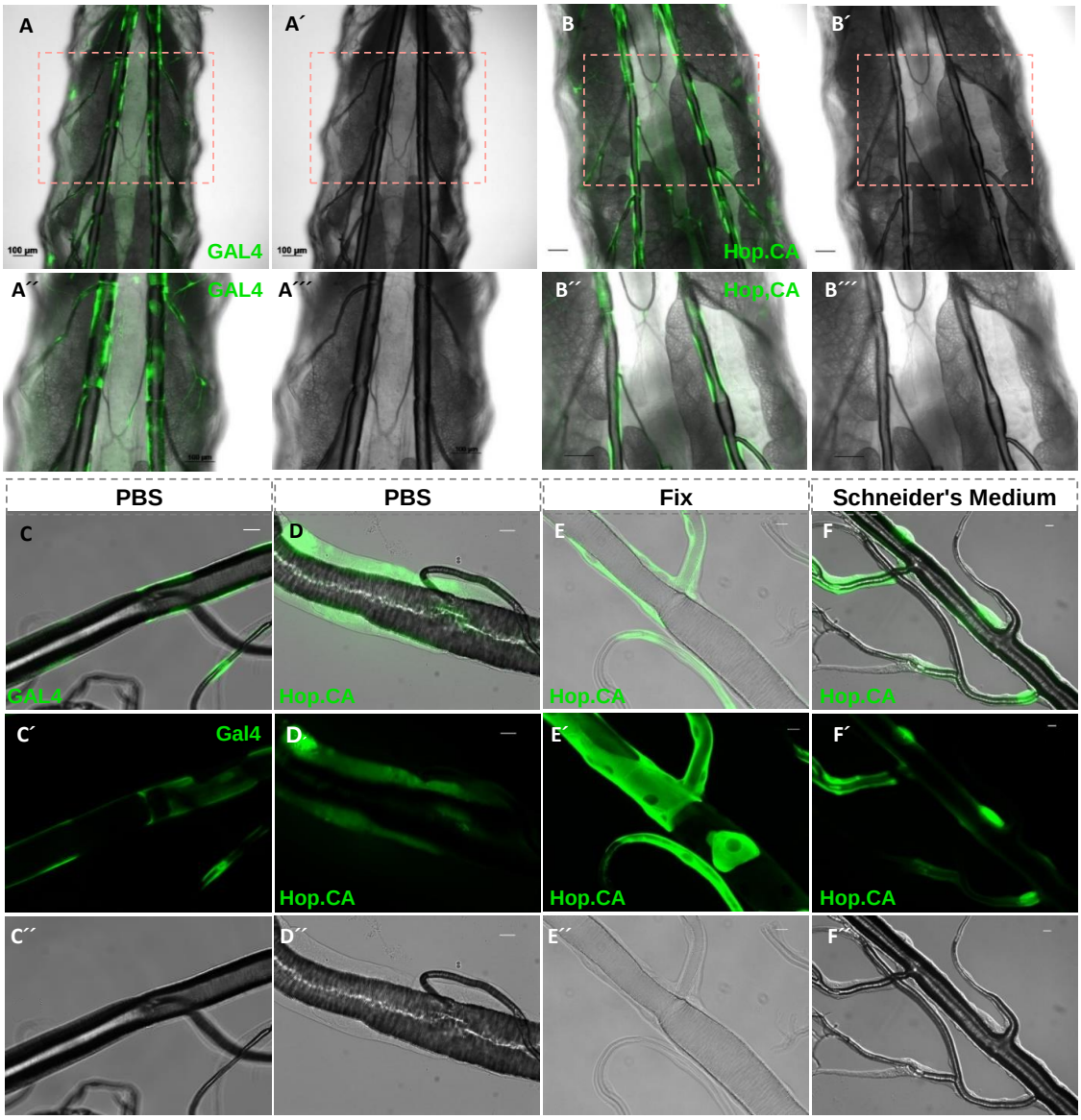

Fig. 12 The observation of changes in cell volume caused by the expression of *hop.CA* in vivo and in some other different solutions in vitro.

(A-B) Micrographs of the posterior of *vvl*-FLP, coin-FLP, *UAS*-EGFP larva(A) and *vvl*-FLP, coin-FLP, *UAS*-EGFP, *UAS-hop.CA* larva(B). Microcopy of the trachea *in vivo* displayed a thicker epithelium in the affected clones(green) compared to the neighbouring cells(B). The cells did not get thickness in the control trachea(A).(C-F) The trachea of *vvl*-FLP, coin-FLP, *UAS*-EGFP larva(c) *vvl*-FLP, coin-FLP, *UAS*-EGFP, *UAS-hop.CA* larva(D-F) were picked out in the PBS(D) or Schneider's medium(F) or fixed immediately in the 4% paraformaldehyde(E) showed a significant increase in the cell volume as well. Scale bar: 100um in A-B; 20um in C-F. n=50.

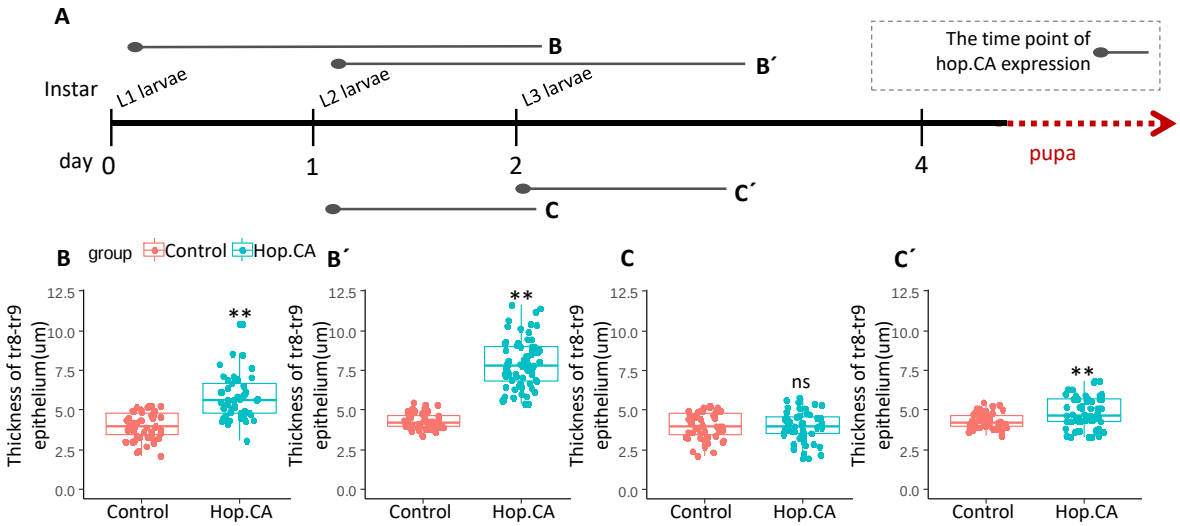

Fig. 13 Changes in epithelial thickness are time-dependent.
(A) Illustration of the time point and period of activation of *hop.CA* expression by using *btl*.ts driver and quantification of the thickness of the tr8-tr9 region of control (*btl*.ts driver, red box) larvae and those experiencing ectopic manipulation (*btl*.ts driver, *hop.CA*, blue box). Compared to the control, 2days expression of *hop.CA* promoted the thickness of trachea significantly (B). 1day expression of *hop.CA* that started at L2 larvae stage didn't promote tracheal thickness(C), but that started at early L3 stage promote epithelial thicker(C´). However, the phenotype is not so strong as 2 days activation of the expression of *hop.CA*. ns means no significant, * P<0.05, ** P<0.01 by Student's t test.

3.1.1.5 JAK/STAT signalling is induced by cigarette smoke.

After demonstrating that JAK/STAT signalling is operative in a fully functional tracheal system and that its deregulation impacts the structure of the airway system dramatically, I aimed to identify situations that are characterized by higher JAK/STAT signalling activities. For this, I subjected the corresponding flies to two different stressful conditions that are related to the airway system; namely, cigarette smoke exposure and hypoxia. Whereas hypoxia had no effects on either the activity of the JAK/STAT pathway reporter or of the corresponding ligands (upd2 and upd3), smoke exposure induced both, upd3 expression and activation of the JAK/STAT pathway reporter: Interestingly, induced expression was mostly confined to a highly sensitive region close to the spiracles (tr9 and tr10) (Fig. 14).

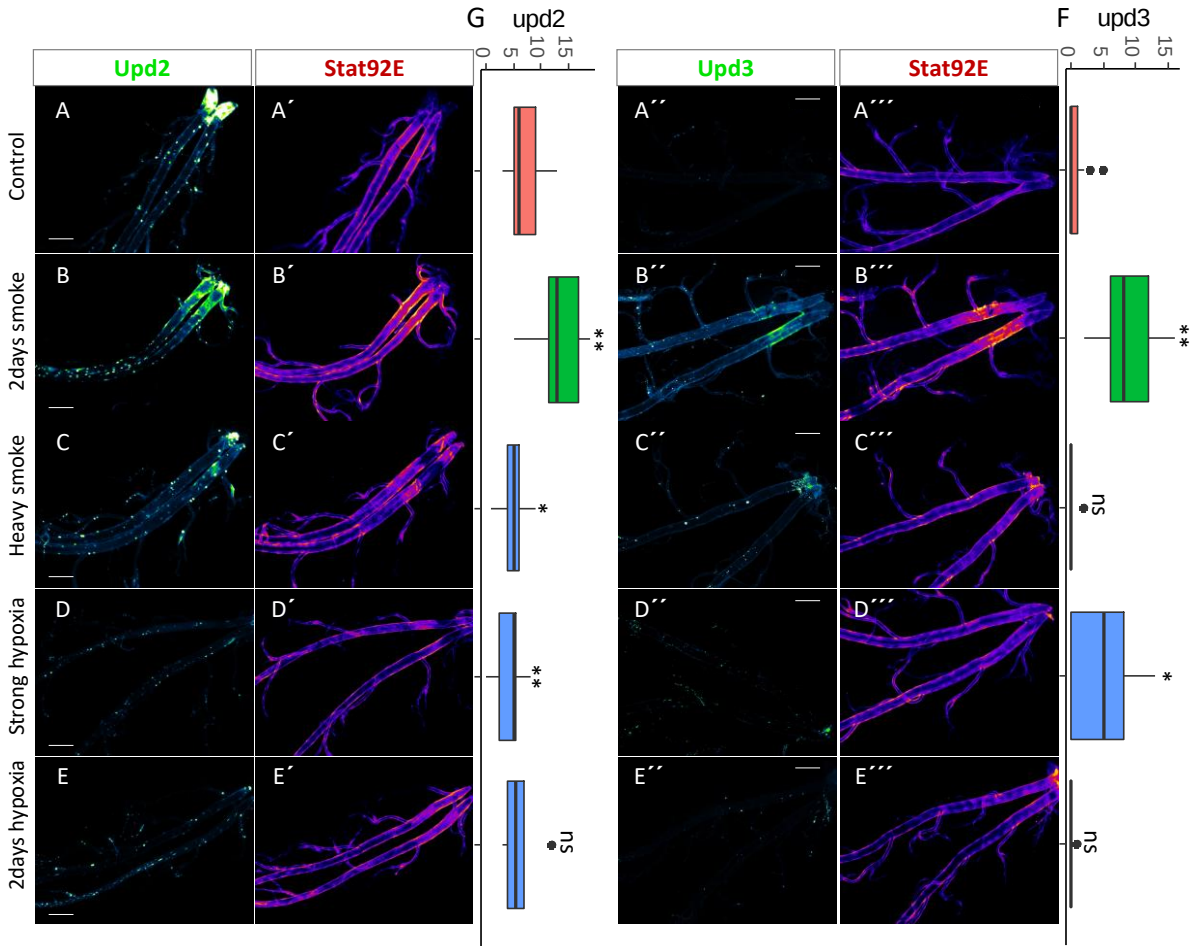

Fig. 14 JAK/STAT signalling in airway epithelial cells is activated by long term cigarette smoke exposure.
(A-E) Fluorescence micrographs of the trachea of *upd2* (left) or *upd3*(right)-*Gal4*; 10XSTAT92E-GFP; *UAS-lacZ.nls* larvae that were exposed for 2 days smoke (B), heavy smoke (C), strong hypoxia (D), and 2days hypoxia (E). (F and G) The number of cells that expressed upd2 and upd3 were counted under these different conditions. ns means no significant, * P<0.05, ** P<0.01 by Student's t test. Scale bar: 200um.

3.1.1.6 Expression of *hop.CA* led to intrinsic changes within the epithelial cells.

To investigate the underlying molecular mechanisms of the effects of chronic activation of JAK/STAT signalling on the airways, I performed RNA-seq analysis of the tracheal cells expressing *hop.CA* in third instar larvae (LL3). This experimental setup revealed that the expression of hopscotch (including *hop.CA*) and Socs36E (one of the best-characterized STAT92E target genes) was up-regulated by 35 folds and 2.7 fold, respectively ($p<10^{-12}$). Among the 13767 genes with uniquely mapped ID, a total of 2004 genes were statistically significantly regulated (2001 genes with unique FlyBase ID), consisting of 1128 downregulated genes and 876 upregulated genes ($p<0.05$). Displayed is a diagram of a circular heatmap of 707 differentially transcribed genes concerning their statistical support ($p<0.01$ and fold changes>2) (Fig. 15A). Moreover, I analysed the changes in expression response to ectopic silencing of the pathway, namely by using the dominant negative isoform of the receptor domeless (*dome.DN*).

Venn diagram analysis revealed a statistically significant overlap in the cohorts of regulated genes between both interventions (Fisher's exact test, $p<0.0001$; Fig. 15B).

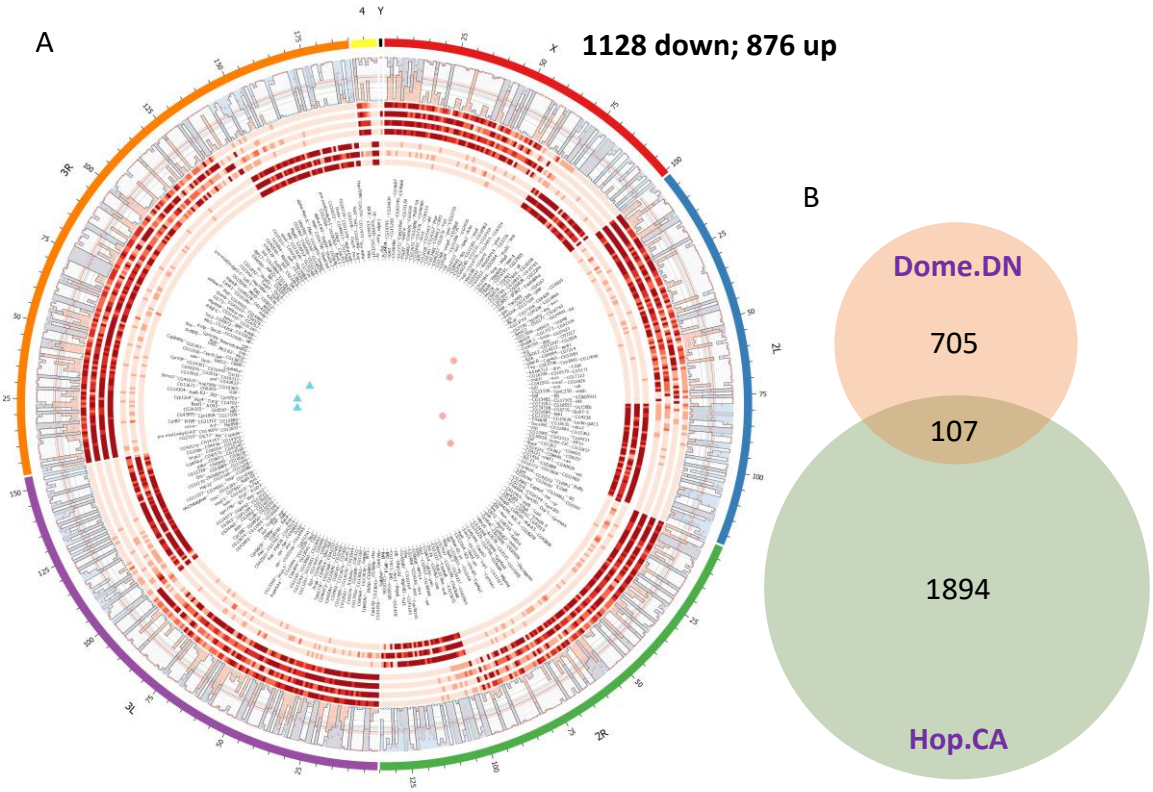

Fig. 15 Global changes provoked by *hop.CA* overexpression at the transcriptional level in the epithelium.
Altered gene expression levels in the trachea caused by 16 h persistent expression of *hop.CA*. In total, 2004 genes were regulated significantly (p<0.05), which 707 genes of (fold change>2, P<0.01) showed even higher levels of significance. (A) These 707 genes were used to visualize the differences of the transcriptional levels between *hop.CA* rich trachea and control trachea. From outside to inside, a histogram for expression mean values (red, control; blue, *hop.CA* group), a heatmap for controls, a heatmap for *hop.CA* expression, gene names, and PCA analysis, are shown separately. According to transcriptome analysis of the tracheal epithelium 1128 genes ($p<0.05$) were down-regulated, 876 genes ($p<0.05$) were up-regulated. The changes in the gene expression total value was not significant in the ectopic expression trachea compared to the controls. (B) The inhibition of the JAK/STAT signalling by ectopic expressing dome.DN for 18 hours affects the transcription of 774 genes, which 107 genes of were regulated by the expression of *hop.CA* as well (B).

To further understand its molecular mechanism in the thickening epithelium, I performed promotor scan studies and GO analyses. The group of genes showing the highest rates of induction supported by the lowest p-values were subjected to a promoterscan (Pscan) analysis. Putative direct JAK/STAT signalling pathway responsive genes were identified by this means (Table 1 and 2). Interestingly, genes with products involved in innate immunity were the largest family among these highly regulated genes that included 7 antimicrobial peptide (AMPs) genes (*IM1, IM2, IM4, IM14, CG5791, CG5778, Drs*). Except for *Drs*, all the other AMPs contain one or two CXXC regions. These CXXC-containing genes belong to a family of the Bomanins (Boms) whose expressions were highly induced after bacterial or fungal infection and their mature

peptides were tested abundant in the hemolymph of infected flies[169,170].

Table 1 Genes with highest rates of upregulation

Name	Max group mean	Fold change	FDR p-value
CG16772	11.85472435	135.4356918	0
hop	286.0640796	35.42957686	0
CG14570	42.20996514	35.3698493	0
CG14147	55.30940549	32.87679686	0
Hsp70Bb	161.511126	29.98530152	0
Ubx	200.4588187	23.51089416	0
pre-mod(mdg4)-I	1.124681971	18.66759173	2.22648E-06
IM14	11.45782606	15.13546529	3.80132E-07
IM4	26.42664387	14.97315552	1.74645E-12
CG14569	1576.880077	14.72575164	0
IM2	7.261319979	14.4714161	2.01792E-06
CG5791	1.786460103	13.80267454	2.90502E-05
CG9121	3.412245019	11.53962271	0
IM1	7.159415315	10.97306621	7.52122E-05
CG11413	35.69960698	10.63636792	3.44242E-07
CG16710	2.132413445	10.32026533	1.72352E-07
CG31960	267.2645814	10.04792875	0
CG16789	1.452007625	9.460811492	5.58576E-09
CG6034	6.915088882	8.468387575	4.7943E-11
Ace	2.056513226	8.187696842	0
CG13059	9.898481009	7.578675956	1.33893E-06
CG31809	8.642528741	7.388263435	0
CG7203	9.406607055	7.213889526	8.66989E-09
Vha14-2	2.510881225	7.050881817	2.31024E-07
wb	7.35456153	6.689915209	0
Drs	8166.473129	6.635790672	0
CG5778	3.202417196	6.607038471	0.000294835
CG3457	2.693960701	6.337465056	2.38755E-06
Lcp65Ad	9.932204556	5.792567795	2.58249E-08
lectin-22C	29.06148461	5.674130819	6.88538E-06
fuss	3.973734058	5.673577323	0
CG43333	2.390923691	5.632143859	1.48392E-09
CG18336	2.963052606	5.485479621	5.52167E-05
CG32563	3.062298877	5.352654098	0.000696584
FASN2	1.651227873	5.340581227	2.95545E-10
Cyp4d21	45.69613978	5.308508635	0
Obp57d	1.797549513	5.276761495	0.000102926
CG17560	2.313559171	5.218521032	0.000766701
CG5888	68.16302548	5.201444372	0

$p<1X10^{-4}$, fold changes>5, Max group mean>1, restricting the list to 39 genes**.**

Matrix ID	Matrix Name	P-value
MA0023.1	dl(var.2)	0.000443261
MA0022.1	dl	0.00407113
MA0532.1	Stat92E	0.00794732
MA0450.1	hkb	0.00811969
MA0197.2	nub	0.0154201
MA0242.1	Bgb::run	0.0371696
MA0204.1	Six4	0.0443521
MA0444.1	CG34031	0.0488169

Table 2 Enriched TF Binding Site Motifs in 41 high up-regulated genes.

133 TF profiles were used

3.1.1.7 An altered biological processing

Then I analysed all significantly regulated genes on the basis of KEGG and GO annotations. In this way, 6 terms in KEGG pathway analysis and 9 categories in GO analysis were enriched according to their predicted functions (Table 3 and Fig. 14).

Table 3 KEGG pathway analysis of the genes regulated by JAK/STAT signalling.

Term	# regulated gene	#REF	corrective p-value
Protein processing in endoplasmic reticulum	37	122	0.000196415
Metabolism of xenobiotics by cytochrome P450	21	62	0.005458041
Glutathione metabolism	20	62	0.006987233
Drug metabolism - cytochrome P450	20	62	0.006987233
Metabolic pathways	143	924	0.010283682
Fatty acid metabolism	14	42	0.033601606

One striking feature of the epithelium with chronically activated JAK/STAT signalling is an induced expression of genes involved in vesicle-mediated transport (Fig. 16). Based on the GO analysis, totally 32 genes are enriched assigned to vesicle-mediated transport and interestingly almost all these genes were up-regulated, except for one gene, namely *CG5946*. However, these genes seem not to be the direct JAK/STAT targets, considering that STAT92E binding is not enriched in these genes as revealed by PSCAN analysis.

Another interesting finding is the reduced transcriptional level of genes related to epicuticle development. 55 genes relevant to cuticle development were regulated, with 40 of them were down-regulated. Besides, muscle cell differentiation was significantly enriched and most corresponding genes were downregulated as well. In this study, cellular protein-containing complex assembly, RNA processing, translation, and detection of chemical stimuli were enriched significantly and the number of up-regulated genes was similar to that of the down-regulated ones.

Drosophila airways need to remodel and expand the tube size during larval growth. The physiological growth process is intimately associated with epithelial lumen morphogenesis and encompasses processes such as the addition of apical membrane by exocytosis occurring in tandem with the removal of luminal products by endocytosis[126,171]. Based on the GO and KEGG analysis several biological processes were found in response to or significantly affected by activation of JAK/STAT signalling. A schematic representation of the different biological process is superimposed on the scheme of an epithelial cell (Fig. 16B). One interesting result was the

observation that endocytosis and vesicle-mediated transport was impaired.

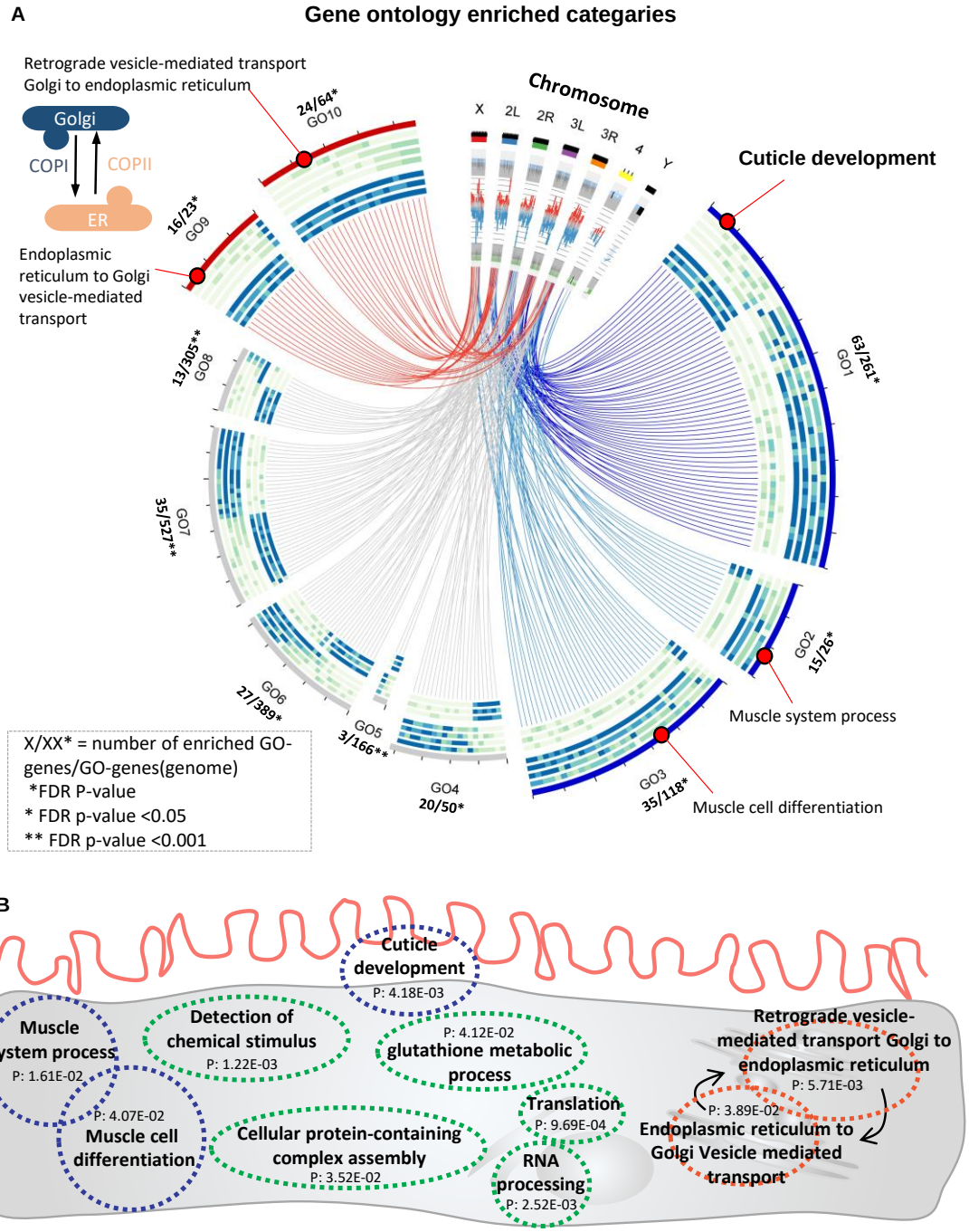

Fig. 16 Gene Ontology (GO) enrichment analysis of 2004 annotated differentially expressed genes induced by *hop.CA*.

(A) Gene ontology analysis showed 10 biological processes that were enriched in *hop.CA* overexpressing airways compared with matching controls. Most regulated genes in the GO1, GO2 and GO3 groups were down-regulated. Most regulated genes in the GO9 and GO10 groups were up-regulated. GO1, cuticle development; GO2, muscle system process; GO3, muscle cell differentiation; GO4, glutathione metabolic process; GO5, detection of chemical stimulus; GO6, cellular protein-containing complex assembly; GO7, RNA processing; GO8, translation; GO9, endoplasmic reticulum to Golgi vesicle-mediated transport; GO10, retrograde vesicle-mediated transport Golgi to endoplasmic reticulum. (B) Enriched biological processes were superimposed on a sketch depicting a tracheal epithelial cell, with the corresponding *p*-value. Blue indicates process where genes were mainly down-regulated; red indicates processes where genes were mainly up-regulated; green indicates processes, where genes were both down-regulated and up-regulated at similar extents. See also table S10 for annotation of genes involved in

each process. All processes shown displayed $p < 0.05$ (Fisher's exact test).

3.1.1.8 Induced JAK/STAT pathway impedes vesicle-mediate transport.

To further analyse this possible effects on the vesicle-mediated transport, I focused on two proteins on two peripheral membrane-binding proteins, namely on Coracle (Cora), a component of the septate junction, and Armadillo (Arm), a component of adherens junctions. Both of them exhibited an effective delivery via vesicles [172,173] (Fig. 17A). Immunofluorescent analysis of *hop.CA* expressing animals revealed the protein hoarding of both Arm and Cora in the cytoplasm, which is indicative for the dysfunctional endosomal transport (Fig. 17B-E). I also observed a stenosis phenotype with a narrowing of the tube. This is associated with epithelial cells expressing *hop.CA* at very high levels as indicated by the strong green fluorescence (Fig. 17F and Fig. 12). Strikingly, the phenotypes of narrowing lumen here are reminiscent of the same phenotype caused by mutants in either COPI or COPII complexes which are required for efficient protein secretion that consequently drives tube expansion[124,174].

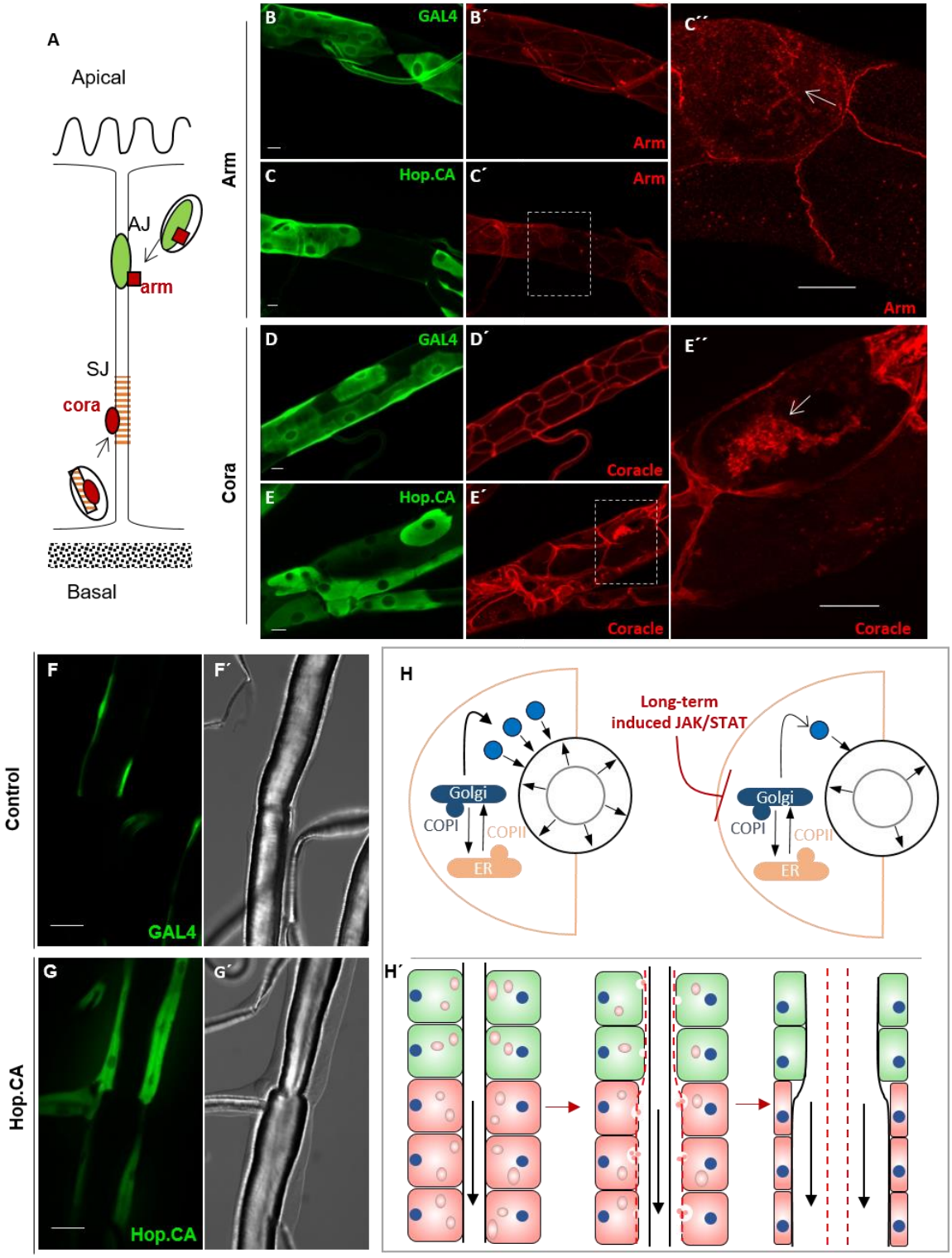

Fig. 17 Activation of airway epithelial JAK/STAT signalling affects vesicle-mediated transport of proteins.
(A-E) The localization of Cora and Arm in control and mutant epithelial cells. (A) shows the schematic orientation of Arm and Cora only at the contact zone between two airway epithelial cells. The trachea of *Vvl*-coin driver larvae (control; B and D) and *Vvl*-coin driver, *UAS-hop.CA* larvae (treatment; C and E) stained for GFP (green, Gal4 positive cells), Arm or Cora (red), respectively. n=30. (F-G) Micrographs of the trachea of *Vvl*-coin driver larvae (control; F) and *Vvl*-coin, *UAS-hop.CA* larvae (treatment; G). White are places where tracheal stenosis took place in the regions with cells expressing *hop.CA* to a high degree. Scale bar: 20um in A-E; 50um in F-G. (H) Schematic illustration of the thickening of the epithelium and narrowing of the tube. In the control epithelium, a secretory burst of luminal proteins drives the diametric expansion of the tubes and this process depends on vesicle-mediated transport. However, long-term induced JAK/STAT activation impedes vesicle-mediated transport, which

contributes to the increase in the cell volume and narrowing the tube size.

3.1.1.9 Induced JAK/STAT pathway affects the cuticle development

Another regulated biological process that was identified by using the transcriptome data is cuticle development. Interestingly, cuticle development in the larval trachea is secretion dependent and a chitin-rich structure, taenidia, is believed to allow the tubes to be flexible while simultaneously providing strength against collapse[171]. The *hop.CA* expressing animals showed an uneven chitin structure within the trachea in comparison with control tubes (Fig. 18 A-B). Chitin staining revealed that the highly organized structure of the chitinous intima (Fig. 18 C) lost its regularity almost completely in the *hop.CA* expressing animals. Using mosaic analysis, presumptive breakpoints could be introduced in the structured at those sites of the trachea, where clones expressed *hop.CA* (Fig. 18 D-F).

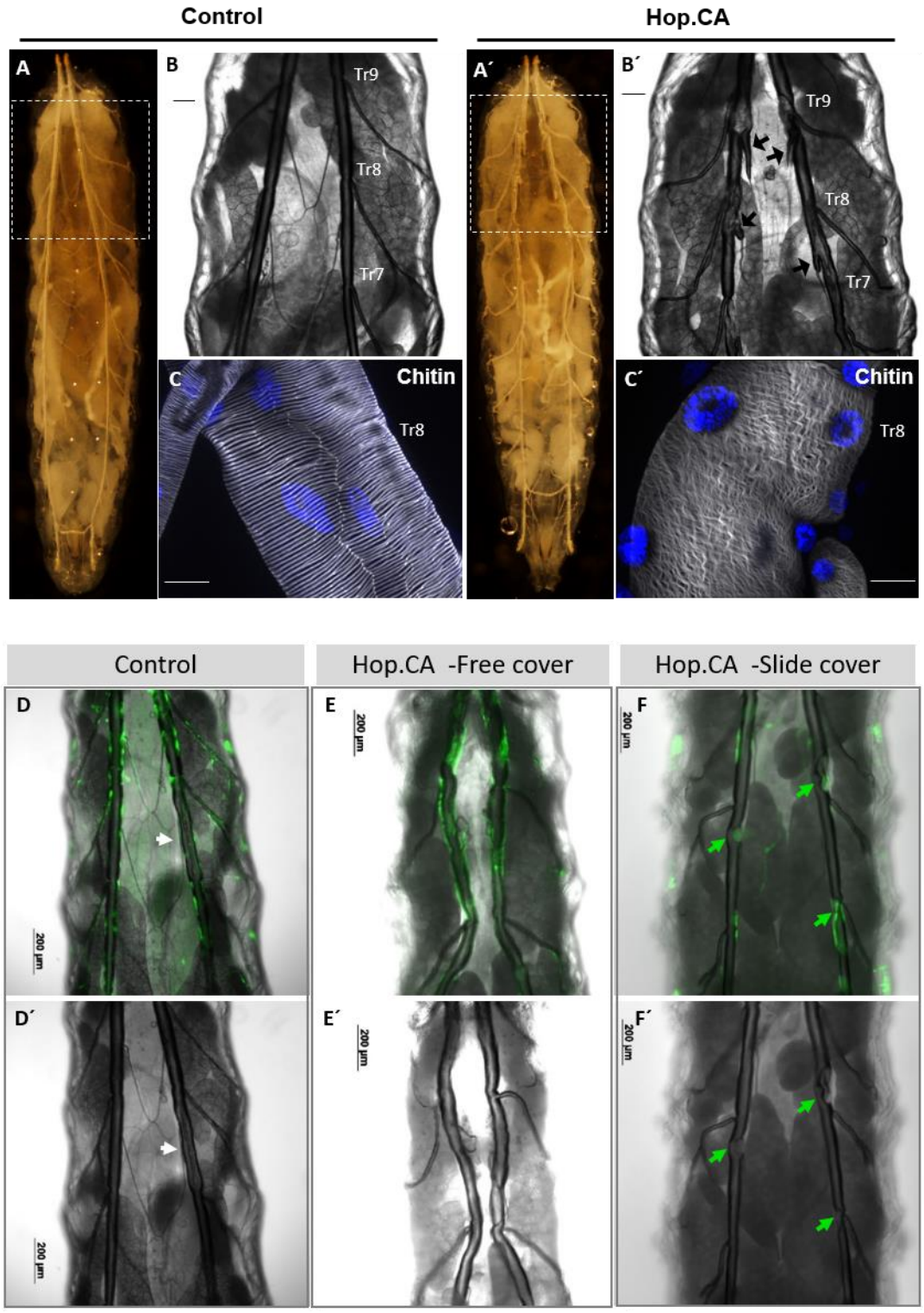

Fig. 18 Activation of JAK/STAT signalling in airway epithelial cells affects the development of the epicuticle.
(A-C) Activation of JAK/STAT signalling in airway epithelia observed in whole larvae by expressing *UAS-hop.CA* under the control of *btl*.ts driver. Controls (A-C) and induction of expression by shifting the temperature to 29°C causes the defects in the tracheal epicuticle (A'-C'). (A, A') Overview of the whole larvae showing the whole tracheal system. In (B, B') the region containing tr7-tr9 is shown). (C, C') Chitin staining of isolated airways (at the tr8 region). (D-F) Micrographs of the trachea of *vvl*-coin driver larvae under different conditions. In D, D' the control is shown, in E, E', the undisturbed larval of animals experiencing *hop.CA* expression are displayed. F, F' similar animals as in E, E', but the animals a covered with a slide, inducing a certain degree of compression. Scale bar: 50um in B; 20um in C; 200 um in D-F.

3.1.1.10 Mild expression of *hop.CA* reduces tracheal epithelial defects.

I found that the effects of inducing the JAK/STAT pathway on the epithelium were time-dependent. To know if the symptoms could also be seen if a milder expression of *hop.CA* is experienced, I additionally used another trachea-specific driver, namely *ppk4*(*nach*)-*Gal4*. *Nach-Gal4* line starts the *Gal4* expression from the late embryo stage and expresses strongly in the early L1, late L2 when the expression is even stronger than of the *btl-Gal4* driver but weakly in the other larval stages[175,176]. Microscopy of trachea showed that this mild expressing *hop.CA* in the trachea promoted epithelial thickness as well (Fig. 19A-B). However, compared to 4 days induction of the JAK/STAT pathway by *btl>hop.CA*, induction of the pathway driven for 4 days by *nach-Gal4>hop.CA* gave rise to a thinner but nevertheless thickened epithelium (Fig. 19D). On the other hand, mild driving upd3 in the trachea resulted in identical changes as observed in response to *btl-Gal4* induced processes (Fig 19C and 19E). Then I used the same driver to inhibit JAK/STAT signalling in the trachea by expressing *dome.DN*. The animals exhibited premature death in the larval stage and their trachea were always filled with the liquid (Fig. 19F).

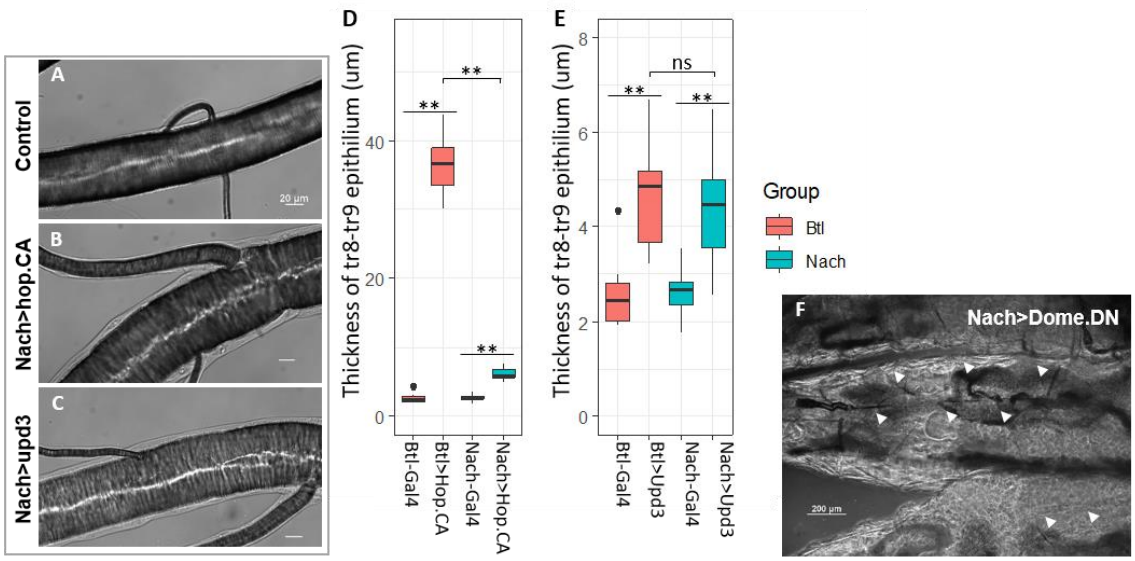

Fig. 19 Mild activation of epithelial JAK/STAT signalling mitigated the thickening phenotype.
(A-C) Micrographs of the tr8-tr9 regions of *nach-Gal4* larvae (control, A), *nach-Gal4*, *UAS-hop.CA* (treatment, B) and *nach-Gal4*, *UAS-upd3* larvae (treatment, C). (D-E) Quantification of the epithelial thickness of the tr8-tr9 region of those larvae whose JAK/STAT signalling were activated by expressing *UAS-hop.CA* or *UAS*-upd3 under the control of *nach-Gal4* and *btl-Gal4*. (F) Micrographs of *nach-Gal4*, *UAS*-Dome.DN larvae experiencing suppression of the JAK/STAT pathway make trachea translucent and filled with fluids (arrows); triangle indicate the tracheal position. Ns means not significant, * $p<0.05$, ** $p<0.01$ by Student's t test. Scale bar: 20 µm in A-C; 200 µm in F.

3.1.2 The investigation of the effects of deregulation of JAK/STAT signalling on the behavior of tracheal stem cells.

Studies in the cellular and molecular mechanisms driving tube morphogenesis in *Drosophila* and mammals have revealed common types of mechanisms in the tracheal formation and maturation and they also revealed the conserved role of key pathways in regulating the growth and elaboration of tubular networks[142,143]. Growth and patterning need to be tightly coordinated for normal development and any errors in these processes may lead to developmental defects and disease. The understanding of the mutant of the key pathways in the tube patterning, outgrowth, ramification and maturation is of clinical relevance, since many factors are evolutionarily conserved and may have similar functions in humans[143]. Previous studies have characterized the *Drosophila* spiracular branch (SB) tracheoblasts during morphogenesis of pupal tracheoles[144] and adult airway system[145]. SB tracheoblasts consist of multipotent progenitors and its lineage cells. They grow slowly before the L3 larval stage, while the SB tracheoblasts in the tr4 and tr5 would promote the speed of cell proliferation and specification in response to paracrine signal. SB tracheoblasts are an emerging and attractive model for studying signalling events that control stem cells homeostasis given that their growth and patterning are tightly coordinated by the similar critical molecular regulators as seen in human lungs, like BMP, Wnt and FGF signalling pathway[1,130,133,142].

Being aware of the importance of JAK/STAT signalling for cell proliferation and specification I investigated the pattern of activation of JAK/STAT signalling and examined the effects of deregulated JAK/STAT signalling on the growing SB tracheoblasts. Interestingly, activation of this signalling pathway is enhanced in the zone of cell proliferation and declined in the zone of cell specification, which embraces the same pattern with the abundance of cut[133]. Through manipulating the activity of JAK/STAT signalling in the trachea I determined the important role of JAK/STAT signalling for cell fate decision. Here, I found that the inhibition of JAK/STAT signalling contributes to cell apoptosis in the SB tracheoblast, On the other hand, activation of the signalling can inhibit cell proliferation and migration of SB tracheoblast by using the *btl-Gal4* driver. Through controlling the activity of JAK/STAT signalling in the tracheal tube and in SB tracheoblast separately I identified up-regulated JAK/STAT signalling in the cells surrounding the SB tracheoblasts, which function as the growth factor secretion cells during morphogenesis of SB tracheoblasts impacted the inhibition of its proliferation and migration. The expression of FGF rescued the defect of cell proliferation and migration, which provided

us with another evidence for the dysfunction of the growth factor secretion cells caused by upregulated JAK/STAT signalling. Additionally, the effects on the cell secretion could be validated by my previous transcriptome analysis that revealed an abnormal vesicle-mediated transport between the endoplasmic reticulum and Golgi and by the study of two membrane-binding proteins requiring vesicle-mediated transport. Thus, I found upregulated JAK/STAT signalling in the trachea can interfere with cellular crosstalk. However, considering that upregulated JAK/STAT signalling did not affect cell proliferation and migration if the targeted regions were restricted to the SB tracheoblast cells, I investigated effects of upregulated JAK/STAT signalling on two additional groups of progenitors in the DT of the tr2(DT2) and the DB of the tr4(DB4). Strikingly, induced JAK/STAT signalling has negative effects on cell proliferation. Although possessing an abundant expression of FGFR, the cells in the two regions cannot be rescued by the overexpression of FGF and in contrast, cell proliferation in the DB4 even was inhibited by the overexpression of FGF. Altogether, I could show the impacts of deregulated JAK/STAT signalling on the growth of progenitors and suggest that the *Drosophila* trachea could be used as a model to study the signalling events relevant to lung disease and development given that the conserved function of signalling events in the tube growth and genetic amiable.

3.1.2.1 The graded activity of JAK/STAT pathway in the SB tracheoblasts regulate proliferation and patterning.

To reveal the importance of JAK/STAT signalling pathway in the normal development of SB tracheoblasts I observed the activity of JAK/STAT signalling pathway in this region at late larval stages, when the SB tracheoblasts are growing, patterning and will form new tracheal branches during metamorphosis.

As an increased abundance of upd could be observed in the zone3 of SB tracheoblasts[133], in this project, I used STAT92E-reporter and ligand (1 kbs upstream enhance traps of *upd*, *upd2*, *upd3*)-*Gal4* driving the expression of lacZ.nls to monitor the activity of the pathway and examine the source of the ligand of this signalling pathway in the SB tracheoblasts. Microscopical analysis showed that *upd2* shows a by far higher expression in this region than *upd* and *upd3*. Compared to the expression of *upd2* in the trachea, *upd* is produced more in other tissues such as an imaginal disc (Fig. 8) and *upd3* is inducible by stressors such as cigarette smoke. *Upd2* is produced all around the trachea, especially it is enriched in the

proliferating parts, such as SB tracheoblasts, DT2 and DB4.

Here I refer to a previous study to divide the SB tracheoblasts into 4 zones[133]. Zone 1, with no detectable *upd2* expression and weak activity of the pathway; zone 2, with intermediate *upd2* amount and activity of the pathway; zone 3, with the highest abundance of *upd2* and activity of the pathway; and zone 4, with low abundance of *upd2* and moderate activity of JAK/STAT (Fig. 20A and B). In the SB tracheoblasts, *upd2* exhibited a graded abundance in the mitosis region and the activation of JAK/STAT signalling pathway coincided with the *upd2* expressing regions.

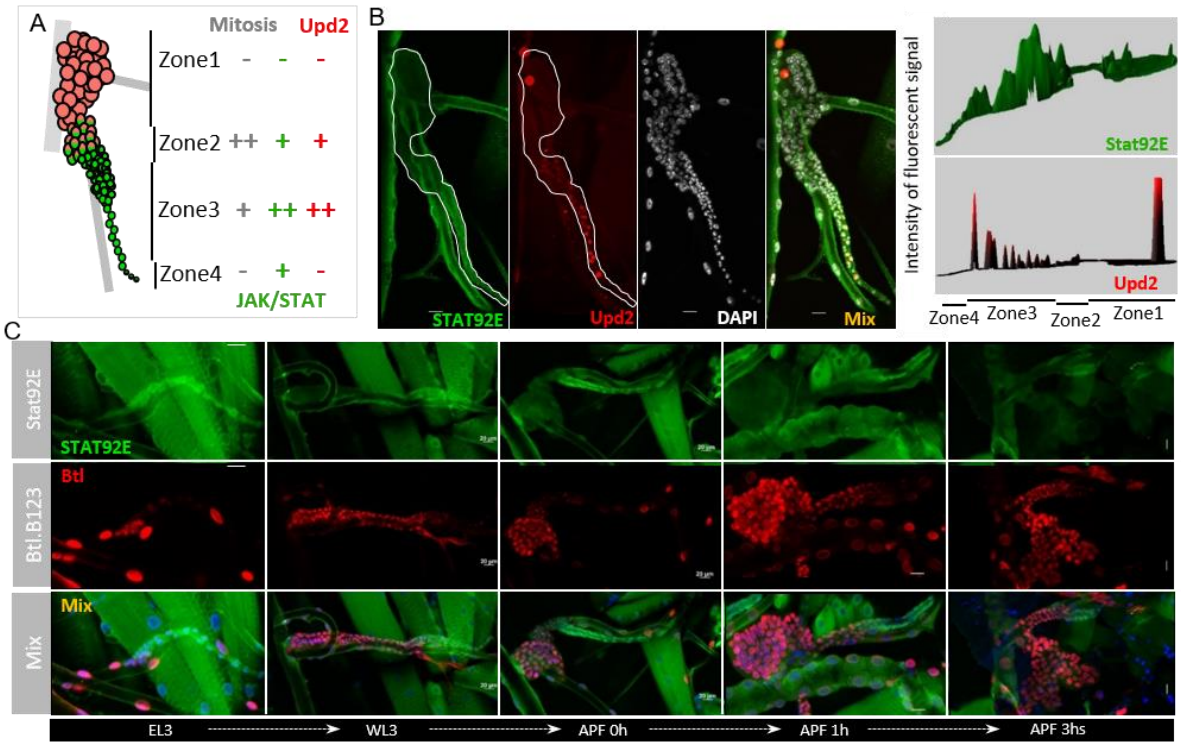

Fig. 20 Active STAT92E signalling was observed in the proliferating region of SB tracheoblasts.
(A) Schematic of the spatial activation of JAK/STAT signalling pathway in the four zones of SB cells (Tr4 and Tr5) during morphogenesis and their corresponding mitotic activity. The solid grey areas lacking cells (circles) represent gas-transporting tracheal tubes. (B) Late L3 larvae with transgenes of 10xSTAT92E-GFP and *upd2-lacZ* stained for active STAT92E(green), ß-galactosidase (red), and 4',6-diamidino-2-phenylindole (DAPI) (blue). White line outlines the entire SB which intensity was analysed by the surface plot. right: surface plot of the intensity of the fluorescent signal driven by active STAT92E and upd2 along the length of the SB. (C) the time-lapse examination for the activity of JAK/STAT pathway from early L3 stage(EL3) to prepupa formed(APF) 3hours. STAT92E were activated strongly in the posterior region during morphogenesis compared with the other regions in the SB tracheoblasts.

In the previous part, I showed the activity of JAK/STAT pathway is enriched in the mitosis regions of SB tracheoblasts in the L3 stage, but it is weak in the specified tracheal cells. Next, I performed a time-lapse analysis for the activity of JAK/STAT signalling from early L3 stage (EL3) to after pupae formation (APF) 3hours. In the EL3, when SB tracheoblasts cells are going to

initiate growth, there is a higher rate of JAK/STAT pathway activated cells in the SB tracheoblasts compared with the following time. At the following time points: wandering L3 2-3hs(WL3), APF0h, APF1h and APF3h, I observed that the differentiated cells (labelled by *btl>lacZ.nls* reporter) moved out from the primordium niche and climbed on the DT while these cells in zone 3 where JAK/STAT signalling pathway is strongly activated still stayed in the TC region. In this way, I found that the JAK/STAT signalling kept strong activity in the mitotic regions, whereas losing the signal after their specification (Fig. 20C).

3.1.2.2 The activity of JAK/STAT signalling in the trachea is critical for the SB tracheoblasts' survival, proliferation and differentiation.

Compounds that could inhibit the JAK/STAT pathway were thought to induce apoptosis in tumorigenesis *in vivo* and *in vitro*[177,178]. Previous studies in *Drosophila* showed that the inhibition of JAK/STAT pathway results in an increase of apoptotic cells and an increase in stalk cell loss in the *Drosophila* egg chamber[179]. In this study, I manipulated the JAK/STAT signalling pathway by driving *dome.DN* expression. Firstly, I used *btl-Gal4*, *tub-Gal80*^{ts} to knock down the signalling pathway in the zone1, zone2 of the primordium and the trachea surrounding the primordium starting from the L2 stage. Strikingly, compared to the primordium in the control, the primordium in the manipulated trachea have a smaller cell cord. Microscopy of the primordium revealed a deduced proliferation and a smaller specificated cell cluster (zone1) (Fig. 21A and B). However, in this study, I did not observe an increase in apoptotic cells in the primordium based on the immunofluorescent assay. To really understand if the cell-autonomous manipulation of JAK/STAT signalling induces cell apoptosis in the trachea, I performed the mosaic analysis by using *vvl*-coin^{ts}. *Vvl*-coin^{ts} consists of *vvl*-FLP[130], CoinFLP-*Gal4*[130] and *tub-Gal80*^{ts} which can drive gene expression massively and ectopically in the trachea. In this way, I found that knock-down of the JAK/STAT signalling pathway for one or two days led to a gradual loss of cell shape in the somatic cells, which implied death of the affected cells. Based on the immunofluorescent assay I confirmed that cell apoptosis would occur in the SB tracheoblasts as well when the signalling was inhibited (Fig. 7 and Fig. 21C).

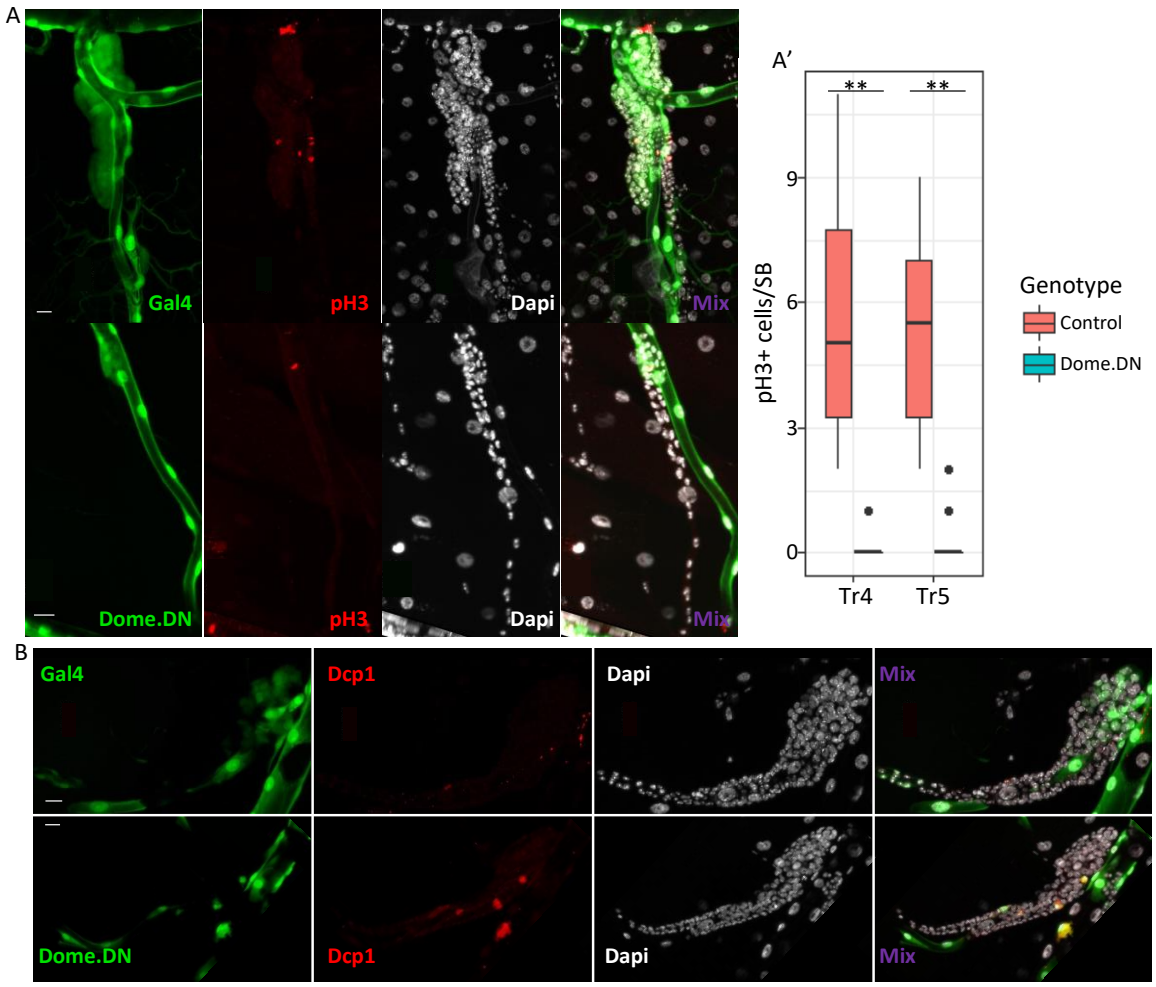

Fig. 21 Inhibition of JAK/STAT signalling induced apoptosis in the SB cells.
(A)*Btl-Gal4*, *UAS-GFP*; *tub-Gal80*^{ts} animals and *btl-Gal4*, *UAS-GFP*, *UAS-Dome.DN*; *tub-Gal80ts* animals reared at 18°C before L2 stage and then transferred to 29°C stained for GFP (green, *Gal4* positive clones), pH3 (red), and DAPI(white) in the wandering L3 stage. (A') The number of mitotic cells in SBs of the trachea without *UAS-dome.DN* and with *UAS-dome.DN* showed a decline of cell proliferation in the *dome.DN* rich trachea. (B) The trachea of *vvl*-coin^{ts}, *UAS-dome.DN* animals stained for GFP (green, *Gal4* positive clones), Dcp1 (red), and DAPI (white) demonstrated that inhibition of JAK/STAT signalling contributes to cell apoptosis in the SB cells. The cells that were expressing of *Dome.DN* can be stained by Dcp-1, a cell apoptotic marker. And no cluster lineaged from *dome.DN* positive progenitors. **p<0.01 by Student's t test.

As an increase in the activity of JAK/STAT signalling has always been found in the proliferating tissue, enhanced JAK/STAT signalling is thought to be a cause of normal proliferation and even a cause of tumorigenesis. To know if upregulated JAK/STAT signalling alone would initiate cell proliferation in the SB cells I drove *hop.CA* expression by *btl-Gal4*, *tub-Gal80*^{ts} driver. Interestingly, contrary to my expectation, upregulating JAK/STAT signalling did not promote cell proliferation in the SB tracheoblasts or anywhere else. In the primordium, upregulating JAK/STAT signalling did not induce cell proliferation but inhibited cell mitosis (Fig. 22A). And

here I am able to show that promoted JAK/STAT signalling inhibits the specification and migration of SB tracheoblasts where cells remained a small size and didn't move out from the niche on the basis of the time-lapse tracing for SB cells from WL3 to APF 3h stage (Fig. 22B and C).

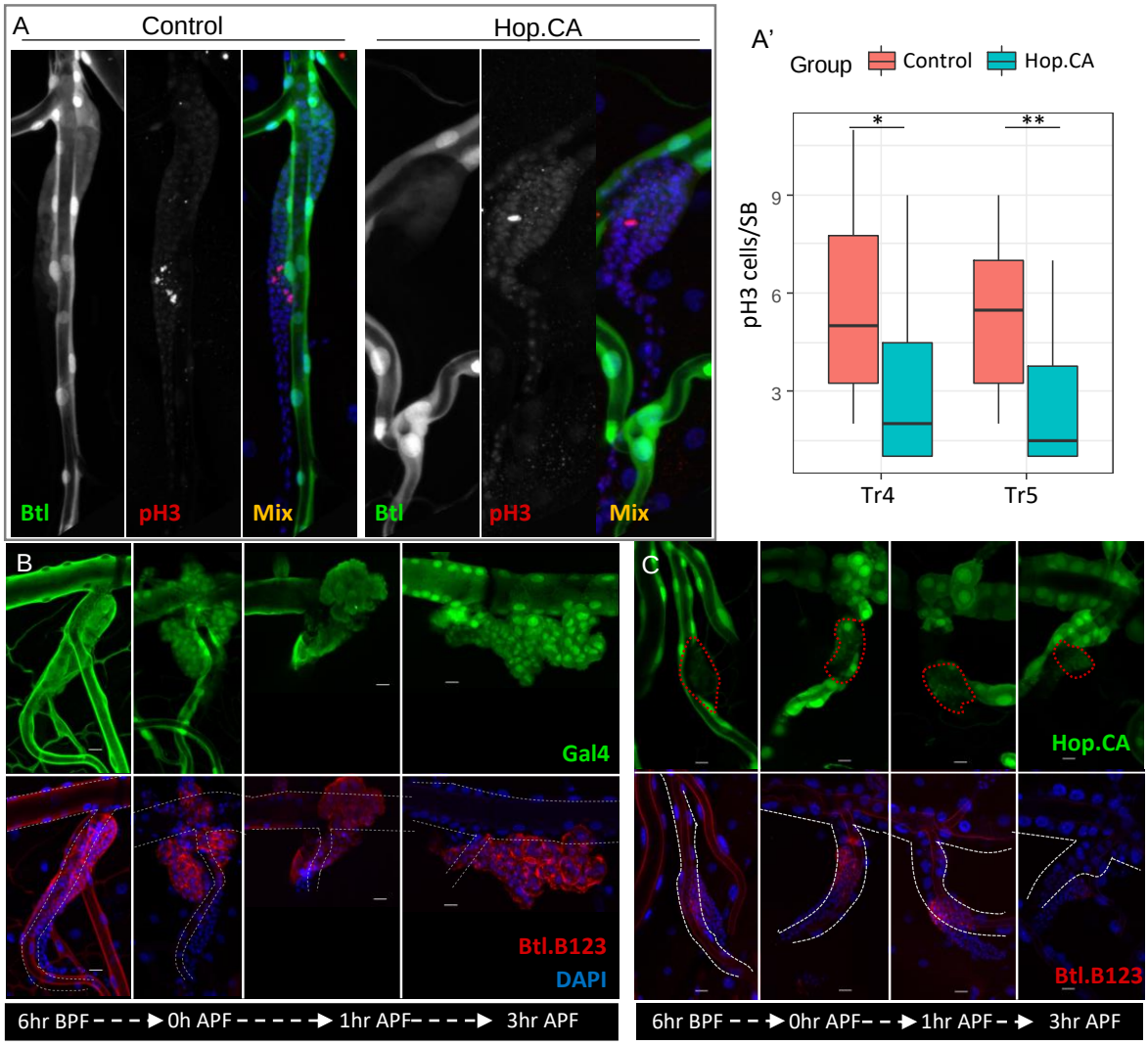

Fig. 22 Upregulating JAK/STAT signalling in the trachea can inhibit cell proliferation and migration of SB tracheoblasts.
(A)*Btl-Gal4*, *UAS-GFP*; *tub-Gal80*^{ts} animals and *btl-Gal4*, *UAS*-GFP, *UAS-hop.CA*; *tub-Gal80*^{ts} animals reared at 18°C before reaching the L2 stage and then they were transferred to 29°C , stained for GFP (green, *Gal4* positive clones), pH3 (red), and DAPI(white) in the wandering L3 stage. (A') The number of mitotic cells in SBs of control trachea without *UAS-hop.CA* and *hop.CA* rich trachea with *UAS-hop.CA* revealed a decline of cell proliferation. (B and C) Fluorescence Micrographs of tr5 SB of *btl-Gal4>UAS-GFP*; *btl*.B123-*RFP-moe* larvae and *btl-Gal4*, *UAS-GFP*, *UAS-hop.CA*; *btl*.B123-*RFP-moe* larvae of the indicated ages. Fluorescence micrographs show moving SB cells (red), targeted cells (green), and nuclei (4',6-diamidino-2-phenylindole, blue). SB cells moved onto the DT in the control during morphogenesis(B), however, these in the *hop.CA* expressing trachea did not(C). * P<0.05, ** P<0.01 by Student's t test.

I illustrated the inhibition of cell proliferation and migration caused by up-regulated JAK/STAT in the (Fig. 23A). To confirm the negative effects of promoted JAK/STAT signalling in the cell

proliferation I drove *upd3* expression by *btl-Gal4* again. In the same way, I got the same phenotype in the primordium when I promoted JAK/STAT signalling by driving the expression of *upd3* instead of *hop.CA* (Fig. 23B).

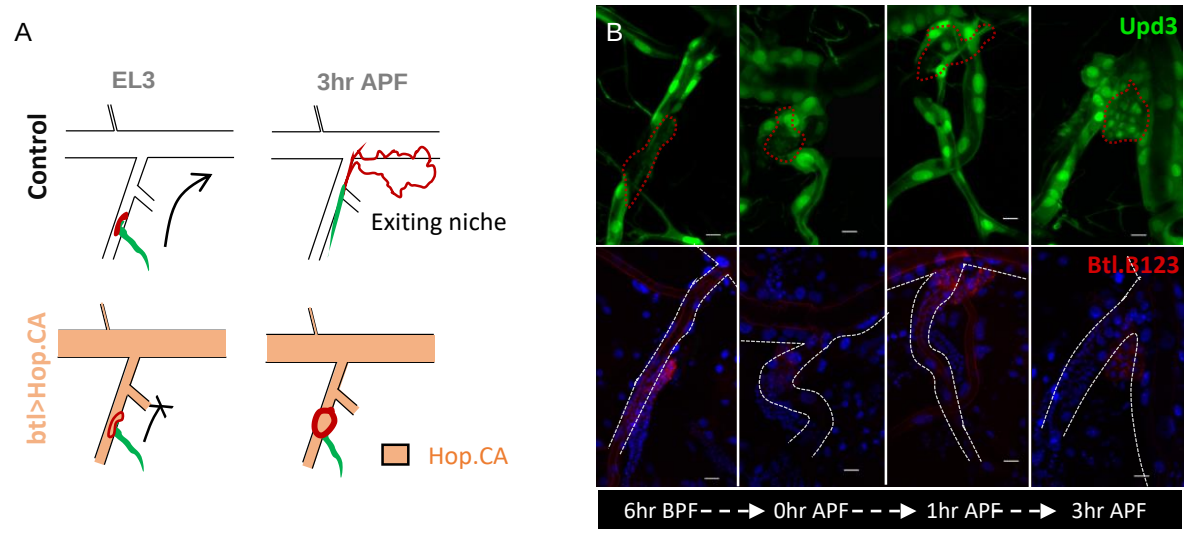

Fig. 23 Upregulating JAK/STAT signalling by driving the expression of *upd3* can inhibit cell proliferation and migration of SB tracheoblasts as well.
(A) Illustration of the inhibition of cell proliferation and migration caused by expression of *hop.CA*. (B) Fluorescence Micrographs of tr5 of *btl-Gal4*, *UAS*-GFP, *UAS*-upd3; *btl*.B123-RFP-moe showed a similar pattern of the location and size of moving SB cells.

3.1.2.3 The cell migration and proliferation could be FGF/FGFR signalling related.

The inhibition of the growth of SB tracheoblasts by activated JAK/STAT signalling may be caused by its influence on the FGF/FGFR (gene *bnl* and *btl* separately) or/and the WNT pathway, which was shown to play a key role in cell migration and proliferation[130,144]. Although, most components in the WNT signalling pathway are not regulated by the expression of *hop.CA*. Quantification of the intensity of RFP which is under the control of the *btl*.B123 upstream fragment[180,181] indicated lower transcriptional levels of *btl* compared to the control (Fig 22 and Fig. 24A). The previous study on the larval wing imaginal-disc revealed the feedback regulation in the FGF/FGFR pathway guided tissue migration, which showed that FGF elicits the positive feedback on the production of PntP1 (gene *pnt*) and FGFR in tracheal cells[182]. Then, I compared the transcriptional level of *pnt, btl, bnl* and *stump* of control trachea with that of *btl>hop.CA* trachea and found all these genes in a lower level in the *btl>hop.CA* trachea (Fig. 24B). This indicates that the decrease in the FGF/FGFR signalling could be the main reason for the growth of SB tracheoblasts.

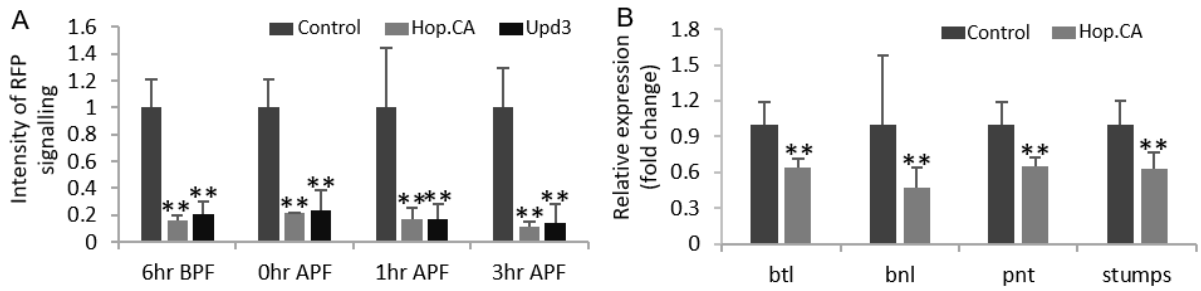

Fig. 24 FGF/FGFR signalling related component were down-regulated when *hop.CA* was expressing.
(A) Quantification of RFP intensity in the tr5 SB tracheolasts of the control animals (*btl-Gal4*, *UAS-GFP*, *btl*.B123-*RFP.moe; tub-Gal80^{ts}* larva) and tracheal mutant animals (*btl-Gal4*, *UAS-GFP*, *UAS-hop.CA* or *upd3, btl.*B123-*RFP-moe; tub-Gal80^{ts}* larva) indicated a deduced expression of FGFR during morphogenesis. (B) Transcriptome analysis of the *hop.CA* rich trachea showed a lower transcriptional level of genes in response to activation of FGF/FGFR pathway.

3.1.2.4 Activation of JAK/STAT signalling affects FGF secreting cells.

In previous studies, I used the btl-Gal4 as a Gal4 line to drive gene expression, which can affect both SB tracheoblasts (FGF receptor positive cells) and tracheal tube (FGF positive cells). So this inhibition of the activity of the FGF/FGFR signalling is possible due to a decrease in the component abundance in FGFR positive cells or a decline in the secretion of FGF. To find out the source of the effects, firstly I drove the expression of *hop.CA* only in the SB tracheoblasts zone 1 and 2 by the *btl*.B123, *tub-Gal80^{ts}* driver. Interestingly, compared to the control, mutant SB tracheoblasts cells in the zone1 and zone2 exhibit a close speed of climbing from LL3 to APF 3hs (Fig. 25A-B). This observation excluded the possibility that promoted JAK/STAT signalling impeded the growth of SB tracheoblasts mainly via the influence in the SB tracheoblasts. Then I drove the expression of *hop.CA* ectopically in the tracheal SB cells by *vvl*-coin that was used before. The results were consistent with the previous presumption, the SB cells that were expressing *hop.CA* proliferated and migrated along tracheal DT (Fig. 25C-D).

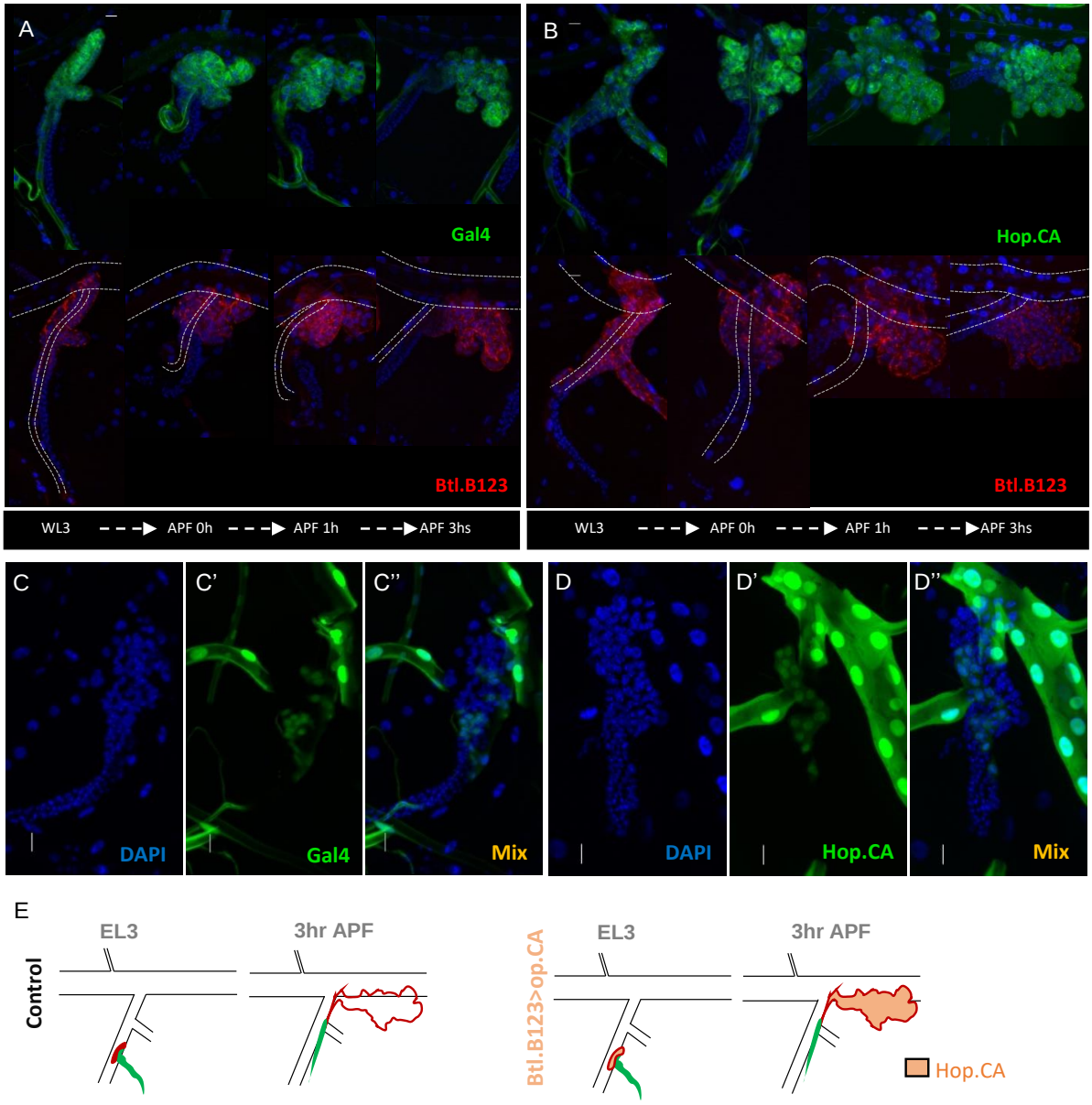

Fig. 25 The inhibition of SB development is not on the SB tracheoblast.
(A-B) Fluorescence micrographs and schematics of Tr5 of *btl*.B123-*Gal4*, *UAS*-GFP; *btl*.B123-RFP-moe larvae and *btl*.B123-*Gal4*, *UAS*-GFP, *UAS-hop.CA*; *btl*.B123-RFP-moe larvae of the indicated ages stained to show moving SB cells (RFP, red), larval tracheal cells (GFP, green), and nuclei (DAPI, blue). The expression of *hop.CA* in the SB cells(B) moved out from the SB niche and had the same speed and size as the control SB cells(A). (C-D) Ectopic analysis of the impacts of the expression of *hop.CA* on the cell migration and proliferation on the SB cells by using *vvl*-coin driver driving *hop.CA* expression. Affected clones in the SB tracheoblast showed normal proliferation and migration. n=30. Figure (E) illustrated that up-regulated JAK/STAT signalling in the SB cells specifically did not cause slower SB development compared to the control.

Thus the impacts should be on the ligand secreting cells. To confirm this assumption I re-observed *hop.CA* mosaic expressing trachea via the *vvl*-coin driver, which can drive the gene expression ectopically not only in the SB tracheoblasts but also in the tracheal tube cells. Interestingly, in WL3 animals, when SB progenitors are observed along the TC branches in the control, SB tracheoblasts cells did not migrate on the *hop.CA* rich cells and the migration could

be stopped by the sites expressing high levels of *hop.CA* rich cells (Fig. 26A-C). This observation proved the previous assumption that the effects of upregulated JAK/STAT signalling on the cell migration derived from the interference with FGF releasing cells. Indeed, as a switch of SB tracheoblast development, FGF abundance plays a key role in the SB tracheoblast proliferation and migration[130] (Fig. 26D-E). To confirm the FGF release to be the leading cause of the inactive SB tracheoblasts I drove the expression of a *UAS-bnl* transgene in the mutant clones, which were expressing *hop.CA*. As a result, progenitors in the SB tracheoblasts climbed on the affected clones and showed an overproliferation (Fig. 26F).

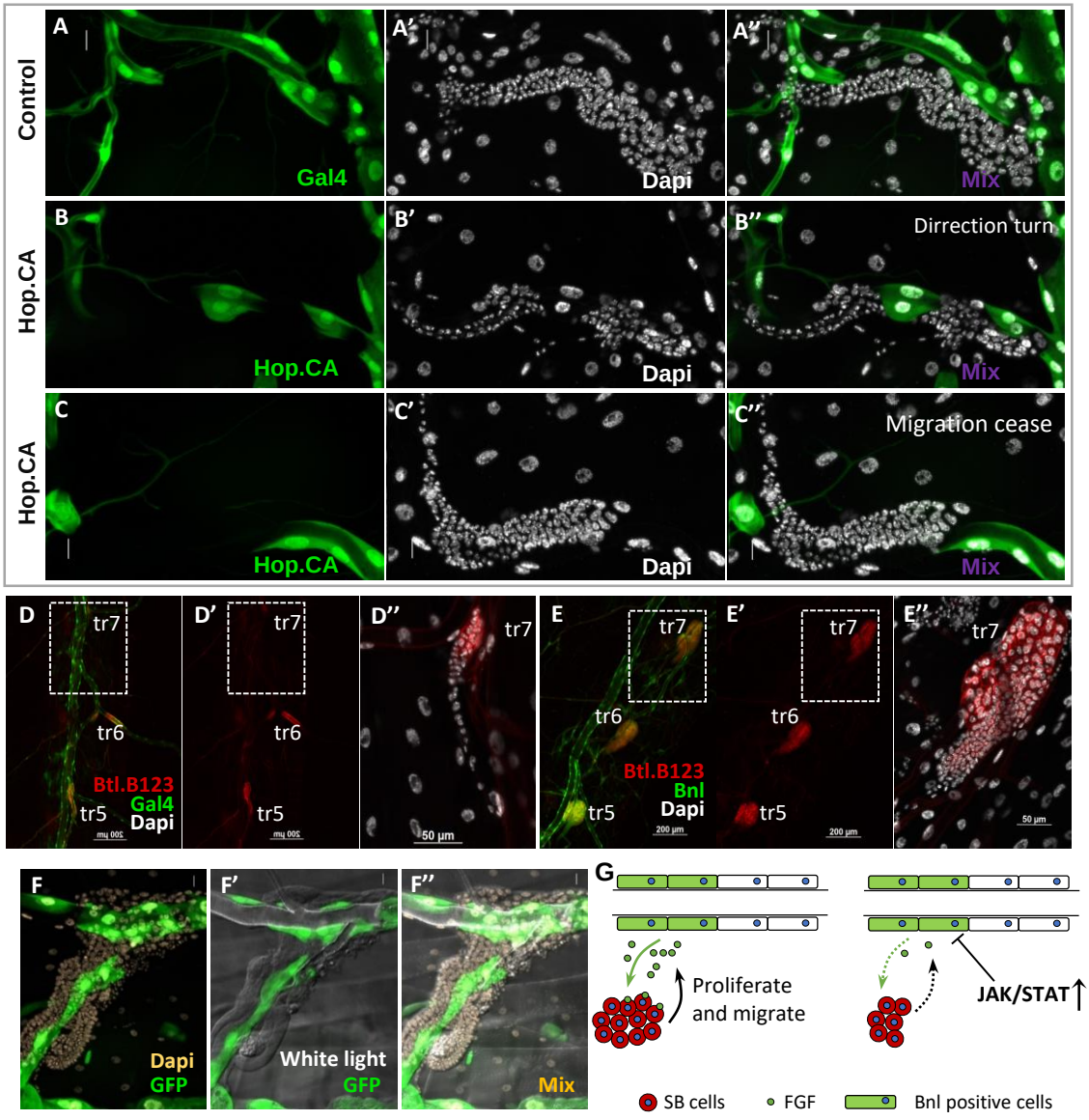

Fig. 26 Enhancing JAK/STAT signalling inhibits bnl secretion.
(A-C) Ectopic analysis of the effects of the expression of *hop.CA* on the developing SB cells by using *vvl*-coin driver driving *UAS-hop.CA* expression. (A) SB cells climbing on the gas-filled trachea straightly. SB cells did not move onto these affected clones on the gas-filled trachea (B). (C) SB would stop their growth at the *hop.CA* positive sites.n=30. (D-E) *Btl*.B123-*RFP-moe, btl-Gal4, UAS-GFP; UAS-bnl, tub-Gal80*^{ts} and *Btl*.B123-*RFP-moe*, *btl-Gal4*, *UAS*-GFP; *tub-Gal80*^{ts} reared at 18°C before the L2 stage and then they were transferred to 29°C. GFP (green, *Gal4* positive

clones), RFP (red, moving SB cells), and DAPI (white). Compared to the animals without the transgene of *UAS*-bnl (D), animals that expressed *bnl* specifically in the trachea with the *btl-Gal4* driver (E) induced cell proliferation and migration in the tr7 where SB cells are relative quiscent compared to tr5 SB tracheoblast. (F) Increasing *bnl* expression in the *hop.CA* rich clones by using additional *UAS*-bnl transgene rescues the phenotype that SB cells cannot migrate on *hop.CA* rich clones. (G) A model demonstrates that promoting JAK/STAT signalling in the trachea contributes to the decline of cell proliferation and migration via a decrease in the secretion of FGF.

3.1.2.5 The decreased release of FGF could be caused by a lower efficiency of vesicle-mediated transport.

The decreased release of ligands is reminiscent of our transcriptomes analysis that regulated genes was highly enriched in vesicle-mediated transport. And apart from CG5946, all the other regulated genes were induced. The upregulated vesicle-mediated transport indicated an increase in the requirement for the secretion, considering I induced the expression of *hop.CA* for a long time (16hs) (Fig. 16). Further studies showed the vesicle-mediated transport at a lower efficiency using localizing Coracle, a core member of the septate junctions (Fig. 17).

3.1.2.6 Upregulating JAK/STAT signalling pathway impedes cell proliferation in the tracheal stem cells.

The JAK/STAT signalling pathway plays a positive role in cell proliferation as shown in previous observation in mammals and *Drosophila* and here I also found a high abundance of active STAT92E in the tracheal mitotic sites. *Btl-Gal4* driver can drive gene expression in the tracheal tube and parts of SB regions, by which I understand the effects of upregulating JAK/STAT on cell secretion. However, I do not know which effects act on the zone 3 of SB tracheoblast that possess a strong JAK/STAT signal and belong to progenitors. Then I upregulated the JAK/STAT signalling pathway in the zone 3 of SB tracheoblasts (Fig. 27A). As a result, promoted JAK/STAT signalling in this region did contribute to a change in cell proliferation (Fig. 27B).

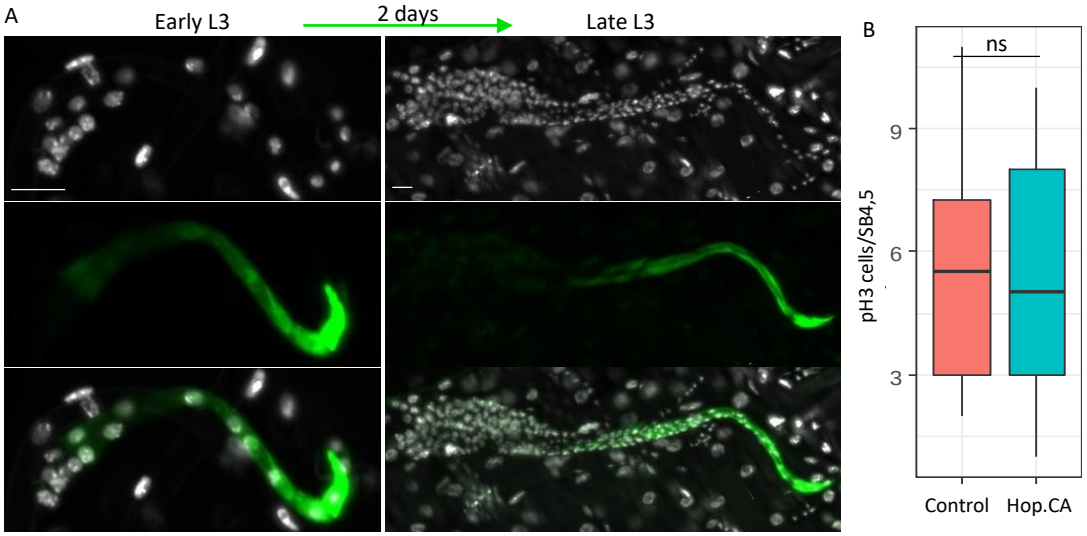

Fig. 27 Upregulating JAK/STAT signalling pathway in the mitotic region did not inhibit cell proliferation.
(A) Fluorescence micrographs of tr5 SB tracheoblasts of *fz3-Gal4*, *UAS*-GFP larvae and *UAS-hop.CA*; *fz3-Gal4*, *UAS*-GFP larvae at early L3 stage and late L3 stage stained for GFP(*Gal4* positive cells), DAPI. (B) The number of mitotic cells in Tr5 SB tracheoblast of *fz3-Gal4*, *UAS*-GFP larvae and *UAS-hop.CA* ;*fz3-Gal4*, *UAS*-GFP. Scale bar: 20um. ns means no significant by Student's t test.

To determine the possibility that upregulated JAK/STAT signalling has a positive effect on cell proliferation in the trachea I examined its effects on two additional groups of progenitors, DT2 and DB4 using the same driver (*btl-Gal4* and *vvl*-coin driver). Interestingly, upregulating JAK/STAT signalling had negative effects on cell proliferation in both areas. In this study, *btl* driving *hop.CA* led to a fewer total number of cells and a fewer average number of $pH3^+$ (pH3, a marker for cells undergoing mitosis) cells in the two distinct regions (Fig. 28A-B and 29A-B). Mosaic analysis confirmed the inhibition on cell proliferation (Fig. 28C and Fig. 29C). The use of *btl*.B123-*RFP.moe* reporter detected a rich expression of FGFR in the two progenitor clusters as well and the proliferation of the progenitors were induced by *btl>bnl* in the DT2 (Fig. 28D-F). Then I presumed that the inhibition on cell proliferation was attributed to the secretion of FGF. Thus, I tried to rescue the inhibition of cell proliferation in the DT2 by *vvl*-coin driving bnl in the mutant clones. As a result, inducing FGF expression in DT2 failed to rescue the inhibition caused by upregulating JAK/STAT signalling (Fig. 25G). On the other hand, the expression of FGF alone inhibited cell proliferation of progenitors in DB (Fig. 29D-E).

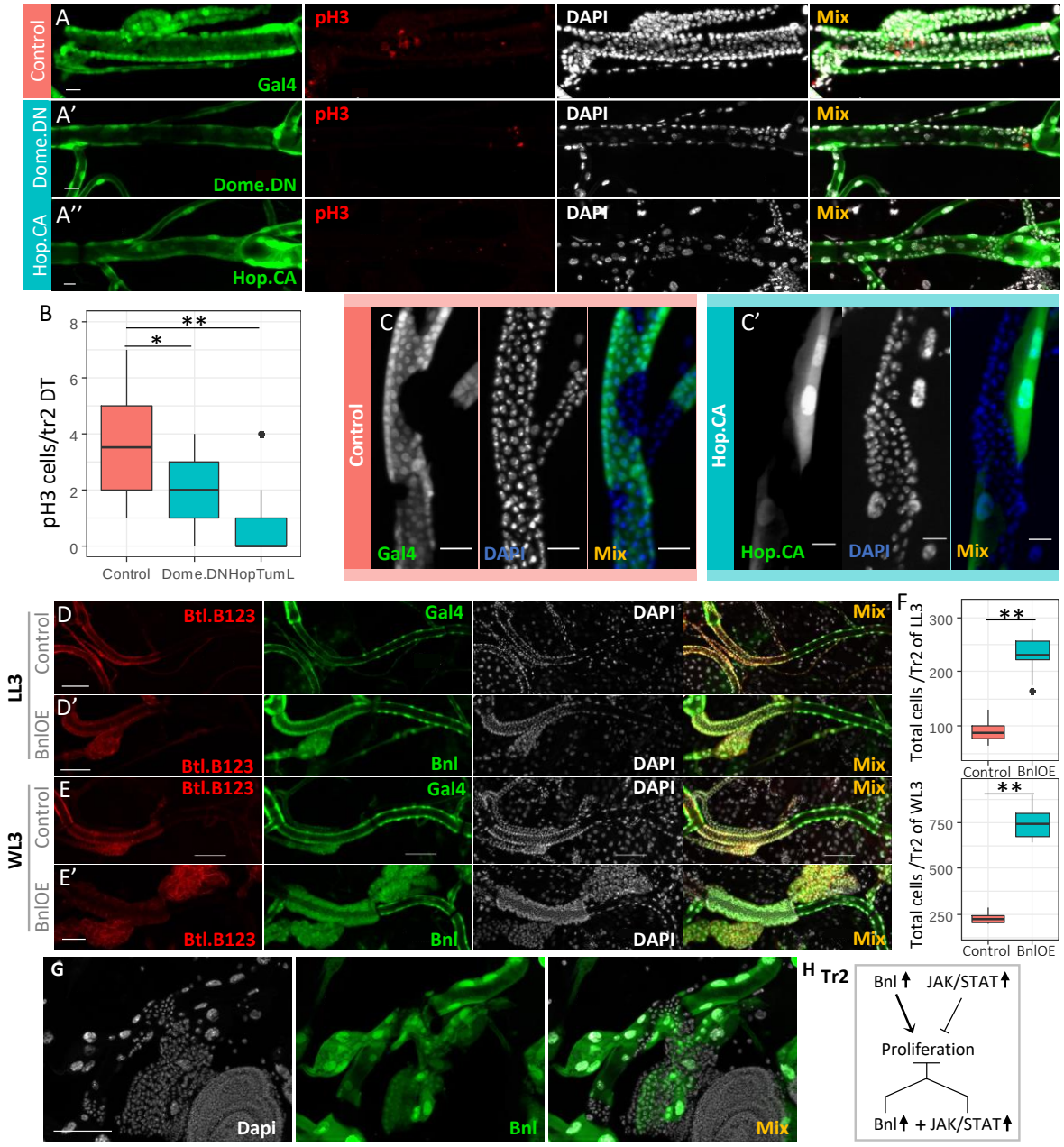

Fig. 28 Deregulated JAK/STAT signalling pathway inhibits the cell proliferation of progenitors in the DT2 region. (A)*Btl-Gal4*, *UAS*-GFP; *tub-Gal80*^{ts} animals and *btl-Gal4*, *UAS-GFP*, *UAS-hop.CA*(or *UAS-dome.DN*); *tub-Gal80*^{ts} animals reared at 18°C before the L2 stage and were then transferred to 29°C, stained for GFP (green, *Gal4* positive clones), pH3 (red), and DAPI (white) in the wandering L3 stage. (B) The number of mitotic cells in DT2 of control trachea without *UAS-hop.CA* nor *UAS*-dome.DN and of the affected trachea with *UAS-hop.CA* or *UAS-dome.DN* showed a decline in cell proliferation in the affected trachea. (C) Ectopic analysis of the effects of the expression of *hop.CA* on cell proliferation in the DT2 by using *vvl*-coin driver. It showed that a cease in cell proliferation in the affected clones in the DT2. n=30. (D-F) *Btl-Gal4*, *UAS-GFP*; *btl*.B123-*RFP-moe*, *tub-Gal80*^{ts} animals and *btl-Gal4*, *UAS-GFP, UAS-bnl*; *btl*.B123-*RFP-moe, tub-Gal80*^{ts} animals reared at 18°C before L2 stage and then transferred to 29°C stained for GFP (green, *Gal4* positive clones), *btl* expressing cells (red), and DAPI(white) in the late L3 stage and wandering L3 stage. The number of the cells in DT2 of control trachea without *UAS-bnl* and mutant trachea with *UAS-bnl* showed cell proliferation is inducible for the FGF (F). (G) Ectopically expressing *hop.CA* together with FGF in the DT2 with *vvl*-coin driver showed that the mutant progenitors can not divide as well. Mutant clones were always large cells and no mutant cell cluster formed. Scale bar 20um in A-C; 100um in E-H. * P<0.05, ** P<0.01 by Student's t test.

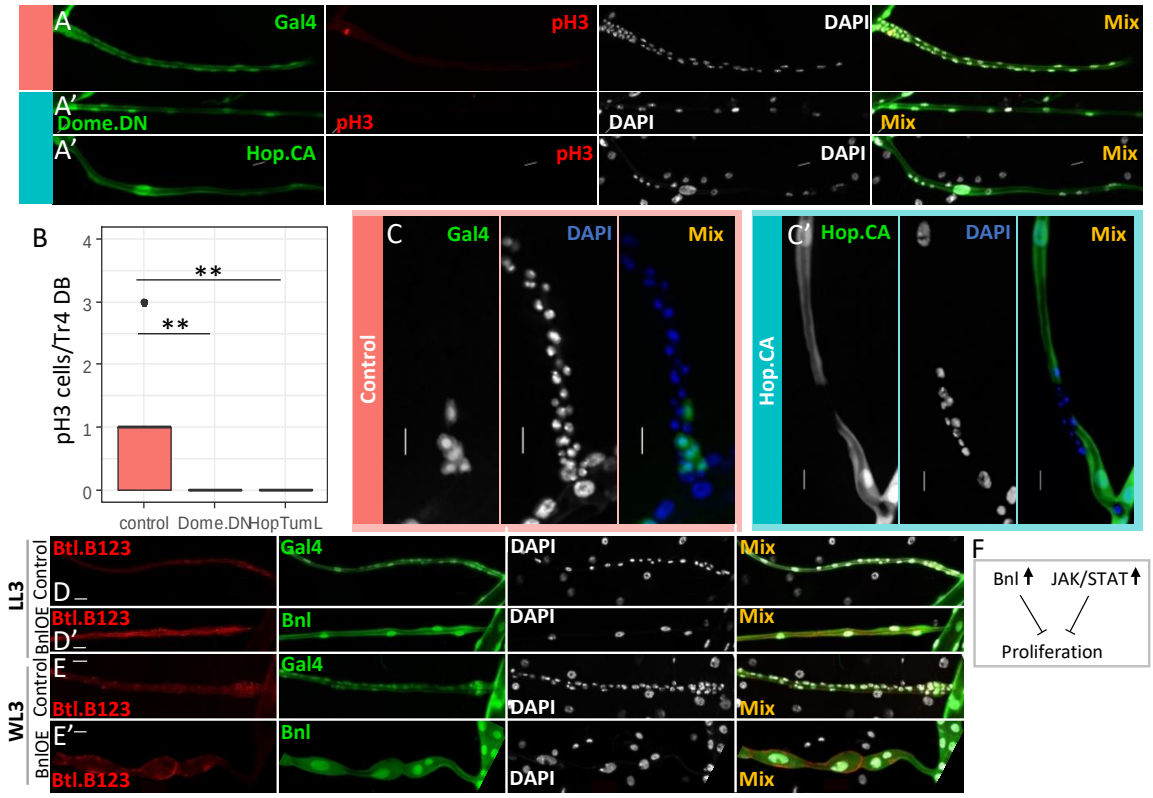

Fig. 29 Upregulating JAK/STAT signalling pathway inhibits the cell proliferation of progenitor cells in the DB4 region.

(A)*Btl-Gal4, UAS-GFP; tub-Gal80ts* animals and *btl-Gal4, UAS-GFP, UAS-hop.CA*(or *UAS-dome*.DN); *tub-Gal80ts* animals reared at 18°C before L2 stage and then transferred to 29°C stained for GFP (green, Gal4 positive clones), pH3 (red), and DAPI(white) in the wandering L3 stage. (B) The number of mitotic cells in DB4 of control trachea without *UAS-hop.CA* nor *UAS-dome*.DN and of the affected trachea with *UAS-hop.CA* or *UAS-dome*.DN displays a decline of cell proliferation in the affected trachea. (C) Ectopic analysis of the impacts of the expression of *hop.CA* on cell proliferation in the DB4 by using vvl-coin driver driving *hop.CA* expression. It showed a cease in cell proliferation in the affected clones in the DB4. n=30. (D-E) *Btl-Gal4, UAS-GFP; btl*.B123-*RFP-moe, tub-Gal80ts* animals and *btl-Gal4, UAS-GFP, UAS-bnl; btl*.B123-*RFP-moe*, *tub-Gal80ts* animals reared at 18°C before L2 stage and then transferred to 29°C stained for GFP (green, Gal4 positive clones), btl expressing cells (red), and DAPI(white) in the late L3 stage and wandering L3 stage showed overexpression of bnl inhibit cell proliferation in DB4. Scale bar: 20um. ** P<0.01 by Student's t test.

3.2 Noncanonical WNT activation of Yki signalling is necessary for epithelial cells to maintain their homeostasis

Emphysematous destruction is another source of airflow limitation in COPD which reduces maximum expiratory flow by decreasing the elastic recoil force[39]. Previous reports revealed its close association with the inadequate repair upon the tissue damage. Among a variety of signal in response to injuries, WNT/ß-catenin signalling pathway seems to play a central role in the repair which contributes to cell differentiation from AT2 to AT1[15,16]. However, the noncanonical WNTs (e.g. WNT5a), which can be induced by cigarette smoke, can alter the WNT/ß-catenin signalling pathway to the noncanonical WNT signalling pathway, which led to the inhibition of genesis of the AT1 cells[108]. Strikingly, a recent study on the noncanonical WNT signalling discovered that YAP/TAZ react to the WNT5a and the activation of YAP/TAZ was proved to inhibit the WNT/ß-catenin signalling[114].

In *Drosophila*, all components of the WNT-YAP/TAZ could be found including WNT2/WNT5 (human analogue, WNT5a), ROR1/ROR2 (human analogue, ROR1/ROR2), protein concertina (human analogue, $G\alpha_{12/13}$), Ras-like GTP-binding protein Rho1 (human analogue, RhoA), Warts (human analogue, Lats1/2), Yorkie/Scalloped (human analogue, YAP/TAZ). In this study, I analysed the relevance of WNT-Yorkie/Scalloped (Yki/Sd) axis in the airway system by using *Drosophila* as a model. As a result, expression of intracellular components of the pathway led to a similar phenotype that the cell morphogenesis and differentiation were inhibited while the overexpression of ligands and receptors did not provoke these changes in tracheal structure. Here I also found that the activity of Yki was induced by severe stress factors. To understand the effects of WNT-Yki/Sd on the cell morphogenesis and differentiation at the molecular level, I performed transcriptome analysis. It ruled out that active Yki reprogramed the cell biological process, inhibited the production of structural substances during the trachea growth and induced noncanonical *wnt* expression. In addition, I found the expression of these noncanonical WNTs could promote the expression of the transcription factor cut that is of relevance for cell differentiation[133].

3.2.1 The activation of yki impedes the growth of trachea.

To understand the effects of long-term induced Yki on the trachea development I drove the

tracheal cell expression of a constitutively active form of Yki (Yki.CA) by using *btl-Gal4*. The expression of *yki.CA* in the trachea led to the premature death of larvae. The animals looked healthy without any defects on the tracheal structure before the L2 larvae stage but would die with small body size at the L3 larval stage (Fig. 30A). Microscopy of the trachea of *btl-Gal4*, *UAS-yki.CA* larvae showed a puffing-like structure of chitin-based epicuticle at L3 the larval stage (Fig. 30A'). Then I observed the morphogenesis of the targeted trachea at different time point. Trachea developed normal before reaching the L3 state, however, the epithelium would be tortuous during forming a new tracheal tube and afterwards no air-filled tube formed. It indicated that the epithelium lost the morphologic structure and functionality in the L3 stage. In this study, I investigated the long-term activation of canonical WNT signalling as well, by driving the expression of a constitutively active form of an armadillo in epithelium cells. Lots of mutant animals survived to flies and their tracheal tubes were filled with gas. One phenotype of these *arm.CA* expressing trachea is the bifurcation structure, which is indicated an over differentiation or disorganization of the epithelium but not inhibition of cell function and other characteristics (Fig. 30D-E).

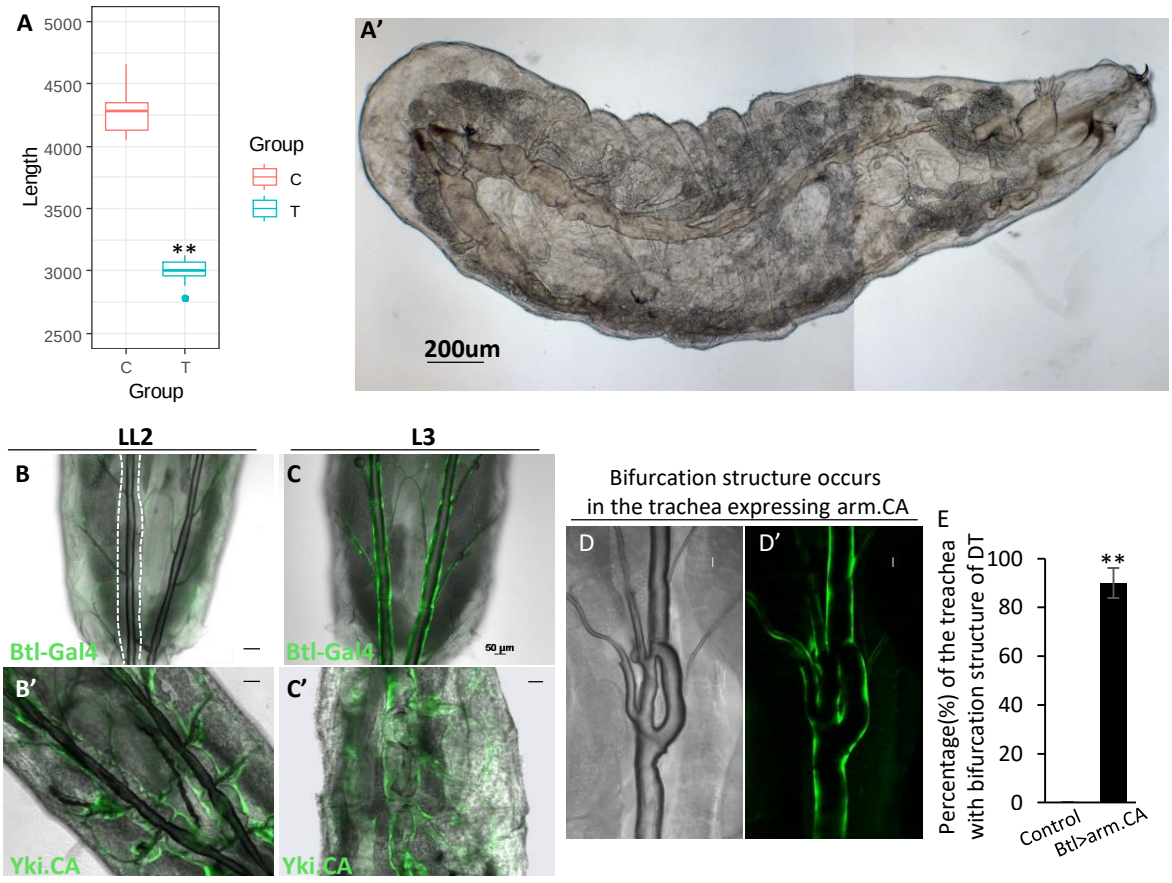

Fig. 30 Expressing *yki.CA* in the trachea impedes the genesis of new tracheal tube between L2 and L3.
(A) *Btl-Gal4*, *UAS*-GFP, *UAS-yki.CA* larvae are smaller than *btl-Gal4*, *UAS*-GFP control larvae in the L3 stage. The

affected trachea were transparent and puffing-like. (B-C) The epithelium of *btl-Gal4*, *UAS*-GFP, *UAS-yki.CA* larvae is tortuous during tracheal tube expansion and no gas-filled trachea formed afterwards. (D-E) The expression of *arm.CA* by using *btl-Gal4* driver contributed to the bifurcation structure of the trachea.

In this study, I also drove the expression of other components in the WNT-Yki/Sd signalling pathway by using the *btl-Gal4* driver to see if there is a similar phenotype in the affected larvae. Interestingly, the expression of ligands (gene, *wnt2, wnt4 and wnt5*) and receptors (gene, *ror1* and *ror2*) did not inhibit the growth of trachea while the expression of the constitutively active form of Cta (gene, *cta.CA*) and Rho (gene, *rho1.CA*) led to the premature death of the animals, but the animals that expressed *rho1.CA* or *cta.CA* in the trachea died earlier than the animals that expressed *yki.CA* driven by the same Gal4 line. Macrographs revealed that the expression of *rho1.CA* interfered with the genesis of the tracheal tree, which was not observed for the expression of *yki.CA*. (Fig. 31).

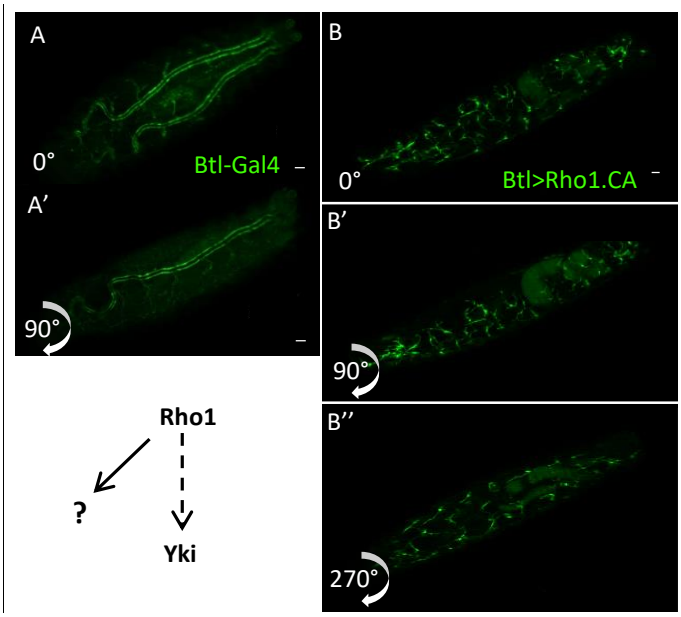

Fig. 31 Larvae that were expressing *Rho1*.CA in the trachea lack an intact trachea.
Fluorescence micrographs of btl-Gal4, UAS-GFP L1 larvae (A) and *btl-Gal4, UAS-GFP; UAS-Rho1.CA* L1 larvae(B).

3.2.2 Similar phenotypes in the trachea expressing *yki.CA*, *rho1.CA* and *cta.CA*.

Considering the expression of *rho1.CA* and *cta.CA* in the whole trachea by *btl-Gal4* driver led to premature death in the early L1 stage, I choose *cut-Gal4* as the driver for *UAS*-gene expression instead. *Cut-Gal4* can drive gene expression in only a part of the trachea and after the trachea has formed(Fig. 32A). Micrographs of the affected larvae that were expressing components of the WNT-Yki/Sd signalling pathway in the specific zones showed the expression of noncanonical ligands (WNT2, WNT4 and WNT5) and receptors (*ror1* and *ror2*) did not contribute to visible changes in the tracheal structure compared to the control, but the

expression of an active form of the intracellular members in the signalling pathway (*rho1.CA*, *cta.CA* and *yki.CA*) impede the formation of the new trachea in the affected zone (tr8-tr10). Here I also compared the effects of *cta.CA* expression to the effects of the expression of another sub-type of G protein, namely Galphaq which does not participate in the WNT-Yki/Sd pathway. It showed that the expression of Galphaq did not contribute to the losses of tracheal structure in the targeted zone as the expression of *rho1.CA*, *cta.CA* and *yki.CA* did(Fig. 32B). Mosaic analysis confirmed the effects of activating WNT-yki signalling on the tracheal growth (Fig. 32F-G).

The effects of expressing *yki.CA* in the trachea mainly occurred in the late larval stage when new tracheal tubes form. To confirm the impacts of the enhanced signalling in this stage, I introduced a new trachea-specific driver (*nach-Gal4*), which start the expression of *Gal4* from larvae stage and have a wave expression in the larval trachea. The expression of *nach* showed a close association with the formation of the new tracheal tube[176]. In this study, I examined the effects of active forms of the three intracellular components (Yki.CA, Rho.CA and Cta.CA) in the trachea by using the *nach-Gal4* driver. As a result, the functional trachea formed in these animals and the animals can survived to flies by using this *nach-Gal4* driver. Furthermore, micrograph analysis of the trachea of the three manipulations of larvae revealed a similar appearance among the affected trachea that were tortuous compared with the control tube. Quantification of the length of the dorsal trunk between tr8 and tr9 indicated the inhibition of trachea growth (Fig. 33 A-E). The mosaic analysis confirmed the effects of activating WNT-Yki/Sd signalling on the tracheal growth that the targeted zones are shorter compared to the normal zones (Fig. 33 F-G).

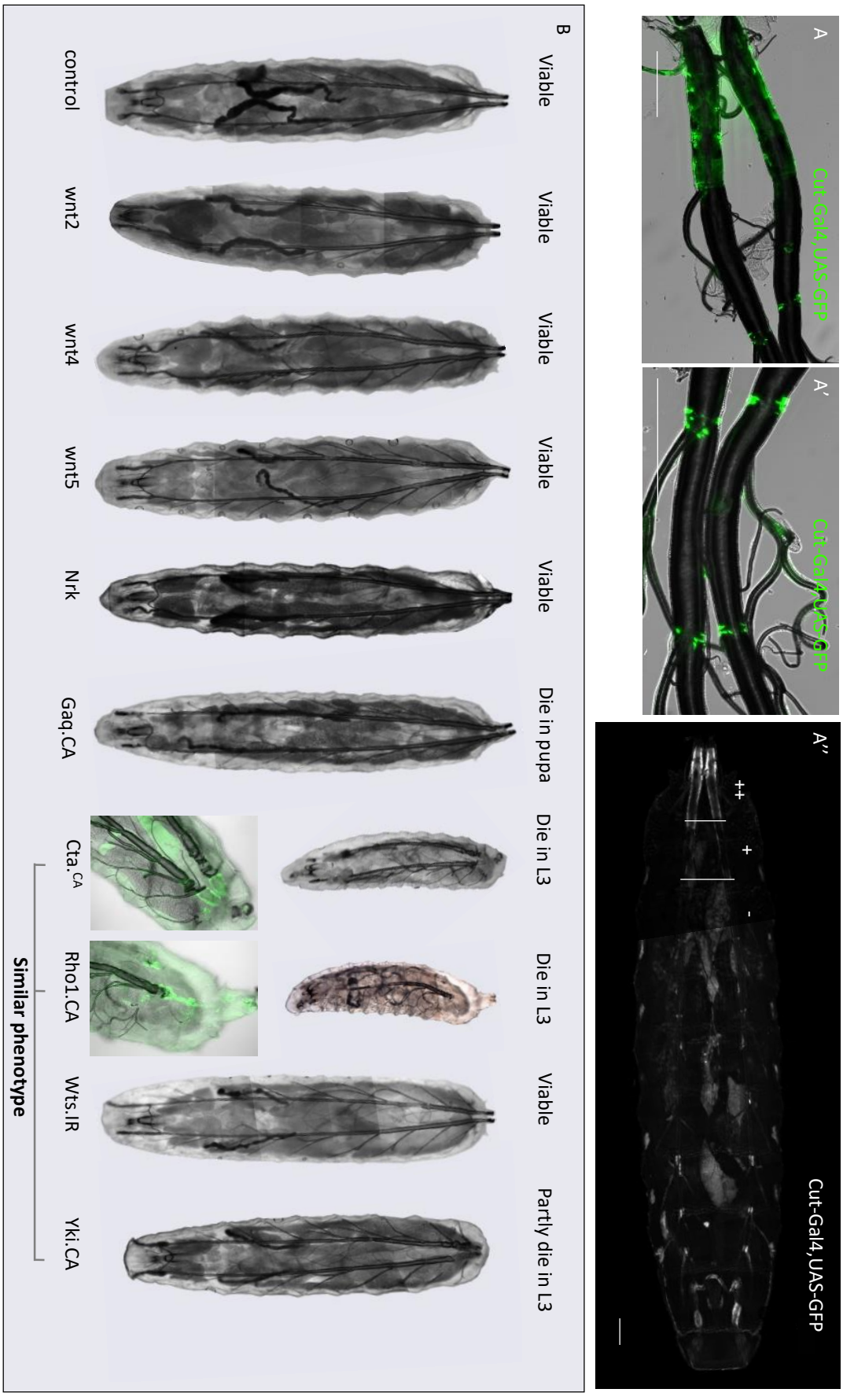

Fig. 32 The overexpression of the component of WNT-Yki pathway impeded the genesis of new trachea.
(A) Micrographs showed the expression zones of *Gal4* under the control of the upsteam regulatory element of

cut. In the tracheal dorsal trunk, *Gal4* expressed in the posterior region of the trachea(A) and the joint between dorsal trunk and branches(A'). Plus means the abundance of *Gal4* driven by cut regulatory element in the dorsal trunk (A''). (B) Micrographs of the larvae that were expressing the members of the WNT-Yki signalling pathway by using *cut-Gal4*. The expression of intracellular components of the WNT-Yki signalling pathway including active Cta, active Rho1, active Yki contributed to shorter trachea or even loss of chitin-based matrix.

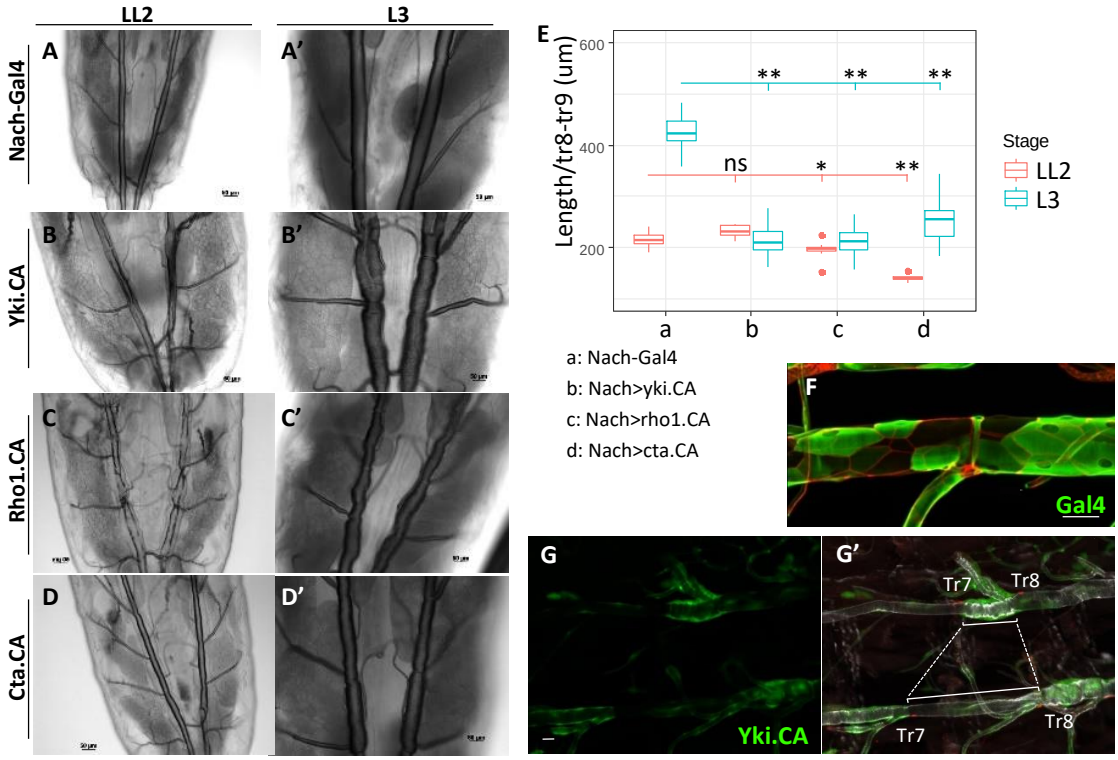

Fig. 33 Temporal and spatial deployment of *yki.CA* confirmed the inhition of tube growth after the new trachea formed.

(A-E) Micrographs of *nach-Gal4*, *UAS-yki.CA*(B); *nach-Gal4*, *UAS-rho1.CA*(C) and *nach-Gal4*, *UAS-cta.CA*(D) larvae showed that the similar appearance of the trachea of the three kinds of affected larvae whose tubes were tortuous compared with the control tube (A). Quantification of the length of the dorsal trunk between tr8 and tr9 showed a shorter tube compared to the control (E). (F) Micrographs of the trachea of *vvl*-coin, *UAS*-EGFP larvae showed the ectopic expressed *Gal4* in the trachea. (G) Mosaic expression of *yki.CA* by using the *vvl*-coin driver confirmed the shorter tube in the *yki.CA* positive regions.

In this study, I also investigated the changes in the activity of Yki in response to overexpression of the components of this pathway, including WNT ligands, wts.IR and rho1 by using *ppk4-GAL4*, *UAS-yki.GFP*. However, there is a contradiction between the phenotype I observed in the tracheal structure and the activation of Yki.GFP. Although having a similar phenotype with the overexpression of Yki.CA, overexpression of Rho1.CA did not activate the Yki.GFP significantly (Fig. 34). By contrast, overexpression of *wnt*, wts.IR did not induce the activation of Yki.GFP strongly as well.

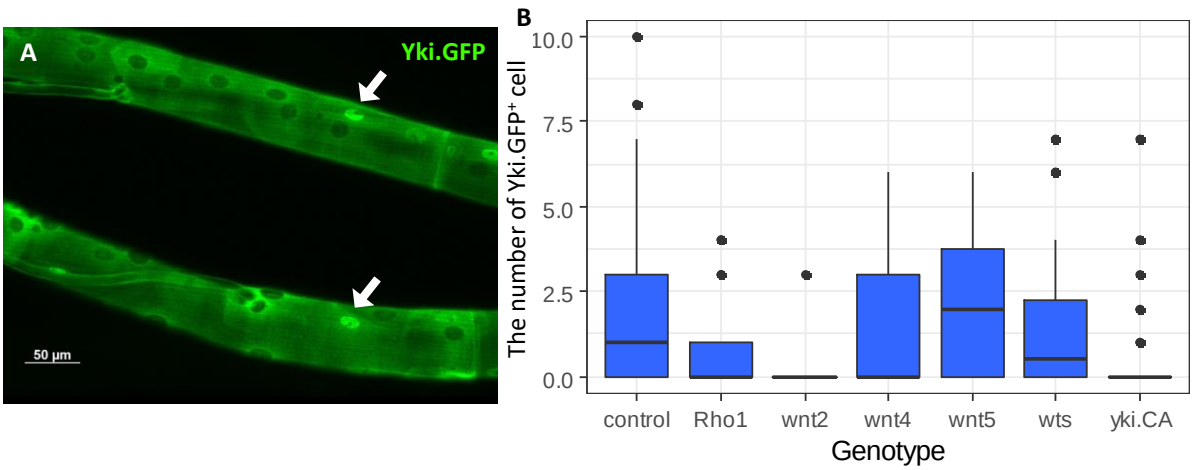

Fig. 34 Yki.GFP did not be activated by the overexpression of the compartments in the signalling pathway by using *ppk4>yki.GFP* reporter.
(A) Micrograph of trachea between tr8 and tr9 of ppk4-Gal4, UAS-yki.GFP larvae showed Yki.GFP was activated in some cells. (B) However, overepression of the compartments in the signalling pathway did not increase the number of cells where Yki.GFP was activated.

3.2.3 Strong smoke exposure contributes to death of epithelial cells.

In this study, I subjected the larvae to a higher intensity of cigarette smoke, which led to a higher mortality of animals compared to the animals exposed to the low intensity smoke for the same time (Fig. 35B and Fig. 38). Through examining the developmental viability of the animals that were exposed to smoke for the different time, I indentified the dose-dependent impact of cigarette smoke on the larval survival. 2 cigarettes smoked for 40 mins (strong smoke exposure) always caused death of more than half of all animals. By using cell death marker I know that there is an increase in the frequency of cell death in the trachea of the animals that were exposed to strong smoke compared to the control (Fig. 35C-E). To know if the cell death can be attributed to apoptosis, I stained the trachea with two different antibodies, namely cleaved caspase-1 (Dcp-1) and cleaved caspase-3 (Casp3), which can mark programmed cell death. However, the trachea of these larvae which had a strong smoke exposure could not be stained by either of these antibodies (Fig. 37)

In this study, I detected the changes of activity of Yki in response to strong smoke exposure as well by the observation of the translocation of the GFP tagged Yki (Yki.GFP) in the tracheal cells. Strikingly, compared to the control larvae, there is a larger number of the trachea where Yki.GFP translocated into the nucleus after the larvae were exposed to strong smoke (Fig. 35 F-H).

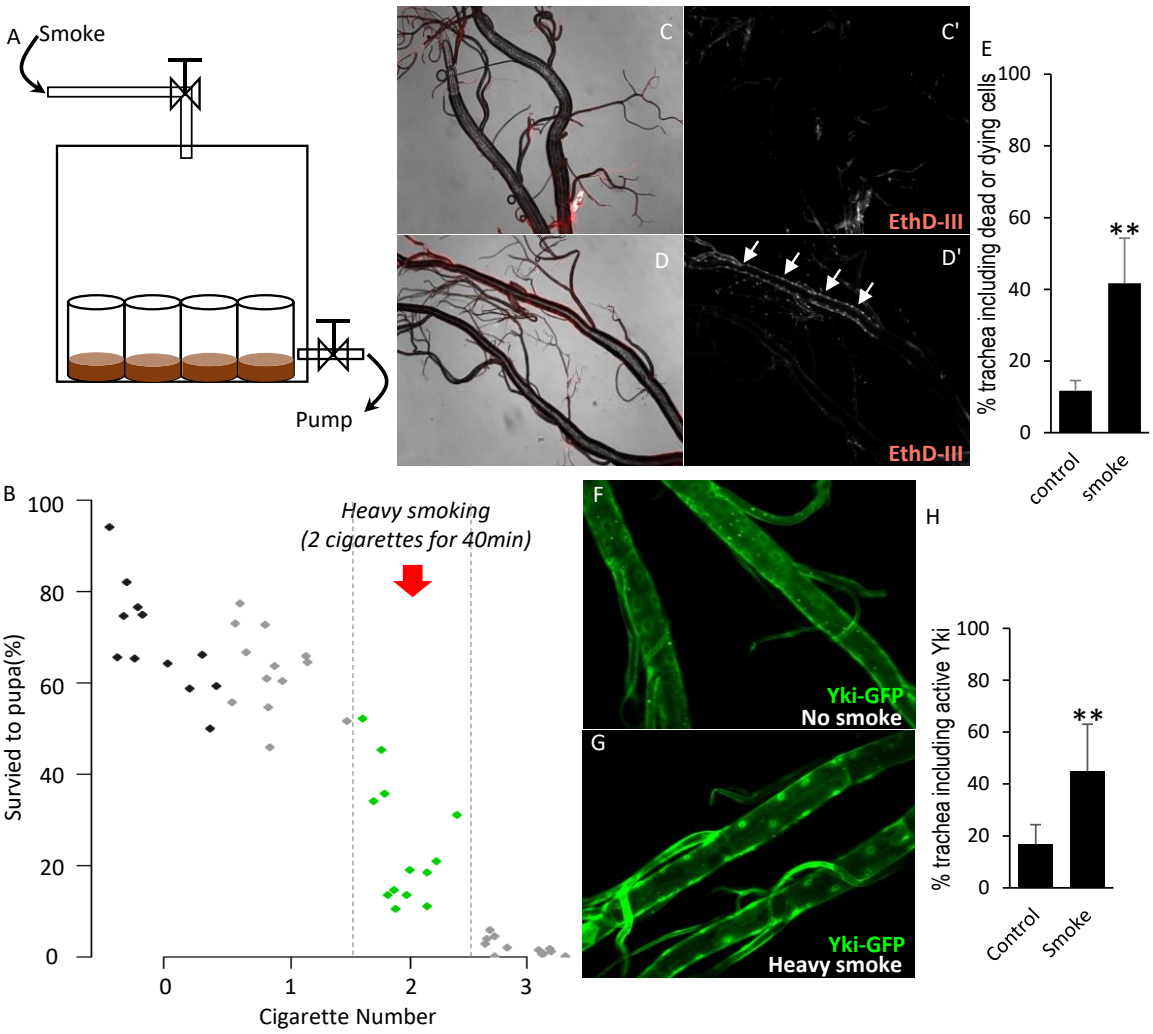

Fig. 35 Heavy smoke cause cell death in the epithelium of dorsal trunk and Yki was activated.
(A) The device for animals smoking. The pump can be adjusted to increase the concentration of the smoke in the device. (B) Time and dose-dependent effects of cigarette smoke on larval developmental viability. Compared to the control (0 CS), the larvae that were exposed to 1 CS for 20mins showed similar developmental viability. However, strong smoke exposure (2 cigarettes for 40mins) caused high mortality of larvae, although some of them survived. 3 CS caused massive death of larvae, only a few larvae could survive to the pupal stage. (C-E) Strong smoke exposure caused cell death in the epithelium of dorsal trunk based on anatomy observation. Microscopy of the trachea of larvae that were exposed to strong smoke exposure (D) showed an increase in the frequency of the trachea that could be stained by ethidium homodimer (a dye to detect dead or dying cells) compared to the control in the normal condition(C). (F-H) Microscopy analysis of the trachea of *nach-Gal4*, *UAS-yki.GFP* larvae that were in the normal condition (F) or exposed to strong smoke(G). Compared to the control more trachea of the heavy-smoked animals possessed translocated Yki from plasmid to nucleus(H).

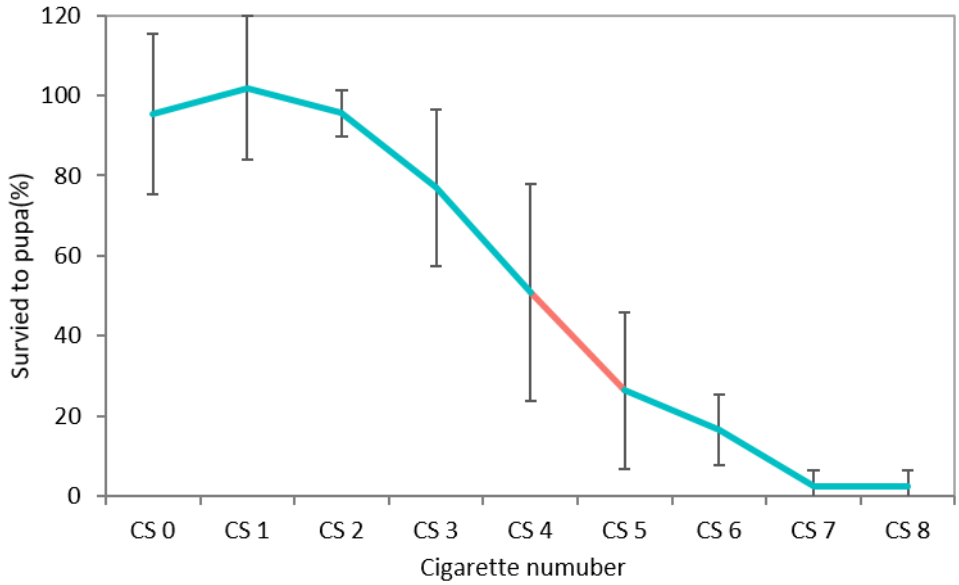

Fig. 36 The mortality rate at larvae after the exposure to the low intensity of smoke.
The low intensity of smoke have a deduced toxicity in the animals. The mortality rate reached 50% until 4 cigarettes smoke for 80mins.

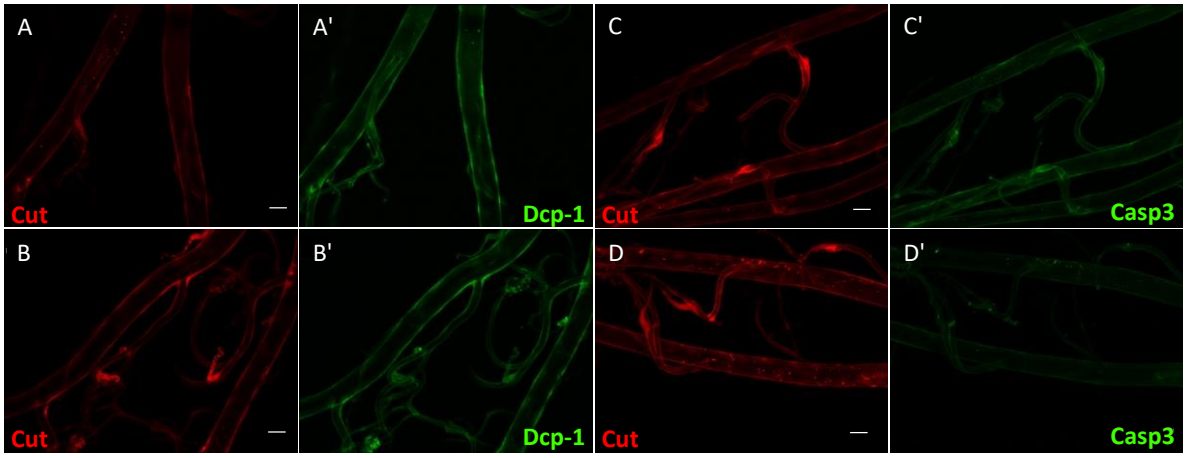

Fig. 37 Smoke didn't initiate cell apoptosis.
Micrographs of the trachea of control larvae (A,C) and the larvae exposed to heavy smoke (B,D) stained for apoptosis marker Dcp-1(green), Caspase 3(green) and positive control cut(red). The trachea of cigarette smoke larvae did not be stained by apoptosis marker. Scale bar: 50um, n=50.

3.2.4 Expression of active *yki* gene alters epithelial cell transcriptome.

To investigate the underlying molecular mechanisms of the effects of the activation of WNT-Yki/Sd on the airways, I performed an RNA-seq analysis of the tracheal cells expressing *yki.CA* in third instar larvae (LL3). This experimental setup revealed that the expression of *yki* (including *yki*.CA) was up-regulated 8 fold, ($p<10^{-14}$) (Fig. 37A). Among 13767 genes with uniquely mapped ID, a total of 3036 genes were statistically significantly regulated, with 1686 genes being downregulated and 1350 genes upregulated ($p<0.05$). Displayed is a diagram of a

heatmap of 3036 differentially transcribed genes concerning their statistical support (p<0.05) (Fig. 38B).

Then I analysed all significantly regulated genes based on GO annotations. In this way, 13 categories were significantly enriched according to their predicted functions (Fig. 38C). Most regulated genes were related to the muscle system process, myofibril assembly, chitin-based cuticle development exhibited a decrease in the transcription level. By contrast, most regulated genes involved in protein folding, glycoprotein metabolic process and RNA processing were induced by long-term expression of *yki.CA*.

One striking feature of the trachea with enhanced WNT-Yki/Sd signalling is the inhibition of the genesis and growth of a new trachea tube in the L3 larval stage. Here, I performed the GO analysis for 78 downregulated genes whose FDR P-value $<10^{-5}$; max expression group> 1; fold change>5 (table 4). Finally, these genes were significantly enriched in two categories (body morphogenesis and chitin-based cuticle development) (Fig. 38D). The mutations of the genes in the two biological process exhibit shorter chitin-based structure[141,183]. Fig. 38E shows that almost all regulated genes involved in body morphogenesis were down-regulated.

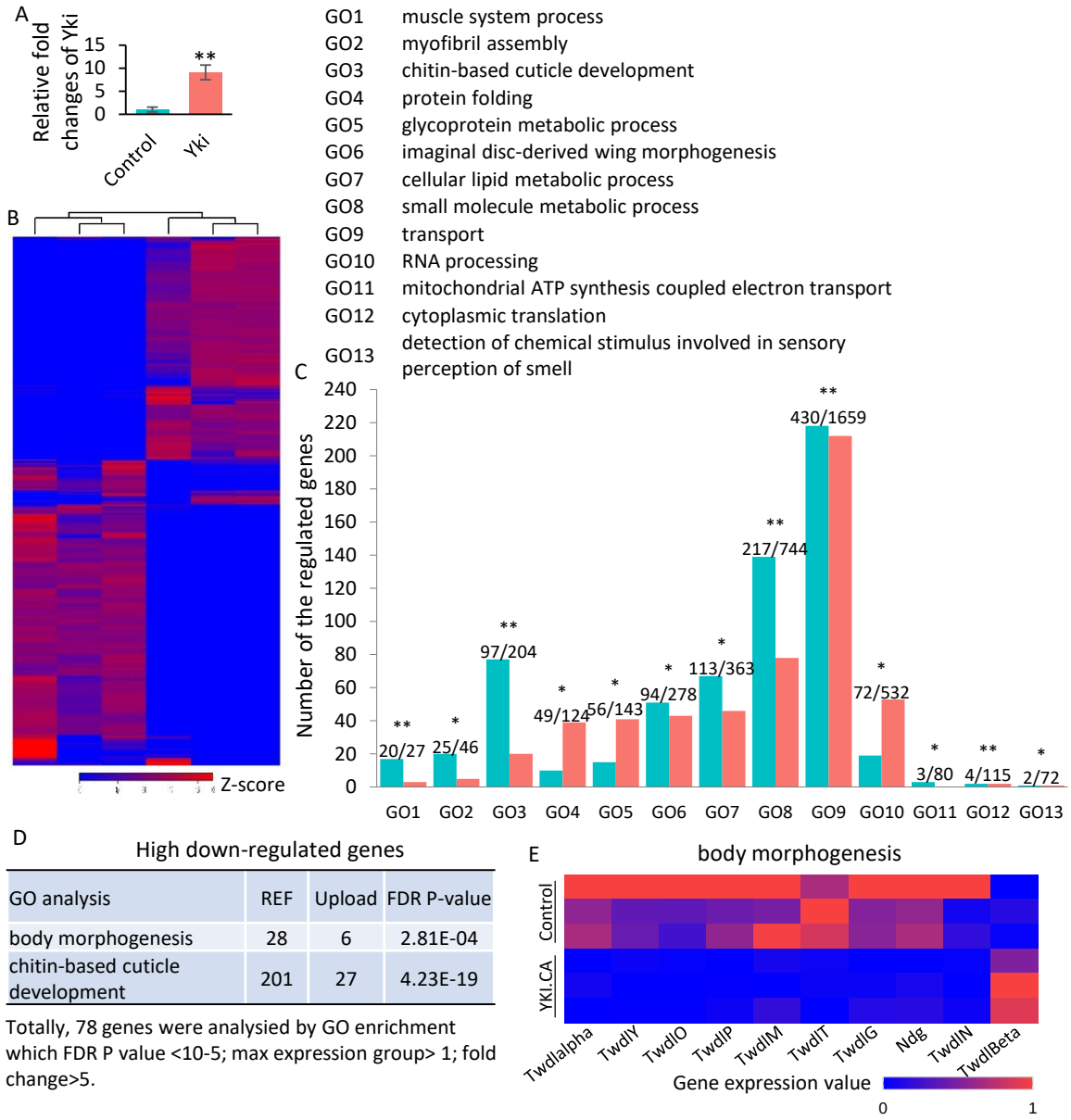

GO analysis	REF	Upload	FDR P-value
body morphogenesis	28	6	2.81E-04
chitin-based cuticle development	201	27	4.23E-19

Totally, 78 genes were analysied by GO enrichment which FDR P value <10-5; max expression group> 1; fold change>5.

Fig. 38 Expression of *yki.CA* alters transcriptome of tracheal cells.
(A-B) Heatmap based on the transcriptome of the trachea of *btl-Gal4*, *UAS-Yki.CA* larvae that were reared in the 18°C all the time (B left) and transferred to 29°C when they grew to L3 larvae (B right). The expression of Yki that contains *yki.CA* and Yki showed an 8 fold increase in the temperature-induced larvae (A). (C) 13 GO terms that all regulated genes were enriched in. (D) genes that FDR P value< 10-5, max expression group> 1 and fold changes> 5 were enriched in two biological processes which could be classified and both of them are relevant to epicuticle development. (E) Heatmap showed the most regulated genes involved in body morphogenesis were down-regulated in response to yki.CA.

Table 4 The genes that were inhibited strongly by expressing *yki*.CA in the trachea.

Name	Max group mean	Fold change	FDR p-value
Lcp65Ag1	2012.35022	-15.4909351	0
CG13051	1959.88807	-8.7733244	3.0563E-13
Cpr65Ax2	1906.28846	-16.365754	0
CG16884	1722.3103	-6.58097142	0
Cpr67Fa1	1521.66543	-7.73973088	0
Cpr47Eg	1374.79258	-28.7812055	0
CG32266	1324.48728	-6.81295477	0
CG13069	1096.55052	-13.2278738	2.1551E-12
CG13047	1031.32705	-12.2142556	0
Lcp65Ag3	917.800304	-25.6931708	0
CG1368	721.995815	-6.54134489	0
Lcp65Ac	676.994523	-16.6090049	0
CG11350	651.692824	-11.47736	0
CG13705	557.066422	-13.3791511	0
Lcp65Ae	544.991078	-13.3834218	0
Ccp84Aa	484.245722	-6.78940944	0
Cpr64Ad	475.664562	-44.2099988	0
Cpr67Fa2	425.63335	-10.4031699	0
Ccp84Ab	424.007275	-8.94296383	0
Lcp65Ag2	416.23834	-10.0872453	0
CG13640	401.296966	-9.65619552	0
CG13674	376.659606	-14.4058517	0
Lcp65Af	345.204645	-76.8953116	0
Cpr65Ax1	273.825247	-17.140516	0
CG34305	266.852444	-11.0954151	0
CG15515	212.517748	-10.8454813	0
CG14564	179.111941	-6.98653725	1.8814E-05
CG13066	162.769552	-69.8633604	8.5424E-15
Cyp313a4	120.506874	-8.06028244	0
TwdlO	96.7145391	-13.3262509	0
CG14569	92.4413609	-10.0144771	2.3983E-05
CG14565	65.4715986	-14.4904172	3.4437E-11
CG34208	63.2850917	-25.5012395	0
CG13722	63.1487364	-6.66345575	0
CG11585	49.92065	-7.15911429	0
CG34327	47.7363115	-10.9441756	0
CG30334	44.1750185	-10.826095	0
TwdlP	39.0774861	-8.56296791	0
CG42821	38.0664841	-8.56922124	0
CG15225	28.9247248	-26.6367982	0
GstD2	26.0625591	-7.38029244	2.5082E-14
CG13618	25.483088	-12.385793	0
CG13041	21.9340906	-16.5615698	0
CG43666	21.6148954	-15.6425315	0
CG10581	19.9466698	-23.0859744	0
CG14419	19.0501471	-9.09367374	0
CG11796	15.0805145	-8.01046739	1.1409E-11
CG31559	14.8505103	-13.8482856	0
Obp99d	13.0975962	-28.0228341	4.8784E-08
sit	12.1448279	-10.8938332	0
Acp65Aa	11.8749979	-15.2998246	3.3571E-10
CG13297	10.3828966	-16.9178092	1.0176E-08
PH4alphaNE1	10.007829	-7.81446465	0
CG16758	9.81107884	-6.19072494	8.5983E-12
Cpr49Ad	9.64083858	-15.2403146	1.6134E-07
CG14191	9.55600705	-11.8137973	5.5879E-07
CG15213	7.2830181	-14.1258318	2.8754E-05
CG13060	6.96290586	-45.7884354	4.4392E-08
CG13157	5.19898438	-14.9915372	3.2883E-14
CG10598	5.09154286	-8.93410417	1.2204E-08
CG15554	5.06935438	-10.1074833	3.4115E-05

Cp7Fc	4.61825173	-14.7578225	3.5373E-07
Cralbp	4.53285865	-8.62452775	9.4273E-07
CG15545	4.39091106	-7.46316209	4.3775E-05
CG6972	4.37600903	-8.12310599	1.901E-05
CG6472	4.21156487	-6.65946757	1.1817E-05
TwdlY	3.60230933	-16.9396549	4.2298E-06
CG14880	3.3630936	-9.62216418	2.8669E-09
Spn100A	2.96334687	-6.83315899	2.8754E-05
CG17290	2.63929346	-16.7053494	4.0208E-07
CG4998	2.5234819	-6.84423692	7.8152E-09
Act88F	2.4595977	-10.4651662	4.6015E-06
CG32719	2.11005171	-18.0374529	2.076E-13
Scgdelta	1.90411916	-6.38135612	1.2291E-05
Twdlalpha	1.89276127	-31.2588419	1.9693E-06
CG8160	1.63255241	-24.8699363	1.286E-05
CG31668	1.54699101	-24.3503301	1.9034E-07
CG43711	1.24760627	-31.8266787	1.4223E-05

$p<1X\ 10^{-4}$, Fold change>6, Max group mean>1.

3.2.5 Expression of active y*ki* gene induced the expression of noncanonical WNTs.

On the basis of analysis of the changes in transcriptomes, I found noncanonical *wnts* were up-regulated by *yki.CA* which is consistent with observation made in human cells[114]. Then, I performed qPCR to validate the positive effect of *yki.CA* on the expression of *wnts*. As expected, noncanonical *wnts* were up-regulated, by contrast, the changes in the expression of canonical *wnt(wg)* was not significant (Fig. 39A). Previous studies identified Cut as a transcription factor that can keep tracheal progenitor cells in an undifferentiated state. In this study, I found *wnt2* and *wnt4* can initiate the expression of *cut* gene (Fig. 39B-E).

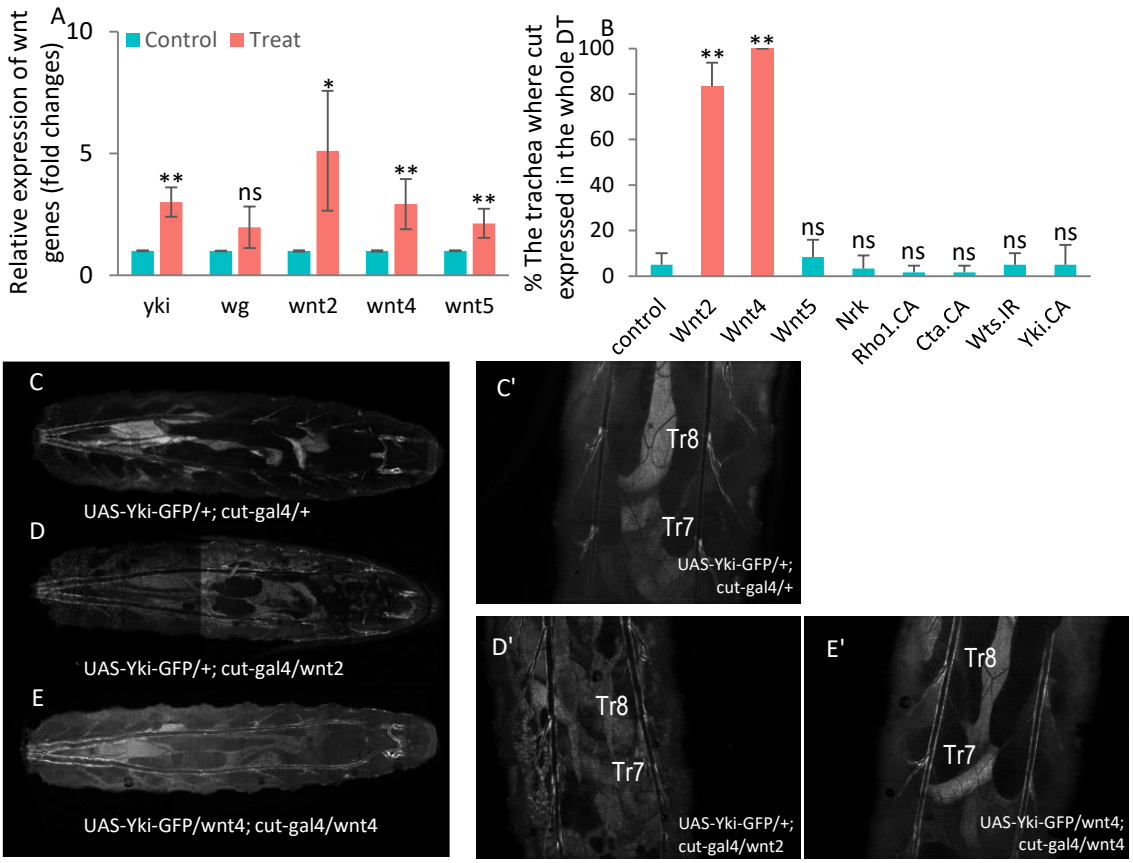

Fig. 39 Yki.CA induced *wnts* expression.
(A) Relative fold changes of *wnts* in the trachea where Yki.CA was expressed by using *nach-Gal4* driver. On the basis of qPCR, the difference of the expression of noncanonical *wnts* (*wnt2*, *wnt4* and *wnt5*) were significant, in contrast, canonical *wnt* (*wg*) was not significant regulated. (B-E) In the control, cut-*Gal4* drive the expression of *UAS*-gene in the specific zone(C), however, the overexpression of *wnt2* and *wnt4* induced the expression of cut in the whole trachea (D-E). (B) The ratio of the cut-induced trachea/total trachea. * $p<0.05$, ** $p<0.01$ by Student's t test.

Discussion

The main objective of the present work was to develop new models for chronic lung diseases using tailor-made *Drosophila*-based systems. At the same time, the aim was to gain further insights into essential signalling pathways in the respiratory tract of the fruit fly, which are also of paramount importance for diseases of the human lung. JAK/STAT and the WNT signalling pathway, each with a central role in the development of the respiratory system, but also in maintaining a homeostatic situation, especially under stress, were the focus of my interest. Although *Drosophila*, like all anthropods, do not have lungs but trachea, this system has been established as a very valuable system to study various human lung diseases[122,184–186]. This is obviously due to the fact that the physiological and structural requirements for effectively working airways are largely identical and thus have developed similar structural, but above all similar molecular mechanisms in the different systems. In the following, I will discuss separately the three main topics that I worked on experimentally in my dissertation. I will start with the two chapters on the function of the JAK/STAT pathway in the airways of the fruit fly and the effects of a misregulation of this pathway on airway structure and functionality.

4.1 Relevance of JAK/STAT signalling for the structure and functionality of airways

I was able to show that balanced JAK/STAT signalling is necessary to ensure the normal functionality of the airway system (trachea) of *Drosophila*. In addition, this signalling pathway takes a central position during the development of this organ. Consistent with the results of the current study are the reports about the role of JAK/STAT signalling during early phases of organ formation[187], but also those that showed a role during the formation of the adult tracheal system[188]. If JAK/STAT signalling is essential for the mammalian lung development is still a matter of debate, but the prevailing view that JAK/STAT signalling is not essential for embryonic lung development[189] has been challenged by recent studies[190]. This uncertainty regarding the role of JAK/STAT signalling for lung development stems from the fact that the complexity and redundancy of this signalling pathway is enormous covering more than 50 ligands and a great number of different receptors[96]. Despite the findings that JAK/STAT signalling is essential for different aspects of tracheal development, the current study focused on the role of this signalling pathway for maintaining homeostasis of a fully functional airway epithelium. I choose *Drosophila* larvae as a model, because of the fully functional airways that

must fulfil the task as a gas exchange organ in order to enable survival and growth of the animal. The respiratory epithelial cells of the larvae are terminally differentiated cells that do no longer divide, but increase in size as they grow. Interestingly, I was able to show that the JAK/STAT signalling pathway is essential for the larval airway epithelium and that blocking this pathway leads to the induction of apoptotic processes. This implies that this pathway plays a central role in maintaining homeostatic processes in this organ, which appears also to be the case for mammalian airway epithelia. Blunting JAK/STAT signalling in cell lines derived from airway epithelia induced cell apoptosis[191], which thus seems to be especially relevant for growing tissues and cells that still can divide or grow[192]. This ability to grow might be one reason for the high susceptibility of the *Drosophila* airway epithelial cells to the blockade of JAK/STAT signalling. Thus, cytokines that activate the JAK/STAT signalling pathway act at least in part as survival factors especially in those situations where repair mechanisms are operative. This dependence on functional JAK/STAT signalling could be shown, for example, in regenerative processes after epithelial damage[189,193], in the response to infections[194], and for the reaction to hyperoxia[194]. It follows from the above that JAK/STAT signalling in mammalian airway epithelial cells and in the *Drosophila* trachea is especially relevant for a protective reaction in response to stressful stimuli. In accordance with this assumption, I could show that JAK/STAT signalling is active during normal life in the airway epithelial cells of *Drosophila* larvae. JAK/STAT signalling could be observed all the time and it is especially activated in response to very strong stressors such as chronic confrontation to cigarette smoke. An organ-autonomous signalling system seems to be operative with induced expression and release of the cytokine Upd3 and the activation of a JAK/STAT dependent response in the same regions of the tracheal system. A comparable, stress induced system has been identified in the intestinal epithelium of the fly, where highly stressful insults targeting the absorptive enterocytes, lead to production and release of the cytokine Upd3[195,196]. In contrast to the situation in the intestine, where the cytokines produced by the stressed enterocytes affect stem cells and induce their proliferation to replenish the enterocyte pool, in the tracheal system, the structure of conventional epithelial cells is altered without employing activation of stem cells.

Besides this obvious requirement of a certain level of JAK/STAT signalling to ensure airway epithelial functionality and survival, excessive activation of the signalling pathway has been associated with a number of different lung diseases, comprising lung cancer, acute lung injury, asthma, pulmonary fibrosis, and COPD[197,198]. This implies that the different facets of this highly

complex signalling pathway are critically involved in the development of the majority of all chronic lung diseases. Thus, keeping a homeostatic balance in the airway epithelium, especially with respect to potential damages and their repair, is essential for a healthy life. In this context, the JAK/STAT signalling pathway seems to take a decisive position[189]. To study this imbalance of JAK/STAT signalling that is causally associated with the majority of chronic lung diseases and that is responsible for structural changes typically seen in these diseases, I used ectopic activation of JAK/STAT signalling restricted to the airway epithelium of *Drosophila* larvae. This intervention induced massive structural changes of the airway epithelium that mainly comprises substantial changes of the architecture of the tracheal cells. This effect induced by ectopically induced JAK/STAT activation was cell-autonomous as demonstrated by mosaic analysis. Major structural changes of the tracheal structure are reminiscent of those seen in the aforementioned lung diseases such as COPD. Structural changes that permit to fulfil the original function of epithelial cells are often part of an epithelial to mesenchymal transition (EMT). In COPD, fibrosis is the main contributor to physiological airway dysfunction and EMT is one mechanism contributing to airway fibrosis[199].

Beside the observed and obvious structural changes of the airways in response to JAK/STAT activation, I observed complex transcriptome alterations. These changes comprise immune relevant genes such as the bomanins. Regulation of antimicrobial responses via JAK/STAT signalling is also typically seen in the human airway epithelium[200]. However, chronically activated JAK/STAT signalling also led to obstruction of basic cellular functions involved in secretory processes and in the formation of the extracellular structure. The defects in the extracellular matrix that were caused by *Hop.CA* expression are also reminiscent of the pathophysiology of the aforementioned chronic lung diseases that comprise acute or chronic injury related responses[201]. Excessive JAK/STAT signalling that induces structural changes aiming to enhance the repair capacities of the epithelial cells are therefore not entirely compatible with normal cell function, which thus also interferes for example with the transport of junctional proteins to the membrane. This defect should consequently lead to not only destruction of epithelial cells (e.g. cilia) but also a reduced barrier function of the epithelium, which is also a hallmark of chronic lung diseases such as asthma or COPD[202–204]. In addition to the changes just described, I also observed epicuticular changes, which influence the structure of the whole organ considerably. In this case, however, it is naturally much more difficult to find an equivalent in vertebrates.

As a final notice, it has to be kept in mind that the vertebrate lung and the insect trachea are not homologous. Nevertheless, they share a high degree of similarities regarding their development, physiology, innate immunity, and the signalling systems operative in these tissues[205,206]. Based on this, the fruit fly has been used as a very valuable tool to study disease-associated genes for a great variety of different chronic lung diseases, comprising asthma, COPD and lung cancer[184,186,207–210]. Thus, using this simple model supplements the experimental toolbox that not only allows us to understand the role of JAK/STAT signalling in the airways and especially the effects of chronic deregulation of the pathway but also provides us with easy access to materials to examine for example disease-targeted compounds at the molecular level.

4.2 Role of JAK/STAT signalling during structuring of adult airways

In this part on my thesis, I will focus on the effects of aberrant JAK/STAT signalling on a certain stem cell group in the larval trachea that is essential for making the adult trachea, the SB tracheoblast in the late larvae stage. The relevant time window was when SB cells grow and move out from the SB niche. I will describe a mechanism by which inhibition of JAK/STAT signalling contributes to the programmed cell death in stem cells and by contrast, enhanced activation of JAK/STAT signalling inhibits cell crosstalk. I identified that inhibition of the secretion of FGF causes a decline in cell proliferation and growth. Furtherly, I noticed that the upregulated JAK/STAT signalling in some other groups of progenitors impedes cell proliferation as well. Based on the comparison of the response of different kinds of progenitors to the activation of FGF/FGFR signalling and JAK/STAT signalling, it can be concluded that the cell proliferation of tracheal progenitors in different regions is controlled by different key signals.

JAK/STAT signalling is involved in the regulation of multiple stem cell activities in *Drosophila*[211]. In the intestine, JAK/STAT signalling is initiated by Upd1 under normal conditions to maintain basal turnover of the epithelium in an autocrine manner. Upon acute stress, Upd3 is recruited to promote cell regeneration[212]. A similar reaction can be observed in the trachea. On one hand, I found that Upd2 is required for the tracheal cells to re-enter into the cell cycle, which possesses a higher transcriptional level in all mitotic department compared to the other two *upd* genes. On the other hand, the expression of *upd3* is also induced by conditional insults such as cigarette smoke. In this study, the regions of *upd2* expression that encompass an

activation of JAK/STAT signalling not only validate the important role of Upd2 in activating the signalling pathway but also imply an autocrine manner of the signalling activation.

The JAK/STAT signalling pathway plays an important role in cell proliferation and differentiation, given that an increase in the activity of the JAK/STAT signalling could be observed in proliferating cells[92] and the expression of constitutively active JAK2 in lymphocyte validated its positive role in cell proliferation[93,94]. Likewise, its inhibition contributed to the reduction of stem cell proliferation and even to programmed cell death [92,95]. But it is not clear if the aberrant JAK/STAT signalling has similar effects on the respiratory system. In *Drosophila*, the investigations in the adult stem cells showed the importance of JAK/STAT signalling in controlling stem cell maintenance in the testis, ovary, and the intestine as well[211]. The previous study revealed the important role of JAK/STAT signalling in tracheal development in the embryonic stage[213–215], whereas the effects of deregulation of JAK/STAT signalling on the homeostasis and regeneration is not clear. To identify the effects of aberrant JAK/STAT signalling on the homeostasis and regeneration of tracheal stem cells, I firstly investigated the effects of aberrant JAK/STAT signalling on the tracheal progenitors, especially the SB tracheoblasts. Cell proliferation and differentiation of SB tracheoblasts are dominantly controlled by functionally conserved signalling pathway such as FGF/FGFR, and the WNT signalling pathway[133], which take the same role for proliferation and differentiation in the human lung[1]. My results showed the importance of JAK/STAT signalling in cell homeostasis and proliferation with consistency to previous reports in human cells[92,95]. On one hand, STAT reporters showed an increase in the activity of STAT92E in mitotic cells in the different regions. On the other hand, the inhibition of JAK/STAT signalling contributed to cell apoptosis in all these cell types.

However, tracheal stimulation with *Hop.CA* did not promote but inhibit cell proliferation and differentiation. The result was unexpected taking the generally positive role of JAK/STAT signalling on cell growth into account. It indicates that up-regulation of the activity of STAT cannot initiate cell division directly and in contrast, the long term up-regulation could antagonise cell cycle progression. The same phenotype could be observed in the FGF/FGFR signalling induced cell proliferation in this study as well. One possibility is that the activation of JAK/STAT signalling is required in part in phases of the cell cycle but is dispensible in others, so long term activation could make the cells stay in a certain phase of their cell cycle. For example, FGF/FGFR signalling was reported in an important role in cell endoreplication[216]. I

also observed an increase in the size of the cell nucleus and cytoplasm but no induction of cell division in the DB cells that expressed the *bnl* gene.

Apart from inflammation, in COPD, there is a significant increase in cell apoptosis and dysfunction of epithelial cells[100,217]. In response to the damages, several types of stem and/or progenitor cells are motivated by up-regulation of specific key signal factors that have the capacity to self- renew and differentiate into multiple cell lineages[1]. Chronic injury and unchecked inflammation, which can provoke irreversible lung remodelling are considered to be the main driver of lung diseases such as COPD. The IL-6 - JAK/STAT signalling axis was found to play an important role in orchestrating defence responses and tissue regeneration. In this study, I showed that the JAK/STAT signalling participates in cell proliferation and also provided another perspective, that long-term up-regulation can impede cell cycle progression and interfere with cell function. Cell development, homeostasis and regeneration are complex biological processes which involve the release of extracellular signalling molecules and changes of the microenvironment. *Drosophila* provides us with an easy model to dissect this enormous complexity. In this study, I benefited from the temporal and spatial expression of genes of interest and found out that defects occurring in this cellular crosstalk caused by aberrant JAK/STAT signaling had dramatic effects on stem cell behavior.

4.3 The WNT signalling pathway in maintaining airway homeostasis

Wnt genes are defined by their sequence, they encode proteins that have a characteristic cysteine pattern plus other conserved residues in a characteristic spatial pattern[218]. So far, 19 *wnt* genes have been found in the human genome that can be assigned either to the ß-catenin dependent or/and ß-catenin independent signalling pathway. Their deregulation has been linked to the pathogenesis of several kinds of chronic lung disease[219]In this study, I investigated the effects of up-regulated WNT-Yki/Sd signalling on the airway system by driving the expression of an active form of *yki* ectopically in the larval trachea. I was able to show that upregulating this signalling pathway can inhibit cell differentiation and function, considering the tracheal defect in the cell differentiation stage. Transcriptomic analysis revealed this highly severe interference with major biological processes, especially with those intimately involved in the synthesis of tracheal structural substances and with components of the extracellular stroma. This phenotype is reminiscent of the pathogenesis of emphysema that is caused by

WNT5a[107,108]. Among the 19 *wnt* genes, WNT*5*a exhibits a rapid reaction to cigarette smoke exposure and seems to be centrally involved in the induced emphysematous destruction. It can not only initiate the noncanonical WNT pathway but also inhibit the canonical WNT pathway that plays a central role in the cell differentiation of AT2 cells. Interestingly, WNT5a also regulates multiple signaling pathway with relevance in cell differentiation, during the lung development and morphogenesis. However, overexpression of it was proved to inhibit cell differentiation of alveolar cells which was thought to trigger emphysema-like phenotypes and facilitated the pathological progress. Previous studies confirmed the important role of WNT5a in the pathological progress. However the key biological process that deregulation of WNT5a initiate and interfere with is not clear, considering that WNT5a is involved in several aspects of the biological process through distinct and indirect downstream responsory component[110]. Strikingly, WNT5a was recently reported to be an activator of the WNT-YAP/TAZ signalling pathway whose components can antagonize the ß-catenin dependent canonical WNT signalling pathway[114,117,118]. One assumption is that overexpression of *wnt5a* induced emphysematous destruction is mainly attributed to its ability to induce the activation of YAP/TAZ. In my thesis, the observation of the effects on the tracheal cell differentiation by activation of Yki in *Drosophila* trachea agrees with this assumption.

To further confirm the inhibition of the pathway in cell differentiation, I investigated the effects of the other components in the pathway on the airway system as well. The phenotype provoked by expression of these intracellular components is similar to the phenotype caused by expression of *yki*.CA. These upstream intracellular components of the pathway, such as Rho1 and Cta($G\alpha_{12/13}$), involve other signal transducing pathway as well, apart from activating Yki/Sd[220,221]. This fact interprets the severe defect in the tracheal structure provoked by overexpression of *Rho1*.CA and *Cta*.CA compared to *yki*.CA if the animals were reared in the same condition. For example, overexpression of *Rho1*.CA and *Cta*.CA can contribute to the defects of the tracheal development when I ectopically drove their expression before the formation of the tracheal tree, whereas active Yki cannot.

In *Drosophila*, *Ror1/2* (human ortholog *Ror1/2)* are expressed in the nervous system (and in other organs) and binds specifically to Wingless (Wg), WNT4 and WNT5[222]. Here I overexpressed these *Ror* genes or/and their ligands in the tracheal system. Interestingly, this activation did not lead to visible changes in the tracheal structure. This very slight effects provoked by the ligands and receptors on the trachea indicated a low level in the activation of

the corresponding signalling pathway, considering that the expression of *yki*.CA led to a visible change in the tracheal structure. The activation of the signalling pathway to the same extents as overexpression of intracellular signalling components implies that other factors are required to cooperate. *Drosophila* Ror displays a similar protein structure if it is compared with the human Ror, both containing FZ domain, protein kinase domain and extracellular Kringle domain. However, human Ror also includes extracellular immunoglobulin domains with yet unknown functions and intracellular proline-rich and serine-threonine-rich domains that are not part of the *Drosophila* Ror protein[223]. The distinct structure of the *Drosophila* Ror indicates that the regulation and activation in response to ligand binding of the receptor involves different mechanisms as in the human system. The activation of Ror involves WNT-dependent coupling to the Frizzled (Fz) coreceptor and recruitment of shared components in both human and *Drosophila*[222,224]. A previous study showed that the *Drosophila* Ror can specifically bind to Frizzled2 (Fz2) and Otk as well[222]. However, Otk is not expressed in the larval trachea (as referred to the information kept in the FlyAtlas 2). One another possibility is that the low activity of the pathway was attributed to the interaction with possible feedback regulators that restrict its activation. This kind of regulation could be examined in other pathways and the inhibition occurs often at the start of the signal transduction process. One paradigm is the regulation of JAK/STAT signalling pathway. Here, windpipe (Wdp), a membrane-bound protein, is positively regulated by JAK/STAT signalling and inhibits the JAK/STAT signalling pathway by directly interacting with the receptor Domeless, thus leading to a lesser degree of activation of the entire signalling pathway [225].

In this study, the observed effects of activated WNT-Yki/Sd signalling always occurred during the tube remodelling process that can be observed in the late L2 larvae stage. The observationof the affected region in the trachea showed that the activation of WNT-Yki/Sd signalling led to smaller cell sizes and an abnormal structure of the chitin layer. Indeed, the tube remodelling process occurring at this stage relies on the structural changes of the cells and the apically-secreted extracellular matrix in the absence of cell division and cell death during embryonic tracheal development[141]. In this study, I was able to show that the activation of WNT-Yki/Sd signalling can impede this process.

To know the underlying molecular mechanism, I performed a comprehensive transcriptomic analysis. The regulated genes can be categorized into 13 GO categories showing significant enrichment. Strikingly the categories that showed in the same direction of change (either up-

or downregulated) in the regulation were mainly of structural relevance. This analysis in the transcriptional level was in accordance with the phenotype I observed in the affected trachea showing structural changes. Here, I also screened the most down-regulated genes and identified tweedle family genes as a major group. Consistently, tweedle proteins regulate the body shape and mutants show shorter body sizes[183]. In this study, I analysed the highest up-regulated genes as well. Interestingly, most of these highly up-regulated genes were not regulated by the transcription factor Sd directly. This information was based on an enrichment analysis of the regulatory elements of these genes. Yki (or the human homolog, YAP) is examined as an oncogene for a long time which contributes to the production of a proliferation signal[226–228]. This big number of highly up-regulated genes, which are predominantly regulated by other transcription factors underline the severe influence of the expression of *yki*.CA on the intrinsic changes within the cells and may be considered as a general cell type transition.

Considering functional conservation between WNT-YAP/TAZ and WNT-Yki/Sd, I determined the effects of the activation of WNT-Yki/Sd on the cellular signal regulation during tracheal remodelling which could be intimately associated with cigarette smoke induced emphysema and implicate inhibition of YAP/TAZ as a potential therapy for emphysema in mammals.

Conclusions

1. The JAK/STAT signalling pathway is an indispensable signalling pathway for maintaining and controlling cell homeostasis and cell function. Its activation can be observed in the tracheal system of *Drosophila* at all developmental stages, having a stereotypical spatial activation pattern in the tracheal zones. For example, there is a stronger JAK/STAT signalling in the niche where stem cells proliferate compared with the zones where cells are quiescent. To elucidate the importance of JAK/STAT signalling in the trachea, I manipulated JAK/STAT signalling by using the UAS/GAL4 system. Cells with substantially reduced JAK/STAT signalling would initiate programmed cell death, showing that this signalling pathway transmits effects of survival factors. On the other hand, cells where JAK/STAT signalling activity was upregulated lost their specific identity as an airway epithelial cell. This deregulation can not only impede the genesis of the tracheal tree at early stages of tracheal development, but also interferes with cell differentiation and cell function after the formation of the tracheal tree, namely in the fully differentiated larval airway epithelial cell. These effects are well shown by the obvious changes in the epithelial structure, cell morphology and the alternation of gene transcription. This ectopic activation of JAK/STAT signaling has a physiological background, as its activity can be induced by cigarette smoke exposure, a result that is also seen in the human lung. Taken together, JAK/STAT signalling in the *Drosophila* airways is required for cell survival, but chronic overexpression has dramatic effects on cell structure and cell identity. Thus, I suppose JAK/STAT signalling to be a potential target for treatment aiming to ease the symptom of cigarette smoke-induced chronic lung disease.

2. I also examined the effects of deregulated JAK/STAT signalling on the progenitor cells in the airway system. Here, I found that activating JAK/STAT signalling can affect the paracrine secretion dependent cell crosstalk. Moreover, a different response of distinct stem cell niches to the deregulation of JAK/STAT signaling was shown. Although cell proliferation requires an increase in the activity of the JAK/STAT signalling, upregulation to a higher level can inhibit cell proliferation substantially.

3. The overexpression of noncanonical WNT (e.g. WNT5a) seems to play a critical role in the development of emphysema. Preliminary evidence suggests that a switch from canonical WNT signalling to noncanonical WNT signalling can cause inhibition of the differentiation of AT2 cells and thus contributes to the pathogenesis of emphysema in general. But it is not clear

which noncanonical WNT signalling pathway reacts to the noncanonical WNT. In this study, I was able to show that the overexpression of components of one noncanonical WNT signalling pathway (WNT-Yki/Sd) led to similar phenotypes characterized by the inhibition of cell differentiation. This strong phenotype was especially evident if the intracellularly acting components of the signalling pathway were activated. In *Drosophila*, Wnt-Yki/Sd can be initiated by cigarette smoke and its activation can induce the expression of noncanonical WNT in turn. A similar phenotype was presented in recent studies based on the exploration of WNT5a induced WNT-YAP/TAZ pathway in mammals. Considering WNT-YAP/TAZ as an important response pathway to WNT5a and its negative effects on cell differentiation, I suppose WNT-YAP/TAZ to be a potential therapeutic target for emphysema treatment in human COPD patients.

Declaration

I, Xiao Niu, here declare that my doctoral thesis entitled “A *Drosophila* model to understand lung disease related regulatory imbalances” and the work presented in it are my own work apart from supervisor’s guidance and design of the paper. This dissertation has not been submitted for the award of doctoral degree to another examining body and was prepared according to the Rules of Good Scientific Practice of the German Research Foundation.

Erklärung

Hiermit erkläre ich, Xiao Niu, dass diese Dissertation mit dem Titel: “ A *Drosophila* model to understand lung disease related regulatory imbalances ”, sowie die darin beschriebenen Arbeiten, abgesehen von der Beratung durch meinen akademischen Lehrer, nach Inhalt und Form meine eigene Arbeit ist. Diese.Arbeit wurde weder im Ganzen noch zum Teil an anderer Stelle im Rahmen eines Promotionsvorhabens eingereicht. Sie wurde nach den Regeln guter wissenschaftlicher Praxis der Deutschen Forschungsgemeinschaft angefertigt.

Kiel, April 2020

Xiao Niu

ACKNOWLEDGMENTS

Thanks to my professor, Prof. Dr. Thomas Roeder. He is very wise. I learned quite a lot from him. Here, I know how to find a question that is my topic relevant and that is worth to study. I promoted a skill to find out solutions. I learned how to present my results. He is very kind as well. I have too lots of questions, but he is always patient with my disturbance.

Thanks to everybody in our lab, AG Roeder, I spent a happy life here. They also provided me with a lot of suggestions in my study and a lot of help in the life trivia. Here especially thanks to Judith Bossen, Christine Fink and Roxy, they help me solve a lot of trouble in my daily life, which help me save time to do what I want and what I need. I also want to thanks to Britta Laubenstein and Christiane Sandberg. They do a lot of repetitive work for us and then we have more time to do creation.

In addition, I must thank ***Deutsche Zentrum für Lungenforschung (DZL)*** *and* ***China Scholarship Council (CSC)*** here. They supported me for my studies here.

Finally, I appreciate my parents and my lover. They are waiting for me for 3+ years and support my choice all the time.

Bibliography

1. Zepp, J. A. & Morrisey, E. E. Cellular crosstalk in the development and regeneration of the respiratory system. *Nature Reviews Molecular Cell Biology* vol. 20 551–566 (2019).
2. Volckaert, T. *et al.* Fgf10-Hippo Epithelial-Mesenchymal Crosstalk Maintains and Recruits Lung Basal Stem Cells. *Dev. Cell* **43**, 48-59.e5 (2017).
3. Lee, J. H. *et al.* Anatomically and Functionally Distinct Lung Mesenchymal Populations Marked by Lgr5 and Lgr6. *Cell* **170**, 1149-1163.e12 (2017).
4. Volckaert, T. *et al.* Parabronchial smooth muscle constitutes an airway epithelial stem cell niche in the mouse lung after injury. *J. Clin. Invest.* **121**, 4409–4419 (2011).
5. Yang, Y. *et al.* Spatial-Temporal Lineage Restrictions of Embryonic p63+ Progenitors Establish Distinct Stem Cell Pools in Adult Airways. *Dev. Cell* **44**, 752-761.e4 (2018).
6. Tata, A. *et al.* Myoepithelial Cells of Submucosal Glands Can Function as Reserve Stem Cells to Regenerate Airways after Injury. *Cell Stem Cell* **22**, 668-683.e6 (2018).
7. Lynch, T. J. *et al.* Submucosal Gland Myoepithelial Cells Are Reserve Stem Cells That Can Regenerate Mouse Tracheal Epithelium. *Cell Stem Cell* **22**, 653-667.e5 (2018).
8. Yin, Y., Wang, F. & Ornitz, D. M. Mesothelial- and epithelial-derived FGF9 have distinct functions in the regulation of lung development. *Development* **138**, 3169–3177 (2011).
9. Que, J. *et al.* Mesothelium contributes to vascular smooth muscle and mesenchyme during lung development. *Proc. Natl. Acad. Sci. U. S. A.* **105**, 16626–16630 (2008).
10. Von Gise, A. *et al.* Contribution of fetal, but not adult, pulmonary mesothelium to mesenchymal lineages in lung homeostasis and fibrosis. *Am. J. Respir. Cell Mol. Biol.* **54**, 222–230 (2016).
11. Yang, J. *et al.* The development and plasticity of alveolar type 1 cells. *Dev.* **143**, 54–65 (2016).
12. Rock, J. R. *et al.* Multiple stromal populations contribute to pulmonary fibrosis without evidence for epithelial to mesenchymal transition. *Proc. Natl. Acad. Sci. U. S. A.* **108**, (2011).
13. Barkauskas, C. E. *et al.* Type 2 alveolar cells are stem cells in adult lung. *J. Clin. Invest.* **123**, 3025–3036 (2013).
14. Frank, D. B. *et al.* Emergence of a Wave of Wnt Signaling that Regulates Lung Alveologenesis by Controlling Epithelial Self-Renewal and Differentiation. *Cell Rep.* **17**, 2312–2325 (2016).
15. Zacharias, W. J. *et al.* Regeneration of the lung alveolus by an evolutionarily conserved epithelial progenitor. *Nature* **555**, 251–255 (2018).
16. Nabhan, A. N., Brownfield, D. G., Harbury, P. B., Krasnow, M. A. & Desai, T. J. Single-cell Wnt signaling niches maintain stemness of alveolar type 2 cells. *Science (80-.).* **359**, 1118–1123 (2018).
17. Oxenius, A., Zinkernagel, R. M. & Hengartner, H. CD4+ T-Cell induction and effector functions: A comparison of immunity against soluble antigens and viral infections. *Adv. Immunol.* **70**, 313–367 (1998).
18. Coffman, R. L., Lebman, D. A. & Rothman, P. Mechanism and regulation of immunoglobulin isotype switching. *Adv. Immunol.* **54**, 229–270 (1993).
19. Le, J. & Vilcek, J. Tumor necrosis factor and interleukin 1: Cytokines with multiple overlapping biological activities. *Laboratory Investigation* vol. 56 234–248 (1987).
20. Soukup, J. M. & Becker, S. Human alveolar macrophage responses to air pollution particulates are associated with insoluble components of coarse material, including particulate endotoxin. *Toxicol. Appl. Pharmacol.* **171**, 20–26 (2001).
21. Becker, S., Soukup, J. M. & Gallagher, J. E. Differential particulate air pollution induced oxidant stress in human granulocytes, monocytes and alveolar macrophages. *Toxicol. Vitr.* **16**, 209–218 (2002).
22. Fujii, T., Hayashi, S., Hogg, J. C., Vincent, R. & Van Eeden, S. F. Particulate matter induces cytokine expression in human bronchial epithelial cells. *Am. J. Respir. Cell Mol. Biol.* **25**, 265–271 (2001).
23. Carter, J. D., Ghio, A. J., Samet, J. M. & Devlin, R. B. Cytokine production by human airway epithelial cells after exposure to an air pollution particle is metal-dependent. *Toxicol. Appl. Pharmacol.* **146**, 180–188 (1997).
24. Gilmour, P. S. *et al.* Adenoviral E1A primes alveolar epithelial cells to PM10-induced transcription of interleukin-8. *Am. J. Physiol. - Lung Cell. Mol. Physiol.* **281**, (2001).
25. Blobe, G. C., Schiemann, W. P. & Lodish, H. F. Role of transforming growth factor β in human disease. *New England Journal of Medicine* vol. 342 1350–1358 (2000).
26. Gorelik, L. & Flavell, R. A. Transforming growth factor-β in T-cell biology. *Nature Reviews Immunology* vol. 2 46–53 (2002).
27. Herfs, M. *et al.* Proinflammatory cytokines induce bronchial hyperplasia and squamous metaplasia in smokers implications for chronic obstructive pulmonary disease therapy. *Am. J. Respir. Cell Mol. Biol.* **47**,

67–79 (2012).
28. Hogg, J. C. Pathophysiology of airflow limitation in chronic obstructive pulmonary disease. *Lancet* **364**, 709–721 (2004).
29. Aubry, M.-C., Wright, J. L. & Myers, J. L. The pathology of smoking-related lung diseases. *Clin. Chest Med.* **21**, 11–35 (2000).
30. Fernandez, I. E. & Eickelberg, O. New cellular and molecular mechanisms of lung injury and fibrosis in idiopathic pulmonary fibrosis. *Lancet* **380**, 680–688 (2012).
31. Vogelmeier, C. F. *et al.* Global strategy for the diagnosis, management, and prevention of chronic obstructive lung disease 2017 report. *American Journal of Respiratory and Critical Care Medicine* vol. 195 557–582 (2017).
32. Neve, M. Smoke: A Global History of Smoking. *BMJ* **330**, 313 (2005).
33. Pauwels, R. A., Buist, A. S., Calverley, P. M., Jenkins, C. R. & Hurd, S. S. NHLBI/WHO Global initiative for chronic obstructive lung disease (GOLD) Workshop summary. *Am J Respir Crit Care Med* **163**, 1256–1276 (2001).
34. Fletcher, C., Peto, R., Tinker, C. & Speizer, F. E. *The natural history of chronic bronchitis and emphysema. An eight-year study of early chronic obstructive lung disease in working men in London.* (Oxford University Press, 37 Dover Street, London. W1X 4AH, 1976).
35. Disease, G. I. for C. O. L. Global strategy for the diagnosis, management and prevention of chronic obstructive pulmonary disease: NHLBI/WHO workshop report. *Bethesda, Natl. Hear. Lung Blood Inst.* (2001).
36. Hogg, J. C., Macklem, P. T. & Thurlbeck, W. M. Site and nature of airway obstruction in chronic obstructive lung disease. *N. Engl. J. Med.* **278**, 1355–1360 (1968).
37. Van Brabandt, H. *et al.* Partitioning of pulmonary impedance in excised human and canine lungs. *J. Appl. Physiol.* **55**, 1733–1742 (1983).
38. Yanai, M., Sekizawa, K., Ohrui, T., Sasaki, H. & Takishima, T. Site of airway obstruction in pulmonary disease: direct measurement of intrabronchial pressure. *J. Appl. Physiol.* **72**, 1016–1023 (1992).
39. Mead, J., Turner, J. M., Macklem, P. T. & Little, J. B. Significance of the relationship between lung recoil and maximum expiratory flow. *J. Appl. Physiol.* **22**, 95–108 (1967).
40. Saetta, M. *et al.* Inflammatory cells in the bronchial glands of smokers with chronic bronchitis. *Am. J. Respir. Crit. Care Med.* **156**, 1633–1639 (1997).
41. Mullen, J. B. M., Wright, J. L., Wiggs, B. R., Pare, P. D. & Hogg, J. C. Reassessment of Inflammation of Airways in Chronic Bronchitis. *Br. Med. J. (Clin. Res. Ed).* **291**, 1235–1239 (1985).
42. Hulbert, W. C., Walker, D. C., Jackson, A. & Hogg, J. C. Airway permeability to horseradish peroxidase in guinea pigs: The repair phase after injury by cigarette smoke. *Am. Rev. Respir. Dis.* **123**, 320–326 (1981).
43. Jones, J. G. *et al.* INCREASED ALVEOLAR EPITHELIAL PERMEABILITY IN CIGARETTE SMOKERS. *Lancet* **315**, 66–68 (1980).
44. Simani, A. S., Inoue, S. & Hogg, J. C. Penetration of the respiratory epithelium of guinea pigs following exposure to cigarette smoke. *Lab. Investig.* **31**, 75–81 (1974).
45. REID, L. Measurement of the bronchial mucous gland layer: a diagnostic yardstick in chronic bronchitis. *Thorax* **15**, 132–141 (1960).
46. Dunnill, M. S., Massarella, G. R. & Anderson, J. A. A comparison of the quantitative anatomy of the bronchi in normal subjects, in status asthmaticus, in chronic bronchitis, and in emphysema. *Thorax* **24**, 176–179 (1969).
47. Peto, R. *et al.* The relevance in adults of air-flow obstruction, but not of mucus hypersecretion, to mortality from chronic lung disease. Results from 20 years of prospective observation. *Am. Rev. Respir. Dis.* **128**, 491–500 (1983).
48. Vestbo, J. & Lange, P. Can GOLD stage 0 provide information of prognostic value in chronic obstructive pulmonary disease? *Am. J. Respir. Crit. Care Med.* **166**, 329–332 (2002).
49. WEIBEL, E. R. Morphometry of the Human Lung. *Anesthesiology* **26**, 367 (1965).
50. Yanai, M., Sekizawa, K., Ohrui, T., Sasaki, H. & Takishima, T. Site of airway obstruction in pulmonary disease: Direct measurement of intrabronchial pressure. *J. Appl. Physiol.* **72**, 1016–1023 (1992).
51. van Brabandt, H. *et al.* Partitioning of pulmonary impedance in excised human and canine lungs. *J. Appl. Physiol. Respir. Environ. Exerc. Physiol.* **55**, 1733–1742 (1983).
52. Hogg, J. C., Macklem, P. T. & Thurlbeck, W. M. Site and nature of airway obstruction in chronic obstructive lung disease. *N. Engl. J. Med.* **278**, 1355–1360 (1968).
53. REID, L. M. Correlation of certain bronchographic abnormalities seen in chronic bronchitis with the pathological changes. *Thorax* **10**, 199–204 (1955).
54. Hogg, J. C. *et al.* The nature of small-airway obstruction in chronic obstructive pulmonary disease. *N. Engl.*

J. Med. **350**, 2645–2653 (2004).
55. Chen, Z. H. *et al.* Autophagy protein microtubule-associated protein 1 light chain-3B (LC3B) activates extrinsic apoptosis during cigarette smoke-induced emphysema. *Proc. Natl. Acad. Sci. U. S. A.* **107**, 18880–18885 (2010).
56. Auerbach, O., Hammond, E. C., Garfinkel, L. & Benante, C. Relation of Smoking and Age to Emphysema: Whole-Lung Section Study. *N. Engl. J. Med.* **286**, 853–857 (1972).
57. Craig, J. M., Scott, A. L. & Mitzner, W. Immune-mediated inflammation in the pathogenesis of emphysema: insights from mouse models. *Cell and Tissue Research* vol. 367 591–605 (2017).
58. Arnson, Y., Shoenfeld, Y. & Amital, H. Effects of tobacco smoke on immunity, inflammation and autoimmunity. *J. Autoimmun.* **34**, (2010).
59. Qiu, F. *et al.* Impacts of cigarette smoking on immune responsiveness: Up and down or upside down? *Oncotarget* **8**, 268–284 (2017).
60. Rose, M. C. & Voynow, J. A. Respiratory tract mucin genes and mucin glycoproteins in health and disease. *Physiological Reviews* vol. 86 245–278 (2006).
61. Simet, S. M. *et al.* Long-term cigarette smoke exposure in a mouse model of ciliated epithelial cell function. *Am. J. Respir. Cell Mol. Biol.* **43**, 635–640 (2010).
62. Elliott, M. K., Sisson, J. H. & Wyatt, T. A. Effects of cigarette smoke and alcohol on ciliated tracheal epithelium and inflammatory cell recruitment. *Am. J. Respir. Cell Mol. Biol.* **36**, 452–459 (2007).
63. Gensch, E. *et al.* Tobacco smoke control of mucin production in lung cells requires oxygen radicals AP-1 and JNK. *J. Biol. Chem.* **279**, 39085–39093 (2004).
64. Jones, J. G. *et al.* INCREASED ALVEOLAR EPITHELIAL PERMEABILITY IN CIGARETTE SMOKERS. *Lancet* **315**, 66–68 (1980).
65. LeVine, A. M. & Whitsett, J. A. Pulmonary collectins and innate host defense of the lung. *Microbes and Infection* vol. 3 161–166 (2001).
66. Abbas, A., Lichtman, A. & Pillai, S. *Innate Immunity. Cellular and Molecular Immunology*. (2012).
67. Chen, Z. H. *et al.* Egr-1 regulates autophagy in cigarette smoke-induced chronic obstructive pulmonary disease. *PLoS One* **3**, (2008).
68. Medzhitov, R. & Janeway, C. Innate immune recognition: Mechanisms and pathways. *Immunological Reviews* vol. 173 89–97 (2000).
69. Richmond, I. *et al.* Bronchus associated lymphoid tissue (BALT) in human lung: Its distribution in smokers and non-smokers. *Thorax* **48**, 1130–1134 (1993).
70. Di Stefano, A. *et al.* Airflow limitation in chronic bronchitis is associated with T-lymphocyte and macrophage infiltration of the bronchial mucosa. *Am. J. Respir. Crit. Care Med.* **153**, 629–632 (1996).
71. O'Shaughnessy, T. C., Ansari, T. W., Barnes, N. C. & Jeffery, P. K. Inflammation in bronchial biopsies of subjects with chronic bronchitis: Inverse relationship of CD8+ T lymphocytes with FEV1. *Am. J. Respir. Crit. Care Med.* **155**, 852–857 (1997).
72. Bosken, C. H., Hards, J., Gatter, K. & Hogg, J. C. Characterization of the inflammatory reaction in the peripheral airways of cigarette smokers using immunocytochemistry. *Am. Rev. Respir. Dis.* **145**, 911–917 (1992).
73. Kemeny, D. M. *et al.* CD8+ T cell subsets and chronic obstructive pulmonary disease. in *American Journal of Respiratory and Critical Care Medicine* vol. 160 (1999).
74. Becker, S., Soukup, J. M. & Gallagher, J. E. Differential particulate air pollution induced oxidant stress in human granulocytes, monocytes and alveolar macrophages. *Toxicol. Vitr.* **16**, 209–218 (2002).
75. Fujii, T. *et al.* Interaction of alveolar macrophages and airway epithelial cells following exposure to particulate matter produces mediators that stimulate the bone marrow. *Am. J. Respir. Cell Mol. Biol.* **27**, 34–41 (2002).
76. Soukup, J. M. & Becker, S. Human alveolar macrophage responses to air pollution particulates are associated with insoluble components of coarse material, including particulate endotoxin. *Toxicol. Appl. Pharmacol.* **171**, 20–26 (2001).
77. Jamil, A., Rashid, A., Naveed, A. K. & Asim, M. Effect of smoking on interleukin-6 and correlation between IL-6 and serum amyloid a-low density lipoprotein in smokers. *J. Postgrad. Med. Inst.* **31**, 336–338 (2017).
78. Glossop, J. R., Dawes, P. T. & Mattey, D. M. Association between cigarette smoking and release of tumour necrosis factor α and its soluble receptors by peripheral blood mononuclear cells in patients with rheumatoid arthritis. *Rheumatology* **45**, 1223–1229 (2006).
79. Bermudez, E. A., Rifai, N., Buring, J. E., Manson, J. A. E. & Ridker, P. M. Relation between markers of systemic vascular inflammation and smoking in women. *Am. J. Cardiol.* **89**, 1117–1119 (2002).
80. Soliman, D. M. & Twigg, H. L. Cigarette smoking decreases bioactive interleukin-6 secretion by alveolar macrophages. *Am. J. Physiol. - Lung Cell. Mol. Physiol.* **263**, (1992).

81. McCrea, K. A., Ensor, J. E., Nall, K., Bleecker, E. R. & Hasday, J. D. Altered cytokine regulation in the lungs of cigarette smokers. *Am. J. Respir. Crit. Care Med.* **150**, 696–703 (1994).
82. Kishimoto, T. & Ishizaka, K. Regulation of antibody response in vitro. Suppression of secondary response by anti-immunoglobulin heavy chains. *J. Immunol.* **107**, 1567–75 (1971).
83. Nishimoto, N. *et al.* Improvement in Castleman's disease by humanized anti-interleukin-6 receptor antibody therapy. *Blood* **95**, 56–61 (2000).
84. Yokota, S. *et al.* Efficacy and safety of tocilizumab in patients with systemic-onset juvenile idiopathic arthritis: a randomised, double-blind, placebo-controlled, withdrawal phase III trial. *Lancet* **371**, 998–1006 (2008).
85. Nishimoto, N. *et al.* Treatment of rheumatoid arthritis with humanized anti-interleukin-6 receptor antibody: A multicenter, double-blind, placebo-controlled trial. *Arthritis Rheum.* **50**, 1761–1769 (2004).
86. Rabe, K. F. *et al.* Roflumilast - An oral anti-inflammatory treatment for chronic obstructive pulmonary disease: A randomised controlled trial. *Lancet* **366**, 563–571 (2005).
87. Savelikhina, I., Ostrovskyy, M., Ostrovska, K., Kulynych-Miskiv, M. & Varunkiv, O. Proinflammatory cytokine IL-6 detetion in severe COPD patients: Focus on roflumilast. in *European Respiratory Journal* vol. 52 OA3267 (European Respiratory Society (ERS), 2018).
88. Papanicolaou, D. A., Wilder, R. L., Manolagas, S. C. & Chrousos, G. P. The pathophysiologic roles of interleukin-6 in human disease. in *Annals of Internal Medicine* vol. 128 127–137 (American College of Physicians, 1998).
89. Van Snick, J. Interleukin-6: An overview. *Annual Review of Immunology* vol. 8 253–278 (1990).
90. Stark, G. R. & Darnell Jr, J. E. The JAK-STAT pathway at twenty. *Immunity* **36**, 503–514 (2012).
91. Villarino, A. V, Kanno, Y. & O'Shea, J. J. Mechanisms and consequences of Jak–STAT signaling in the immune system. *Nat. Immunol.* **18**, 374 (2017).
92. Fragiadaki, M. *et al.* STAT5 drives abnormal proliferation in autosomal dominant polycystic kidney disease. *Kidney Int.* **91**, 575–586 (2017).
93. Peeters, P. *et al.* Fusion of TEL, the ETS-variant gene 6 (ETV6), to the receptor- associated kinase JAK2 as a result of t(9;12) in a lymphoid and t(9;15;12) in a myeloid leukemia. *Blood* **90**, 2535–2540 (1997).
94. Lacronique, V. *et al.* A TEL-JAK2 fusion protein with constitutive kinase activity in human leukemia. *Science (80-.).* **278**, 1309–1312 (1997).
95. Vier, J., Groth, M., Sochalska, M. & Kirschnek, S. The anti-apoptotic Bcl-2 family protein A1/Bfl-1 regulates neutrophil survival and homeostasis and is controlled via PI3K and JAK/STAT signaling. *Cell Death Dis.* **7**, e2103–e2103 (2016).
96. O'Shea, J. J. *et al.* The JAK-STAT Pathway: Impact on Human Disease and Therapeutic Intervention. *Annu. Rev. Med.* **66**, 311–328 (2015).
97. Wang, C., Ding, H., Tang, X., Li, Z. & Gan, L. Effect of liuweibuqi capsules in pulmonary alveolar epithelial cells and COPD through JAK/STAT pathway. *Cell. Physiol. Biochem.* **43**, 743–756 (2017).
98. Yew-Booth, L. *et al.* JAK–STAT pathway activation in COPD. *Eur. Respir. J.* **46**, 843–845 (2015).
99. Bhalla, D. K., Hirata, F., Rishi, A. K. & Gairola, C. G. Cigarette smoke, inflammation, and lung injury: A mechanistic perspective. *Journal of Toxicology and Environmental Health - Part B: Critical Reviews* vol. 12 45–64 (2009).
100. Hodge, S., Hodge, G., Holmes, M. & Reynolds, P. N. Increased airway epithelial and T-cell apoptosis in COPD remains despite smoking cessation. *Eur. Respir. J.* **25**, 447–454 (2005).
101. Bakakos, P., Patentalakis, G. & Papi, A. Vascular Biomarkers in Asthma and COPD. *Curr. Top. Med. Chem.* **16**, 1599–1609 (2015).
102. Eapen, M. S. *et al.* Epithelial–mesenchymal transition is driven by transcriptional and post transcriptional modulations in copd: Implications for disease progression and new therapeutics. *International Journal of COPD* vol. 14 1603–1610 (2019).
103. Guha, A. & Kornberg, T. B. Tracheal branch repopulation precedes induction of the Drosophila dorsal air sac primordium. *Dev. Biol.* **287**, 192–200 (2005).
104. Harris-Johnson, K. S., Domyan, E. T., Vezina, C. M. & Sun, X. β-Catenin promotes respiratory progenitor identity in mouse foregut. *Proc. Natl. Acad. Sci. U. S. A.* **106**, 16287–16292 (2009).
105. Goss, A. M. *et al.* Wnt2/2b and β-Catenin Signaling Are Necessary and Sufficient to Specify Lung Progenitors in the Foregut. *Dev. Cell* **17**, 290–298 (2009).
106. Kneidinger, N. *et al.* Activation of the WNT/β-catenin pathway attenuates experimental emphysema. *Am. J. Respir. Crit. Care Med.* **183**, 723–733 (2011).
107. Jiang, Z. *et al.* A chronic obstructive pulmonary disease susceptibility gene, FAM13A, regulates protein stability of β-catenin. *Am. J. Respir. Crit. Care Med.* **194**, 185–197 (2016).
108. Baarsma, H. A. *et al.* Noncanonical WNT-5A signaling impairs endogenous lung repair in COPD. *J. Exp. Med.*

214, 143–163 (2017).
109. Semenov, M. V, Habas, R., MacDonald, B. T. & He, X. SnapShot: Noncanonical Wnt Signaling Pathways. *Cell* vol. 131 1378.e1-1378.e2 (2007).
110. van Amerongen, R. Alternative Wnt pathways and receptors. *Cold Spring Harb. Perspect. Biol.* **4**, a007914 (2012).
111. Yuzugullu, H. *et al.* Canonical Wnt signaling is antagonized by noncanonical Wnt5a in hepatocellular carcinoma cells. *Mol. Cancer* **8**, 90 (2009).
112. Bradley, E. W. & Drissi, M. H. WNT5A regulates chondrocyte differentiation through differential use of the CaN/NFAT and IKK/NF-κB pathways. *Mol. Endocrinol.* **24**, 1581–1593 (2010).
113. Yang, Y., Topol, L., Lee, H. & Wu, J. Wnt5a and Wnt5b exhibit distinct activities in coordinating chondrocyte proliferation and differentiation. *Development* vol. 130 1003–1015 (2003).
114. Park, H. W. *et al.* Alternative Wnt Signaling Activates YAP/TAZ. *Cell* **162**, 780–794 (2015).
115. Imajo, M., Miyatake, K., Iimura, A., Miyamoto, A. & Nishida, E. A molecular mechanism that links Hippo signalling to the inhibition of Wnt/β-catenin signalling. *EMBO J.* **31**, 1109–1122 (2012).
116. Barry, E. R. *et al.* Restriction of intestinal stem cell expansion and the regenerative response by YAP. *Nature* **493**, 106–110 (2013).
117. Seo, E. *et al.* SOX2 Regulates YAP1 to Maintain Stemness and Determine Cell Fate in the Osteo-Adipo Lineage. *Cell Rep.* **3**, 2075–2087 (2013).
118. Blauwkamp, T. A., Nigam, S., Ardehali, R., Weissman, I. L. & Nusse, R. Endogenous Wnt signalling in human embryonic stem cells generates an equilibrium of distinct lineage-specified progenitors. *Nat. Commun.* **3**, (2012).
119. Liu, A. *et al.* Wnt5a through noncanonical Wnt/JNK or Wnt/PKC signaling contributes to the differentiation of mesenchymal stem cells into type II alveolar epithelial cells in vitro. *PLoS One* **9**, (2014).
120. Mirzoyan, Z. *et al.* Drosophila melanogaster: A model organism to study cancer. *Frontiers in Genetics* vol. 10 (2019).
121. Prange, R. *et al.* A Drosophila model of cigarette smoke induced COPD identifies Nrf2 signaling as an expedient target for intervention. *Aging (Albany. NY).* **10**, 2122–2135 (2018).
122. Kallsen, K. *et al.* ORMDL deregulation increases stress responses and modulates repair pathways in Drosophila airways. *J. Allergy Clin. Immunol.* **136**, 1105–1108 (2015).
123. Bodenstein, D. The postembryonic development of Drosophila. in *Biology of Drosophila* 275–367 (1950).
124. Jayaram, S. A. *et al.* COPI vesicle transport is a common requirement for tube expansion in Drosophila. *PLoS One* **3**, (2008).
125. Grieder, N. C. *et al.* γCOP is required for apical protein secretion and epithelial morphogenesis in Drosophila melanogaster. *PLoS One* **3**, e3241 (2008).
126. Dong, B., Kakihara, K., Otani, T., Wada, H. & Hayashi, S. Rab9 and retromer regulate retrograde trafficking of luminal protein required for epithelial tube length control. *Nat. Commun.* **4**, (2013).
127. Ribeiro, C., Neumann, M. & Affolter, M. Genetic control of cell intercalation during tracheal morphogenesis in Drosophila. *Curr. Biol.* **14**, 2197–2207 (2004).
128. Shaye, D. D., Casanova, J. & Llimargas, M. Modulation of intracellular trafficking regulates cell intercalation in the Drosophila trachea. *Nat. Cell Biol.* **10**, 964–970 (2008).
129. Luschnig, S. & Uv, A. Luminal matrices: An inside view on organ morphogenesis. *Experimental Cell Research* vol. 321 64–70 (2014).
130. Chen, F. & Krasnow, M. A. Progenitor outgrowth from the niche in drosophila trachea is guided by FGF from decaying branches. *Science (80-.).* **343**, 186–189 (2014).
131. Manning, G. & Kasnow, M. Development of the Drosophila tracheal system. *The Development of Drosophila melanogaster Vol. 1* 609–685 (1993).
132. Weaver, M. & Krasnow, M. A. Dual origin of tissue-specific progenitor cells in Drosophila tracheal remodeling. *Science (80-.).* **321**, 1496–1499 (2008).
133. Pitsouli, C. & Perrimon, N. The homeobox transcription factor cut coordinates patterning and growth during drosophila airway remodeling. *Sci. Signal.* **6**, (2013).
134. Ugur, B., Chen, K. & Bellen, H. J. Drosophila tools and assays for the study of human diseases. *DMM Disease Models and Mechanisms* vol. 9 235–244 (2016).
135. Millburn, G. H. *et al.* Fly Base portals to human disease research using Drosophila Models. *DMM Dis. Model. Mech.* **9**, 245–252 (2016).
136. Chen, H. W. *et al.* mom identifies a receptor for the Drosophila JAK/STAT signal transduction pathway and encodes a protein distantly related to the mammalian cytokine receptor family. *Genes Dev.* **16**, 388–398 (2002).
137. Agaisse, H., Petersen, U. M., Boutros, M., Mathey-Prevot, B. & Perrimon, N. Signaling role of hemocytes

in Drosophila JAK/STAT-dependent response to septic injury. *Dev. Cell* **5**, 441–450 (2003).
138. Binari, R. & Perrimon, N. Stripe-specific regulation of pair-rule genes by hopscotch, a putative Jak family tyrosine kinase in Drosophila. *Genes Dev.* **8**, 300–312 (1994).
139. Hou, X. S., Melnick, M. B. & Perrimon, N. marelle acts downstream of the Drosophila HOP/JAK kinase and encodes a protein similar to the mammalian STATs. *Cell* **84**, 411–419 (1996).
140. Yan, R., Small, S., Desplan, C., Dearolf, C. R. & Darnell, J. E. Identification of a Stat gene that functions in Drosophila development. *Cell* **84**, 421–430 (1996).
141. Loganathan, R., Cheng, Y. L. & Andrew, D. J. Organogenesis of the Drosophila respiratory system. in *Organogenetic Gene Networks: Genetic Control of Organ Formation* 151–211 (Springer International Publishing, 2016). doi:10.1007/978-3-319-42767-6_6.
142. Andrew, D. J. & Ewald, A. J. Morphogenesis of epithelial tubes: Insights into tube formation, elongation, and elaboration. *Developmental Biology* vol. 341 34–55 (2010).
143. Behr, M. Molecular aspects of respiratory and vascular tube development. *Respiratory Physiology and Neurobiology* vol. 173 S33–S36 (2010).
144. Miguel, C., Cruz, J., Martín, D. & Franch-Marro, X. Dual role of FGF in proliferation and endoreplication of Drosophila tracheal adult progenitor cells. *J. Mol. Cell Biol.* 0 (2019) doi:10.1093/jmcb/mjz055.
145. Pitsouli, C. & Perrimon, N. Embryonic multipotent progenitors remodel the Drosophila airways during metamorphosis. *Development* **137**, 3615–3624 (2010).
146. Brand, A. H. & Perrimon, N. Targeted gene expression as a means of altering cell fates and generating dominant phenotypes. *Development* **118**, 401–415 (1993).
147. Del Valle Rodríguez, A., Didiano, D. & Desplan, C. Power tools for gene expression and clonal analysis in Drosophila. *Nature Methods* vol. 9 47–55 (2012).
148. Yoshida, T. & Tuder, R. M. Pathobiology of cigarette smoke-induced chronic obstructive pulmonary disease. *Physiol. Rev.* **87**, 1047–1082 (2007).
149. Jiang, X. *et al.* Effect of simvastatin on 5-HT and 5-HTT in a rat model of pulmonary artery hypertension. *Cell. Physiol. Biochem.* **37**, 1712–1724 (2015).
150. Yang, S.-R. *et al.* IKKα causes chromatin modification on pro-inflammatory genes by cigarette smoke in mouse lung. *Am. J. Respir. Cell Mol. Biol.* **38**, 689–698 (2008).
151. Bodas, M., Min, T. & Vij, N. Critical role of CFTR-dependent lipid rafts in cigarette smoke-induced lung epithelial injury. *Am. J. Physiol. Cell. Mol. Physiol.* **300**, L811–L820 (2011).
152. De Rose, V., Molloy, K., Gohy, S., Pilette, C. & Greene, C. M. Airway epithelium dysfunction in cystic fibrosis and COPD. *Mediators Inflamm.* **2018**, (2018).
153. Bach, E. A. *et al.* GFP reporters detect the activation of the Drosophila JAK/STAT pathway in vivo. *Gene Expr. Patterns* **7**, 323–331 (2007).
154. Brand, A. H. & Perrimon, N. Targeted gene expression as a means of altering cell fates and generating dominant phenotypes. *development* **118**, 401–415 (1993).
155. Olson, E. R. *et al.* Yan, an ETS-domain transcription factor, negatively modulates the Wingless pathway in the Drosophila eye. *EMBO Rep.* **12**, 1047–1054 (2011).
156. Brown, S., Hu, N. & Hombría, J. C.-G. Identification of the first invertebrate interleukin JAK/STAT receptor, the Drosophila gene domeless. *Curr. Biol.* **11**, 1700–1705 (2001).
157. Harrison, D. A., Binari, R., Nahreini, T. S., Gilman, M. & Perrimon, N. Activation of a Drosophila Janus kinase (JAK) causes hematopoietic neoplasia and developmental defects. *EMBO J.* **14**, 2857–2865 (1995).
158. Fuse, N., Yu, F. & Hirose, S. Gprk2 adjusts Fog signaling to organize cell movements in Drosophila gastrulation. *Dev.* **140**, 4246–4255 (2013).
159. Gibson, D. G. *et al.* Enzymatic assembly of DNA molecules up to several hundred kilobases. *Nat. Methods* **6**, 343–345 (2009).
160. Gibson, D. G., Smith, H. O., Hutchison, C. A., Venter, J. C. & Merryman, C. Chemical synthesis of the mouse mitochondrial genome. *Nat. Methods* **7**, 901–903 (2010).
161. Bownes, M. The Embryonic Development of Drosophila Melanogaster. Jose A. Campos-Ortega , Volker Hartenstein. *Q. Rev. Biol.* **61**, 404–404 (1986).
162. Levi, B. P., Ghabrial, A. S. & Krasnow, M. A. Drosophila talin and integrin genes are required for maintenance of tracheal terminal branches and luminal organization. *Development* **133**, 2383–2393 (2006).
163. Jeon, M., Nguyen, H., Bahri, S. & Zinn, K. Redundancy and compensation in axon guidance: genetic analysis of the Drosophila Ptp10D/Ptp4E receptor tyrosine phosphatase subfamily. *Neural Dev.* **3**, 3 (2008).
164. Patterson, R. A. *et al.* Serine Proteolytic Pathway Activation Reveals an Expanded Ensemble of Wound Response Genes in Drosophila. *PLoS One* **8**, e61773 (2013).
165. Kallsen, K. *et al.* ORMDL deregulation increases stress responses and modulates repair pathways in

Drosophila airways. *J. Allergy Clin. Immunol.* **136**, 1105–1108 (2015).
166. Martin, M. Cutadapt removes adapter sequences from high-throughput sequencing reads. *EMBnet. J.* **17**, 10–12 (2011).
167. Hoskins, R. A. *et al.* The Release 6 reference sequence of the Drosophila melanogaster genome. *Genome Res.* **25**, 445–458 (2015).
168. Shiga, Y., Tanaka-Matakatsu, M. & Hayashi, S. A nuclear GFP/β-galactosidase fusion protein as a marker for morphogenesis in living Drosophila. *Dev. Growth Differ.* **38**, 99–106 (1996).
169. Clemmons, A. W., Lindsay, S. A. & Wasserman, S. A. An effector peptide family required for Drosophila Toll-mediated immunity. *PLoS Pathog.* **11**, (2015).
170. Uttenweiler-Joseph, S. *et al.* Differential display of peptides induced during the immune response of Drosophila: A matrix-assisted laser desorption ionization time-of-flight mass spectrometry study. *Proc. Natl. Acad. Sci. U. S. A.* **95**, 11342–11347 (1998).
171. Glasheen, B. M., Robbins, R. M., Piette, C., Beitel, G. J. & Page-McCaw, A. A matrix metalloproteinase mediates airway remodeling in Drosophila. *Dev. Biol.* **344**, 772–783 (2010).
172. Oshima, K. & Fehon, R. G. Analysis of protein dynamics within the septate junction reveals a highly stable core protein complex that does not include the basolateral polarity protein Discs large. *J. Cell Sci.* **124**, 2861–2871 (2011).
173. Lock, J. G. & Stow, J. L. Rab11 in recycling endosomes regulates the sorting and basolateral transport of E-cadherin. *Mol. Biol. Cell* **16**, 1744–1755 (2005).
174. Tsarouhas, V. *et al.* Sequential Pulses of Apical Epithelial Secretion and Endocytosis Drive Airway Maturation in Drosophila. *Dev. Cell* **13**, 214–225 (2007).
175. Wagner, C. & Roeder, T. Infection induces a survival program and local remodeling in the airway epithelium of the fly. *Artic. FASEB J.* (2009) doi:10.1096/fj.08-114223.
176. Liu, L., Johnson, W. A. & Welsh, M. J. Drosophila DEG/ENaC pickpocket genes are expressed in the tracheal system, where they may be involved in liquid clearance. *Proc. Natl. Acad. Sci. U. S. A.* **100**, 2128–2133 (2003).
177. Thoennissen, N. H. *et al.* Cucurbitacin B induces apoptosis by inhibition of the JAK/STAT pathway and potentiates antiproliferative effects of gemcitabine on pancreatic cancer cells. *Cancer Res.* **69**, 5876–5884 (2009).
178. Diaz, T. *et al.* Lestaurtinib inhibition of the jak/stat signaling pathway in hodgkin lymphoma inhibits proliferation and induces apoptosis. *PLoS One* **6**, (2011).
179. Borensztejn, A., Mascaro, A. & Wharton, K. A. JAK/STAT signaling prevents excessive apoptosis to ensure maintenance of the interfollicular stalk critical for Drosophila oogenesis. *Dev. Biol.* **438**, 1–9 (2018).
180. Ohshiro, T. & Saigo, K. Transcriptional regulation of breathless FGF receptor gene by binding of TRACHEALESS/dARNT heterodimers to three central midline elements in Drosophila developing trachea. *Development* **124**, 3975–3986 (1997).
181. Jin, J. *et al.* Regulation of Drosophila Tracheal System Development by Protein Kinase B. *Dev. Cell* **1**, 817–827 (2001).
182. Du, L., Sohr, A., Yan, G. & Roy, S. Feedback regulation of cytoneme-mediated transport shapes a tissue-specific FGF morphogen gradient. *Elife* **7**, (2018).
183. Guan, X., Middlebrooks, B. W., Alexander, S. & Wasserman, S. A. Mutation of TweedleD, a member of an unconventional cuticle protein family, alters body shape in Drosophila. *Proc. Natl. Acad. Sci. U. S. A.* **103**, 16794–16799 (2006).
184. Roeder, T., Isermann, K. & Kabesch, M. Drosophila in asthma research. *American Journal of Respiratory and Critical Care Medicine* vol. 179 979–983 (2009).
185. Roeder, T., Isermann, K. & Kabesch, M. Drosophila in asthma research. *American Journal of Respiratory and Critical Care Medicine* vol. 179 979–983 (2009).
186. Bossen, J. *et al.* An EGFR-induced Drosophila lung tumor model identifies alternative combination treatments. *Mol. Cancer Ther.* **18**, 1659–1668 (2019).
187. Hombría, J. C.-G. & Sotillos, S. JAK-STAT pathway in Drosophila morphogenesis. *JAK-STAT* **2**, e26089 (2013).
188. Powers, N. & Srivastava, A. JAK/STAT signaling is involved in air sac primordium development of Drosophila melanogaster. *FEBS Letters* vol. 593 658–669 (2019).
189. Tadokoro, T. *et al.* IL-6/STAT3 promotes regeneration of airway ciliated cells from basal stem cells. *Proc. Natl. Acad. Sci. U. S. A.* **111**, (2014).
190. Piairo, P., Moura, R. S., Baptista, M. J., Correia-Pinto, J. & Nogueira-Silva, C. STATs in Lung Development: Distinct Early and Late Expression, Growth Modulation and Signaling Dysregulation in Congenital Diaphragmatic Hernia. *Cell. Physiol. Biochem.* **45**, 1–14 (2018).
191. Zheng, X. J. *et al.* Downregulation of leptin inhibits growth and induces apoptosis of lung cancer cells via

the Notch and JAK/STAT3 signaling pathways. *Biol. Open* **5**, 794–800 (2016).
192. Quinton, L. J. & Mizgerd, J. P. NF-κB and STAT3 signaling hubs for lung innate immunity. *Cell and Tissue Research* vol. 343 153–165 (2011).
193. Kida, H. *et al.* GP130-STAT3 regulates epithelial cell migration and is required for repair of the bronchiolar epithelium. *Am. J. Pathol.* **172**, 1542–1554 (2008).
194. Hokuto, I. *et al.* Stat-3 is required for pulmonary homeostasis during hyperoxia. *J. Clin. Invest.* **113**, 28–37 (2004).
195. Jiang, H. *et al.* Cytokine/Jak/Stat Signaling Mediates Regeneration and Homeostasis in the Drosophila Midgut. *Cell* **137**, 1343–1355 (2009).
196. Miguel-Aliaga, I., Jasper, H. & Lemaitre, B. Anatomy and physiology of the digestive tract of drosophila melanogaster. *Genetics* **210**, 357–396 (2018).
197. Zhang, X. *et al.* Orally bioavailable small-molecule inhibitor of transcription factor Stat3 regresses human breast and lung cancer xenografts. *Proc. Natl. Acad. Sci. U. S. A.* **109**, 9623–9628 (2012).
198. Dutta, P., Sabri, N., Li, J. & Li, W. X. Role of STAT3 in lung cancer. *JAK-STAT* **3**, e999503 (2014).
199. Sohal, S. S. & Walters, E. H. Role of epithelial mesenchymal transition (EMT) in chronic obstructive pulmonary disease (COPD). *Respiratory Research* vol. 14 1–3 (2013).
200. Kao, C.-Y. *et al.* IL-17 Markedly Up-Regulates β-Defensin-2 Expression in Human Airway Epithelium via JAK and NF-κB Signaling Pathways. *J. Immunol.* **173**, 3482–3491 (2004).
201. Fahy, J. V. & Dickey, B. F. Medical progress: Airway mucus function and dysfunction. *New England Journal of Medicine* vol. 363 2233–2247 (2010).
202. Gon, Y. & Hashimoto, S. Role of airway epithelial barrier dysfunction in pathogenesis of asthma. *Allergology International* vol. 67 12–17 (2018).
203. Heijink, I. H., Brandenburg, S. M., Postma, D. S. & Van Oosterhout, A. J. M. Cigarette smoke impairs airway epithelial barrier function and cell-cell contact recovery. *Eur. Respir. J.* **39**, 419–428 (2012).
204. Georas, S. N. & Rezaee, F. Epithelial barrier function: at the front line of asthma immunology and allergic airway inflammation. *The Journal of allergy and clinical immunology* vol. 134 509–520 (2014).
205. Andrew, D. J. & Ewald, A. J. Morphogenesis of epithelial tubes: Insights into tube formation, elongation, and elaboration. *Developmental Biology* vol. 341 34–55 (2010).
206. Bergman, P., Seyedoleslami Esfahani, S. & Engström, Y. Drosophila as a Model for Human Diseases—Focus on Innate Immunity in Barrier Epithelia. in *Current Topics in Developmental Biology* vol. 121 29–81 (2017).
207. Prange, R. *et al.* A Drosophila model of cigarette smoke induced COPD identifies Nrf2 signaling as an expedient target for intervention. *Aging (Albany. NY).* **10**, 2122–2135 (2018).
208. Levine, B. D. & Cagan, R. L. Drosophila Lung Cancer Models Identify Trametinib plus Statin as Candidate Therapeutic. *Cell Rep.* **14**, 1477–1487 (2016).
209. Almqvist, C. *et al.* ORMDL deregulation increases stress responses and modulates repair pathways in Drosophila airways. *J. Allergy Clin. Immunol.* **136**, 1105–1108 (2015).
210. Roeder, T., Isermann, K., Kallsen, K., Uliczka, K. & Wagner, C. A Drosophila asthma model - What the fly tells us about inflammatory diseases of the lung. *Adv. Exp. Med. Biol.* **710**, 37–47 (2012).
211. Bausek, N. JAK-STAT signaling in stem cells and their niches in Drosophila. *JAK-STAT* **2**, e25686 (2013).
212. Osman, D. *et al.* Autocrine and paracrine unpaired signaling regulate intestinal stem cell maintenance and division. *J. Cell Sci.* **125**, 5944–5949 (2012).
213. Brown, S., Hu, N. & Hombría, J. C. G. Identification of the first invertebrate interleukin JAK/STAT receptor, the Drosophila gene domeless. *Curr. Biol.* **11**, 1700–1705 (2001).
214. Sotillos, S., Espinosa-Vázquez, J. M., Foglia, F., Hu, N. & Hombría, J. C. G. An efficient approach to isolate STAT regulated enhancers uncovers STAT92E fundamental role in Drosophila tracheal development. *Dev. Biol.* **340**, 571–582 (2010).
215. Li, J. *et al.* Patterns and functions of STAT activation during Drosophila embryogenesis. *Mech. Dev.* **120**, 1455–1468 (2003).
216. Miguel, C., Cruz, J., Martín, D. & Franch-Marro, X. Dual role of FGF in proliferation and endoreplication of Drosophila tracheal adult progenitor cells. *J. Mol. Cell Biol.* (2019) doi:10.1093/jmcb/mjz055.
217. Hogg, J. C. Pathophysiology of airflow limitation in chronic obstructive pulmonary disease. in *Lancet* vol. 364 709–721 (2004).
218. Nusse, R. Wnt signaling in disease and in development. *Cell Research* vol. 15 28–32 (2005).
219. Königshoff, M. & Eickelberg, O. WNT signaling in lung disease: A failure or a regeneration signal? *American Journal of Respiratory Cell and Molecular Biology* vol. 42 21–31 (2010).
220. Fukuhara, S., Chikumi, H. & Gutkind, J. S. Leukemia-associated Rho guanine nucleotide exchange factor (LARG) links heterotrimeric G proteins of the G12 family to Rho. *FEBS Lett.* **485**, 183–188 (2000).
221. BISHOP, A. L. & HALL, A. Rho GTPases and their effector proteins. *Biochem. J.* **348**, 241–255 (2000).

222. Ripp, C. *et al.* Drosophila Ror is a nervous system-specific co-receptor for Wnt ligands. *Biol. Open* **7**, (2018).
223. Borcherding, N., Kusner, D., Liu, G. H. & Zhang, W. ROR1, an embryonic protein with an emerging role in cancer biology. *Protein Cell* **5**, 496–502 (2014).
224. Grumolato, L. *et al.* Canonical and noncanonical Wnts use a common mechanism to activate completely unrelated coreceptors. *Genes Dev.* **24**, 2517–2530 (2010).
225. Ren, W. *et al.* Windpipe Controls Drosophila Intestinal Homeostasis by Regulating JAK/STAT Pathway via Promoting Receptor Endocytosis and Lysosomal Degradation. *PLoS Genet.* **11**, e1005180 (2015).
226. Overholtzer, M. *et al.* Transforming properties of YAP, a candidate oncogene on the chromosome 11q22 amplicon. *Proc. Natl. Acad. Sci. U. S. A.* **103**, 12405–12410 (2006).
227. Huang, J., Wu, S., Barrera, J., Matthews, K. & Pan, D. The Hippo signaling pathway coordinately regulates cell proliferation and apoptosis by inactivating Yorkie, the Drosophila homolog of YAP. *Cell* **122**, 421–434 (2005).
228. Student, P. D. & Benazzo, A. ISCRA Application form Curriculum Vitae. *Mol. Biol. Evol* **23**, 1–7 (2010).

Apendix

Regulated genes of trachea that expressed *hop.CA* for 16h.

Name	Max group mean	Fold change	FDR p-value
CG16772	11.854724	135.435692	0.000000
hop	286.064080	35.429577	0.000000
CG14570	42.209965	35.369849	0.000000
CG14147	55.309405	32.876797	0.000000
Hsp70Bb	161.511126	29.985302	0.000000
Ubx	200.458819	23.510894	0.000000
CG14569	1576.880077	14.725752	0.000000
CG9121	3.412245	11.539623	0.000000
CG31960	267.264581	10.047929	0.000000
Ace	2.056513	8.187697	0.000000
CG31809	8.642529	7.388263	0.000000
wb	7.354562	6.689915	0.000000
Drs	8166.473129	6.635791	0.000000
fuss	3.973734	5.673577	0.000000
Cyp4d21	45.696140	5.308509	0.000000
CG5888	68.163025	5.201444	0.000000
CG8785	136.298256	4.458476	0.000000
Cadps	5.524383	3.897700	0.000000
Klp54D	18.833178	3.716956	0.000000
GstD9	56.870065	3.710962	0.000000
CG8665	40.234016	3.601481	0.000000
CG33169	53.910223	3.449518	0.000000
IP3K2	38.951190	3.418464	0.000000
CG5618	17.688615	3.387744	0.000000
dome	65.400962	3.195578	0.000000
CG17931	31.349028	3.178920	0.000000
18w	73.379610	3.098589	0.000000
CG1888	7.964757	3.082247	0.000000
Arc1	1138.103362	3.000099	0.000000
rau	14.519143	2.993672	0.000000
Sgt1	75.257539	2.963803	0.000000
CG31370	18.670205	2.898682	0.000000
CG6753	50.706373	2.840493	0.000000
osp	18.121932	2.811527	0.000000
CG33939	88.486758	2.739233	0.000000
ImpL2	105.713953	2.728543	0.000000
Socs36E	69.101575	2.718119	0.000000
CG14439	37.844464	-2.494412	0.000000
CG4300	23.775793	-2.575114	0.000000
CG17026	45.221460	-2.589154	0.000000
CG10311	51.352459	-2.695897	0.000000
CG14304	9.051145	-2.756092	0.000000
spel1	6.621450	-2.810730	0.000000
CG7402	65.704608	-2.827244	0.000000
CycB3	11.532503	-2.859139	0.000000
l(2)efl	131.475752	-3.037773	0.000000
CG4267	17.806650	-3.116341	0.000000
Pif1B	15.027811	-3.121636	0.000000
Hsp70Ab	12.086546	-3.134836	0.000000
CG40486	138.257301	-3.208869	0.000000
CG2016	40.008943	-3.210035	0.000000
CG4630	7.806743	-3.285255	0.000000
CG13044	2246.898811	-3.337172	0.000000
CG12880	12.742673	-3.344687	0.000000
CG17108	67.427967	-3.367940	0.000000
CG31313	435.133499	-3.447822	0.000000
CG10365	14.906757	-3.474743	0.000000
CG7497	54.222859	-3.576049	0.000000
GstT4	71.602532	-3.757575	0.000000
Cyp313a4	25.275761	-3.763362	0.000000
Cpr49Ah	218.366005	-3.889471	0.000000
St4	59.408589	-3.938712	0.000000
Pxd	92.637901	-4.134562	0.000000
CG32091	10.330166	-4.598884	0.000000
TwdlT	47.883608	-4.779702	0.000000
shf	9.771067	-4.868660	0.000000
CG40472	60.541488	-4.873136	0.000000
CG34305	343.222014	-5.090618	0.000000
Kif3C	2.770395	-5.224220	0.000000
pip	4.147840	-5.610002	0.000000
PGRP-SA	68.285490	-5.765730	0.000000
Alp4	15.071432	-6.383382	0.000000
AANATL2	40.766581	-7.153932	0.000000
CG42822	49.513917	-9.294354	0.000000
CG7888	10.018308	-10.324450	0.000000
CG9509	9.622277	-12.041928	0.000000
CG13639	100.942179	-18.042578	0.000000
CG34327	44.712987	-42.520124	0.000000
CG10581	21.035419	-84.806824	0.000000
Jhl-21	31.556438	2.668225	0.000000
Sry-delta	20.217111	2.385151	0.000000
CG13679	68.813927	-3.131506	0.000000
CG4914	17.964918	-3.155866	0.000000
CG16798	9.124597	-3.942597	0.000000
CG18278	7.508935	-5.837595	0.000000
CG15497	6.095070	-10.594500	0.000000
CG14275	33.433070	3.319846	0.000000
CG11550	36.415996	-2.822174	0.000000
fau	120.610360	-3.094293	0.000000
CG6845	13.493134	2.643726	0.000000
CG1418	32.876999	2.264537	0.000000
CG14356	57.631490	-3.010943	0.000000
CG13042	18.287726	-7.251824	0.000000
Cyp312a1	38.632944	-2.726693	0.000000
CG14567	108.577458	2.520129	0.000000
CG14401	20.218391	-2.560428	0.000000
Sulf1	5.107241	-3.687210	0.000000
CG43693	3.525883	-7.154876	0.000000
Snoo	8.492142	-2.558064	0.000000
CG15629	152.191155	3.958465	0.000000
Lst	37.603062	-2.864281	0.000000
CG6293	3.488642	-6.735744	0.000000
CG45069	5.822081	-4.466864	0.000000
CG10232	217.903101	2.782978	0.000000
CG9449	105.054238	-3.124522	0.000000
CG13101	126.719703	2.748773	0.000000
Snmp1	7.091945	-3.595888	0.000000
CG45095	9.197982	-7.511155	0.000000
Dmtn	32.223071	2.187606	0.000000
Best1	21.943737	-2.346415	0.000000
MFS14	36.041291	2.452892	0.000000
CG12288	13.756708	-2.544275	0.000000
pwn	41.816296	2.544868	0.000000
CG2121	42.174373	-2.322638	0.000000
CG13640	206.600612	-3.768879	0.000000
Acp65Aa	26.569155	-5.189508	0.000000
IM4	26.426644	14.973156	0.000000
CG1265	40.959128	-2.728833	0.000000
GstD6	7.380641	-18.981786	0.000000
geko	74.087401	2.169597	0.000000
Cyp12a4	11.081276	-4.230509	0.000000
caix	1362.473877	-4.983557	0.000000
obst-B	304.799818	-2.850874	0.000000
QC	147.259184	2.872641	0.000000
Ucp4B	3.597695	-25.800969	0.000000
CG14880	5.165499	-4.937949	0.000000

CG14301	12.351209	-2.790221	0.000000
CkIIalpha-i3	14.950945	2.744750	0.000000
ppk22	7.026391	-6.868606	0.000000
MFS3	301.176725	3.231625	0.000000
pre-mod(mdg4)-AD	3.005253	-11.500547	0.000000
CG32719	2.083357	-7.909394	0.000000
CG9257	30.082111	2.271450	0.000000
NT1	1.971373	-6.445788	0.000000
Cpr65Au	337.406811	-6.564471	0.000000
Mgat2	45.735305	2.906197	0.000000
Buffy	30.363306	-2.221109	0.000000
Dif	30.427112	2.195793	0.000000
pigs	5.107064	-2.650240	0.000000
sel	95.212248	2.143766	0.000000
Cyp301a1	62.266162	2.171914	0.000000
CG6034	6.915089	8.468388	0.000000
CG4000	307.931159	-5.177909	0.000000
CG1461	8.990483	-3.236138	0.000000
CG4455	85.592441	2.256094	0.000000
Gbs-76A	5.941284	-2.537584	0.000000
gpp	5.808390	-2.284411	0.000000
CG17104	11.275269	-2.754820	0.000000
CG40439	126.882010	2.095604	0.000000
CG7227	7.407010	-3.988884	0.000000
mino	11.698176	-2.057640	0.000000
Lsd-1	23.120488	-2.914862	0.000000
CngA	18.101353	-2.508266	0.000000
Osi9	16.087569	-2.616305	0.000000
CG7860	28.032689	-2.921367	0.000000
FASN2	1.651228	5.340581	0.000000
jumu	8.103262	-2.536514	0.000000
GMF	26.171705	-2.182220	0.000000
robo2	29.357055	2.241004	0.000000
CG14566	1767.781053	2.931409	0.000000
CG7378	7.149757	-3.306359	0.000000
Cyp318a1	59.741204	-2.130868	0.000000
CG8654	102.917858	2.599393	0.000000
Tsp29Fb	16.966577	-2.349675	0.000000
Hmgcr	489.274922	2.510333	0.000000
Acf	2.913585	-3.119116	0.000000
Cyp6a2	5.610124	-5.355657	0.000000
CG10962	44.845120	-2.862907	0.000000
CG10089	3.519784	3.449613	0.000000
NaPi-III	134.065910	3.074924	0.000000
Atg1	18.627009	2.215009	0.000000
CNPYb	38.426782	1.915724	0.000000
CG13063	1371.521319	-3.867161	0.000000
CG13297	21.927454	-5.773767	0.000000
CG42749	47.927688	-2.034384	0.000000
CG43333	2.390924	5.632144	0.000000
AOX2	38.954312	-2.590335	0.000000
CG4666	12.627466	-3.016958	0.000000
CG32808	9.575243	-3.822539	0.000000
C901	3.303082	-7.040365	0.000000
Rich	14.582196	2.080905	0.000000
CG13369	32.824160	2.133712	0.000000
Hex-A	75.637017	2.227498	0.000000
CG5171	3.882869	-6.089206	0.000000
CG10623	14.162865	-2.578487	0.000000
CG9747	25.506766	2.301369	0.000000
CG45087	67.317418	2.510957	0.000000
AdoR	16.072154	-2.216576	0.000000
CG16789	1.452008	9.460811	0.000000
sals	7.369046	-2.869830	0.000000
Osi24	14.536810	2.028875	0.000000
CG30059	4.341070	-6.703428	0.000000
Zasp66	63.561325	-2.719463	0.000000

inv	1.806076	-3.884701	0.000000
Antp	8.821283	-2.180641	0.000000
yellow-d2	51.764431	-4.368065	0.000000
CG8560	37.412688	-2.244099	0.000000
spok	5.326661	-122.089270	0.000000
CG7203	9.406607	7.213890	0.000000
CG9737	17.901852	2.839530	0.000000
CG15715	52.116958	1.864194	0.000000
CG2930	15.686047	-2.223602	0.000000
grk	6.308052	-3.408313	0.000000
Ude	147.530633	-2.171016	0.000000
CG30197	124.233831	-2.185062	0.000000
dmGlut	8.431542	-2.785022	0.000000
CG1416	94.466632	2.120169	0.000000
phm	3.261333	-48.732225	0.000000
Grip	4.818285	2.678211	0.000000
CG11537	49.370693	2.056371	0.000000
CG13674	32.577387	-4.227086	0.000000
CG10005	33.400631	-2.333977	0.000000
GlcAT-S	33.051430	2.294892	0.000000
CG10764	16.984019	3.086586	0.000000
pdm3	1.587068	-5.267677	0.000000
l(3)mbn	53.958537	-2.317591	0.000000
Vps24	19.993250	-1.951122	0.000000
CG17600	30.379672	2.080917	0.000000
Cyp6d4	18.617712	-2.039536	0.000000
CG6084	155.546595	2.074643	0.000000
Cyp12e1	66.154373	-1.908165	0.000000
Efa6	20.029989	2.105067	0.000000
CG2310	24.571156	-2.015084	0.000000
CG10802	19.983299	2.011086	0.000000
CG5866	12.324439	-15.458414	0.000000
CG45076	48.509493	-2.926869	0.000000
Lcp65Ad	9.932205	5.792568	0.000000
CG13796	15.271770	-4.674285	0.000000
CG7011	52.771130	1.986896	0.000000
Pepck	67.432615	2.468207	0.000000
Act87E	230.839122	-3.518488	0.000000
CG17027	18.879186	-2.964287	0.000000
Cpr97Ea	120.990553	-2.561019	0.000000
Est-P	14.680913	-4.764686	0.000000
CG9338	296.365476	-2.189667	0.000000
CG42259	44.890190	-1.877457	0.000000
bbg	18.658930	2.001460	0.000000
nw	299.842208	-2.851993	0.000000
CG5646	8.198951	3.310238	0.000000
Ccp84Ab	361.910281	-3.076009	0.000000
CG13041	5.232770	-12.472597	0.000000
CG17036	6.836976	-3.191391	0.000000
CG7772	24.999034	-2.113117	0.000000
CNT2	3.061189	-4.811475	0.000000
SelD	80.262844	2.061837	0.000000
tkv	25.157259	-1.987864	0.000000
CG4607	24.745516	-2.042246	0.000000
CycB	15.846751	-1.973875	0.000000
CG46317	9.389722	-3.169741	0.000000
CG7720	57.137171	2.149868	0.000000
CG11854	315.385834	-4.035246	0.000000
Ilp2	10.035876	-4.729992	0.000000
Wsck	16.708293	1.823662	0.000000
CG34347	16.315278	1.943363	0.000000
CG15210	21.295468	-2.725928	0.000000
CG1827	17.820297	-2.267353	0.000000
maf-S	45.995288	1.904597	0.000000
Lcp4	14147.871787	-2.291050	0.000000
CRMP	9.335336	-2.227406	0.000000
ck	7.360069	1.935938	0.000000
ArfGAP1	47.904889	1.845626	0.000000
NLaz	20.806583	-2.285907	0.000000

foi	61.924748	1.936328	0.000000
CG17572	4.982425	-4.730716	0.000000
CG8320	46.150245	1.853542	0.000000
CG18258	5.127136	4.729961	0.000000
Mal-A5	9.697340	-2.945478	0.000000
CG44245	120.452392	-2.754219	0.000000
CG16710	2.132413	10.320265	0.000000
mre11	14.640960	-1.885268	0.000000
Tsf3	276.271478	2.316150	0.000000
RIC-3	11.321183	-2.881885	0.000000
Vha14-2	2.510881	7.050882	0.000000
CG30148	4.554450	-5.181749	0.000000
CG32407	23.368756	-2.005347	0.000000
lawc	9.608159	1.922476	0.000000
Nse4	6.444369	3.797120	0.000000
mu2	6.982018	2.270676	0.000000
Tsp42Ek	15.614922	-2.605852	0.000000
CG44215	22.570158	-3.214791	0.000000
l(2)41Ab	5.232879	2.791911	0.000000
CG2200	35.028958	1.881045	0.000000
CG5162	2395.220141	2.302364	0.000000
CycA	25.638732	-1.924835	0.000000
CG8888	57.872115	-2.658983	0.000000
Hsp23	75.929180	3.670432	0.000000
CG11413	35.699607	10.636368	0.000000
Cpr100A	382.150327	-2.666982	0.000000
CG12290	9.365540	2.168325	0.000000
fax	39.711337	-2.303539	0.000000
CG12075	30.850652	-1.964802	0.000000
IM14	11.457826	15.135465	0.000000
Cpr92F	510.161732	-2.440768	0.000000
Sodh-2	72.735388	-1.996133	0.000000
CG31689	50.021919	2.399693	0.000000
Neurochondrin	24.940820	-3.072541	0.000000
CG5599	25.388109	1.932667	0.000000
CG8620	5.974228	-5.972863	0.000000
Adgf-C	18.644474	-2.259531	0.000000
borr	14.862451	-2.281898	0.000000
CG9304	25.629147	1.844849	0.000001
Cpr67B	149.401940	-2.167126	0.000001
Cyp4e1	4.886522	-4.050757	0.000001
CG15485	1.907813	-11.949326	0.000001
CG13043	1370.536940	-2.951858	0.000001
CG14095	30.937726	-4.069729	0.000001
Dgp-1	16.413673	1.792863	0.000001
Jheh1	58.508227	-1.969074	0.000001
Mlc2	1314.583559	-3.249296	0.000001
mth	42.947499	1.865679	0.000001
CG15362	14.989688	2.654889	0.000001
CG31729	46.757028	1.881828	0.000001
CG33521	15.264348	-2.231380	0.000001
path	59.875830	1.923165	0.000001
Hsp68	20.123937	-3.802880	0.000001
Gk2	12.954950	-1.938024	0.000001
CG7530	23.513272	1.920043	0.000001
Cpr78E	446.195858	-6.181515	0.000001
CG33178	42.313791	-2.254232	0.000001
Cyp9h1	2.886027	-5.019208	0.000001
CG16786	49.007360	-1.887535	0.000001
CG13059	9.898481	7.578676	0.000001
CG42500	520.373190	-6.160848	0.000001
Cda5	10.497338	-2.071997	0.000001
Spn77Bc	10.679456	3.037445	0.000001
CG43103	41.677553	2.381856	0.000001
Lcp2	2306.588339	-2.464167	0.000001
CG43394	17.244797	-1.730365	0.000001
CG30154	214.183574	-1.809992	0.000001
Cpr67Fb	12.003930	-4.034271	0.000001
spg	3.362159	2.034461	0.000001

Cyp4g1	59.236076	4.571334	0.000002
Gs2	1493.034191	-2.584441	0.000002
CG3770	30.334039	-1.730908	0.000002
CG3386	9.164331	2.227648	0.000002
NimC2	1.669399	-4.976867	0.000002
drongo	48.180021	1.887031	0.000002
Slc45-1	7.066684	-2.182019	0.000002
Spindly	7.811678	-2.032824	0.000002
Dp1	177.563348	2.124982	0.000002
Arc2	45.881231	1.829796	0.000002
CG3226	87.187367	1.800447	0.000002
agt	7.034721	-2.869467	0.000002
CG4576	17.473687	-2.269909	0.000002
Oatp30B	35.412638	1.802592	0.000002
CG3847	41.927069	1.712528	0.000002
haf	17.902549	-2.208780	0.000002
CrzR	1.597155	-8.680843	0.000002
TM9SF4	36.389417	1.770304	0.000002
IM2	7.261320	14.471416	0.000002
CG33333	30.706674	-32.989606	0.000002
kek1	9.110679	2.063914	0.000002
SpdS	27.441089	-1.768337	0.000002
pre-mod(mdg4)-I	1.124682	18.667592	0.000002
CG13069	79.196290	-4.183332	0.000002
Cyp6a17	7.291486	-3.198888	0.000002
CG42709	16.994803	-1.686202	0.000002
CG3457	2.693961	6.337465	0.000002
CG5177	276.874213	-2.831410	0.000002
heix	15.678337	1.680871	0.000003
Glycogenin	47.087301	-2.267798	0.000003
CG14879	16.980478	2.109971	0.000003
CG10570	22.860715	-2.372522	0.000003
CG5254	19.638108	-1.919620	0.000003
vas	1.305617	-31.784214	0.000003
Gcn2	7.093201	1.897144	0.000003
Pu	28.455800	1.897927	0.000003
GstE14	5.667583	-3.903620	0.000003
CG6310	58.955107	1.957607	0.000003
GstE3	50.346337	-1.909243	0.000003
CG11275	38.347922	1.891183	0.000003
CHORD	33.766182	1.743484	0.000003
Vha36-3	24.004213	-1.912607	0.000003
CG4962	3505.124505	-2.554620	0.000003
Jupiter	25.909525	-1.792937	0.000004
drm	9.402490	-2.124209	0.000004
CG6565	14.325495	1.693554	0.000004
cbt	24.973417	1.802290	0.000004
CG13047	137.031821	-2.909245	0.000004
CG17646	39.338505	-2.034489	0.000004
CG40485	2.309244	-6.919822	0.000004
pAbp	640.419416	2.021439	0.000004
CG34398	33.364859	2.005456	0.000004
CG13403	75.011510	-2.213941	0.000004
CG11377	30.268726	1.691950	0.000004
CG15225	32.615146	-4.046751	0.000004
CG30151	47.458091	1.853687	0.000004
Dlip2	15.568268	2.434547	0.000005
Cyp6a8	2.957691	-11.002171	0.000005
Hsp70Ba	0.771236	-10.879155	0.000005
CG1368	639.037584	-2.894093	0.000005
HmgZ	211.509207	-1.963115	0.000006
l(2)34Fc	5056.003286	1.982780	0.000006
CG3009	18.204606	-1.696052	0.000006
CG32564	545.312256	2.177726	0.000006
CG34208	40.828198	-3.242737	0.000006
Lcp65Ac	559.393850	-2.346058	0.000006
CG18067	29.344332	-1.927487	0.000006
ect	11.845695	-3.355384	0.000007

CG8492	196.845986	3.599732	0.000007
lectin-22C	29.061485	5.674131	0.000007
CG34199	9.420678	-9.702194	0.000007
CG8736	544.048795	-2.735463	0.000007
CG32276	508.163421	2.061002	0.000007
CG7900	76.205714	-1.825629	0.000007
glob1	95.844979	-1.853514	0.000008
CG9914	119.787222	-1.823744	0.000008
ImpL3	102.880883	-2.204942	0.000008
Tsp42Eh	4.186599	-6.154247	0.000008
Cdk1	26.914334	-1.865303	0.000009
pgant2	12.927212	-1.765233	0.000009
Ret	2.662078	2.603055	0.000010
rn	2.306576	-3.187416	0.000010
Cat	1197.615887	1.982710	0.000011
Hmgs	42.238579	1.750325	0.000011
scat	15.166172	1.739356	0.000011
yellow-h	15.202220	1.917735	0.000011
atilla	208.784785	-1.767101	0.000011
CG14572	3157.958662	1.990943	0.000011
thw	6.873346	-2.388404	0.000012
twz	1.490501	-5.304685	0.000012
Dsp1	33.549945	-1.744730	0.000012
tsh	4.848419	-2.386219	0.000012
Ipp	28.948549	1.753173	0.000012
GstS1	101.555640	1.900878	0.000013
GM130	29.728023	1.684735	0.000013
c11.1	11.146557	1.724327	0.000013
UbcE2H	23.707234	1.781621	0.000013
TRAM	201.805188	2.112497	0.000013
CG10205	35.123140	-2.017131	0.000013
mbl	4.271190	-1.826580	0.000013
Hsp60A	268.907968	2.039425	0.000013
Ndae1	4.024469	1.986433	0.000013
tok	3.592946	-3.132552	0.000014
Cpr97Eb	112.044395	-2.657088	0.000014
RpS5b	3.237232	-13.209875	0.000014
Oaz	4.800478	2.008786	0.000014
CG3902	155.206444	2.007050	0.000014
St1	12.199834	-2.150758	0.000015
CG2233	28.689371	-2.810457	0.000015
CG43781	54.833448	-1.651018	0.000015
Cpr49Ac	14.571560	-3.060899	0.000015
CG3700	32.251597	-1.772327	0.000016
Ufm1	111.231482	1.730451	0.000016
CG4822	7.092118	-1.956889	0.000017
CG11658	7.094260	2.262345	0.000017
MESR3	26.929699	1.901360	0.000017
lds	12.969511	-1.666497	0.000018
barc	23.157477	1.715728	0.000018
AGBE	68.248475	-1.773786	0.000018
CG10098	48.675451	1.782374	0.000019
ko	36.335676	-1.867927	0.000020
CG42806	17.347564	-2.283597	0.000020
CG13671	13.949500	1.704819	0.000020
CG9471	39.161065	-1.829487	0.000021
HmgD	291.992196	-2.045606	0.000021
Osi19	1.449217	-12.964818	0.000021
Dbi	115.202123	-1.964992	0.000021
CG13051	153.693699	-3.454835	0.000022
Rh50	3.190264	-2.600659	0.000023
CysRS	38.614719	1.665223	0.000023
Plc21C	5.837516	-1.636623	0.000024
kcc	4.918290	-1.964328	0.000025
CG16799	8.084936	-2.350345	0.000027
SclA	71.858315	-2.427202	0.000028
CG1943	147.408900	1.744725	0.000029
CG32249	2025.476851	-3.294426	0.000029
CG5791	1.786460	13.802675	0.000029
stan	1.247581	-2.265652	0.000030
alpha-Est8	203.100575	2.030569	0.000030
ckd	73.942566	-1.829451	0.000030
ap	4.839601	-2.857413	0.000030
CG13678	3499.717546	-2.339836	0.000030
CG7432	13.910441	1.986630	0.000031
Gbs-70E	5.805179	1.978583	0.000032
CG7556	37.129575	1.665147	0.000032
CG11306	44.357195	1.655861	0.000032
CG42502	22.505339	-2.198988	0.000032
APC7	1.274463	-7.824859	0.000032
CG45078	27.812744	-2.616292	0.000033
CG5597	18.869867	-2.693724	0.000033
pav	11.906725	-1.968687	0.000034
CG15308	658.114629	-2.563423	0.000034
CG9782	128.687433	-1.767886	0.000034
CG11576	24.588417	1.691539	0.000034
jv	18.775162	1.704605	0.000035
CG42562	31.415434	-2.229365	0.000035
TpnC25D	9.355681	-3.902823	0.000035
CG3097	78.380310	-1.692443	0.000036
GILT3	6.156812	-4.253058	0.000036
CG31102	22.926360	-1.678406	0.000036
CG42336	46.958280	1.713731	0.000038
x16	57.243615	-1.669823	0.000039
CG7997	8.660442	-3.095369	0.000039
Tet	2.632079	-2.056748	0.000040
CG14770	33.213912	-5.157553	0.000041
Phk-3	1649.866267	1.944411	0.000042
Argk	429.850213	-2.659739	0.000043
ncd	10.332523	-1.771177	0.000043
pch2	11.440998	-1.977401	0.000043
CG6012	22.079692	-2.105902	0.000044
garz	13.834061	1.719567	0.000044
CG43780	54.120197	-1.660173	0.000045
Lcp1	4510.011959	-2.446887	0.000045
nub	2.444930	-3.095181	0.000046
Cyp313a3	35.174534	-1.865378	0.000048
mlt	22.108464	1.776555	0.000049
rut	11.194335	1.699743	0.000049
alpha-Est5	7.064135	2.023015	0.000051
GABPI	24.926015	1.662457	0.000052
CG9413	4.327959	-2.534446	0.000052
CG6739	241.967922	2.492256	0.000054
CG33230	11.875009	1.792775	0.000054
CG30463	5.472097	-1.820023	0.000054
CG18336	2.963053	5.485480	0.000055
CG15611	143.947911	1.681566	0.000057
Incenp	12.708909	-1.940944	0.000057
PAPLA1	18.718168	1.703538	0.000058
Mlp60A	76.210545	-2.878989	0.000058
Hsp22	1.542377	4.917111	0.000058
Cralbp	3.371441	-5.736289	0.000058
Dcp-1	5.784766	-2.378605	0.000058
Nep2	15.908687	1.651459	0.000059
Zip48C	31.514923	1.890449	0.000061
Mlp84B	71.861278	-2.401647	0.000061
CG5381	33.203750	-1.644807	0.000062
CG13630	52.832599	-1.677257	0.000062
CG32369	5.696091	1.700528	0.000062
bnb	415.212465	2.276900	0.000063
CG9095	14.252281	-1.939226	0.000063
feo	13.430429	-1.786192	0.000064
qkr58E-3	50.228440	-1.660729	0.000065
CG10420	17.551221	1.595172	0.000066
Cpr	90.976551	1.833916	0.000066
CG6299	22.246894	1.678841	0.000068
GstD10	15.039428	-2.368708	0.000069
CG3108	0.688716	-5.572575	0.000071

Sec61beta	445.750027	1.837771	0.000071
CG15011	8.694877	1.808208	0.000073
CG2224	10.680015	1.782529	0.000074
tun	5.716369	1.650033	0.000074
CG4702	7.610297	-2.900665	0.000074
IM1	7.159415	10.973066	0.000075
CG9119	39.596884	1.665553	0.000076
CG15343	9.173299	-2.605048	0.000076
nAChRalpha4	1.932567	2.462985	0.000076
CG7280	13.739361	1.643876	0.000076
CG31999	51.822055	1.669559	0.000077
veli	25.880371	1.645584	0.000077
CG1674	35.558554	-2.240662	0.000080
CG32170	43.690981	1.620118	0.000081
CG6912	13.811780	-1.750684	0.000081
Gal	30.031881	-1.903569	0.000082
CG9757	320.842077	-2.371342	0.000082
CG8129	1.133215	-9.162593	0.000083
Mpc1	68.891373	1.716073	0.000084
Klp64D	18.435375	1.599228	0.000085
CG15747	8.745997	1.778455	0.000086
CG13983	2.297060	-48.871048	0.000087
CG11155	6.475685	-1.633755	0.000088
Cyp4e3	4.627238	-3.458744	0.000088
CG7872	28.873197	1.578868	0.000088
armi	11.205414	1.671794	0.000091
CG6145	16.837079	-1.703853	0.000091
neo	8.760494	-2.200850	0.000091
Dscam1	5.132669	1.740682	0.000092
Egm	20.113722	1.665245	0.000092
Timp	5.783033	-2.517396	0.000092
sls	4.952237	-2.059482	0.000093
CG43668	6.139819	-8.592015	0.000093
zld	13.547957	1.723161	0.000093
Tep4	296.732014	1.980058	0.000095
CG11555	31.443577	-1.660309	0.000096
CG6923	6.303302	1.775994	0.000096
LanB2	19.695562	1.660564	0.000098
Cyp313a5	17.208852	-1.770317	0.000098
rho	2.953147	-2.380996	0.000098
Tsp	2.780611	-2.204566	0.000100
CG14258	448.872876	-2.411753	0.000100
Obp57d	1.797550	5.276761	0.000103
Su(z)2	4.679810	1.671570	0.000108
7B2	7.840582	-2.467105	0.000110
ninaC	0.470290	-5.971055	0.000110
Fim	40.422197	-1.667794	0.000110
CG13833	3.899174	-4.036578	0.000110
CG12204	8.358192	2.508234	0.000112
coil	13.030746	1.650089	0.000112
nop5	75.935930	-1.648128	0.000114
CG6126	47.358511	-1.693323	0.000119
CG5002	9.184673	-2.464791	0.000120
CG34227	3173.100437	-3.992515	0.000120
scyl	88.236009	-1.809807	0.000124
Sfxn1-3	26.633202	-1.613093	0.000125
Art1	84.130258	-1.701593	0.000125
CG10863	70.083969	1.824849	0.000125
CG10026	7.153439	-2.445865	0.000126
CG34462	31.809245	2.204696	0.000130
SmydA-5	1.426835	-5.390983	0.000131
Sox15	3.550709	-2.790795	0.000132
CG14971	16.219524	1.651332	0.000134
Jabba	30.831177	-1.887635	0.000135
CG1532	62.250948	1.641754	0.000139
wg	3.230253	-2.707243	0.000141
Zasp52	15.622712	-2.123846	0.000146
Cpr66Cb	2.434349	-6.035289	0.000146
CG4975	5.147804	-1.993144	0.000147
CG9572	790.818818	1.851584	0.000148
sti	6.093017	-1.942318	0.000150
Cpr51A	928.634259	-1.941012	0.000153
CG31321	26.865212	-1.760543	0.000155
CG4239	17.489508	-1.859305	0.000155
Ccp84Aa	263.771285	-2.305341	0.000155
TpnC73F	339.963380	-2.418497	0.000155
CG32368	6.837324	-5.151012	0.000155
CG15905	1.084845	-14.294313	0.000155
NUCB1	128.098646	1.703442	0.000156
polo	22.295419	-1.728019	0.000156
CREG	138.279811	-3.824964	0.000157
CG12594	0.343268	8.095786	0.000157
CG11671	2.152538	-6.892196	0.000157
Mst89B	1.314168	-5.596999	0.000159
l(3)neo38	8.913041	-1.856539	0.000160
Schip1	95.205709	1.652763	0.000161
CG4839	1.253528	-2.609982	0.000172
CG8314	48.782534	1.689157	0.000172
Tsp74F	72.977766	-1.628381	0.000178
CG13606	7.899008	-2.229584	0.000185
Pde9	1.224799	2.059309	0.000192
nonA-l	6.231381	-1.970947	0.000192
CG31248	14.732202	2.879458	0.000200
Ufl1	30.156446	1.583250	0.000203
Mp20	531.287329	-2.524116	0.000203
CG12099	64.846277	1.612522	0.000203
AGO3	3.687932	2.710693	0.000208
raw	13.995212	-1.676970	0.000213
KrT95D	4.400682	-1.733119	0.000213
ImpE3	7.927054	-3.302324	0.000214
adp	14.808137	1.621074	0.000217
CG13793	1.079329	-6.152756	0.000220
Mlc1	626.725533	-2.677314	0.000222
CG3649	1.295667	-6.040313	0.000222
CG12877	8.042211	1.701823	0.000228
CG8100	1.547625	-3.999941	0.000228
Akh	2.720852	-13.141814	0.000230
CG14292	6.372206	-9.239545	0.000231
Tango14	30.176220	1.620052	0.000233
CG15766	2.604830	4.666144	0.000233
CG7453	39.814789	1.614874	0.000233
CG31344	24.626604	1.674325	0.000233
CG9636	9.181548	-1.632563	0.000236
CG9689	10.360415	-2.130547	0.000237
CG17323	2.610797	-2.991414	0.000238
Cyt-c-p	242.598283	1.812514	0.000245
CG5612	4.547556	-3.535865	0.000245
scaf	484.180387	2.146111	0.000247
Dgkepsilon	25.130215	1.577871	0.000247
CG1969	55.968920	1.577735	0.000247
tyn	3.191303	-2.514688	0.000247
CG32191	3.139854	-4.290626	0.000247
alt	72.790832	1.827334	0.000250
CG2846	36.874207	1.550433	0.000256
CG14131	10.023978	1.741575	0.000256
Ncc69	23.518075	1.625738	0.000257
EMRE	72.898718	1.612752	0.000260
Ptr	6.461264	1.736762	0.000266
Ir76a	4.865386	2.249159	0.000271
Ptp61F	18.463638	1.614712	0.000272
CG3655	14.506487	1.745071	0.000272
Cyp4aa1	3.635979	-5.879917	0.000273
GlcAT-I	23.730641	1.686384	0.000276
l(2)k14710	13.611642	1.522267	0.000279
mud	2.740405	-2.018604	0.000279
Nmdmc	32.810410	1.601247	0.000279
CG9436	61.098772	-1.526454	0.000279
RabX1	12.372534	1.675863	0.000283

CG13038	10.291797	-2.943935	0.000284
CG42240	8.382353	-2.596898	0.000288
CG13024	10.619650	-1.764602	0.000294
CanA1	3.735666	-2.799166	0.000294
CG5778	3.202417	6.607038	0.000295
pain	7.643406	-1.800391	0.000297
CG5065	9.887152	2.084167	0.000300
Dip-C	36.834718	-1.594581	0.000301
CG14075	3.036655	-85.748387	0.000301
eIF3j	163.028014	1.648238	0.000310
mav	99.906356	1.664544	0.000317
CG33155	23.373824	1.624458	0.000321
CG9547	19.652717	1.590367	0.000325
l(1)G0020	12.123217	-1.557395	0.000326
Klp67A	5.020732	-2.046610	0.000337
CG46314	26.089722	1.592675	0.000342
Cyp9f2	77.769794	-1.612701	0.000346
CG42673	20.308442	1.748528	0.000353
Picot	71.752901	1.633444	0.000358
Tm2	226.026976	-2.573559	0.000358
Vamp7	90.769788	1.597249	0.000361
alpha-Est9	37.404513	-1.647835	0.000363
Oamb	0.793806	-3.902862	0.000366
CG42788	11.081889	-1.610361	0.000377
pon	3.954039	-2.184935	0.000382
CG4456	3.393859	2.872127	0.000383
CG13138	0.535130	-17.725311	0.000383
gt	1.167093	4.550475	0.000385
CG3630	6.865660	-2.177007	0.000386
CG14109	5.042951	-3.442818	0.000389
Pcyt1	33.676916	1.561234	0.000397
fzy	10.727758	-1.839242	0.000397
comt	2.842963	-2.270882	0.000406
blow	27.222084	-1.570105	0.000410
CG3301	15.509152	-2.784165	0.000411
yellow-e	65.903186	-1.691052	0.000414
CG14564	37.894518	1.818189	0.000415
Pcd	113.638594	1.522677	0.000417
CG4998	1.246972	-2.971835	0.000418
CG43367	6.611183	1.562937	0.000424
CG4603	24.167119	1.620974	0.000430
CG43245	4.299808	3.104187	0.000437
cyc	9.159330	-2.035092	0.000437
Nf-YA	7.999380	1.882227	0.000437
GstE1	85.360424	1.598727	0.000443
CG3631	6.516879	1.940507	0.000447
CG17105	91.978161	-3.564890	0.000449
firl	3.288171	-2.463917	0.000450
CG2812	11.596799	2.416603	0.000451
CG45093	8.799911	-1.619723	0.000451
CG4069	15.081708	-1.596496	0.000454
CG42326	13.272171	-1.726336	0.000454
CG2736	5.732474	-2.627983	0.000454
CG12164	1.959394	-4.969963	0.000464
serp	2079.909746	1.677632	0.000468
CG10550	54.512117	1.727536	0.000470
SPoCk	26.108885	1.653898	0.000470
ng1	3.895962	-8.108367	0.000470
CG42571	0.709268	12.642472	0.000490
CG18858	21.717377	1.519447	0.000494
CG8372	36.662711	1.572777	0.000501
CG1208	11.446265	-1.731026	0.000508
kuk	22.389099	-1.728129	0.000524
wupA	303.505009	-2.442877	0.000526
CG9279	1.005518	-2.700536	0.000528
Tsp97E	21.148172	1.615907	0.000532
GstT3	11.843193	1.853499	0.000533
Skeletor	44.220905	-1.644252	0.000534
bip1	11.420023	1.826272	0.000535
CG13239	5.247933	-3.927372	0.000542
Sec31	49.017395	1.658867	0.000545
rpk	0.765245	-4.811784	0.000547
CG8336	16.879688	1.569758	0.000550
CG4872	11.257893	-1.807484	0.000556
rasp	26.230734	1.544522	0.000558
CG12643	35.913887	1.722787	0.000558
CG42514	5.113129	-2.220776	0.000573
CrebA	20.505368	1.614080	0.000575
Tapdelta	246.018728	1.611908	0.000579
CG9220	21.028787	1.576198	0.000587
Ugt36Bc	37.669697	2.177459	0.000588
CG18508	24.642818	1.652274	0.000591
corto	20.295134	1.665032	0.000595
Actn	70.744894	-2.166698	0.000595
CG9911	108.532670	1.581500	0.000596
alphaTub84D	101.196497	-1.608209	0.000606
CG3760	132.165122	1.584401	0.000612
CG14183	0.737725	4.399855	0.000612
CG17493	18.247707	1.559943	0.000622
PI4KIIIalpha	17.213319	1.630364	0.000627
zye	35.542191	-2.767866	0.000627
RhoGAP1A	12.128909	2.165149	0.000630
PsGEF	0.131532	-4.803616	0.000634
Mur2B	0.844041	2.827666	0.000654
Vps11	15.196650	1.520456	0.000655
yellow-e3	1.907467	-4.343962	0.000661
CNMa	1.462468	-5.190015	0.000663
IntS2	11.837667	1.514360	0.000676
CG9372	1066.084305	1.790552	0.000679
deltaCOP	103.710606	1.565510	0.000680
Stip1	118.452282	1.566724	0.000683
Cdc37	57.948652	1.528192	0.000689
uif	19.571139	-1.723554	0.000689
vg	2.437004	-2.920681	0.000689
alpha-Man-Ic	0.523597	8.112270	0.000692
Yp3	0.692961	-8.895698	0.000692
CG32563	3.062299	5.352654	0.000697
Mvl	40.958157	-1.665875	0.000701
CG14636	17.728755	1.994278	0.000709
crc	473.755168	1.710944	0.000709
sip2	13.625623	-1.698180	0.000709
CG2794	17.331134	1.580381	0.000714
CG30497	8.880688	-1.612770	0.000714
CG3823	18.683761	-1.751925	0.000718
CG7841	7.196194	2.083614	0.000719
pre-mod(mdg4)-C	2.510323	-4.547392	0.000736
ine	4.053004	-1.890629	0.000736
rumi	15.290648	1.708524	0.000739
GstD2	14.318448	-2.412007	0.000744
CG6071	1.004616	3.601045	0.000746
CG10462	12.384747	1.553085	0.000746
Nop60B	67.117217	-1.568941	0.000746
ash2	18.373929	1.523456	0.000749
Nox	1.891132	-2.165452	0.000749
nmo	3.086985	-1.718304	0.000755
ste24a	59.810476	-1.544855	0.000764
prage	11.659115	1.553514	0.000767
CG17560	2.313559	5.218521	0.000767
CG6638	27.289065	1.504750	0.000767
CG18558	0.887777	5.320195	0.000768
CG32603	752.361188	-2.236989	0.000769
fu12	6.851434	-1.849844	0.000777
Xpc	9.343069	-1.557765	0.000780
CG12995	8.905528	3.058409	0.000783
CG3838	7.669333	1.616290	0.000783
Sec13	103.067303	1.556802	0.000783
CG13060	1.651742	-15.258777	0.000783

mahe	11.874943	-1.583759	0.000789
CG4404	1.639294	-3.685166	0.000790
CG9662	50.687342	1.517374	0.000793
Cpr47Eb	6417.327400	1.674969	0.000796
Girdin	10.801591	1.644180	0.000796
CG5346	65.269479	1.598107	0.000796
CG13905	3.138696	-22.352570	0.000809
Hsc70-3	382.540067	1.734910	0.000846
CG9590	27.884872	1.481637	0.000865
Mf	100.567999	-2.369453	0.000879
CG6204	12.964356	1.613680	0.000887
stx	14.527620	1.593485	0.000890
CG4662	26.531134	1.584691	0.000891
CG8908	0.575107	3.716505	0.000894
CG7016	30.384616	-1.560329	0.000900
CG15506	3.876836	-2.922839	0.000906
CG34325	68.778293	-1.551415	0.000908
Usp32	14.429446	1.567087	0.000911
HDAC1	89.574344	-1.550394	0.000911
dgt5	3.611855	-2.247600	0.000914
jing	2.529306	-1.739440	0.000922
Obp83cd	5.390350	3.129908	0.000923
ergic53	180.258203	1.749912	0.000928
nord	1.157077	-3.888086	0.000928
Vha68-1	3.264175	-2.467577	0.000942
CG3744	12.676880	1.612743	0.000961
CG3961	5.808822	-1.798845	0.000968
CG5439	20.257145	1.600374	0.000968
loj	137.751237	1.573849	0.000975
CG18557	18.733531	2.355090	0.000976
CG7408	5.538633	-1.943214	0.000976
CG1662	15.481088	1.586538	0.000978
Act57B	2512.663423	-2.392506	0.000978
CG10918	1.673250	-14.114529	0.000978
tutl	0.910005	-2.403927	0.000981
CG3609	105.258880	1.595019	0.000994
Ppr-Y	0.620203	-18.031406	0.000996
reb	74.200969	-1.562437	0.000997
Reph	3.820781	1.904224	0.001001
sn	167.370414	1.818426	0.001003
CG18081	60.771169	1.609756	0.001011
ab	3.505669	-2.115680	0.001034
CG14573	19.192324	2.897965	0.001039
kon	1.112205	-2.245849	0.001080
bowl	96.430095	1.741153	0.001113
Tango10	12.641703	1.492844	0.001134
CG14795	19.483930	-2.189081	0.001144
CG10178	47.831057	-1.634381	0.001151
Cyp4d2	5.043605	1.909010	0.001153
CG17109	45.483346	-2.008243	0.001160
CG42542	23.235759	-1.539408	0.001164
Obp99d	7.397889	5.211721	0.001166
Pen	46.957098	-1.635824	0.001172
Pde1c	3.017856	-1.828484	0.001185
CG7456	23.948297	1.537314	0.001188
ETHR	4.548535	1.661155	0.001194
Ssl2	0.569953	6.439453	0.001196
mRF1	5.115868	2.513207	0.001197
CG8507	80.255250	1.537992	0.001197
CG13124	63.220459	-1.611383	0.001205
kibra	14.107924	1.507945	0.001211
Tom	8.304521	-2.692274	0.001211
CG32521	60.007052	1.611649	0.001214
CG32486	16.218727	1.596075	0.001218
Galphaf	4.907433	-2.088317	0.001219
msb1l	6.298096	-2.275921	0.001223
CG3652	35.493290	1.543435	0.001228
Poc1	8.765819	-1.825065	0.001228
CG13157	2.379985	-4.820951	0.001228
if	22.465119	-1.745851	0.001232
PK2-R2	0.944265	-3.607587	0.001232
CG11670	8.506014	2.117919	0.001233
ey	0.691693	3.677898	0.001240
CG1136	5.263047	-1.813920	0.001242
dpp	3.509285	-2.008398	0.001243
pre-lola-G	5.440879	-1.755322	0.001251
CG17816	1.492852	-2.031757	0.001268
pll	20.055463	1.561754	0.001277
GILT2	1.548478	-6.183666	0.001309
mab-21	48.997227	-1.593336	0.001333
NijA	53.109933	1.616128	0.001342
Esp	7.453142	1.646722	0.001342
salt	0.625922	-14.035888	0.001342
Phax	12.312302	1.676645	0.001348
CG5867	169.256484	-1.644820	0.001379
qkr58E-1	20.756168	-1.587587	0.001391
CG4213	1.317371	-2.910380	0.001391
frac	6.838229	-2.436676	0.001393
CG4115	323.399267	-1.804501	0.001404
DOR	66.625591	-1.581401	0.001410
ZnT77C	18.372775	-1.860344	0.001429
NFAT	7.443378	1.550938	0.001444
IM3	3.962671	5.279836	0.001445
JhI-26	146.986596	2.074976	0.001446
IleRS-m	6.381815	1.841397	0.001446
CG4558	16.075789	1.566524	0.001446
CG15445	16.442000	1.557699	0.001446
eIF4G2	4.125212	1.713487	0.001448
nab	2.157548	-2.769120	0.001452
IleRS	42.561232	1.528540	0.001454
tn	5.724161	-2.285283	0.001469
Prm	121.556799	-2.485098	0.001469
trio	13.222187	1.559852	0.001482
beta-PheRS	47.553527	1.494898	0.001508
DCP1	20.458759	1.530071	0.001516
CG42307	7.592677	1.469313	0.001517
Rsf1	48.019970	-1.514806	0.001518
CG5021	37.872218	1.489139	0.001522
mey	0.886116	-4.245457	0.001523
CG32485	6.981125	-2.341494	0.001530
mbf1	81.347359	1.556834	0.001540
CG42337	0.604472	-3.638905	0.001554
CG10064	0.370224	-8.040407	0.001562
CG41128	117.861962	1.521448	0.001564
CG5987	1.810852	3.349232	0.001571
Spc25	8.346840	-2.294614	0.001574
CG6867	2.743624	-2.352469	0.001574
m	1.141614	-3.199159	0.001584
mtsh	0.387488	-7.656745	0.001603
hdc	7.969130	-1.644692	0.001607
CG3168	2.981849	-1.843483	0.001607
MtnD	3.263452	-8.191720	0.001608
CG3264	1.253983	-6.148658	0.001614
Zip99C	18.908033	-1.515797	0.001621
CG4259	10.514466	-1.676533	0.001621
CG31030	6.529614	-2.027492	0.001621
CG10280	1.523615	-4.950465	0.001624
CG10899	0.887699	-11.492990	0.001626
CG42507	0.984837	-3.355292	0.001662
CG17843	38.341610	-1.567729	0.001686
CG1358	0.263787	-5.404131	0.001689
CG1812	15.154030	1.494032	0.001694
CG16884	1983.367936	-2.034055	0.001705
CG7791	14.556574	1.511061	0.001716
CG9586	52.202323	1.512632	0.001737
CG6321	5.089931	-2.113108	0.001738
Ac76E	5.714080	-1.837199	0.001739
Mink	10.204906	-1.642125	0.001740

Spase22-23	106.108225	1.541535	0.001767
CG2100	16.841181	-1.541399	0.001771
Gs1	8.870170	-1.764165	0.001771
l(2)k05911	137.584175	-3.032392	0.001771
RyR	2.133114	-2.510766	0.001843
Lectin-galC1	16.880364	2.950116	0.001846
Kal1	5.107522	-2.283881	0.001846
cmet	3.100303	-1.749350	0.001898
betaCOP	95.960359	1.602758	0.001899
Unc-115b	22.732650	1.544187	0.001902
Mur18B	3.156324	-6.112813	0.001902
sage	0.984315	4.621985	0.001905
CG6746	43.611601	-1.512792	0.001911
Tsp66E	24.260586	-1.574737	0.001916
CG8160	1.237406	-4.966201	0.001920
CG2065	13.785975	-2.024672	0.001936
CG12655	11.214035	-2.574831	0.001936
Diap2	28.110810	1.572285	0.001968
CG43897	23.089466	-2.000597	0.001974
CG11147	201.011626	1.944715	0.001979
CG14695	6.318274	-2.546001	0.001986
fal	16.791366	-1.515202	0.001999
Adk1	11.446209	-1.768607	0.002008
CG14408	4.588230	1.781642	0.002012
CG13300	2.376128	-2.212257	0.002019
CG4825	30.412466	1.501399	0.002020
CG16885	2688.213214	-1.906915	0.002020
Fer3	0.715004	13.491777	0.002030
Vps28	35.434079	-1.457774	0.002048
CG17260	7.281352	1.952152	0.002050
Atg2	10.809809	1.525494	0.002050
Tsp42Ei	5.496405	-3.034762	0.002058
CG6083	0.893327	-4.690694	0.002073
Twdlalpha	2.066224	11.333811	0.002080
CG5070	6.150996	-10.102437	0.002091
CG10171	21.974090	-1.508132	0.002096
CG11267	151.173243	1.536124	0.002096
CG31287	1.539827	-3.695591	0.002107
CG13012	14.770109	3.086383	0.002120
Su(dx)	16.904722	1.464483	0.002120
btl	26.892806	-1.549871	0.002134
Nek2	2.660704	-2.628339	0.002144
Cks30A	15.679945	-1.973124	0.002147
CG5885	320.350917	1.641809	0.002187
CG32816	88.727925	1.654821	0.002207
CG10062	1.174814	-3.363836	0.002223
SMSr	10.741592	1.528326	0.002248
Lsd-2	67.044701	-1.648075	0.002254
CG6613	14.340944	1.530860	0.002367
CG6972	4.984895	-3.206654	0.002367
TrissinR	0.947971	3.181097	0.002442
CG42570	0.287027	9.959647	0.002447
pre-mod(mdg4)-B	2.859385	1.828192	0.002459
Drip	24.346236	1.890951	0.002475
Sec24CD	53.796864	1.555751	0.002476
CG8230	35.549239	1.496363	0.002476
CG1814	12.340206	-1.522210	0.002476
CG13046	32.001306	-1.688915	0.002481
Hsp70Bbb	0.629495	-24.907466	0.002485
sky	20.748944	-1.519035	0.002488
CG14785	2.021227	3.108540	0.002516
ex	8.949870	-1.607882	0.002516
CG12481	1.732714	-5.706800	0.002516
stc	18.539155	1.494060	0.002533
Ndg	6.249381	-2.099689	0.002533
tum	12.917469	-1.549025	0.002537
CG7884	17.658576	1.634255	0.002565
Drice	40.643959	-1.467813	0.002567
CG32459	0.386371	16.855922	0.002579
Tmc	0.661356	3.304185	0.002579
CG42821	12.403052	-3.179039	0.002614
SMC1	19.718983	1.544754	0.002617
CG42319	1.164522	-3.781848	0.002685
CG2145	226.528078	1.718258	0.002686
CG10737	46.927203	-1.555203	0.002722
p115	23.553022	1.500032	0.002750
CG8728	40.887424	1.483253	0.002762
CG12237	34.761592	1.556986	0.002796
RhoGEF4	6.672111	-1.848782	0.002796
CG7781	2.760493	-2.362755	0.002796
CG43355	1.463540	-3.781860	0.002834
Obp83g	105.594589	-1.835311	0.002865
CG16820	253.507669	-1.845061	0.002865
pit	24.901050	-1.473065	0.002885
CG3176	10.327183	-2.328643	0.002925
CG6231	36.693887	-1.510388	0.002930
CG42246	147.057037	1.533095	0.002983
pr	46.659235	1.493096	0.003030
Hr38	2.299962	-1.739788	0.003030
CG7328	8.393617	-1.836415	0.003030
up	409.775233	-2.283546	0.003030
CG14893	1.112640	4.576802	0.003049
Samuel	13.339389	-1.582071	0.003050
Ama	19.095872	1.677243	0.003054
CG32448	29.660922	-1.765621	0.003102
CG4294	8.802395	1.496470	0.003129
Cyp12b2	9.509073	-1.864826	0.003138
CG14718	0.261536	9.658623	0.003140
CG12910	1.460687	-3.048931	0.003140
Sp212	9.865206	-1.958050	0.003145
lush	3.433659	3.255661	0.003152
CG13728	0.635908	4.498628	0.003164
pdgy	34.030958	-1.572090	0.003178
KFase	13.202909	-1.834751	0.003210
Msh6	4.695103	-1.796406	0.003211
aurA	5.151520	-2.140881	0.003211
goe	22.988216	1.471998	0.003213
CG2918	96.407250	1.604717	0.003244
CG17385	32.777355	1.481372	0.003244
nos	0.477659	-46.231979	0.003289
CG14132	45.460315	-1.477130	0.003308
CG8370	8.991580	1.512557	0.003309
mRpL53	31.485701	1.496222	0.003311
CG15211	10.709669	-1.903396	0.003312
CG6409	10.444229	-2.519888	0.003327
zetaCOP	96.311301	1.510022	0.003362
Tfb5	26.755513	1.605901	0.003364
CG6006	6.259097	-1.548516	0.003364
stumps	12.671895	-1.570397	0.003371
CG1582	12.583346	1.546467	0.003406
eca	159.275148	1.512845	0.003406
Osi15	2.010600	-3.515640	0.003424
PH4alphaMP	14.887330	-1.681300	0.003459
CG32266	283.097498	-1.927082	0.003464
mthl15	0.993686	-3.343852	0.003476
CG4050	17.850039	1.512952	0.003479
Listericin	86.618274	-3.158247	0.003544
l(2)tid	21.643641	1.431793	0.003563
RpL22-like	1.714166	-13.017473	0.003568
sano	18.117586	1.517833	0.003570
CG8206	31.013655	-1.518362	0.003581
CG30008	1.962597	4.328309	0.003589
gb	6.754087	-1.658061	0.003589
CG31817	0.254547	3.525384	0.003679
CdsA	28.687772	-1.444831	0.003682
Wnt6	11.492923	-1.579302	0.003682
CG44013	2.352781	5.872513	0.003685

CG17490	9.786350	1.486889	0.003694
Hydr1	8.589558	-1.502746	0.003726
CG33281	0.612695	-10.386029	0.003726
CG14642	8.141859	-1.930592	0.003733
CG34408	12.826833	1.489966	0.003745
Doa	14.989613	1.503861	0.003765
CG8635	56.223658	1.458244	0.003791
CG7289	27.924135	1.526227	0.003800
JhI-1	13.029523	1.520391	0.003803
CG7214	1716.446314	-2.156929	0.003814
CG42808	15.147227	-1.966750	0.003892
Srp14	82.885874	1.502302	0.003959
CG7110	3.690841	-1.991732	0.003998
Sox102F	0.938138	-3.043160	0.004008
CG13003	18.808160	-1.644011	0.004027
alpha-Man-Ib	14.116164	1.417152	0.004033
CG11905	2.670717	-2.079362	0.004045
CG2962	2.159765	-448.682424	0.004055
CG5391	11.850117	-2.315121	0.004063
CG30291	40.552311	1.480730	0.004118
CG10166	73.656396	1.532908	0.004132
pgant8	6.466381	1.852773	0.004153
GLS	3.884557	-1.849336	0.004153
Syn1	4.053642	1.862939	0.004164
CG13631	41.322871	1.452985	0.004168
CG10948	11.303038	1.493554	0.004179
fz3	5.143257	-1.684211	0.004201
Fhos	2.129499	-1.706673	0.004234
nbs	7.535415	1.517454	0.004246
Toll-7	8.852207	1.615625	0.004255
Impbeta11	15.234610	1.508032	0.004270
CG3719	76.705020	1.629760	0.004313
gwl	2.647947	-2.091248	0.004326
CG7342	0.522124	-5.854279	0.004326
CG8745	2.981954	-2.460608	0.004350
CG9925	0.371216	-20.163981	0.004377
CG9664	2.521144	-2.343232	0.004421
CG4950	1.695175	-3.883987	0.004423
CG1218	15.360917	-1.557128	0.004447
bnl	7.760830	-2.084881	0.004522
CG3149	11.943426	-1.478503	0.004523
Pka-R2	69.348344	1.579859	0.004552
CG18549	61.703695	1.965742	0.004553
CG9505	3.519283	-2.359811	0.004593
oxt	13.104129	1.404464	0.004619
zyd	6.325330	1.598746	0.004621
CG15365	4.215500	-1.702049	0.004626
AsnS	16.334088	-1.573933	0.004628
CG42238	3.971420	-1.789970	0.004651
BubR1	5.011822	-1.698291	0.004727
CG4293	30.328887	1.492049	0.004753
GstE12	202.968428	-1.565674	0.004753
scra	11.530978	-1.618230	0.004772
CG33655	3.585798	-3.073416	0.004778
CG9945	9.520384	-1.508810	0.004785
betaTub60D	30.395153	1.575580	0.004824
ZAP3	17.766440	1.510508	0.004869
jtb	6.264551	2.403938	0.004986
CG16717	16.378241	1.600446	0.005015
Ino80	6.632528	1.559143	0.005022
IntS3	27.029181	1.455721	0.005022
Unc-89	6.460007	-2.095082	0.005054
Hrb87F	105.507594	-1.549613	0.005091
CG9149	20.961876	1.477327	0.005138
fabp	450.417788	1.635541	0.005157
CG31436	16.044139	1.552599	0.005157
Cypl	28.795239	1.491148	0.005188
CG9399	40.364849	1.592057	0.005273
Eip71CD	59.093953	-1.557642	0.005273

CG10467	71.196324	-1.550662	0.005277
CG10877	22.704097	-1.512546	0.005284
wit	9.838572	-1.455310	0.005286
Sf3a2	32.664539	1.466036	0.005313
Pof	9.508329	-1.538992	0.005313
RPA2	37.189118	-1.501675	0.005317
brv3	0.577218	-4.401182	0.005381
yellow-f	5.365905	-2.115603	0.005382
St3	5.796045	-2.242436	0.005413
Ets98B	8.734288	-1.509583	0.005435
CG9123	2.317723	-2.941229	0.005439
esg	3.972562	-2.017844	0.005467
bt	17.184749	-2.306502	0.005467
Hayan	21.258315	-1.576341	0.005515
tbrd-1	0.626439	5.512368	0.005572
Wnt10	0.905694	-3.586282	0.005572
aurB	13.546137	-1.790731	0.005604
Karybeta3	149.296842	1.620917	0.005612
CG5023	96.379718	-1.729485	0.005612
CG3726	1.443080	2.859927	0.005634
CG12338	9.117756	1.824576	0.005634
Ppt1	18.139097	-1.528260	0.005634
CG2076	61.473306	1.444369	0.005642
rg	3.838628	1.475640	0.005658
CG13323	0.235680	-14.841604	0.005660
CG43954	9.098986	-1.442130	0.005696
Mgat1	12.107113	1.481693	0.005765
CG40298	4.475003	-2.571807	0.005798
zf30C	23.620624	1.486523	0.005811
Gmer	23.167066	1.475821	0.005857
FASN3	5.306838	2.322551	0.005858
sgll	128.751885	-1.480351	0.005919
ssp	18.614065	1.452546	0.005949
Bet1	36.371979	1.509118	0.005981
CG11892	0.457745	-7.862198	0.006159
CG13721	8.870624	3.138289	0.006171
CG18765	0.555583	5.705003	0.006206
en	1.871062	-2.756898	0.006210
Mpcp1	27.026386	-2.142944	0.006225
SerRS	130.333411	1.480747	0.006305
CG10337	19.329679	1.446594	0.006334
Uch-L5	55.204247	-1.403429	0.006334
PNPase	12.234341	1.452166	0.006339
CG18853	2.317071	-413.800894	0.006353
CG11858	52.395717	-1.463206	0.006396
SPARC	69.844969	-1.535193	0.006398
Gagr	2.116032	2.534720	0.006398
Spt-I	34.173064	1.460184	0.006427
CG17119	5.300411	-1.896931	0.006438
Cpr62Bc	1396.941301	-1.944234	0.006456
CG13857	0.369848	-13.008808	0.006456
CG31469	16.423868	-1.840569	0.006456
Faa	11.245235	-2.415514	0.006456
Cyp6g1	2.446047	-3.053905	0.006495
CG8202	9.976814	1.421300	0.006511
CaBP1	233.698223	1.630351	0.006517
l(1)1Bi	10.740184	-1.429006	0.006525
uri	10.329625	1.469740	0.006569
Sid	1.441157	-4.126798	0.006659
CG11961	18.140464	1.451610	0.006661
mthl3	1253.941168	1.542704	0.006695
CG32344	15.116025	-1.418928	0.006712
hbs	2.435541	-1.884413	0.006712
CG41284	5.023718	2.418245	0.006718
CG5823	30.322928	1.487454	0.006742
CG8945	0.241207	-4.559205	0.006790
CG14997	198.723944	-1.615080	0.006826
Hydr2	27.986676	1.440521	0.006858
nrm	4.275325	-1.771666	0.006862

CG14191	10.879613	3.889612	0.006870
KCNQ	28.101168	1.468162	0.006870
Dro	33.530214	2.316678	0.006930
CG5946	43.550118	-1.481447	0.006965
CG6805	53.918324	-1.457032	0.007041
Duox	25.123628	1.514843	0.007147
oys	27.685733	1.513604	0.007148
CG4984	4.180782	-2.222256	0.007176
Idgf3	230.196436	1.603537	0.007238
ksh	55.658810	1.491374	0.007276
Edg91	1041.667207	-1.660755	0.007347
NaPi-T	0.905719	-3.422512	0.007365
CG8435	15.768223	-1.553346	0.007426
CG42329	2.055502	-2.359790	0.007457
Tim8	56.748668	1.427565	0.007465
CG5087	6.739063	1.466448	0.007470
CG1143	16.313812	-2.091502	0.007470
CG13293	0.699266	-2.932833	0.007515
Lam	38.379305	-1.521935	0.007515
D19B	12.085182	1.471898	0.007599
Manf	187.598341	1.467416	0.007708
mRpL12	49.816379	1.477846	0.007834
CG3603	39.866618	-1.404039	0.007874
CG6324	0.259386	-5.719732	0.007877
CG3505	30.610049	-1.519617	0.007986
subdued	15.252391	1.455824	0.007990
CG13397	2.759003	-2.019026	0.008008
CG31955	14.479984	1.658112	0.008010
Lcp65Ab1	18759.859563	-1.839159	0.008062
Fcp3C	1.538410	3.565949	0.008096
CG14712	7.600762	1.472427	0.008099
CG15021	1.483004	3.729788	0.008146
CG2004	73.980824	1.472021	0.008146
CG17111	27.992737	1.774881	0.008173
Ack-like	10.843024	-1.510626	0.008179
Kif19A	0.246487	-8.797684	0.008245
a	5.238090	-1.491086	0.008305
CG7376	3.376494	-1.629975	0.008343
Ocho	1.373823	-3.471322	0.008395
CG13227	9.199967	-3.308317	0.008416
Spn43Ab	25.202805	-1.560327	0.008452
CG8630	310.023569	1.758191	0.008502
dpr17	0.267889	-5.507125	0.008502
Jafrac1	335.494667	1.741257	0.008565
CG5853	10.688287	1.446883	0.008565
CG7102	9.324686	-1.554962	0.008567
CG6660	3.979020	3.764339	0.008568
d4	57.437062	1.447610	0.008572
Pms2	6.139044	-1.497502	0.008572
CG43102	0.589570	-2.261530	0.008611
CG44242	87.503474	1.432177	0.008617
Srp54k	121.265416	1.464217	0.008738
CG31098	27.818255	-1.395240	0.008746
CG6294	9.062904	1.508188	0.008780
DMAP1	19.198981	-1.439972	0.008861
Ilp3	0.831210	-6.721323	0.008918
ara	2.264247	-2.255847	0.008927
CG11581	0.438241	-7.254138	0.008948
CG9330	47.079302	1.442519	0.009080
CG13995	1.109982	2.815039	0.009080
Cyp28d1	1.701787	-2.972916	0.009107
Cyp6v1	12.980797	-1.398368	0.009164
CG4991	8.622408	-1.673292	0.009200
GluProRS	37.838005	1.475204	0.009213
AstA-R2	1.810756	-2.562456	0.009248
rdgA	2.576707	-1.482481	0.009325
Pgm	69.634300	-1.526848	0.009333
CG15635	0.175300	6.536995	0.009359
CG6230	30.643261	1.491351	0.009388
ArfGAP3	56.549614	1.430628	0.009402
CG6978	0.449851	4.534331	0.009473
aux	17.598527	1.372730	0.009473
CG9864	4.759854	-1.935574	0.009473
CG4238	1.724351	2.114577	0.009476
CG8173	8.785126	-1.649381	0.009476
CG42565	0.508596	-4.381408	0.009476
foxo	9.298941	-1.438699	0.009546
CG34348	13.161589	-1.480378	0.009564
CG15083	189.996231	-1.502620	0.009564
CG5863	11.954855	-1.637687	0.009564
CG9312	11.635448	-1.905926	0.009564
CG34031	1.285095	4.246993	0.009585
TMEM216	8.796356	-1.437903	0.009614
Adk2	221.580891	1.457750	0.009668
Oga	19.402918	1.501517	0.009688
pkaap	24.501936	-1.442051	0.009768
CG5522	3.992504	-1.656471	0.009768
tld	1.686460	-2.629338	0.009768
CG2839	0.708396	-3.400255	0.009768
CG8303	91.240739	1.607162	0.009796
rgr	1.151923	-2.279450	0.009796
CG31883	1.369620	3.416321	0.009837
CG14223	2.693184	-2.119276	0.009844
CG16743	2.885673	-3.080298	0.009879
CG10254	9.570644	1.430261	0.009944
Hn	9.428728	-1.678042	0.009945
CG30101	10.218154	-1.896488	0.009949
dao	0.494967	-2.998488	0.009949
yip2	178.556916	-1.495258	0.010053
nudC	55.467877	1.420831	0.010071
qsm	174.440989	-1.570193	0.010071
CG6142	3.182583	-2.340180	0.010084
sqa	1.184048	-2.214165	0.010088
CG12868	25.923636	-1.601016	0.010093
CG10348	1.607298	-2.826767	0.010159
Ste:CG33237	1.462327	-6.852411	0.010230
CG12116	7.518962	-2.374128	0.010285
CG42747	2.371724	-2.212718	0.010288
CG12404	65.053795	1.389054	0.010411
Cln7	15.123271	-1.523145	0.010416
CG14434	16.524879	-1.452548	0.010425
Tsp42Ej	3.386011	2.640982	0.010474
CG17292	48.340586	-1.446051	0.010474
jigr1	11.023709	-1.452725	0.010474
CG18869	0.507233	-4.665977	0.010474
CG31712	21.156632	1.461613	0.010521
Prip	23.686712	-1.498475	0.010521
az2	4.879370	1.825503	0.010749
isoQC	12.156576	1.460423	0.010820
fs(1)N	0.070703	6.682360	0.010836
RanBP3	64.676713	1.443170	0.010836
THADA	4.424540	-1.479152	0.010836
CG15414	84.756045	1.518602	0.010883
CG10175	1.403571	-2.157817	0.010883
CG15599	0.625595	-10.511457	0.010883
CG2816	126.337251	1.463616	0.010908
Sec23	122.680024	1.544822	0.010929
CG3967	11.771887	-1.393345	0.010929
CG11345	19.845666	-2.172860	0.010961
AP-1gamma	22.718115	1.484767	0.010966
Abd-B	13.225166	-1.453687	0.010966
EndoGI	144.875657	-1.435102	0.011022
viaf	50.557452	-1.434510	0.011030
CG15247	1.863612	-2.870931	0.011100
CG13659	14.104978	-1.581858	0.011105
Eip74EF	14.879115	-1.527259	0.011254
verm	3576.231080	1.497634	0.011303
CG42231	13.005110	1.489486	0.011361

PMP34	13.206586	-1.474173	0.011428
Ppt2	20.749974	1.500903	0.011457
Ars2	42.441640	1.423959	0.011459
dgt3	4.643440	-1.927651	0.011494
pHCl-2	0.184677	-9.291174	0.011504
epsilonCOP	76.103623	1.399189	0.011535
CG46319	8.281306	1.556354	0.011563
CG43711	1.146656	-5.027038	0.011695
yin	7.444412	-1.710171	0.011713
CG12773	34.990437	1.458959	0.011800
CG9521	9.484200	2.614773	0.011804
GalNAc-T1	35.734772	1.417795	0.011807
CG9427	64.195746	-1.428083	0.011835
rost	11.340134	-1.460028	0.011882
AdenoK	21.639082	1.396078	0.011963
Nca	97.993310	1.417793	0.012009
CG13314	20.822002	-2.146865	0.012036
CLS	17.985236	1.437086	0.012053
CG2147	24.059928	1.658366	0.012068
Sec24AB	22.086892	1.427689	0.012235
Dcr-1	6.092430	1.394471	0.012235
GluRIID	3.282436	-2.122152	0.012235
Nos	0.105902	-7.236109	0.012235
CG16886	1.701349	-2.843682	0.012246
comm2	19.313542	1.474958	0.012364
CG8012	551.147686	-1.685434	0.012384
CG14907	15.542166	-1.634078	0.012423
CG9804	20.578607	1.514823	0.012429
CG1764	10.318202	1.564526	0.012429
CG7265	36.295640	-1.457534	0.012429
CG18155	1.645218	-2.609295	0.012429
Gad1	0.233145	-5.882819	0.012429
CG11529	7.115620	-2.503020	0.012566
Sdic2	8.875366	2.574529	0.012605
CG7255	7.134322	1.529370	0.012605
CG7766	19.911159	1.431873	0.012605
CG5532	60.797009	-1.368361	0.012605
CG10341	17.472902	-1.449231	0.012605
CG3588	119.558885	-1.664273	0.012605
Mul1	8.751342	-1.621698	0.012633
Cog7	15.977011	1.443630	0.012736
Scgdelta	1.595117	-2.819460	0.012736
CG17065	18.840740	-1.430644	0.012791
GNBP2	1.782306	-2.804349	0.012791
g	14.982191	1.443259	0.012816
nkd	3.651869	-1.608939	0.012831
Sep5	4.885688	-1.834584	0.012831
CG33993	0.634393	-3.820681	0.012831
CG6788	0.994226	-4.022151	0.012831
tup	2.221572	-2.097979	0.012869
CG32055	0.499581	-5.010680	0.012869
Meics	6.878594	1.696659	0.012893
CG5913	18.071304	1.416617	0.012893
CG8927	550.961857	-1.563705	0.012899
Cpr60D	274.985802	-1.642401	0.013237
CG10560	0.697296	-5.242589	0.013237
CG5484	49.657660	1.398318	0.013244
ringer	34.489469	-1.576874	0.013313
Msr-110	801.929629	1.519932	0.013322
CG8239	8.702888	1.667557	0.013379
Lac	156.253704	-1.542092	0.013395
Nna1	1.225158	-1.890857	0.013395
CG14610	6.275078	2.779008	0.013400
Xbp1	284.102804	1.568462	0.013402
CG9723	11.713569	1.457902	0.013402
twe	2.115334	-2.228684	0.013402
FDY	19.199828	-8.905091	0.013567
tapas	24.228972	1.432740	0.013618
GalNAc-T2	41.359086	1.425638	0.013635
CG14968	26.314058	-1.479968	0.013635
CG4415	0.988422	-7.642367	0.013645
Spp	170.975633	1.491827	0.013693
mag	0.862045	-22.097896	0.013719
Cpr78Ca	44.420754	-1.572099	0.013826
mEFTu1	62.186836	1.413886	0.013840
l(1)G0320	327.762054	1.556539	0.013866
nemy	1.623924	-2.240099	0.013866
l(2)01289	15.229113	-2.141872	0.013867
CG10345	12.600441	-1.550121	0.014055
CG45075	0.803498	-7.596276	0.014114
CAH1	1134.537883	-1.576297	0.014141
CG3940	26.034947	-2.074785	0.014141
CG4017	20.073323	-3.045356	0.014177
CG7945	30.955063	1.446074	0.014216
CG14441	2.071055	1.586693	0.014259
CG10598	2.198405	-2.778169	0.014259
WRNexo	14.989633	1.508449	0.014306
CG3107	39.613267	1.405816	0.014359
tth	14.880783	1.392877	0.014359
Cht7	55.873990	-1.525468	0.014359
Atg10	4.993941	-1.932489	0.014359
Grasp65	70.108526	1.450031	0.014418
CG44085	3.446765	-1.692831	0.014438
CG11221	1.872767	-2.291739	0.014438
CG9628	65.512872	-1.513080	0.014486
MtnE	1.517300	-4.666321	0.014486
Uro	1.462880	-4.913977	0.014501
CG42486	9.492591	-1.911641	0.014529
Asph	13.370469	-1.666698	0.014548
CG15930	0.560489	-4.899868	0.014552
Nnf1b	2.185208	2.997384	0.014570
Acsl	47.252159	-1.443732	0.014841
CG11448	28.288813	1.440979	0.014843
Srp68	64.040039	1.415516	0.014890
CG2818	16.533800	1.387420	0.014890
Glt	56.481605	-1.506386	0.014890
antdh	0.624885	-5.433262	0.014890
Nle	18.082000	-1.408918	0.014914
CG5945	13.320290	-2.129264	0.014989
Ufc1	102.247427	1.423670	0.015092
CG9192	74.919034	2.082784	0.015122
CG14961	0.597970	3.126678	0.015131
CG5376	4.773727	-2.863493	0.015131
Snmp2	2.685963	2.166707	0.015219
CG6785	0.603667	2.770656	0.015356
CG3552	13.847966	1.497401	0.015436
CG34232	39.474513	-1.538693	0.015436
CG1988	0.265069	-6.305350	0.015436
CG33331	6.742999	1.895839	0.015558
Spn28Dc	75.331553	-1.442731	0.015572
CG33080	30.381827	1.677117	0.015625
nec	15.941549	1.464288	0.015665
CG17271	69.112124	1.459902	0.015714
CG34165	31.168790	-1.647473	0.015753
Ptpmeg2	8.863439	1.406583	0.015909
sau	77.498812	1.431877	0.016050
SP1029	344.908517	-1.700494	0.016050
Eip63E	24.900514	1.399078	0.016136
Mur89F	2.155096	-3.659227	0.016291
Hlc	39.427343	1.382617	0.016292
CG9953	67.601691	-1.481421	0.016292
CG3918	21.465234	1.409979	0.016300
Mon1	15.605361	1.400156	0.016393
lva	16.884948	1.433303	0.016441
YME1L	36.054462	1.395847	0.016441
CG30285	9.037221	-2.071779	0.016449
Arr2	1.172224	3.115140	0.016496
c(2)M	0.607290	3.804728	0.016646

CG42700	1.189603	-2.110992	0.016759
CG8229	7.708053	1.673707	0.016771
CG3570	11.725399	1.684134	0.016890
brm	27.226956	1.426774	0.016908
CG13893	8.271008	-1.503434	0.016908
mthl8	4.723243	1.605359	0.016930
Mal-B2	1.998087	-2.311598	0.016938
CG1486	23.025967	1.393879	0.016999
CG31710	49.496300	-1.414599	0.017026
sbb	5.922185	-1.488777	0.017069
CG31627	0.745434	-5.203335	0.017096
Mhc	240.398049	-2.192979	0.017162
MFS18	18.794420	1.444409	0.017175
CG31917	25.593364	1.488596	0.017183
CG11127	16.510201	-1.432378	0.017229
CG11374	1.036664	-3.259074	0.017313
CG10924	3.943346	1.850457	0.017319
frm	313.438429	-1.684572	0.017319
CG42342	10.482212	-1.686314	0.017319
CG11882	14.435672	-1.657715	0.017326
Thor	508.348374	1.660453	0.017450
CG9297	43.105972	-1.888442	0.017710
lcs	1.374390	-7.245215	0.017819
Taf8	9.108170	1.687471	0.017842
Scox	34.350738	1.461627	0.017885
CG31869	7.717893	1.467758	0.018046
Glut4EF	1.163423	-1.503133	0.018080
thr	1.849966	-1.927963	0.018180
sqh	277.657809	1.591753	0.018231
CG4670	69.573609	1.428365	0.018237
CG10731	18.328747	-1.473193	0.018242
mdy	5.488418	-1.598403	0.018330
CG11400	4.353510	-2.081929	0.018422
veil	21.658028	1.430864	0.018468
dac	0.438944	-4.408304	0.018502
Ste:CG33246	1.535001	-7.159777	0.018502
CG32335	5.178695	-2.125311	0.018542
CG17739	0.483936	-3.713015	0.018568
CCAP-R	3.218340	-2.034729	0.018688
PH4alphaEFB	10.930387	1.421112	0.018708
Gabat	4.927909	-1.724351	0.018729
GCS2beta	99.193766	1.405050	0.018798
Rrp1	17.890958	-1.429450	0.018798
cert	35.394899	-1.434147	0.018798
CG10237	11.451363	-1.496208	0.018798
stai	37.354144	1.484605	0.019176
Slmap	29.787674	1.398478	0.019215
CG34450	0.807886	3.800238	0.019263
hwt	0.287308	-2.886043	0.019263
Smvt	0.604607	-4.789456	0.019263
hh	1.466968	-2.814869	0.019286
CG15431	0.293134	-3.129947	0.019412
br	16.633784	-1.721038	0.019456
GstE13	43.980444	-1.401840	0.019459
CG14752	4.805567	-2.785171	0.019534
CG18622	7.841462	-1.802510	0.019558
GstD3	82.657151	1.490204	0.019578
Spn100A	1.527427	-3.901432	0.019613
zpg	0.396921	-25.666993	0.019648
CG12702	2.960663	-1.785699	0.019682
EndoB	9.986881	-1.401330	0.019698
sob	3.519431	-1.737699	0.019757
CG7365	8.392341	1.845445	0.019916
Rab32	2.811698	-1.712513	0.019944
Mpcp2	383.811719	1.545913	0.020061
CG12017	5.881631	-1.805098	0.020100
CG13896	8.292483	1.755777	0.020184
ade2	10.359785	1.377501	0.020184
CG3356	14.360889	1.425311	0.020329
CG1637	22.548900	1.415736	0.020491
Ccp84Ag	222.646718	-1.501886	0.020491
Hers	3.374229	-1.430375	0.020502
mRNA-cap	28.161661	1.382769	0.020737
CG17258	0.590238	2.901582	0.020796
vri	9.110819	-1.472540	0.020938
krimp	4.359478	1.671656	0.020956
FMRFaR	0.643861	-3.023534	0.020995
mthl4	166.989740	1.474199	0.021144
Ppat-Dpck	14.286333	1.415769	0.021340
CG31157	1.120876	3.090794	0.021346
Acp1	839.454942	-1.913257	0.021402
ImpE2	6.838869	-2.735733	0.021407
Tango1	26.833742	1.451327	0.021437
Syx18	28.093937	1.355287	0.021462
Gapdh2	1537.077618	-1.485950	0.021462
CG8915	2.964970	-1.598741	0.021462
CG17574	16.816216	-1.372857	0.021617
trn	5.678784	-1.547512	0.021617
CG9135	52.304195	-1.425668	0.021742
Kaz1-ORFB	55.779078	-1.444619	0.021742
nahoda	42.053523	-1.479675	0.021750
pnt	3.559932	-1.523717	0.021778
CG4927	3.333024	-2.148933	0.021881
SmydA-9	6.282956	-2.204873	0.021915
Tsp42Ea	19.868714	-1.360430	0.022223
CG4496	8.584481	1.516114	0.022305
CG31038	15.121111	-1.428243	0.022386
CG33332	12.712127	-1.600476	0.022397
CG7115	11.184680	-1.402332	0.022514
c12.2	7.231523	1.425170	0.022595
nrv2	33.390919	-1.423696	0.022662
Pfk	49.728922	-1.425726	0.022672
CG30403	9.966893	-1.654607	0.022726
eRF3	82.294856	1.515204	0.022802
CG9328	24.380619	1.485062	0.022896
Cerk	23.889700	-1.415508	0.022940
ppk6	1.532024	5.242040	0.022942
VGAT	0.176243	-6.370216	0.022942
Cam	297.081446	1.487102	0.022970
Dr	2.275701	-2.259114	0.023024
mRpL14	22.223080	-1.579200	0.023058
CG33054	24.798293	-1.436677	0.023115
CG14866	0.715712	-3.386437	0.023115
PlexB	15.579512	1.394417	0.023123
Snx1	42.802827	1.372941	0.023123
rpr	5.051699	-2.140202	0.023123
Gp93	327.721405	1.513351	0.023149
pan	4.282826	-1.404868	0.023149
CG1550	24.074641	1.365156	0.023251
CG9743	6.431750	-1.729848	0.023297
Ttc19	8.822151	-1.638991	0.023344
eloF	0.447822	7.237785	0.023352
Octbeta2R	2.088080	-1.766992	0.023403
CG12948	21.205639	-1.415210	0.023407
Cyp6w1	6.409624	-1.781164	0.023409
CG30080	0.206685	-6.265633	0.023587
svr	20.678308	1.404013	0.023590
CG5953	5.255377	1.389951	0.023590
CG7058	0.195517	-3.550802	0.023632
CG17329	0.875674	-5.201105	0.023632
PHGPx	157.044788	-1.413985	0.023700
CG11563	28.343821	-1.394104	0.023738
eco	15.220858	1.421827	0.023849
l(2)35Bd	14.441658	-1.397008	0.023851
Fbp1	40.889946	-3.576099	0.023936
CG13748	4.537259	-3.195416	0.024110
CG42564	0.968600	2.821650	0.024115
Irk1	14.732176	1.357728	0.024392

cnn	2.298840	-1.640571	0.024392
CG8602	46.524428	1.403598	0.024463
Dad	15.990922	-1.401905	0.024463
metro	1.559327	-2.515514	0.024463
CG12998	3.068132	-2.516755	0.024482
Gr39b	0.609318	4.227593	0.024566
L2HGDH	17.687167	-1.420091	0.024664
B4	7.577973	1.408611	0.024711
CG5745	20.319338	1.399939	0.024711
alpha-Est3	15.884956	1.377385	0.024711
CG7201	4.040661	2.028460	0.024749
wus	7.559834	1.614521	0.024779
Cyp6a20	2.786151	2.407487	0.024908
CG8353	5.945604	-2.137969	0.024939
LeuRS	34.860743	1.388566	0.025052
Cpr12A	129.594555	-1.886708	0.025110
CG32437	1.191960	2.555635	0.025131
SMC5	7.384654	-1.435011	0.025131
wgn	11.028558	1.401499	0.025159
CG12811	32.735152	-1.417822	0.025159
CG9289	0.466757	-3.754990	0.025167
holn1	17.415709	1.447582	0.025182
CG9467	22.418653	1.378176	0.025233
CG43666	17.036267	-2.596073	0.025234
bai	264.609272	1.394544	0.025263
Ack	17.842941	1.488642	0.025707
regucalcin	195.599477	-1.620044	0.025707
lbl	0.383899	-3.933326	0.025707
phr	8.885188	-1.515461	0.025715
Smyd4-4	19.694992	1.386137	0.025923
Cpr47Ee	1.412975	-3.002840	0.025923
CG7272	59.875451	-1.387035	0.026106
CG15625	0.379400	4.899611	0.026347
Aprt	16.116089	1.594015	0.026354
Calr	1012.435466	1.476644	0.026385
CG43658	3.858581	1.400567	0.026390
Taf6	15.555852	1.375391	0.026555
Adat1	4.668082	-1.623026	0.026743
CG46310	9.630800	1.408097	0.026795
Pli	14.625256	-1.378076	0.026795
CG13643	0.902562	-2.591204	0.026795
spz3	13.827037	1.438779	0.026918
stac	19.946916	1.389173	0.027030
otk2	2.558265	-2.211718	0.027030
CG9960	12.944069	1.553763	0.027033
Ady43A	10.950394	1.405443	0.027033
Irp-1A	27.617372	1.339112	0.027039
Lcp3	3971.634572	-1.714363	0.027178
CG2187	0.271047	-9.289657	0.027771
Spc105R	2.410237	-1.720312	0.027781
Dll	2.350001	-2.209801	0.027991
CG17454	45.153968	1.396917	0.028134
Liprin-beta	26.262211	1.330604	0.028134
SsRbeta	380.464641	1.512149	0.028137
Wnt5	6.020542	1.541188	0.028239
CG12213	26.752900	1.369241	0.028270
CG9536	23.156287	1.351438	0.028270
RagC-D	26.044093	1.330097	0.028271
Ku80	8.773645	-1.437754	0.028343
nompB	0.151439	-17.639941	0.028451
CG34057	4.233900	2.044401	0.028509
Dak1	88.029257	1.370241	0.028535
CG31125	2.190545	-2.520330	0.028571
ed	28.745281	-1.429613	0.028714
CG32163	17.080573	1.549997	0.028787
PSR	26.134463	1.339667	0.028787
CG14767	86.921036	-1.400528	0.028787
CG31301	35.369491	-1.402894	0.028844
tal-1A	4.349147	-1.935931	0.028873
Doc3	0.868198	-2.953511	0.028889
CG2747	10.991502	1.357473	0.028916
CG3520	6.809740	1.371282	0.028921
RSG7	0.563026	-2.441413	0.029415
Eglp4	22.285872	-1.679035	0.029621
CG4645	25.065309	1.343611	0.029624
CG1632	15.309763	-1.532013	0.029655
Muc30E	0.140929	-5.098411	0.029701
alphaCOP	74.650621	1.449250	0.029706
AIMP2	73.842116	1.376590	0.029994
Nipped-A	10.354226	1.408972	0.030065
Adk3	19.418961	-1.381362	0.030065
CG1607	17.360434	-1.449327	0.030065
r-l	23.732054	-1.397001	0.030071
CG5235	3.966809	-1.756878	0.030226
CG13454	0.787469	5.034015	0.030260
CG11899	35.237247	-1.716401	0.030269
CG11399	7.635535	-1.421161	0.030274
CG1142	31.787687	-1.342903	0.030276
CG6426	119.086131	-1.379622	0.030365
Cyp4c3	34.107701	-1.474331	0.030390
pix	166.270107	1.496969	0.030537
CG32645	10.154336	-1.423469	0.030537
emb	43.217338	1.419190	0.030601
Acer	5.417340	-1.702763	0.030601
CG7294	182.724262	-1.742085	0.030601
SmydA-4	1.650900	-2.677041	0.030774
CG32284	2.660721	-3.159379	0.030854
dve	0.700478	-2.588831	0.030912
r2d2	23.612527	1.337567	0.031006
pre-mod(mdg4)-U	1.294942	2.365762	0.031015
CG43740	0.302783	3.895359	0.031073
Rbbp5	13.784813	1.390230	0.031228
Tailor	47.296850	-1.351210	0.031242
Lip1	0.680805	-3.200466	0.031242
CG10512	23.992717	1.617401	0.031279
CG9701	70.180913	1.496035	0.031351
Ten-a	0.829906	-1.855629	0.031351
CG10096	0.099147	-5.601022	0.031351
GV1	70.544759	-1.465572	0.031357
mirr	4.132321	-1.698737	0.031367
Sec22	72.301989	1.402676	0.031492
CG5991	8.592474	1.495720	0.031627
CG5225	1.768163	-2.434232	0.031652
CG11474	16.336810	-1.352809	0.031660
CG4793	2.017979	-1.960691	0.031893
Krn	8.181220	1.641097	0.031965
CG4041	18.155533	1.400269	0.032018
Ppi1	0.117683	-9.607726	0.032018
CG6295	0.688933	-18.625772	0.032018
Gtp-bp	102.528518	1.391052	0.032078
Arv1	14.312561	-1.486849	0.032217
mrt	19.944998	1.369745	0.032244
beg	13.672663	1.549191	0.032303
CG34451	0.304037	5.457237	0.032429
Achl	4.205841	1.756321	0.032429
rnh1	16.689398	1.453669	0.032429
CG6910	8.699763	-2.332766	0.032455
CG6985	3.168080	1.944130	0.032459
CG5984	0.403711	-4.596095	0.032600
CG30015	11.416545	-1.405131	0.032624
CG5270	4.173702	1.374471	0.032629
CG30380	10.419433	-2.069327	0.032758
CG10165	5.439622	1.702313	0.032825
CG16762	1.229539	-4.628674	0.032885
Tg	32.585553	1.579989	0.032905
CG42741	0.214430	-4.573416	0.032905
TwdlG	2.047358	2.823698	0.032998

SK	0.276321	-2.589153	0.032998
SerRS-m	9.284908	-1.353258	0.033182
Spn43Aa	12.124537	3.751083	0.033259
CG13318	8.366829	-1.705927	0.033416
gskt	0.184066	7.433375	0.033425
CG4928	39.342563	1.384810	0.033425
gem	11.059624	1.366070	0.033433
Obp56a	1015.067441	-1.698334	0.033433
Prx2540-1	10.134212	-1.787756	0.033433
Set1	14.646284	1.365124	0.033436
CG11807	22.041525	1.346944	0.033624
cyr	0.733352	-2.740737	0.033624
CG7800	10.020601	1.494754	0.033665
CG14526	3.351826	-1.898725	0.033665
TppII	51.458136	1.414695	0.033706
Proc	2.101806	-2.198060	0.033855
CG13531	6.768741	1.367084	0.033921
CG17359	5.383328	1.903919	0.033957
CG33298	11.815726	1.334107	0.034060
CG43124	20.952445	-1.629201	0.034091
KdelR	165.642883	1.434894	0.034105
Mal-A6	0.308694	-5.582631	0.034160
Pkc98E	7.536461	-1.374526	0.034262
trol	190.453352	1.443622	0.034278
shams	15.440788	1.452299	0.034325
Taf1	10.815826	1.396027	0.034339
corn	5.824624	-1.427641	0.034339
CG3397	3.071811	-2.885867	0.034408
tgo	26.874525	1.361879	0.034464
CG15269	3.033262	-2.149842	0.034469
CG8788	2.881314	1.980996	0.034635
RpI135	8.574442	-1.361169	0.034635
CG42524	1.673963	-2.236164	0.034680
GstO3	223.577966	-1.399210	0.034948
mahj	12.040432	1.386086	0.035002
Cpr11B	26.346004	-4.476631	0.035002
mRpS31	23.843567	1.354609	0.035153
Ste:CG33242	0.730219	-10.674157	0.035366
stwl	3.544617	-1.597954	0.035384
Spn27A	57.798650	-1.383642	0.035524
Asator	3.948026	-1.374485	0.035723
CG5835	32.411121	-1.387275	0.035790
CG16974	36.721707	1.401107	0.036507
Npc1a	55.469495	-1.426717	0.036507
CG11261	1.811493	2.267476	0.036577
Hdc	0.071900	8.798234	0.036654
dpr7	0.989143	2.890320	0.036964
Strn-Mlck	5.859921	1.376134	0.037112
CG31100	8.136281	1.490423	0.037196
hid	1.726194	-2.016730	0.037196
msd1	9.417508	-2.034445	0.037472
wech	2.650627	-1.439274	0.037727
CG44247	0.740473	2.344743	0.037802
CG2865	7.450642	-1.369012	0.037805
Usp8	13.194402	1.329353	0.037867
CG10283	22.015317	1.370321	0.037917
Ugt36Ba	11.488864	2.152976	0.037998
prom	0.168376	-3.827443	0.038018
CG9269	4.282116	-3.236861	0.038038
CG9205	41.484911	1.344294	0.038093
CG5039	22.985187	-1.560491	0.038093
gas	1.421831	-2.397611	0.038362
CG10151	0.606370	-2.973439	0.038424
CG7028	12.317682	1.342140	0.038465
wls	9.077399	-1.408258	0.038465
CG10068	16.479932	1.354722	0.038484
CG32241	526.561319	-1.583383	0.038484
CG11249	0.194073	-6.973528	0.038878
ste24b	1.168671	2.590075	0.038990
CG10184	13.480799	1.510215	0.039109
Vps53	9.677910	1.364583	0.039212
CG14291	60.329588	-1.391563	0.039301
CG2010	3.924166	-2.013263	0.039375
Rh5	0.684348	3.047852	0.039449
CG42235	0.195407	-4.571138	0.039542
Sdic1	0.208374	-5.872308	0.039542
Elo68alpha	11.775412	3.736975	0.039581
sand	0.896498	-2.873347	0.039631
Hsc70-5	104.021157	1.424015	0.039663
CG3634	15.688280	1.355014	0.039663
egl	31.724434	1.392767	0.039665
CG43293	10.204123	1.909185	0.039667
Rnb	3.879058	1.605788	0.039669
CG3045	5.589085	-1.630567	0.039669
DIP2	14.055725	1.353691	0.039683
T48	10.618212	-1.374755	0.039683
Pka-C3	3.427464	-1.682547	0.039683
Scp2	2.627602	-3.770395	0.039683
miple1	3.534640	-1.923211	0.039952
boi	4.290463	-1.569056	0.039974
CG32708	12.994303	1.615732	0.040070
CG14245	0.886718	-13.096580	0.040158
Npc2h	2.624359	-3.117562	0.040391
CG18596	11.650771	1.324658	0.040451
CG7394	17.242940	1.361473	0.040460
CG17636	0.135462	8.797618	0.040556
m-cup	8.275412	1.362927	0.040604
Jheh3	279.049279	1.521631	0.040778
CG5116	7.254884	-1.383145	0.040778
CG3880	5.855460	-1.804731	0.040778
GstD8	4.859430	-2.244628	0.040778
CG44006	0.349704	4.541792	0.040870
Galk	6.803240	1.430780	0.040913
CG1998	17.322933	-1.408206	0.041093
CG8852	1.897063	-2.298652	0.041225
CG13482	1.666216	-3.867359	0.041245
CG3594	23.071633	-1.411601	0.041296
strat	25.873499	1.401900	0.041418
CG33253	0.190779	3.882657	0.041469
tilB	0.679849	-3.491139	0.041649
Ih	5.092477	1.354987	0.041711
pyr	3.682682	-1.633214	0.041759
fz4	6.988506	-1.358877	0.041840
Sec16	12.412644	1.385734	0.041951
CG32687	3.242492	-1.742015	0.042036
ITP	20.853624	-1.343274	0.042048
CG11584	0.388865	-3.441433	0.042048
ena	8.917321	1.403139	0.042126
CG1902	69.126200	1.382843	0.042126
tau	1.489077	-1.811528	0.042126
CG11816	0.249344	79.750559	0.042152
dunk	0.462678	-5.532466	0.042152
CG3040	20.182274	1.423650	0.042257
Sec63	95.473795	1.412314	0.042257
CG16782	0.852187	-3.101616	0.042257
CG43291	0.222656	-4.381866	0.042257
CG4557	10.615687	1.410895	0.042521
GluRIIE	1.432985	-1.943594	0.042664
Osbp	37.512118	1.390014	0.042722
sty	6.547141	-1.396101	0.042729
Chd64	808.880321	-1.472992	0.043231
CG5167	54.460725	-1.348650	0.043321
sub	4.797924	-1.620246	0.043630
RAF2	14.138185	1.353997	0.043735
GstD5	1.846339	-3.187668	0.043742
Hsp70Bc	0.596289	-3.608056	0.043983
CG14262	0.436429	-4.780910	0.043983
Obp18a	0.902532	-6.053598	0.043983

CG10953	320.986796	-1.903830	0.044020
RpL37b	1.132725	-19.847152	0.044086
CG8097	2.714555	-1.923159	0.044196
ninaD	0.227848	-7.007506	0.044305
pre-mod(mdg4)-AB	3.230815	2.360536	0.044620
spidey	10.930629	1.772626	0.044658
CG9186	102.862566	1.354035	0.044800
spag	9.895027	1.453967	0.044815
CG6695	17.061245	1.403823	0.044824
CG15067	0.484508	11.169895	0.045164
tnc	0.806436	1.942000	0.045303
CG8549	26.648490	-1.343952	0.045307
Dup99B	1.269686	6.649555	0.045411
Dat	6.921171	-1.645848	0.045602
Gpb5	2.403902	2.618422	0.045621
Dlic	83.004434	1.428482	0.045745
Pym	17.465450	1.534219	0.045762
Orc6	10.150548	-1.644554	0.045813
CG5382	42.527062	1.369445	0.045917
Pkcdelta	0.602518	-2.083904	0.045940
CG7763	2.425461	3.261104	0.045996
bun	20.640317	-1.429612	0.045996
tal-2A	4.489210	-1.881846	0.045996
CG15369	9.964354	-2.934775	0.045996
TfIIEalpha	18.533846	1.338497	0.046045
CG17752	0.456689	-4.813645	0.046086
CG3819	0.373473	-22.865859	0.046263
CG34383	6.132274	1.343648	0.046294
Tis11	26.088942	1.406684	0.046337
CG3868	0.564733	-4.120083	0.046337
CG14598	19.775335	-1.757599	0.046382
CG9522	0.288456	4.340882	0.046561
Zyx	38.832983	-1.347387	0.046561
GstE2	1.472228	-3.240890	0.046561
dgt2	16.312340	-1.540822	0.046722
Tret1-1	4.335348	-1.526156	0.046822
CG32640	1.910923	-135.007394	0.046822
CG9302	69.882230	1.359490	0.047137
CG11857	79.553068	1.348644	0.047345
CG9062	13.487337	1.328637	0.047616
Spn55B	21.774122	-1.367171	0.047616
CG4587	0.027668	8.260831	0.047777
Cpr47Ea	4.942057	2.354015	0.047788
Fib	64.834264	-1.341129	0.047792
CG3036	510.738255	1.453179	0.047827
Obp99a	4.469928	-2.560820	0.047861
mAChR-A	0.169725	-3.488179	0.047986
Hs6st	71.449325	-1.373358	0.048047
CG6791	12.111761	1.461785	0.048085
Lip4	0.520974	-3.358708	0.048116
CG12592	5.252022	-1.705736	0.048184
Hrd3	29.321749	1.333521	0.048255
CG31826	15.188047	-1.486882	0.048255
CG43134	161.936318	-1.576435	0.048255
CG4306	5.052785	-2.008834	0.048255
P5cr	24.035738	1.361607	0.048297
HPS1	4.659367	-1.598790	0.048328
CG10333	15.570108	-1.311021	0.048361
CG14327	0.444239	5.652280	0.048428
CG12935	11.054221	1.575149	0.048428
prel	32.277675	1.375192	0.048428
CG12003	0.920794	-2.699981	0.048428
SCCRO	20.161357	1.312561	0.048592
CG12173	32.699687	-1.329296	0.048603
CG14882	5.259508	-1.591057	0.048654
Art3	21.460913	-1.312228	0.048771
CG13604	3.866483	-1.536141	0.048775
Tsp42Eo	4.330146	-2.238963	0.048775
Cyp4d20	28.608154	1.456055	0.048885
CG43078	3.966558	-1.706527	0.048885
Cln3	2.288877	-2.208182	0.048885
ord	0.200211	-118.920635	0.048885
CG9281	71.584056	1.357261	0.048910
Pcyt2	4.763470	1.835422	0.048942
Vsp37A	30.783157	1.318966	0.048988
CG5151	6.115141	-1.386460	0.049133
CG11752	69.083550	1.382339	0.049374
CG6675	0.931940	-2.918481	0.049374
Aef1	14.196037	1.371031	0.049417
twr	247.267222	1.362579	0.049425
Idgf2	359.110354	1.468328	0.049425
CG34281	2.025882	3.421916	0.049428
fz2	18.010508	1.409288	0.049521
CG8778	97.885597	1.365346	0.049521
asp	2.652656	-1.701849	0.049549
Cyp6a21	4.339897	-1.952517	0.049651
CG9920	0.921421	3.322985	0.049651
Rpb10	72.081649	1.347984	0.049651
repo	0.384052	-2.955060	0.049651
CG32803	19.958798	-1.382794	0.049659

Regulated genes of trachea that expressed *Yki.CA* for 16h.

Name	Max group mean	Fold change	FDR p-value
CG32783	0.523619	262.528480	0.006489
CG13299	44.423524	231.633649	0.000000
CG32640	2.381703	172.080619	0.025378
Sgs4	0.807213	116.965693	0.027339
CG7587	1.265834	105.683405	0.033187
Sgs5	1.043434	100.523818	0.036219
Sgs3	3.211140	60.130363	0.000000
Sgs7	9.696916	40.583444	0.000000
Pcp	125.921702	38.503630	0.000000
CG14332	45.349013	31.784481	0.000000
Mal-A2	0.846974	29.178482	0.000001
CG12715	0.317420	27.878224	0.004298
CG14960	28.317353	27.839584	0.000000
CG7142	6.249322	23.387797	0.000000
Eig71Ee	0.923827	23.238625	0.000007
CG14545	0.685893	23.210048	0.006197
Sgs8	1.511472	22.551300	0.006659
CG13280	0.311144	22.549286	0.006345
CG42834	6.790593	21.094655	0.000000
CG42296	0.141463	19.280453	0.019375
CG43737	3.344682	16.459331	0.000000
Hsp70Bb	253.368988	16.189958	0.000000
Cyp6g2	1.220147	16.064271	0.000004
ppk6	2.731780	15.183768	0.000000
Sgs1	0.152242	14.505045	0.003379
Amy-d	37.922072	13.809758	0.000000
CG15696	0.480307	13.764910	0.031457
CG2663	182.355222	13.523049	0.000000
CG33333	239.349445	12.944396	0.000162
pre-mod(mdg4)-I	1.497281	12.927868	0.000000
CG42798	9.124990	12.798693	0.000000
Fer3HCH	0.399436	12.481420	0.049655
CG4382	1.920727	11.954048	0.000000
Ubx	258.062246	11.855396	0.000000

CG7991	5.119101	11.848532	0.000000
spok	6.928995	10.974787	0.043445
CG30080	0.156944	10.698276	0.012722
Hsp23	93.586888	10.622595	0.000000
CG16710	1.435721	10.580742	0.000001
BoYb	0.175721	10.571605	0.002046
CG4325	0.677426	10.296015	0.002548
CG15919	2.558578	10.264791	0.000029
ltl	35.789702	9.973813	0.000000
CG13177	1.940035	9.857189	0.000000
CG14662	0.368858	9.643401	0.000884
jhamt	0.720431	9.570661	0.039800
CG43998	0.328739	9.125716	0.029407
CG9121	3.637197	8.902407	0.000000
yki	920.607658	8.773738	0.000000
Cpr76Bd	0.080721	8.769165	0.029779
CG17083	0.184764	8.756397	0.025361
CG16789	1.749331	8.665691	0.000000
CG44956	0.942827	8.388706	0.028458
Tdc2	28.938558	8.086497	0.000000
Amy-p	12.729235	7.750632	0.000000
CG13272	8.263040	7.337703	0.000000
CG11714	0.118949	7.060688	0.030006
sage	2.634219	7.055825	0.000000
CG13692	1.362446	6.983892	0.000525
Cyp304a1	0.595386	6.882820	0.000670
Spn43Aa	10.399970	6.721229	0.000000
CG6034	4.212183	6.464283	0.000000
CG5646	7.443814	6.452500	0.000000
sad	4.444655	6.128103	0.008899
CG42249	0.674964	5.876332	0.000066
Jon25Bii	0.490008	5.816617	0.023306
Vha14-2	0.509549	5.815995	0.000962
CG14221	0.264412	5.776091	0.014393
CG33946	1.409598	5.760964	0.030734
Arr2	0.798160	5.664856	0.000464
CG42500	284.118736	5.660815	0.000000
CG14183	1.207367	5.593444	0.000000
CG17105	46.684556	5.573591	0.000000
Hsp22	0.478120	5.560085	0.002088
CG18258	2.465340	5.462941	0.000000
Jon25Bi	0.468493	5.310782	0.049845
CG44013	42.882116	5.210903	0.000000
CG46312	0.325289	5.199357	0.016298
CG32073	1.323999	5.179135	0.005616
CG3457	1.828406	5.127996	0.000025
Fbp1	34.162184	5.125392	0.000026
CG18563	1.399821	5.104423	0.000450
CG3812	1.167146	5.033246	0.000004
gt	1.232617	4.925680	0.000014
pre-mod(mdg4)-AE	2.411214	4.867868	0.000000
CG13062	1.819519	4.784750	0.000409
CG5921	1.437974	4.689472	0.000000
c(2)M	0.558594	4.680917	0.001066
NimC3	0.701547	4.668107	0.023125
Timp	89.406546	4.617369	0.000000
CG6660	1.315793	4.524456	0.042134
CG18558	0.315171	4.460249	0.020634
krimp	4.594455	4.419833	0.000000
CG9411	1.786425	4.327273	0.000000
CG42564	0.864895	4.269725	0.001036
CG5987	2.012241	4.253295	0.000000
mthl6	1.288687	4.207614	0.000146
CG16984	1.014723	4.100474	0.011152
l(2)41Ab	4.275125	4.065940	0.000000
CG8908	0.932821	4.022427	0.000000
CG4570	0.455893	3.966496	0.043969
CG4020	0.649338	3.899286	0.015254

DptA	2.106836	3.860065	0.009929
Mst36Fb	0.928550	3.845719	0.001640
CG18336	1.996892	3.824248	0.001223
Osi15	21.384254	3.785413	0.000000
CG6785	0.590428	3.771098	0.000049
CG46316	0.525989	3.757285	0.009997
CG6071	0.686306	3.748012	0.000422
CG34215	25.053321	3.705015	0.000000
alrm	0.648333	3.684461	0.010875
CG33655	0.775179	3.654333	0.044567
CG32563	2.738298	3.637861	0.002318
CG42662	39.488647	3.567907	0.000000
Lcp65Ad	4.543198	3.543705	0.001604
Ace	0.781931	3.536017	0.000000
Osi24	23.385030	3.450803	0.000000
CG5999	0.740005	3.440932	0.009645
Pebp1	2.669312	3.433459	0.009349
fuss	1.822136	3.333870	0.000000
Obp57d	2.239048	3.312652	0.000010
phm	6.078566	3.310805	0.026244
Ccp84Ae	20.781472	3.309410	0.000008
Pex7	0.441355	3.307659	0.046935
CG4238	2.231994	3.302589	0.000000
CG40498	0.380893	3.300441	0.008110
CG13445	3.542115	3.293255	0.002597
CG17107	35.329784	3.287217	0.000017
CG5866	32.323433	3.269262	0.000000
pyr	31.563103	3.260774	0.000000
ppk13	22.278735	3.238748	0.000000
Ir76a	6.109032	3.217540	0.000000
CG42342	24.344960	3.207441	0.000000
PH4alphaEFB	47.508657	3.175593	0.000000
CG15766	4.401802	3.165831	0.000011
CG11475	0.535520	3.108135	0.031985
CG31676	15.720744	3.075071	0.000000
Cpr64Aa	4.579658	2.983229	0.008428
CG34164	0.944718	2.941383	0.011298
Taf12L	5.729142	2.937668	0.000106
CG15909	0.850186	2.930107	0.033187
CG42807	3.569362	2.927657	0.000000
alpha-Est4	0.448541	2.925925	0.034476
CG14102	6.441745	2.905978	0.000000
CG18754	0.545717	2.904605	0.029720
CG31817	0.150594	2.888521	0.023353
CG43293	6.789641	2.851356	0.000041
CG17018	1.253528	2.842268	0.000001
Tep1	3.055146	2.835044	0.000000
CG17803	6.407069	2.831815	0.000000
Mst36Fa	0.791105	2.798925	0.026595
CG5888	17.450715	2.795578	0.000000
GstD9	42.860655	2.795511	0.000000
CG13627	0.630112	2.770518	0.009695
Dlip2	18.400257	2.766445	0.000000
CG43163	21.458563	2.753955	0.000000
CG34330	5.654427	2.743473	0.009645
ect	57.773568	2.740160	0.000000
CG7300	4.778951	2.726849	0.000010
nyo	15.487399	2.672014	0.000000
CG9444	0.802262	2.658256	0.020354
CG10019	2.075011	2.648262	0.000000
Hsp67Ba	3.355721	2.644790	0.001154
NijC	12.843591	2.625634	0.000000
Cpr67Fb	12.166670	2.623171	0.000042
CG17931	31.876386	2.622533	0.000000
CG14454	6.724240	2.622191	0.002451
stg	58.928631	2.619474	0.000000
Pvf2	12.498653	2.614337	0.000000
sing	1.001156	2.589611	0.019368
sxe2	4.310520	2.589486	0.000001

CG7201	5.542206	2.573510	0.000000
CG5618	16.067559	2.558239	0.000000
CCKLR-17D3	0.808713	2.542512	0.020160
CG6845	14.095159	2.510908	0.000000
Prip	65.499260	2.508990	0.000000
CG6770	2483.322293	2.487168	0.000000
Sry-alpha	1.275746	2.484788	0.001066
rk	3.187379	2.483574	0.000000
CG14131	7.324622	2.481125	0.000000
CG6753	20.339656	2.474183	0.000000
Fuca	17.289029	2.465609	0.000000
Cat	1037.654248	2.463057	0.000000
CG43980	2.698609	2.460671	0.000000
Tdc1	73.041040	2.447939	0.000000
Rh5	2.143235	2.410870	0.001853
CG6484	0.890727	2.408008	0.049044
TotA	6.295406	2.401971	0.007942
Reg-5	354.258313	2.399486	0.000000
CG11261	1.948470	2.393087	0.001567
CG10960	24.642939	2.388921	0.000000
CkIIalpha-i3	14.535823	2.357319	0.000000
Klp54D	10.932260	2.351832	0.000000
Cyp4d2	3.732389	2.351520	0.000000
CG5096	1.282771	2.341872	0.011523
CG42231	12.365229	2.337824	0.000000
pgant5	52.777894	2.321758	0.000000
CG2812	13.344322	2.321549	0.000000
Toll-7	9.766167	2.314815	0.000000
pre-mod(mdg4)-AB	2.744338	2.307316	0.007721
Sgt1	59.168617	2.305174	0.000000
cry	1.431486	2.296249	0.005893
CG4766	8.525990	2.293619	0.000000
PGRP-LB	9.658735	2.291914	0.000000
CNPYb	46.040241	2.281747	0.000000
ppk28	0.885782	2.276046	0.019457
NimB4	12.344703	2.271997	0.000000
Cadps	4.269412	2.249206	0.000000
CG10098	48.827392	2.242067	0.000000
kon	2.854572	2.241769	0.000000
CG13728	1.368032	2.227286	0.011040
Nse4	5.480418	2.224649	0.000008
CG12204	8.775250	2.221637	0.000001
CG8854	7.356295	2.220442	0.000000
Hsc70-3	644.259136	2.212673	0.000000
Nnf1b	2.896281	2.205212	0.026880
Gp93	597.813926	2.192916	0.000000
Cyp313a3	20.743134	2.192034	0.000000
CG14879	15.622454	2.186965	0.000000
CG6923	6.593900	2.184492	0.000000
Pu	49.539388	2.177802	0.000000
CG14785	1.765167	2.172459	0.010991
Syn1	3.848685	2.162667	0.000000
ste24b	1.574116	2.147239	0.043752
CG6910	5.182500	2.144956	0.001499
cib	1036.537754	2.130517	0.000000
CG6023	2.879622	2.129760	0.004218
Indy	129.605783	2.120080	0.000000
CG15362	11.223788	2.117807	0.000002
pre-mod(mdg4)-U	1.258799	2.117651	0.003617
Hsp27	87.125550	2.112028	0.000000
CG6409	12.564506	2.104704	0.024484
l(2)k05911	266.167758	2.103132	0.000000
CG3386	7.214663	2.102235	0.000000
CG8372	42.312751	2.100826	0.000000
CG15628	0.857498	2.099237	0.011702
CG3502	19.955415	2.097748	0.000003
hng3	6.901419	2.096679	0.000006
CG43333	1.577101	2.093421	0.000536
CG33169	29.330221	2.087897	0.000000
CG9098	3.909066	2.086844	0.000000
CG12237	39.869115	2.085681	0.000000
Npc2a	56.262454	2.080003	0.000000
spir	12.086468	2.072838	0.000000
CG9257	26.830793	2.067303	0.000000
CG12017	8.197091	2.060476	0.000000
CG3323	1.052244	2.051132	0.017239
Cyp4d14	1.947528	2.047394	0.022193
CG11529	56.276041	2.044667	0.000000
CG9095	106.576344	2.044304	0.000000
mRF1	5.640376	2.028393	0.000067
Cpr65Aw	40.058743	2.027582	0.001333
fax	195.857955	2.024363	0.000000
Ilp2	4.184914	2.017084	0.038537
CG16717	17.966891	2.014191	0.000000
CaBP1	305.446077	2.012278	0.000000
Mis12	7.007365	2.008893	0.002145
Wsck	27.318295	2.008122	0.000000
CG7203	8.576477	2.007092	0.006134
Obp99b	220.031077	2.003140	0.001895
bip1	11.631075	1.997726	0.000000
CG10462	16.986405	1.993249	0.000000
Cpr11B	75.360542	1.991381	0.000009
mu2	8.904426	1.990433	0.000000
Sodh-2	291.834497	1.988697	0.000000
CG17350	7.093909	1.988086	0.000372
CG1673	111.690214	1.982051	0.000003
CG31473	5.416509	1.980607	0.007259
Nf-YA	9.201248	1.980272	0.000000
LManI	3.142833	1.961441	0.000046
Pkc53E	1.597761	1.959990	0.000085
CG6310	73.226441	1.955916	0.000000
CG44249	1.987258	1.947103	0.035512
CG12224	2.286733	1.929591	0.029864
pre-mod(mdg4)-X	2.782777	1.922957	0.000959
CG4456	1.612944	1.922633	0.027339
CG1418	31.040274	1.913985	0.000000
CG34057	5.056869	1.913027	0.003123
CG13995	1.179049	1.912108	0.027722
CG33509	8.199063	1.910604	0.000015
Drs	54.618209	1.909419	0.014011
Dtg	48.448573	1.905283	0.000000
CG7763	2.873315	1.904737	0.043445
CG10089	3.553676	1.900651	0.000001
CG17359	5.477039	1.898341	0.001112
CG6055	5.711141	1.897501	0.007364
Oscillin	30.400630	1.896453	0.000000
CG18853	12.353351	1.884851	0.001031
ver	6.780665	1.881099	0.012263
Dp1	175.660044	1.878930	0.000000
Wnt5	8.953020	1.878090	0.000000
CG13896	7.988697	1.877819	0.000284
CG43107	12.216893	1.877252	0.018581
CG3631	5.137613	1.873032	0.000004
CG40439	89.542443	1.870799	0.000000
CG12213	38.142581	1.867391	0.000000
DnaJ-1	57.025806	1.866696	0.000027
CG1416	100.395314	1.858449	0.000000
CG32564	367.392377	1.854039	0.000001
Hsp70Ab	3.723488	1.847420	0.018560
Meics	7.904369	1.847055	0.000005
CG6511	5.336671	1.842847	0.000000
az2	5.483752	1.840080	0.000044
JhI-21	22.343986	1.826341	0.000000
Rich	15.275405	1.820265	0.000000

CG17121	198.513591	1.818889	0.000004
CG33331	6.414414	1.816623	0.000666
ry	6.332936	1.812602	0.000009
CG9723	15.333584	1.811919	0.000000
CG13314	24.471391	1.809162	0.000000
Ipp	26.040237	1.806494	0.000000
CG12877	9.603349	1.806466	0.000000
CG15747	8.414884	1.804416	0.000000
Gcn2	7.940693	1.802638	0.000000
HEATR2	2.825443	1.801231	0.000367
Alp1	28.635841	1.795884	0.000000
MFS3	139.920438	1.795557	0.000001
barc	25.199441	1.789539	0.000001
CG7985	6.857646	1.787730	0.000003
CG1943	173.887442	1.785397	0.000000
FASN3	1.869777	1.779366	0.018099
eater	10.002462	1.774942	0.000000
CG9759	27.628702	1.774279	0.002393
loj	119.010934	1.771635	0.000000
CG3226	90.837423	1.771480	0.000000
LManII	26.336664	1.768981	0.000000
Hsp26	9.419524	1.767473	0.000300
nmdyn-D7	6.512203	1.766683	0.000502
CG13369	28.373309	1.764632	0.000000
Mst85C	12.405212	1.763618	0.000002
mth	33.558078	1.763506	0.000000
tapas	37.110191	1.763121	0.000000
CG4306	8.248287	1.760073	0.000592
CG31075	97.299232	1.757995	0.000000
CG32855	4.862623	1.756179	0.008678
CG1764	14.079279	1.755218	0.000000
Tango9	16.305315	1.755103	0.000000
RhoGDI	389.619794	1.754801	0.000001
CG15011	9.075367	1.748613	0.000000
CG7456	23.315845	1.748295	0.000000
Calr	1535.383665	1.744961	0.000000
CG13116	12.921819	1.742782	0.000826
CG32276	361.481570	1.741742	0.000001
CG5391	15.772238	1.740751	0.008420
stx	26.956621	1.739386	0.000000
CG9662	51.854537	1.738626	0.000000
bnl	10.248312	1.738431	0.000000
SelD	89.866783	1.737864	0.000000
CG11382	11.179421	1.735734	0.030766
Lamp1	280.134923	1.730151	0.000031
CG8336	21.102722	1.728152	0.000000
mthl8	4.208530	1.726538	0.000047
kibra	54.305709	1.723974	0.000005
rumi	20.469369	1.723381	0.000000
ergic53	190.763130	1.723370	0.000008
Sry-delta	19.660767	1.723223	0.000000
CG7800	14.222043	1.721128	0.000000
CG14353	9.552123	1.715546	0.000017
nbs	8.419794	1.713878	0.000000
Elo68alpha	54.103362	1.711899	0.000126
CG4050	22.099629	1.711260	0.000000
Cht10	448.223336	1.711037	0.000000
dnt	9.826711	1.707535	0.000000
CG5335	15.626677	1.703933	0.000000
Fdh	256.268590	1.697761	0.000015
IleRS-m	6.258582	1.694165	0.000037
CG45071	15.813346	1.693801	0.000000
CG31370	15.325984	1.689283	0.000000
et	2.347117	1.688042	0.042348
TRAM	150.997655	1.686002	0.000052
Gld	53.836934	1.685995	0.000013
CG6749	18.229712	1.684286	0.000000
Ncc69	27.381612	1.682181	0.000000
CG8507	78.856490	1.682103	0.000001

GCS2beta	122.502436	1.680060	0.000009
CLS	20.535528	1.678977	0.000000
wbl	19.820785	1.677706	0.000000
CG13671	12.145049	1.677379	0.000000
CG15715	48.514039	1.676260	0.000000
CG14906	6.405982	1.674519	0.006859
shu	5.867878	1.672669	0.001125
CG32428	27.470802	1.671052	0.000000
pre-mod(mdg4)-L	2.792306	1.670470	0.025420
pAbp	712.096619	1.669045	0.000000
CG7255	13.544357	1.668709	0.000000
Impbeta11	17.761157	1.666812	0.000000
heix	16.844707	1.666599	0.000021
crc	422.082652	1.664918	0.000001
sced	5.091280	1.664614	0.000155
Pgant35A	15.514748	1.662946	0.000000
Dscam1	8.703741	1.662598	0.000000
scat	14.381227	1.662502	0.000037
SMSr	11.654384	1.660399	0.000000
Gasp	1137.541396	1.659656	0.000002
sqh	204.711268	1.655270	0.000022
CG33465	5.666105	1.653812	0.003824
CG3355	5.420931	1.652958	0.020517
CG5087	8.235219	1.651595	0.000000
Cpr78Ca	132.781936	1.650248	0.000000
PIG-V	10.228116	1.649120	0.000019
Cdc37	70.947551	1.648265	0.000000
CG11377	28.308668	1.647441	0.000000
CG7011	38.331714	1.646973	0.000027
koko	12.740685	1.646228	0.000065
CG40486	209.051573	1.645810	0.000000
grass	124.473191	1.643792	0.000000
tw	34.828018	1.642877	0.000003
rasp	19.889930	1.642717	0.000000
Spt-I	40.300577	1.637159	0.000000
pr	37.920895	1.636400	0.000000
His4r	574.945182	1.632838	0.000069
CG15435	4.224485	1.632148	0.005423
CG12009	61.097403	1.631434	0.000000
armi	14.595141	1.630822	0.000000
CG34227	1391.546529	1.625432	0.000088
Tango6	6.272819	1.625217	0.000162
TM9SF4	35.441283	1.625158	0.000003
CG31917	24.649516	1.624413	0.000000
CG3918	25.002072	1.623087	0.000000
ERp60	1223.783428	1.621845	0.000003
CG42336	41.410957	1.620861	0.000000
Culd	2.748050	1.620687	0.006833
Ccp84Af	42.970802	1.619968	0.000040
pll	19.462669	1.618880	0.000000
CHORD	31.721872	1.618799	0.000000
CG7453	42.990314	1.617331	0.000000
GABPI	22.401817	1.616264	0.000000
Pcd	156.316077	1.616161	0.000000
mib1	19.967213	1.615175	0.000000
sro	6.776292	1.613132	0.046935
CG6985	4.289244	1.610691	0.011351
CG33155	20.960016	1.610166	0.000000
CG2147	22.511791	1.609560	0.000403
grnd	39.490322	1.608853	0.000000
CG11306	41.598584	1.608827	0.000000
zip	128.640494	1.607048	0.000040
Tapdelta	241.305341	1.606590	0.000000
CG7294	159.044285	1.606433	0.000014
CG1888	5.390812	1.606007	0.000000
MP1	43.759799	1.605853	0.000000
CG2941	5.305820	1.604942	0.000000
CG2200	26.847558	1.603334	0.000000

gny	5.069064	1.602551	0.000259
CG12338	8.066328	1.602487	0.002597
CG42307	7.988482	1.601110	0.000000
Tfb5	24.567159	1.599996	0.000000
CG9304	20.327568	1.598019	0.000114
adp	13.519571	1.597476	0.000000
CG31100	20.653707	1.597291	0.000365
Sans	4.357584	1.597216	0.004297
CG6695	21.826609	1.595872	0.000000
CG9114	6.772223	1.594719	0.000758
CG9590	26.997289	1.594163	0.000000
CG11267	178.610285	1.593663	0.000009
CG10131	6.684562	1.592746	0.027041
tud	57.195814	1.592199	0.000060
CG33303	124.206248	1.589671	0.000134
CG4860	21.292755	1.587953	0.000000
Drep1	8.136597	1.587336	0.000296
CG11695	6.046914	1.587056	0.003824
VhaAC39-1	188.210811	1.585572	0.000556
GstT3	11.525257	1.585071	0.001452
Sec61beta	357.379215	1.582748	0.000113
Stip1	127.470093	1.582360	0.000084
GstS1	65.610117	1.579520	0.000000
Rab30	11.430112	1.579374	0.000000
CG1812	13.323207	1.578536	0.000000
PIG-K	32.702779	1.578428	0.000000
tun	5.760981	1.574596	0.000000
CG15098	319.651322	1.574405	0.000134
CG16989	17.534833	1.574268	0.000000
CG5126	19.314899	1.572659	0.000000
p115	29.393151	1.571266	0.000000
Pa1	26.079394	1.570183	0.000000
CG10907	10.505395	1.568962	0.000715
CG9547	15.574899	1.568588	0.000001
Cyp301a1	42.953339	1.568219	0.000000
Hmu	204.076333	1.567807	0.000382
CG43345	4.217622	1.567782	0.004909
CG14408	4.834958	1.567744	0.001315
Ets97D	10.932315	1.565033	0.000001
Vamp7	71.293907	1.564989	0.000000
CG7289	29.071523	1.563869	0.000000
Cip4	36.326137	1.562510	0.000000
Dgkepsilon	27.096646	1.561721	0.000365
drl	15.758359	1.560844	0.000012
Smyd3	9.684678	1.559142	0.001149
Nha1	172.934687	1.557570	0.000553
EMRE	73.212426	1.557469	0.000286
Pym	19.976776	1.556542	0.000002
shams	19.201620	1.554147	0.000001
CG5273	157.898600	1.552238	0.001193
CG32473	57.216780	1.551318	0.000163
veli	27.554966	1.549096	0.000000
CG6726	8.971352	1.548428	0.000001
CG13014	18.176334	1.548099	0.000109
Rcd6	39.132728	1.547477	0.000013
CG1662	16.635406	1.547102	0.000001
Coprox	35.622032	1.544735	0.000405
GlcAT-I	21.645866	1.543773	0.000001
CG17721	14.855668	1.541943	0.001774
CG9467	21.425781	1.540640	0.000000
mus304	4.164094	1.540545	0.012741
CG2004	100.745349	1.540310	0.000028
CG4041	19.252163	1.539243	0.000566
CG2852	582.126459	1.539172	0.000254
CG12159	19.684349	1.537201	0.000004
pie	4.331733	1.536953	0.009645
defl	8.173580	1.536693	0.000002
CG18858	20.842007	1.536437	0.000000
slif	25.086116	1.534968	0.000000
CG3570	12.124465	1.533547	0.001684
CG1632	39.457420	1.533347	0.000000
CG7420	9.716294	1.533231	0.003563
CG9267	16.999664	1.533213	0.000003
UK114	14.121078	1.533126	0.015129
CG2938	11.857580	1.532641	0.000000
CG13895	12.804272	1.528855	0.000003
CG8314	45.151348	1.524151	0.000000
CG4293	21.092679	1.523259	0.000001
CG6294	7.973319	1.522712	0.000003
CG8320	37.622264	1.522165	0.000000
sel	76.267307	1.520034	0.000000
wus	9.902816	1.519639	0.000007
CG6565	13.081351	1.518184	0.000002
mRpL53	26.594294	1.517750	0.000006
sofe	4.328401	1.517637	0.011098
CG4558	13.671846	1.517548	0.000003
CG32939	7.320660	1.517520	0.014782
IntS2	12.536889	1.516580	0.000001
CG4825	32.537170	1.515572	0.000000
CG7646	7.116991	1.514764	0.003980
Swim	672.060663	1.514755	0.000601
CG32809	1.003190	1.514135	0.031447
maf-S	37.720304	1.513491	0.000005
CG8230	34.996218	1.513475	0.000000
MED16	5.479349	1.513299	0.004019
CG2794	14.117783	1.512027	0.000002
CG1532	87.615510	1.511929	0.000033
Tspo	295.448204	1.511037	0.000529
CG5913	19.139956	1.510813	0.000003
alt	85.110816	1.510810	0.002987
CG17271	70.654617	1.509568	0.000000
Act5C	2784.374405	1.507279	0.000052
Vhl	5.680017	1.506966	0.047839
CG32163	16.385748	1.506468	0.007457
Tgi	28.380095	1.506329	0.000001
D19B	12.437038	1.505954	0.000003
fy	6.008424	1.505586	0.016704
Diap2	24.161408	1.505512	0.001112
CG43739	4.253102	1.505475	0.038694
nudC	47.454380	1.505442	0.000000
CG12024	17.339504	1.504074	0.000003
Usp8	15.960140	1.502611	0.001223
Rtca	7.198983	1.497245	0.004737
Krn	8.196398	1.496996	0.010224
CG18081	68.549654	1.496890	0.000000
OstDelta	173.058154	1.496564	0.004091
CG7744	13.490333	1.496275	0.000004
rg	5.679373	1.496063	0.000000
Nca	77.798174	1.494870	0.000001
CG11961	19.111935	1.494273	0.000001
CG32708	16.252541	1.493881	0.004829
CG4455	54.387663	1.492557	0.000001
Akap200	159.503984	1.492425	0.000783
NUCB1	146.381209	1.491915	0.002093
CG44242	82.479432	1.491437	0.000000
Rpb5	46.223806	1.491258	0.000002
msk	138.553773	1.490073	0.000869
Klp64D	16.202514	1.490009	0.000003
CG32521	49.213378	1.489522	0.000000
CG18542	14.734492	1.489254	0.001436
Arc1	426.803577	1.489068	0.000861
CG8202	12.041706	1.488782	0.000000
qua	2.628247	1.488679	0.014904
Atac2	7.083777	1.488665	0.002325
Pdi	892.081858	1.486777	0.000078
Taf7	6.237175	1.486642	0.003837
Eip63E	16.502986	1.486640	0.000077
CG11964	27.495467	1.484957	0.001466

CG5835	80.702854	1.484774	0.002196
CG8239	5.434121	1.483721	0.013030
CG7841	4.744727	1.482812	0.045828
CG17493	16.162078	1.482804	0.000001
Pdxk	26.061688	1.482320	0.000004
lectin-28C	5.557269	1.481325	0.046390
CG11686	119.779643	1.481063	0.000002
CG43143	7.122807	1.480796	0.000988
Mgat1	10.799676	1.480737	0.000010
hd	4.916962	1.480303	0.025384
Smyd4-4	23.194064	1.479606	0.000003
CG4000	232.589276	1.476848	0.000771
CG1667	26.677280	1.476772	0.000005
CG32249	895.459955	1.476548	0.032808
CG8370	10.129278	1.475857	0.000003
CG8420	17.201826	1.475270	0.000006
PIG-F	15.744128	1.472063	0.006223
kto	7.420717	1.471519	0.000004
mbf1	71.280221	1.469283	0.000001
CG9911	96.178859	1.469063	0.000001
Gdi	223.810758	1.468662	0.001540
l(1)G0320	315.798904	1.468386	0.001520
CG13796	25.505249	1.468259	0.000003
CG5554	166.787373	1.468233	0.001977
Ssl1	18.287836	1.467545	0.000015
CG2918	118.457999	1.466752	0.008135
CrebA	15.400885	1.466443	0.000003
CG11134	22.740834	1.466153	0.000046
CG10222	6.867960	1.466005	0.027467
Hsp60A	223.536048	1.465541	0.001623
CG6791	15.064779	1.465247	0.000004
PPP4R2r	47.063771	1.465162	0.000002
CG2145	125.156193	1.465073	0.001793
CG3107	37.435620	1.463132	0.000002
Lk6	80.787742	1.462156	0.001967
CG4646	24.540235	1.460201	0.000076
CanA-14F	25.297220	1.459049	0.000002
Spase25	119.493871	1.458917	0.000002
spag	12.258328	1.457316	0.000056
CG17260	5.879244	1.457192	0.047843
Trs20	24.405401	1.455257	0.007066
dlt	2.563315	1.455030	0.031693
CG6398	402.014854	1.452257	0.002624
CG3408	18.153246	1.450953	0.000024
CG7322	13.061900	1.450711	0.014037
Phax	12.488400	1.449489	0.000105
Fit2	7.402242	1.448353	0.000098
CG8229	8.004914	1.448175	0.006682
mav	69.779215	1.447996	0.000003
CG4496	6.260396	1.447930	0.004198
mus312	5.282518	1.446693	0.000095
CG8311	22.174685	1.446442	0.000019
sev	1.017938	1.446343	0.042902
CG5439	19.026737	1.445598	0.000028
CG30499	62.074372	1.445585	0.000009
CG32537	5.840815	1.445333	0.012050
CG1550	24.483144	1.445292	0.000015
Vps13B	3.374191	1.444962	0.000000
Ppt2	16.297907	1.444620	0.000408
CG2321	3.236620	1.444480	0.023714
CG3652	30.642750	1.444226	0.000057
Sec31	47.697058	1.444112	0.000004
csul	15.658778	1.444089	0.000038
Sod3	89.517570	1.444029	0.000004
CG17385	30.541556	1.443822	0.000012
uri	10.982534	1.443510	0.000063
CG17490	10.145145	1.443452	0.000047
gukh	5.471171	1.443159	0.000021
alpha-Man-Ib	15.913244	1.442881	0.005014

HP4	33.776775	1.442787	0.000077
pcs	35.596497	1.442475	0.000008
Hexo1	93.903345	1.442373	0.000004
CG18011	3.832473	1.439007	0.024481
CG14291	84.719094	1.438516	0.000131
GatC	9.862859	1.438510	0.011298
CG31712	20.203089	1.437797	0.000014
Bet1	33.979838	1.437663	0.000043
VhaM8.9	335.756427	1.436866	0.004801
CG30427	7.522525	1.436809	0.009616
ave	16.423513	1.436625	0.045792
goe	27.620994	1.436578	0.002873
CG14414	14.378261	1.436188	0.008963
Ssrp	49.120998	1.436134	0.000007
Tctp	771.436214	1.436047	0.000723
CG33230	8.942190	1.435245	0.011650
pix	151.196005	1.435161	0.009734
CG43103	28.097782	1.434901	0.013102
Ars2	47.169631	1.433991	0.000006
sn	54.316533	1.433961	0.000006
Stt3B	158.773691	1.433807	0.007003
ProRS-m	6.763492	1.433513	0.035466
CG10420	15.989881	1.433151	0.000069
CG31460	25.652450	1.433026	0.007394
Ing5	13.755490	1.432834	0.011287
Liprin-beta	31.027920	1.432600	0.000869
stc	20.663975	1.431828	0.000591
CG42503	11.741171	1.431718	0.012465
GCS2alpha	227.514012	1.431502	0.003712
KdelR	153.616510	1.430485	0.004621
Dak1	90.417850	1.430438	0.000347
CG3356	15.827135	1.429952	0.000020
CG6613	10.052843	1.429527	0.000123
deltaCOP	98.528042	1.429252	0.000007
Lap1	5.566979	1.429157	0.000109
VhaAC45	269.468948	1.429014	0.004588
CG6115	111.194542	1.428625	0.000015
Unc-115b	21.885142	1.428116	0.000299
CG3744	13.108761	1.427908	0.000022
ash2	20.219778	1.427737	0.000036
CG7685	9.052313	1.427682	0.044620
Gp210	26.865562	1.427563	0.000008
GM130	25.211233	1.427298	0.000019
CG30291	35.379377	1.426993	0.000024
Dlc90F	133.793398	1.426863	0.000012
O-fut1	58.442534	1.426844	0.000903
eca	155.531711	1.426494	0.000010
Charon	12.637199	1.425521	0.000167
CG15353	147734.934577	1.425500	0.000728
CG8038	21.199322	1.425370	0.002937
Evi5	7.725787	1.424284	0.005592
ebd2	5.098165	1.424047	0.038961
TBCB	31.557437	1.423554	0.000000
CG10948	13.166242	1.423167	0.000000
sprt	9.697220	1.421824	0.000125
CG9147	8.904498	1.421818	0.012297
CG14971	12.898202	1.421507	0.000093
r2d2	27.764032	1.420049	0.007534
boca	57.292630	1.419960	0.000000
zf30C	27.496062	1.419872	0.000022
ntc	6.543210	1.419803	0.045631
CG9149	30.649664	1.419408	0.000052
mld	12.433602	1.418724	0.003809
Mmp2	2.927960	1.417891	0.025813
Galphaf	9.830977	1.417435	0.001425
ZnT77C	21.912746	1.417362	0.016522
coil	12.990012	1.416466	0.000000
CG10602	91.581979	1.416022	0.000013
Mocs2	11.579843	1.415250	0.016664

Alg10	15.834272	1.414742	0.000210
CG12935	10.245613	1.414668	0.013081
Cypl	26.326991	1.414224	0.002024
mdlc	8.602726	1.414205	0.014589
CG15445	14.879740	1.413101	0.000000
CG4266	38.016307	1.411673	0.000018
h	49.443390	1.410735	0.006533
Miga	7.172116	1.410062	0.000193
Cnb	8.575521	1.409716	0.000351
CG6299	16.418629	1.408953	0.008060
Mlh1	6.403765	1.408522	0.020199
CG7414	163.319484	1.407953	0.011021
26-29-p	257.084692	1.407400	0.005378
alpha-Est3	7.715211	1.407199	0.025009
Sym	12.966758	1.406949	0.011900
CG18476	3.406056	1.406943	0.048258
Tango14	30.736235	1.406276	0.000000
IleRS	48.700402	1.405984	0.000022
PGAP5	9.410157	1.405743	0.013116
CadN	0.850016	1.404492	0.022465
CG7872	24.852677	1.404286	0.000108
Taf2	9.064661	1.404264	0.000000
CG13531	6.594398	1.404262	0.000000
CG10166	60.890872	1.403828	0.009607
Ufm1	76.902261	1.403588	0.009849
ade2	13.265882	1.402768	0.000068
Cog7	11.888753	1.402591	0.000239
CG42498	16.444962	1.401878	0.023720
CG3040	17.097987	1.400201	0.006057
Mer	11.938113	1.399609	0.000132
CG12643	30.844890	1.398922	0.000209
CG5745	20.935120	1.398806	0.000000
Rcd4	16.253061	1.398547	0.026686
Vps11	14.119701	1.398081	0.000143
CG10217	155.510982	1.398031	0.021318
CG8531	44.337024	1.397631	0.003456
wek	7.245796	1.397550	0.036191
CG5021	34.220153	1.397172	0.000000
CG3732	24.770762	1.396752	0.000235
Hsc70-4	1852.646996	1.396561	0.002041
Zw	33.097070	1.396394	0.002401
Tango10	12.533426	1.394659	0.000160
Egm	19.154989	1.394541	0.000000
Spase22-23	85.924552	1.394535	0.000043
Gmer	16.895895	1.394384	0.000746
Rnb	3.959341	1.394243	0.020105
18w	21.636378	1.393450	0.000052
sra	13.169924	1.393320	0.000267
CG7946	26.641334	1.392946	0.016419
Vha13	427.691932	1.392396	0.030734
RagC-D	28.162448	1.392387	0.000155
mEFTu1	67.398550	1.392352	0.000054
Nipped-A	11.571994	1.392271	0.000000
CG2614	13.484253	1.391336	0.000305
eEF1beta	915.483486	1.391186	0.007507
ex	45.592995	1.391162	0.013948
DCP1	19.632512	1.390942	0.000320
IntS3	26.882604	1.390699	0.003049
CG11790	111.868103	1.389769	0.000000
E2f1	28.295769	1.389715	0.000047
Epg5	12.857627	1.389630	0.000070
CG8010	12.632875	1.389594	0.000707
CG5885	234.444399	1.388896	0.008453
chic	299.182004	1.387239	0.008665
Vha16-1	854.015985	1.386961	0.002573
Torsin	57.748448	1.386692	0.000095
Rrp4	25.047085	1.386227	0.000408
Dhod	44.444121	1.385917	0.000120
ORMDL	21.031836	1.385791	0.024057

Fili	8.699902	1.385290	0.000194
CG5270	4.196004	1.384690	0.000364
PSR	28.630661	1.384677	0.000200
CG12404	57.859352	1.384188	0.000121
CG5510	56.935247	1.383761	0.000111
regucalcin	109.632510	1.383591	0.014011
ksr	7.137709	1.383395	0.000000
Twdlbeta	614.587981	1.381839	0.027124
Rab40	14.776217	1.381085	0.000604
Ih	4.198305	1.380624	0.015361
CG7791	13.651394	1.380520	0.000444
CG17059	62.941858	1.379693	0.000583
Sema2b	5.058524	1.378541	0.000630
ssp	18.260286	1.377726	0.000662
CG3368	16.875014	1.377087	0.000190
Atg14	13.666819	1.377031	0.000691
zetaCOP	76.205514	1.376914	0.000126
CG6454	16.310871	1.376735	0.001436
CG7277	20.230900	1.376646	0.000455
MESR3	14.059127	1.376519	0.000541
CG9804	19.768834	1.376448	0.000955
Gga	22.388916	1.376446	0.019638
CG43343	3.743391	1.376286	0.037330
CG11999	68.231431	1.375939	0.000193
CG7766	22.302803	1.375887	0.000113
JhI-1	12.804598	1.375311	0.000429
Nop17l	15.383741	1.375056	0.000201
CG10904	13.674406	1.374741	0.040769
Den1	19.415157	1.374610	0.000002
Paip2	43.321878	1.374220	0.004989
mi	7.147352	1.373594	0.000677
Picot	33.551744	1.373226	0.000131
omd	9.020451	1.372127	0.000563
Spp	139.767207	1.371513	0.011822
Scox	31.460709	1.371113	0.000549
Ublcp1	28.338218	1.371085	0.000516
MED7	26.029497	1.370823	0.001000
PlexB	18.578367	1.370593	0.000000
CG42557	11.161993	1.370380	0.040377
GSS	29.712635	1.369967	0.003787
gry	21.865462	1.369350	0.008420
Galt	16.904974	1.369157	0.000930
Irp-1A	26.497204	1.368582	0.000000
asun	5.174477	1.368388	0.035527
Cpsf100	13.752940	1.367393	0.000606
norpA	3.837609	1.367057	0.000662
Rpb10	78.065947	1.366957	0.000670
PIG-S	19.880237	1.366840	0.000001
bai	241.129966	1.366137	0.000132
primo-1	18.478761	1.365884	0.001065
Sec61alpha	327.087455	1.365504	0.012783
Ankle2	16.637261	1.365167	0.000273
CG6928	5.451186	1.365052	0.038489
CG12772	6.571496	1.364945	0.001423
Sec13	93.229977	1.364761	0.000149
CG2224	10.305019	1.364122	0.001393
Slmap	28.007826	1.363737	0.004909
Hlc	44.740216	1.363398	0.000221
CG32533	6.288734	1.362967	0.001374
CG31999	37.709494	1.362960	0.000178
alphaCOP	71.661475	1.362525	0.024196
CG15629	66.072257	1.362515	0.028674
Rpb11	38.860542	1.362291	0.001767
Mon1	15.465042	1.362138	0.000003
CG11851	14.992986	1.361637	0.000001
CG14803	7.206833	1.361571	0.001231
lok	14.255275	1.360583	0.000723
GalNAc-T2	38.296409	1.360581	0.000195
CG10802	21.514141	1.359434	0.000869

wol	46.744403	1.359178	0.000373
Mob4	66.131412	1.358437	0.000273
VhaPPA1-1	318.595864	1.357874	0.030708
Smox	23.280367	1.357447	0.006151
Ppat-Dpck	13.310203	1.357381	0.001612
CG11073	45.350344	1.356925	0.013315
CG31368	10.407333	1.356657	0.024827
Manf	231.600489	1.356359	0.000202
Dbp45A	17.671839	1.355745	0.001104
Tim8	59.703953	1.355010	0.000621
RabX1	10.871398	1.354906	0.018059
Jheh3	285.290992	1.354371	0.032497
CG4294	9.664533	1.353991	0.000644
CG8728	34.871979	1.353939	0.000425
CG30438	23.884062	1.353907	0.000372
anne	36.871227	1.353632	0.017363
CG3847	36.648252	1.353348	0.000384
cv-2	15.890427	1.353005	0.000433
CG31121	59.827954	1.352526	0.000232
Lpt	6.340288	1.352242	0.001259
Act42A	478.361399	1.351500	0.019573
CysRS	32.964855	1.351139	0.000408
Snx1	46.990150	1.351098	0.000365
CG7280	15.618041	1.350601	0.001110
Syx18	28.357421	1.349648	0.000859
CG11388	12.032060	1.349484	0.002685
crok	83.595528	1.349455	0.015328
CG5877	4.426576	1.348684	0.019800
Larp7	8.351569	1.347551	0.019375
Grip128	6.172793	1.347529	0.002440
RpII140	40.690080	1.347457	0.000317
isoQC	9.811466	1.347207	0.002547
Dcr-1	6.438024	1.347172	0.000847
amx	8.609447	1.346863	0.048735
wb	1.292925	1.346105	0.038933
mRpS34	28.307936	1.345857	0.002901
Stt3A	94.890693	1.345472	0.024519
SMC1	22.784854	1.345030	0.012722
MED14	11.782046	1.344942	0.000626
CG15544	10.296663	1.344748	0.000955
Srp54k	98.924697	1.344622	0.000332
CG15237	21.900623	1.344278	0.039892
Su(z)2	4.344271	1.344150	0.001641
CG1665	42.895172	1.344062	0.039363
Rcd5	24.516045	1.343913	0.035279
SsRbeta	311.049741	1.343772	0.031457
CG9302	71.827415	1.343471	0.000398
Tpr2	84.070054	1.343010	0.026820
PGRP-LE	16.135777	1.342932	0.001418
CG33774	71.551607	1.342433	0.002703
CG5382	39.871154	1.341715	0.026578
Vha55	328.810814	1.341404	0.029888
sog	22.538575	1.341217	0.011157
Glg1	50.801302	1.340498	0.000380
Ufl1	26.523386	1.340342	0.000713
CG10347	16.459111	1.339522	0.001502
ast	8.204852	1.339306	0.002896
CG12104	12.101666	1.339006	0.030766
ZAP3	19.586490	1.338953	0.000000
Sec61gamma	127.730461	1.338801	0.006221
CG31365	10.761381	1.338526	0.002492
CG6142	8.214704	1.337309	0.033491
CG45049	22.799492	1.336607	0.001975
CG17002	12.873993	1.336379	0.003261
lqf	20.137952	1.336279	0.000000
Ubc7	38.102875	1.336024	0.000809
Sin	23.534979	1.335950	0.001458
Naa20A	29.671680	1.334777	0.000005
Jwa	199.201832	1.334038	0.005567

CG5521	7.426916	1.333890	0.001059
l(1)G0007	20.626401	1.333559	0.002920
cathD	151.943901	1.333034	0.033863
Vha68-2	431.822513	1.332750	0.018862
CG9240	28.499696	1.332354	0.002547
Lrch	2.797248	1.332031	0.009704
CG9586	42.100288	1.332017	0.001603
Gs2	1690.553860	1.331966	0.010196
CtsB1	106.730456	1.331551	0.000603
brm	35.324567	1.331225	0.000580
mRpL21	12.272007	1.330983	0.004255
muskelin	7.508757	1.330280	0.003611
Nurf-38	154.472006	1.330262	0.004135
CG5516	20.777940	1.329652	0.033256
CG11029	34.243946	1.328831	0.001193
Usp47	40.762207	1.328725	0.013434
CG7239	10.414540	1.328043	0.020928
CG5339	17.689813	1.327825	0.004299
Ugt	42.130932	1.327744	0.008326
Sk2	22.426194	1.327347	0.001330
HDAC3	13.492032	1.327113	0.004255
TfIIA-L	48.273533	1.326929	0.001064
CG31249	15.220079	1.326576	0.043930
Plap	32.491023	1.326432	0.000980
RhoGAP5A	10.818088	1.326391	0.004838
CG4332	32.502964	1.326347	0.001148
CG11417	14.946095	1.326197	0.000009
oys	20.924852	1.325740	0.004862
Ino80	7.952252	1.325700	0.001953
CG2846	24.726400	1.325633	0.002914
CG5728	17.026384	1.325520	0.001129
Uch	71.481016	1.325493	0.015208
ogre	57.331402	1.325107	0.004307
CHOp24	171.104871	1.323124	0.000801
Bdbt	20.898240	1.323058	0.005336
Tsp97E	17.138283	1.323044	0.001967
Idgf2	139.017881	1.322782	0.040457
Lmpt	19.392249	1.322266	0.031145
put	23.109784	1.321903	0.001164
CG5484	49.120366	1.321818	0.000001
mip40	21.890689	1.321769	0.004518
capt	91.814035	1.321287	0.049188
CG11699	50.035378	1.321032	0.000010
mRpL12	51.732162	1.320929	0.000010
CG6650	15.337045	1.320712	0.043793
ade5	41.066561	1.320630	0.014476
PGAP3	15.232777	1.320467	0.006008
Mkp	17.359108	1.320327	0.003046
m-cup	8.826238	1.319574	0.003077
stai	33.095848	1.319171	0.001112
garz	13.816458	1.318946	0.001278
RhoGAP15B	11.504764	1.318265	0.001600
RpII15	36.968481	1.318085	0.000012
Xbp1	260.909795	1.318049	0.042170
CG42671	18.869360	1.318001	0.001157
Cam	375.863213	1.317828	0.018600
D19A	12.476150	1.317713	0.002647
c11.1	12.767387	1.317139	0.001530
in	5.959976	1.316744	0.026228
hfw	24.204328	1.316049	0.001668
Edem1	11.966914	1.314682	0.002135
CG32495	29.588588	1.313844	0.015243
CG7778	55.442234	1.313650	0.022238
WRNexo	14.975133	1.313594	0.006318
Sf3a2	33.532908	1.313086	0.003839
CG1371	48.265168	1.310482	0.001347
VhaM9.7-b	143.265363	1.309992	0.001404
XNP	30.401841	1.309854	0.001507
S2P	14.951532	1.309775	0.004793

CG5854	55.888238	1.309022	0.020936
Nup93-2	12.345240	1.308888	0.004802
Uba5	67.564983	1.308766	0.001864
CG3907	32.744431	1.308538	0.002615
Vps16A	19.679379	1.308492	0.007254
APC4	6.470675	1.308466	0.049235
NELF-B	9.137481	1.308456	0.008400
Jafrac2	34.372447	1.308222	0.003379
CG12333	8.738173	1.308099	0.009448
drosha	8.488184	1.307949	0.000027
Pex1	10.264311	1.307791	0.004490
CG2258	3.089884	1.307747	0.009181
Not10	11.074572	1.307674	0.006744
alpha-Est7	26.875811	1.307578	0.002840
CG17266	19.329781	1.307488	0.039771
Rho1	297.339464	1.307482	0.043892
CG12081	20.467814	1.307239	0.003795
LpR1	4.158513	1.307205	0.005784
GNBP1	18.883314	1.306753	0.004642
CG6406	10.810200	1.306695	0.005380
Pmm2	34.435471	1.306397	0.004991
CG7044	11.735965	1.306242	0.000028
CG5323	35.973331	1.306138	0.005817
twr	219.815591	1.305795	0.001603
CG7556	28.675395	1.305298	0.006101
Nup93-1	29.808065	1.304663	0.007947
CG15118	27.581891	1.304524	0.002440
strat	26.116662	1.304475	0.007848
CG9328	13.060358	1.304260	0.005716
mRNA-cap	29.838889	1.303888	0.002769
CG32486	10.475768	1.303531	0.015129
tth	14.102270	1.303441	0.003919
CG6040	33.246937	1.303351	0.001697
Fhos	2.924364	1.303342	0.005906
betaggt-I	19.202716	1.303125	0.005094
Cog3	10.700552	1.302955	0.005567
CG31751	28.842885	1.302461	0.003132
CG12279	47.812073	1.301483	0.006545
mRpS29	23.094710	1.300971	0.005641
A16	22.935478	1.300964	0.006023
ksh	43.891725	1.300936	0.011298
CG3760	121.573333	1.300498	0.002097
CG7071	11.592143	1.300470	0.009938
thoc5	13.385842	1.300388	0.000128
CG18012	27.433103	1.300269	0.004348
Gtp-bp	92.058506	1.300037	0.002000
Sac1	58.673073	1.299971	0.002169
luna	4.096414	1.299956	0.005365
Rbp1	57.048837	1.299576	0.030467
CG17565	17.919341	1.299461	0.007147
YME1L	34.701333	1.299059	0.014842
CG11279	9.214637	1.298790	0.043445
sll	12.340909	1.298509	0.008623
Tor	10.296416	1.298264	0.020092
Rassf	24.035376	1.298201	0.022392
ttv	5.145349	1.297938	0.000052
TAF1B	4.950126	1.297663	0.038441
Spn88Ea	1268.246307	1.297605	0.017731
CG31344	19.206766	1.297337	0.007706
vtd	30.761741	1.297013	0.003226
mxc	4.332588	1.296770	0.000160
CG5708	33.487136	1.296403	0.004928
CG13551	287.561080	1.296344	0.002325
kek1	4.689645	1.295858	0.008292
Hsepi	6.516083	1.295704	0.012269
CG3793	14.266894	1.295517	0.009336
her	11.694533	1.295340	0.008168
Dad1	152.441232	1.295247	0.003379
CG10778	16.312259	1.294901	0.010875
CG6654	12.634914	1.294061	0.000150
AIMP2	71.379271	1.293972	0.012722
Rm62	201.442761	1.293855	0.037387
CG8635	57.397783	1.293548	0.033187
CG5004	11.123238	1.291944	0.004385
hrg	28.385630	1.290613	0.000003
CG4502	11.650776	1.290408	0.011091
CG4853	18.097943	1.290270	0.005140
CG17068	11.585324	1.289871	0.008189
psidin	18.417380	1.289493	0.000015
cta	23.687784	1.289454	0.000014
Fibp	14.444456	1.287949	0.013054
CG10283	12.591209	1.287603	0.000078
Dcr-2	28.256666	1.287137	0.003400
CG15814	31.673757	1.286645	0.005371
Cortactin	58.663118	1.286039	0.003668
CG3634	16.356607	1.285462	0.000089
mRpS7	36.348867	1.285401	0.009093
Arfip	22.850473	1.284973	0.006974
CG6488	9.682079	1.284752	0.018581
CG8300	33.317793	1.284696	0.000121
mRpL49	28.484743	1.284242	0.032620
Arpc2	77.016071	1.284176	0.003858
PAPLA1	15.134894	1.283955	0.004411
CG4098	54.452373	1.283699	0.005806
P5cr	22.039255	1.283641	0.012470
TfIIEalpha	19.287476	1.283576	0.010216
Cbp20	37.705928	1.283177	0.014636
EloB	70.363209	1.282714	0.046371
CG12259	14.207195	1.282142	0.044086
CngA	52.625335	1.281819	0.046748
rngo	35.470766	1.281657	0.013105
IP3K1	67.287532	1.281496	0.004344
ApepP	48.070319	1.281283	0.004864
PNPase	10.725542	1.281074	0.010285
Tep2	32.332480	1.280530	0.004263
nes	31.908356	1.280509	0.005806
RpS29	1217.752592	1.280153	0.040873
CG8665	5.780135	1.279943	0.017572
CG4287	20.090575	1.279923	0.010800
Mtch	88.911879	1.279597	0.004744
RecQ4	4.520763	1.279332	0.016201
CG4603	22.256760	1.279243	0.010800
eEF1gamma	1206.926130	1.279237	0.022193
CG2225	4.022124	1.279107	0.014517
Nbr	15.564562	1.278989	0.000153
Ntf-2	39.016283	1.278672	0.004778
cdm	16.529756	1.278577	0.007024
RpI1	19.913287	1.278380	0.031646
Pngl	27.578490	1.277803	0.006466
eIF4G2	4.052359	1.277624	0.000158
CASK	7.679785	1.277323	0.007028
rnh1	16.857136	1.277026	0.021861
pasi1	71.130196	1.277007	0.007304
kni	10.979962	1.276617	0.016200
Snap29	25.560274	1.276608	0.012601
CG6287	44.825063	1.276158	0.007878
CG14764	6.952702	1.276138	0.018523
Kr-h1	11.009144	1.275851	0.007876
CG3409	4.056301	1.275642	0.016218
CG5815	10.357092	1.275497	0.017093
CG5721	37.515516	1.275398	0.007857
CG34408	13.954499	1.275280	0.006267
Muted	11.820076	1.275278	0.020085
Myt1	9.554379	1.275195	0.023124
PI4KIIIalpha	17.464685	1.274443	0.005817
gbb	77.421353	1.274306	0.000011
CG4789	61.132505	1.273878	0.008453
Dhx15	42.740137	1.273849	0.006047

p130CAS	6.297069	1.273758	0.016433
ArfGAP1	32.294700	1.273460	0.007837
CG1968	14.739178	1.272967	0.014124
Myo31DF	38.873220	1.272439	0.005716
SIDL	6.670910	1.271994	0.018536
Reck	6.784992	1.271720	0.015440
sav	11.258855	1.271660	0.017952
emb	51.212949	1.271118	0.021181
NaCP60E	1.315869	1.271059	0.022742
pck	98.875046	1.270794	0.006282
CG9356	12.119679	1.270695	0.024975
wts	34.062743	1.270511	0.005882
CG5196	19.305375	1.270446	0.011683
d4	45.509387	1.270060	0.007066
Mical	7.901507	1.269949	0.006712
SCCRO	18.564583	1.269818	0.000227
CG34383	7.055596	1.269310	0.027504
CG2061	10.051636	1.269159	0.020652
Camta	2.345769	1.269021	0.020589
Mkp3	7.188962	1.268651	0.014613
SelR	7.646698	1.268328	0.020768
CG10338	8.198153	1.267843	0.025752
Parg	7.813489	1.267234	0.025442
Odj	12.892423	1.266832	0.024544
Reps	12.819190	1.266224	0.010385
CG7739	26.907700	1.265409	0.010716
mlt	10.723587	1.264521	0.017239
Tfb1	36.802053	1.264468	0.031730
CG1582	13.189894	1.263772	0.011832
Mcm3	21.762767	1.263374	0.011555
CG13367	13.044361	1.263060	0.028383
e(r)	36.768834	1.262854	0.011516
Slh	16.155473	1.262338	0.011174
Rac1	85.247799	1.262288	0.008296
CG1427	19.415648	1.262273	0.019347
CG42232	8.792814	1.261916	0.009737
CG10425	17.725607	1.261891	0.023697
CG3815	6.680290	1.261887	0.027274
MAN1	14.770744	1.261509	0.000399
CG15514	22.769933	1.261193	0.019638
Jheh2	104.009566	1.260739	0.008255
Ric	19.893010	1.260456	0.014947
Fpps	52.668363	1.260202	0.011285
Ccm3	35.602737	1.259619	0.013384
DPCoAC	8.023906	1.259389	0.034743
AspRS	81.809901	1.259324	0.008795
Srp68	61.815010	1.258474	0.000035
MFS18	15.860748	1.258377	0.022401
Grasp65	55.805038	1.258248	0.049235
svr	21.520433	1.257806	0.009299
CG6664	28.060366	1.257802	0.012264
SamDC	27.755511	1.257348	0.020378
l(2)SH0834	35.900822	1.257186	0.020637
SP2637	10.757582	1.256820	0.030766
Vps8	6.294694	1.256657	0.027592
Srp14	69.630487	1.255755	0.022193
CG7656	29.102153	1.255664	0.014359
tgo	19.760204	1.255461	0.014589
Vsp37A	26.939732	1.255431	0.000536
Bin1	6.802018	1.255226	0.030766
Pop2	41.347200	1.254643	0.011811
epsilonCOP	66.570376	1.254636	0.013706
NFAT	6.362357	1.254035	0.000161
lft	72.554101	1.253951	0.012722
Invadolysin	7.534944	1.253870	0.026950
Sec8	21.035288	1.253534	0.014474
CG5447	27.421439	1.253506	0.020802
Pka-R2	41.362490	1.253378	0.010615
CG31650	22.520224	1.252883	0.018862
Vps53	10.101385	1.252699	0.025745
Cyp6u1	14.576578	1.252539	0.026093
Vps39	7.556489	1.252504	0.033770
Taf6	15.262785	1.252404	0.024950
CG7049	19.364178	1.251907	0.034835
CG9248	29.830405	1.251652	0.016747
spoon	30.916085	1.251487	0.011568
CG13994	29.953067	1.251207	0.040636
CG45092	3.895261	1.251072	0.032491
dre4	49.580324	1.250864	0.011713
CycH	19.085504	1.250655	0.038285
Srp72	42.729854	1.250592	0.014289
CG7379	20.920225	1.250409	0.023083
CG12393	12.517877	1.249748	0.034642
Mrtf	4.526420	1.249496	0.023102
CG8771	9.348548	1.249109	0.019064
Pvr	19.708548	1.249052	0.013403
CG8032	7.385428	1.248875	0.039414
Utx	9.278599	1.248871	0.022632
CG7099	3.362360	1.248869	0.040180
CG6230	28.440685	1.248839	0.013744
Srp9	53.834179	1.248656	0.021686
Tsp42Ef	136.334855	1.248616	0.012601
CG9062	13.645831	1.248512	0.022708
Hrd3	30.793037	1.248171	0.044620
CG9947	30.362047	1.248082	0.019428
Ice1	4.608703	1.247929	0.039814
CG6015	13.717691	1.247893	0.031204
CG4386	132.855291	1.247792	0.012722
mRpS26	24.798107	1.247658	0.040980
mam	7.619699	1.246538	0.018433
vir-1	107.435619	1.245717	0.044620
Gal	23.980873	1.245608	0.020698
CG12099	64.800021	1.245333	0.013989
p38b	29.190689	1.244516	0.022044
CG8066	54.391806	1.244444	0.000299
l(2)tid	27.434099	1.244121	0.021515
LanB2	19.364131	1.243956	0.016426
FAM21	4.417285	1.243289	0.045631
Hira	7.244081	1.243145	0.038489
msl-2	8.267592	1.242623	0.032123
cnk	9.862402	1.242439	0.022516
Su(fu)	27.914836	1.242242	0.026008
Tnpo-SR	6.649376	1.241809	0.041106
CG9669	100.102817	1.241660	0.001139
Gem3	5.315081	1.240132	0.047628
TBC1D5	13.503315	1.239424	0.035195
CG1233	5.747343	1.238441	0.045426
Uba3	21.474615	1.238354	0.035792
PIG-T	21.685367	1.238346	0.026035
beta-Man	29.421803	1.238129	0.020928
Spt5	29.895032	1.237994	0.020517
CG32581	39.031098	1.237108	0.026710
Nup154	23.050093	1.237055	0.000172
Hexo2	13.638227	1.236899	0.039673
CG5001	50.191648	1.236761	0.049041
fz2	21.552781	1.235479	0.019996
Hrs	15.488608	1.234927	0.032249
l(2)k14710	11.549096	1.234848	0.001731
zld	6.244829	1.234644	0.026595
ArfGAP3	50.243905	1.234618	0.021236
Top3alpha	6.424493	1.234295	0.047252
Fnta	50.697751	1.233126	0.027362
Dgp-1	10.528442	1.232543	0.042219
olf186-F	7.446372	1.231954	0.036853
wdp	47.940292	1.231600	0.022465
dap	13.032378	1.231149	0.042255
Rab10	63.868667	1.231100	0.023192
AspRS-m	20.160196	1.230701	0.026818

TBCD	17.004351	1.230694	0.029781
CG41378	37.957144	1.230663	0.043146
Arpc1	123.325111	1.230538	0.022216
bonsai	28.528005	1.229502	0.003879
CG40178	10.782809	1.228824	0.044620
CG9527	21.258123	1.228648	0.032576
Jra	40.318778	1.228435	0.031792
Hem	24.521130	1.228410	0.028327
Pez	12.264307	1.228174	0.034293
rad50	9.859170	1.227701	0.041074
CG8818	36.952991	1.227005	0.035145
bbg	14.963871	1.226994	0.026345
scf	27.285513	1.226675	0.040328
Sec24AB	23.686433	1.226495	0.028172
AP-1mu	54.180579	1.225979	0.030270
Atg2	11.172723	1.225234	0.033991
CG4119	18.430512	1.224995	0.034025
ifc	50.241685	1.224956	0.029949
asrij	32.061567	1.224898	0.003073
ytr	64.717089	1.224845	0.028331
CG13631	34.394473	1.224466	0.038489
CG2076	51.110472	1.224168	0.034010
Myc	8.083002	1.223717	0.034821
su(w[a])	32.197458	1.223317	0.028414
eco	16.363255	1.221873	0.039811
CG4291	32.333154	1.221769	0.046651
Clc	151.139707	1.221759	0.029178
RNASEK	122.683851	1.220999	0.031867
CG44774	7.808283	1.220134	0.001053
Sep2	92.056424	1.219930	0.032368
mthl10	35.001713	1.219383	0.033211
CG14683	29.885958	1.218022	0.049971
Eps-15	20.394530	1.217540	0.037068
homer	25.555666	1.217395	0.041000
mtm	28.946125	1.216885	0.044272
SerRS	108.518710	1.216396	0.034293
CG4557	10.669565	1.215173	0.004793
Pih1D1	17.040806	1.214850	0.044572
CG8613	20.482525	1.214733	0.048000
beta-PheRS	45.224062	1.214129	0.043383
CG3797	23.932067	1.213778	0.045775
CG1317	22.556872	1.213432	0.043828
CG11360	8.879765	1.213229	0.049012
CG34056	96.565076	1.213102	0.041106
Ctr9	30.764473	1.213034	0.041650
fj	20.775760	1.212152	0.048283
Chro	26.349438	1.211972	0.043445
egl	34.414072	1.211883	0.041000
Snx3	73.148645	1.211434	0.042475
CG2118	30.364846	1.211415	0.046715
E2f2	13.108937	1.211126	0.009802
RpII18	65.241269	1.210286	0.005766
CG18343	56.725508	1.209618	0.005805
P58IPK	70.902996	1.209344	0.043930
Ostgamma	138.714735	1.209307	0.043445
Galphas	93.897840	1.208060	0.044086
GV1	121.786703	1.206818	0.047155
CG4552	12.983365	1.203838	0.007818
CG17202	48.721728	1.203506	0.006968
bsf	27.826957	1.203373	0.001528
imd	17.157096	1.201418	0.014630
slpr	6.330464	1.201306	0.008525
CG1646	25.483974	1.200291	0.001853
CG6420	9.034747	1.198191	0.008912
Eogt	38.458189	1.198101	0.003622
Dpit47	24.634911	1.196083	0.011105
Atg3	28.957540	1.186237	0.016521
Ranbp9	37.495160	1.186061	0.004229
g	14.081567	1.183720	0.009015
CG9346	11.847498	1.182442	0.019378
Pi4KIIalpha	9.777925	1.182314	0.018897
pea	9.195977	1.178741	0.022286
CG14646	19.986975	1.170216	0.033504
CG6418	13.024266	1.169824	0.032251
CG32147	28.163082	1.169437	0.049133
IntS4	10.715236	1.166600	0.034476
Traf6	12.176168	1.162428	0.044820
Mo25	53.617884	1.156355	0.020530
Arp2	46.500256	1.136550	0.049981
scramb2	72.739833	-1.137392	0.048246
Doa	8.022979	-1.154255	0.022789
trc	21.078322	-1.160440	0.025725
CG15099	7.653860	-1.163164	0.020937
MFS15	16.296383	-1.167293	0.037341
CG1882	11.234402	-1.167320	0.035049
mle	13.929961	-1.169814	0.015384
CG2310	26.615675	-1.171398	0.028383
Sik3	4.503539	-1.172593	0.031145
ND-13A	32.757705	-1.172799	0.029920
Rab18	37.088690	-1.173951	0.028931
wrd	14.449548	-1.174496	0.007991
CG31122	8.790159	-1.185191	0.018089
Vps52	10.720886	-1.185290	0.028248
Gale	13.394751	-1.193807	0.020097
CG17574	12.376606	-1.205509	0.007762
ghi	46.301258	-1.207491	0.006469
CG17065	14.339496	-1.209469	0.010432
ALiX	54.018091	-1.210609	0.041814
CG5028	51.132701	-1.210729	0.043450
bowl	36.330025	-1.211344	0.041016
hdc	9.412932	-1.211560	0.041306
CG6700	26.276298	-1.212754	0.041208
CG7630	241.191777	-1.213580	0.041625
CG17919	182.793906	-1.213586	0.038944
Mvb12	10.381502	-1.214708	0.008094
Synd	57.242024	-1.215880	0.036716
nop5	94.481725	-1.215964	0.045614
colt	40.883167	-1.216673	0.044036
CG1890	92.227163	-1.216765	0.043001
CG11876	56.222507	-1.216857	0.036793
RtGEF	3.614708	-1.218168	0.004242
CG32103	21.916513	-1.218234	0.036640
Hs6st	41.515597	-1.219178	0.033560
Kul	17.678079	-1.220189	0.032347
snama	9.631391	-1.220248	0.046788
CG10470	46.467584	-1.220885	0.003390
Csp	49.436237	-1.222392	0.029720
Khc-73	7.542923	-1.223110	0.035070
Acf	6.725772	-1.223896	0.047098
Pitslre	24.257361	-1.226353	0.028069
Rsf1	36.113496	-1.226479	0.032906
mxt	24.917522	-1.226742	0.028248
CG17841	14.804915	-1.226852	0.041751
CG5567	22.924007	-1.227012	0.047392
ATPsynB	196.338225	-1.227055	0.025080
mura	8.702982	-1.227181	0.032347
CG13585	35.645177	-1.227347	0.041016
bsk	35.039395	-1.227512	0.030780
CG12567	27.561088	-1.227678	0.031705
SpdS	28.623438	-1.227895	0.035134
r-l	26.426385	-1.228375	0.033240
Swip-1	29.688390	-1.228764	0.032599
CG12129	21.136938	-1.228816	0.049044
nuf	14.960719	-1.229378	0.027582
Pkc98E	6.580604	-1.230139	0.037535
CG7083	12.496000	-1.230567	0.048110
La	98.803038	-1.231429	0.022454
simj	7.634888	-1.232955	0.034138

Jarid2	8.518487	-1.233233	0.025875
CG8891	29.740071	-1.235704	0.045631
kek5	5.546117	-1.235771	0.033491
Atf6	16.007987	-1.236148	0.024602
CG31688	6.309077	-1.236588	0.026244
CG8026	9.491911	-1.237416	0.037068
sxc	43.924841	-1.237507	0.018359
out	18.602990	-1.237916	0.023569
Cyp4e2	28.908139	-1.239268	0.024174
PHGPx	88.953925	-1.239934	0.000131
CG13921	3.924563	-1.240016	0.046006
Max	27.244715	-1.240404	0.001079
tai	5.602083	-1.241065	0.021004
CG12811	24.367942	-1.241069	0.002522
CG5044	42.796382	-1.241276	0.020195
Wwox	13.254472	-1.242751	0.043213
CG7639	13.089218	-1.243035	0.036582
CG6051	12.369058	-1.245091	0.020174
CG9135	49.490684	-1.245274	0.015170
stv	24.004911	-1.245576	0.042538
Drip	47.687852	-1.246345	0.014630
Nle	19.621660	-1.247019	0.001031
comm2	22.396437	-1.247074	0.025378
viaf	44.908691	-1.247803	0.019245
Mulk	14.680215	-1.247936	0.039599
moody	6.944574	-1.249116	0.028138
ATPsynO	227.830399	-1.249156	0.012174
Glut1	2.738798	-1.249352	0.026093
l(2)37Bb	15.923326	-1.249729	0.027746
CG9821	21.895360	-1.249810	0.012506
Alas	22.864296	-1.249939	0.020307
CG14434	16.956300	-1.249941	0.029072
mnb	4.820023	-1.250051	0.000727
mre11	12.201465	-1.250668	0.001587
CG12880	8.933602	-1.250956	0.041389
cer	137.317493	-1.251120	0.015170
CG9636	8.016014	-1.251479	0.031145
CRAT	22.895912	-1.251891	0.015586
CG11050	13.450263	-1.252478	0.000697
Spn43Ab	23.489323	-1.253020	0.022755
CG7510	6.936970	-1.253455	0.023127
NaPi-III	45.681927	-1.254927	0.010213
Msh6	6.136695	-1.255239	0.025752
qm	10.187647	-1.255480	0.024824
CG8677	7.776803	-1.256028	0.012722
Dyb	13.894025	-1.256240	0.014289
GstO2	55.070384	-1.256336	0.011298
CG10055	8.063193	-1.258030	0.030228
CG1827	12.680164	-1.258878	0.034010
RN-tre	7.664288	-1.259069	0.016053
RhoGAP92B	13.018765	-1.259175	0.013503
Rac2	25.166154	-1.259998	0.012051
Dscam4	2.555834	-1.260124	0.027657
ptc	12.235558	-1.260129	0.011468
mRpL44	23.277328	-1.260309	0.021558
CG11837	17.356869	-1.260702	0.028773
hui	214.483431	-1.261258	0.008163
CG31038	15.348841	-1.262159	0.009334
CG42637	5.390885	-1.263384	0.015364
Ire1	13.166536	-1.264597	0.011287
l(1)G0156	85.761382	-1.264968	0.007150
aurB	19.337370	-1.265145	0.021430
CG7206	17.999393	-1.266365	0.016237
CG2656	15.218617	-1.266534	0.043890
CdsA	22.497685	-1.266774	0.009949
CG3625	32.503225	-1.267468	0.009303
CG14812	24.416289	-1.267604	0.023569
mahe	10.650852	-1.267738	0.043679
CG11399	6.887797	-1.270191	0.014630
Cyp6a9	28.363616	-1.271799	0.008691
gb	6.747752	-1.272613	0.023124
qkr58E-3	31.747355	-1.273731	0.008255
wnd	11.879748	-1.273829	0.007669
Nadsyn	7.550007	-1.273852	0.000174
Cyt-b5	204.500143	-1.274394	0.005070
geko	19.787200	-1.274434	0.014470
CG10916	8.816352	-1.274441	0.021515
Ppa	33.708024	-1.275501	0.005283
Orct2	11.137157	-1.276890	0.011756
muc	47.797959	-1.277252	0.000009
trbd	8.027745	-1.277430	0.011746
KrT95D	4.477794	-1.277664	0.012900
Dad	22.928944	-1.278338	0.005529
Gs1l	16.594280	-1.278668	0.016277
miple2	38.035271	-1.278952	0.006791
ND-MLRQ	200.781578	-1.278954	0.005021
CG1218	14.841274	-1.280088	0.014501
Arp1	123.859638	-1.280829	0.004056
LRR	13.553332	-1.280883	0.004885
Nmd3	31.577478	-1.284031	0.005778
THADA	4.725902	-1.284162	0.011298
CG43783	3.621087	-1.285059	0.014613
pgant2	14.481366	-1.285795	0.005772
CG6340	16.771099	-1.286421	0.005567
Pino	63.930783	-1.286916	0.003348
CG5946	31.463463	-1.288103	0.004021
ImpL2	28.120272	-1.288173	0.037521
ITP	12.131406	-1.288480	0.004951
ND-49	84.949702	-1.289269	0.003218
blow	18.345032	-1.290058	0.004972
GstO3	183.092615	-1.290431	0.002920
sqz	8.690779	-1.290587	0.008303
CG31475	13.546664	-1.291112	0.006394
CG1998	14.865175	-1.291116	0.008060
Aldh-III	40.946541	-1.292286	0.002798
CG5191	15.012184	-1.292690	0.004711
Usp12-46	9.303152	-1.292862	0.011253
CG17162	11.723230	-1.293107	0.004215
CG6028	142.639401	-1.293513	0.002632
cdc14	9.452920	-1.293537	0.004508
CG5535	12.520059	-1.294526	0.007257
CG17292	72.147106	-1.294763	0.002544
CG4670	39.270929	-1.295110	0.002864
sti	9.811651	-1.297330	0.003543
Unc-115a	40.357123	-1.297481	0.002198
RhoGAP93B	6.887923	-1.297864	0.005073
da	15.747050	-1.298294	0.003543
CalpB	20.119193	-1.298681	0.002726
CG6126	32.663771	-1.300505	0.002868
Cad74A	16.801875	-1.300809	0.002224
elB	19.523511	-1.303511	0.002684
CG10663	45.883553	-1.303929	0.001813
CG11309	12.622938	-1.304897	0.005458
CG31357	18.137867	-1.305025	0.004909
CG32758	7.136798	-1.305347	0.000034
rudhira	8.269206	-1.305520	0.009340
ATP7	8.012196	-1.305957	0.003508
Tsp42Ea	17.563917	-1.306174	0.000023
CG14259	18.477613	-1.306502	0.008017
mmy	54.518009	-1.306597	0.001755
CG7512	14.134715	-1.306746	0.035277
Cyp4c3	30.581039	-1.307827	0.002482
RhoGAPp190	7.969310	-1.309427	0.002174
Msp300	15.880047	-1.309450	0.031608
Cyp6v1	10.035315	-1.310437	0.004157
Sox14	11.694452	-1.311859	0.002823
CG18812	15.182437	-1.312000	0.020864
blot	28.026912	-1.313337	0.001322

CG2121	30.625487	-1.315093	0.001776
CG18809	6.721609	-1.315163	0.007782
Gyc76C	5.696049	-1.315616	0.002783
sesB	681.646561	-1.316845	0.020447
CG11858	45.159559	-1.317724	0.004912
Ack-like	21.718059	-1.317784	0.001017
Gug	9.646058	-1.318122	0.001336
RPA2	38.753752	-1.318203	0.002556
CG42668	11.191644	-1.318313	0.001598
Asator	3.188685	-1.318746	0.003380
CG3594	24.673792	-1.319165	0.004991
Zyx	30.548387	-1.319707	0.001387
ACC	20.376489	-1.320332	0.000891
Rtnl1	182.073464	-1.320868	0.037012
CG7966	368.045656	-1.321645	0.037147
CG14572	829.003924	-1.321864	0.045679
wech	2.665228	-1.321999	0.004621
Mipp1	20.322833	-1.322540	0.001942
corn	4.218031	-1.323301	0.003824
HDAC4	5.859915	-1.323512	0.001868
fng	25.731962	-1.323695	0.001574
CG33170	23.042108	-1.324261	0.003075
Vps28	28.367118	-1.324308	0.000010
Nsun2	24.565083	-1.324492	0.001327
sona	45.022509	-1.325270	0.048530
CG8206	24.977329	-1.325578	0.002598
pkaap	24.463534	-1.326027	0.001259
Cks30A	20.146633	-1.326047	0.003612
Gp150	617.432994	-1.326152	0.008453
CG13255	23.445137	-1.326190	0.002344
sd	17.138012	-1.328523	0.000687
Lrt	4.443578	-1.328691	0.017363
ND-AGGG	240.158241	-1.329040	0.000634
CG8321	16.011448	-1.329682	0.004315
grn	5.423935	-1.330763	0.003305
SCOT	32.967272	-1.331047	0.016395
NijA	19.345468	-1.331540	0.003234
CG2100	14.395021	-1.331768	0.003040
CG3702	64.501431	-1.332815	0.000575
CG10311	32.827526	-1.333658	0.001577
Art1	85.507376	-1.334137	0.000580
Cad87A	10.693934	-1.336350	0.004447
melt	17.304557	-1.336777	0.000703
Rbp1-like	19.568101	-1.337569	0.000761
CG30022	31.108958	-1.337587	0.001138
C1GalTA	8.650995	-1.337917	0.002984
CG42673	9.497804	-1.338042	0.000746
CG8786	5.889051	-1.338257	0.019064
yellow-b	32.106148	-1.338333	0.000801
CG16700	14.170865	-1.338710	0.000003
CG1698	6.391875	-1.338734	0.027915
pelo	56.534028	-1.340291	0.000476
Pli	16.762768	-1.340707	0.012470
prtp	52.656053	-1.340779	0.000481
zfh2	12.940815	-1.342177	0.000627
cact	33.468536	-1.343337	0.002192
NKAIN	26.051310	-1.343542	0.000368
CG42327	8.758776	-1.344544	0.047574
bnb	66.359837	-1.345197	0.008612
grh	9.663803	-1.345345	0.000450
cher	169.616176	-1.346431	0.007447
Abd-B	12.810021	-1.347326	0.000318
AGO2	137.560250	-1.347353	0.020398
CG43340	2.802420	-1.347543	0.000872
Tep3	79.998017	-1.348660	0.039101
CG7457	4.504066	-1.349317	0.001242
Mnt	5.312126	-1.349471	0.001587
CG31793	3.594587	-1.350299	0.025861
AGBE	46.869547	-1.350803	0.000321
ftz-f1	4.363366	-1.350920	0.000809
CG43427	22.887968	-1.351354	0.025384
CG7860	22.469418	-1.351855	0.031873
Thor	121.680478	-1.352193	0.028033
CG3700	26.746587	-1.352338	0.000963
to	150.950184	-1.353003	0.000229
l(2)34Fc	541.522754	-1.354011	0.032612
ETHR	4.809369	-1.354470	0.005894
mrj	24.008539	-1.354615	0.002302
alpha-Man-IIb	2.729468	-1.354837	0.046006
CngB	29.415412	-1.354963	0.000284
Ptr	6.691017	-1.355979	0.029801
CG14566	978.499353	-1.357003	0.017228
CG11138	11.712792	-1.358033	0.000328
CG13516	13.895958	-1.359101	0.002557
CG2975	8.972482	-1.359251	0.021822
unc-119	7.225464	-1.359933	0.007810
CG10657	39.968788	-1.361116	0.000322
Men-b	24.839041	-1.361476	0.006944
Atg5	12.425692	-1.361827	0.008513
Plc21C	7.967057	-1.362062	0.000000
jumu	11.089549	-1.362470	0.000446
Eip71CD	46.516776	-1.363948	0.026578
Hr39	10.915004	-1.364041	0.000321
CG6950	23.156883	-1.364335	0.007160
REPTOR	7.958911	-1.364383	0.000304
CG3603	19.153941	-1.364486	0.001439
CG10903	14.837767	-1.366161	0.001476
Mef2	4.982705	-1.366601	0.021318
pch2	14.678099	-1.366625	0.000602
AdoR	41.143027	-1.366983	0.004508
zormin	30.957208	-1.369049	0.041106
pip	4.345812	-1.369546	0.040266
CG12065	42.958034	-1.371540	0.000125
ETH	350.473489	-1.373511	0.013400
DMAP1	20.226029	-1.374955	0.000419
Cks85A	7.564534	-1.376086	0.010838
EndoB	8.587112	-1.376612	0.000851
bru2	9.905179	-1.376753	0.000172
Atg18b	7.355870	-1.377208	0.001146
CG11601	11.884809	-1.380001	0.004655
Gfat1	126.741253	-1.381141	0.012722
CG12288	16.048969	-1.381896	0.000502
chrb	5.746424	-1.382629	0.000000
elav	1.486772	-1.382920	0.006490
HmgD	276.438052	-1.383475	0.016237
CG32645	15.800649	-1.383975	0.000139
Tsp	3.080417	-1.386056	0.015884
fu12	7.292710	-1.388069	0.040647
CG9436	49.156820	-1.389129	0.000097
PMP34	10.330461	-1.389731	0.024398
CG6357	8.338722	-1.390143	0.027680
salm	10.124893	-1.391151	0.000092
ATP8B	3.287586	-1.396531	0.000320
Drice	30.346651	-1.398012	0.000074
l(3)neo38	8.793732	-1.398634	0.000073
rols	3.856578	-1.398687	0.001370
ct	2.723900	-1.399672	0.000166
CG10550	22.557011	-1.399824	0.000000
Mob2	5.050988	-1.401122	0.000195
Sema1b	42.914155	-1.401229	0.000026
slim	18.330933	-1.401868	0.000065
CG2837	19.401757	-1.402119	0.000243
Spindly	5.669379	-1.402537	0.017519
fal	10.529502	-1.403467	0.000177
CG6767	58.510993	-1.404976	0.000840
schlank	35.893207	-1.405514	0.002328
CG9338	250.173731	-1.406123	0.007577
Dredd	28.926431	-1.406888	0.010198

CG7896	34.249750	-1.408060	0.000020
path	12.713267	-1.412021	0.000068
HPS4	4.440549	-1.412466	0.001572
TMEM216	7.078619	-1.413090	0.000281
RfC3	13.196557	-1.414650	0.017904
Chd64	702.072714	-1.416281	0.001949
HDAC1	85.077667	-1.417262	0.000013
CG11594	4.084260	-1.417455	0.037068
CG10467	55.533796	-1.418553	0.017364
jvl	8.704696	-1.419396	0.001975
cic	7.223616	-1.419515	0.000018
Mgstl	235.203808	-1.420849	0.007058
CG31102	14.349447	-1.423106	0.000112
CG41520	22.028461	-1.423389	0.000021
CG7702	5.482050	-1.423716	0.015884
fz4	7.303414	-1.424003	0.000082
Vdup1	118.928925	-1.424340	0.006394
jigr1	10.798769	-1.424638	0.006415
CG32174	3.380327	-1.425871	0.011693
tfc	15.985699	-1.427479	0.000034
Peritrophin-A	253.864445	-1.428736	0.017519
CG13678	10778.256629	-1.430512	0.001425
InR	1.327080	-1.431691	0.031876
PyK	237.751099	-1.432476	0.004837
Pax	62.335767	-1.433494	0.009340
CG3961	4.005430	-1.433858	0.033863
CG33199	21.452032	-1.434787	0.000041
mtg	20.124459	-1.435201	0.007553
Hrb87F	91.142185	-1.438132	0.004807
CG7220	13.070424	-1.438697	0.000030
Trf2	7.014295	-1.438809	0.000010
Pde11	5.235271	-1.438827	0.000023
Tig	9.728190	-1.438851	0.002645
elm	48.495032	-1.439550	0.000011
CG8303	74.544137	-1.439650	0.000005
SPARC	49.870254	-1.439879	0.001863
CG5009	44.095427	-1.442369	0.000005
CG31710	94.136700	-1.444180	0.000004
scyl	88.352989	-1.444278	0.004054
Ets98B	9.530390	-1.446318	0.000000
msd1	14.250834	-1.446820	0.040190
Cpr97Eb	1592.426320	-1.447145	0.001975
CG9691	158.864668	-1.448638	0.003965
Fas2	34.727034	-1.449646	0.002740
CG14258	349.793888	-1.450316	0.009535
Est-P	9.710369	-1.450987	0.007018
CG34125	35.622046	-1.452073	0.000044
SP1173	107.059133	-1.452589	0.003731
pain	9.197932	-1.453198	0.000028
CG17829	5.804693	-1.453690	0.012383
CG9737	6.980974	-1.454301	0.025138
CG17816	1.125720	-1.454329	0.038453
Cdc7	5.348365	-1.454454	0.001295
PGRP-SA	144.139986	-1.455966	0.000002
CG9967	6.540873	-1.455995	0.006368
CG42321	5.490138	-1.456608	0.004187
CG5639	29.053971	-1.456649	0.001975
CG9757	200.490729	-1.458207	0.045713
Spn42Dc	8.301902	-1.458921	0.010851
baz	10.894589	-1.459577	0.000062
Pbgs	39.052205	-1.460356	0.000004
IscU	54.316796	-1.460508	0.000386
Col4a1	47.238895	-1.462434	0.016237
Buffy	68.121051	-1.462555	0.000003
Acsl	52.695053	-1.463535	0.002358
CG32407	29.895552	-1.465251	0.001060
CG3764	3.530204	-1.465498	0.001020
fru	13.596023	-1.465781	0.002769
Sfxn1-3	18.849292	-1.470789	0.000009
CG15706	9.664291	-1.471086	0.000014
vvl	49.868296	-1.473013	0.001225
CG43394	21.094250	-1.473257	0.002388
CG18428	11.764653	-1.473404	0.026806
rt	5.388480	-1.473409	0.000433
Cht6	35.182013	-1.474742	0.002175
jing	2.957388	-1.474830	0.000012
yip2	132.595702	-1.475547	0.000001
IA-2	0.890948	-1.475848	0.021282
wg	4.342565	-1.476843	0.002483
CG31301	37.073800	-1.477112	0.000002
CG32373	3.307225	-1.477865	0.045614
RhoGAP102A	1.495682	-1.477866	0.045372
CG9399	25.693673	-1.479005	0.000005
CG1814	10.993742	-1.479119	0.000018
Dbp80	32.861403	-1.479818	0.000001
Treh	13.780441	-1.480090	0.000002
frc	9.506858	-1.480265	0.000005
B4	5.305389	-1.482309	0.000003
alphaTub84D	97.547683	-1.483469	0.000000
CG7884	15.294886	-1.484723	0.000348
CG42747	3.210620	-1.485228	0.014030
Mocs1	19.347784	-1.485914	0.000003
CG6805	39.776077	-1.486712	0.000001
CG31743	4.043873	-1.486733	0.014516
slow	6.859380	-1.488642	0.004621
Reep1	20.357438	-1.488649	0.000001
drd	66.946931	-1.488664	0.002153
Dip-C	27.465028	-1.489034	0.000002
CG3588	81.603329	-1.490721	0.001561
CG5973	43.622036	-1.491662	0.000000
MagR	11.729257	-1.492869	0.012058
Dr	3.541236	-1.493646	0.012783
CG5039	13.173746	-1.493802	0.013595
CG43102	1.835521	-1.494066	0.000011
CG32017	8.747379	-1.494321	0.000003
Pmp70	21.740956	-1.495144	0.000108
CG6847	55.886123	-1.495223	0.002647
SKIP	3.152912	-1.495389	0.000011
CG34462	23.798160	-1.495654	0.000005
eas	16.399747	-1.498693	0.000001
CG16786	32.561447	-1.498784	0.000000
CG2017	18.702825	-1.499689	0.002288
ome	68.552009	-1.499970	0.002891
Piezo	16.305643	-1.501782	0.000000
CG3376	8.338427	-1.502479	0.000002
CG3149	9.351267	-1.502609	0.000013
CG9628	141.965870	-1.502743	0.000000
D2hgdh	12.014112	-1.503719	0.000004
CG4975	4.893461	-1.504787	0.006383
CG2277	7.110864	-1.504877	0.000014
aay	6.550108	-1.505107	0.026616
CG34248	91.430929	-1.505176	0.017127
CG42268	10.050952	-1.505476	0.000000
Cpr57A	183.618127	-1.508434	0.000938
Sesn	2.999683	-1.510346	0.004984
MRP	49.392702	-1.510372	0.003919
CG9312	8.042385	-1.511154	0.029024
brat	4.944378	-1.511320	0.001135
CG14907	9.020422	-1.511442	0.012437
daw	2.440805	-1.511754	0.021182
Keap1	6.083899	-1.512184	0.000007
CG8560	30.266792	-1.512270	0.002135
msi	1.727494	-1.513872	0.000963
CG3009	14.399514	-1.516159	0.000000
rdgA	1.809488	-1.516169	0.000004
Pka-C3	3.258136	-1.517095	0.030154
Acox57D-p	6.101337	-1.518560	0.014505
CG6428	4.952508	-1.520247	0.002773

CG11474	11.484572	-1.522061	0.000005
CG5381	27.606415	-1.522164	0.000000
CG15211	8.843098	-1.524170	0.011934
AhcyL2	10.925004	-1.525032	0.000004
CG1136	10.754692	-1.525782	0.000001
MFS10	5.006452	-1.526620	0.000005
CG10623	7.390390	-1.527303	0.002331
Cyt-b5-r	8.927772	-1.527732	0.035070
Fatp	18.234289	-1.529244	0.000000
CG45093	17.146340	-1.530216	0.000000
CG6912	10.159075	-1.530394	0.002645
kdn	85.397691	-1.530495	0.000776
CAP	12.627963	-1.530995	0.000267
Cln7	10.056435	-1.531617	0.000003
CG7029	25.890874	-1.533793	0.000003
Vps24	14.606663	-1.536340	0.000466
Cad86C	23.267507	-1.538993	0.000002
CG13630	41.160624	-1.539416	0.000007
CG33939	17.140775	-1.540976	0.003890
CG11147	52.884525	-1.541701	0.000001
pgant8	3.740409	-1.541726	0.010432
tkv	21.109469	-1.542911	0.000068
bs	3.886134	-1.543732	0.000087
Pof	9.332645	-1.546425	0.000003
Tsp42Ek	9.489608	-1.546658	0.010216
pnt	4.310162	-1.550090	0.000000
raw	13.380639	-1.551471	0.000001
CG7272	59.909611	-1.552037	0.000000
aralar1	18.141916	-1.552597	0.000000
fz3	5.517205	-1.555432	0.000001
Cyp6a17	37.591624	-1.555913	0.000000
obst-B	224.870473	-1.556376	0.000218
CG17734	49.816823	-1.559091	0.000000
CG14696	18.285047	-1.559291	0.000013
lute	56.375633	-1.560767	0.000030
drm	12.242357	-1.560905	0.000000
PRAS40	42.297510	-1.562458	0.000000
CG30497	17.916527	-1.565606	0.000000
CG9815	21.208181	-1.566893	0.000355
Tsp96F	13.774703	-1.568731	0.000029
Ddc	18.926320	-1.569595	0.000376
CG6836	13.615930	-1.569701	0.000334
Tob	1.346087	-1.569766	0.009333
HmgZ	154.857984	-1.570531	0.000307
Cpr65Au	81.843810	-1.572875	0.001481
Cyp28a5	386.883615	-1.575355	0.000126
CG4594	6.018077	-1.576320	0.013571
CG13046	63.654062	-1.577657	0.004362
Lpin	13.545594	-1.577690	0.000000
CG46339	40.181535	-1.578888	0.000000
Esyt2	91.592151	-1.579980	0.000413
CG31808	4.178576	-1.580487	0.012643
CG14301	10.654715	-1.581015	0.000001
stan	2.860190	-1.583380	0.000000
Pif1A	4.542678	-1.586150	0.000000
CG6746	49.273928	-1.586596	0.000267
CG4615	5.232834	-1.588210	0.004221
CG2254	7.743300	-1.590210	0.009051
Tsp42El	68.336627	-1.591046	0.000000
CG2865	7.827571	-1.591960	0.000000
spz3	20.391461	-1.592078	0.000397
caup	2.893930	-1.592159	0.001000
Dsp1	31.755098	-1.592555	0.000000
CG32549	4.281980	-1.594249	0.000642
Jupiter	26.399629	-1.594988	0.000000
CG34437	8.062275	-1.597789	0.024824
CG32638	57.714868	-1.599261	0.000014
Tmhs	26.219779	-1.600551	0.000000
unc-13-4A	0.987994	-1.601193	0.004991
dsx	0.754051	-1.602228	0.032963
CG4829	18.998103	-1.605607	0.000000
CG5805	7.610225	-1.606919	0.000006
CG18530	5.533708	-1.607284	0.017954
Prestin	9.138172	-1.607465	0.000000
wat	288.649365	-1.607955	0.000052
nmo	2.952278	-1.608674	0.000174
CG8563	14.798273	-1.608784	0.000262
jdp	17.842225	-1.608854	0.000000
Ccp84Ac	16.570227	-1.610729	0.008698
CG42259	28.913290	-1.612492	0.000000
Oaz	2.915023	-1.614063	0.000482
CG5958	20.282962	-1.615605	0.001320
ken	20.495501	-1.616510	0.000000
caps	16.716123	-1.617376	0.000000
frm	356.986952	-1.618958	0.000068
CG8738	5.704215	-1.619454	0.005190
gol	4.620930	-1.620159	0.000000
lama	18.323388	-1.625157	0.000000
St4	17.766218	-1.627523	0.000000
SLC5A11	7.130171	-1.628041	0.000002
Hayan	12.475866	-1.628342	0.000000
CG10365	11.582336	-1.629194	0.000016
CG30196	20.865120	-1.629276	0.003125
Cyp4d1	4.497549	-1.630141	0.041233
CycB3	9.196784	-1.632814	0.000002
bi	4.893688	-1.634498	0.000000
Ugt36Bc	21.295970	-1.635650	0.000000
CG4267	11.402147	-1.636132	0.000000
CG8483	131.075746	-1.636396	0.001604
bond	595.188491	-1.636511	0.000004
CG8630	410.071863	-1.637401	0.000050
CG5167	34.567324	-1.637577	0.000001
CG10359	34.532516	-1.637876	0.000000
CG32448	21.172655	-1.639643	0.001178
ine	8.064595	-1.640934	0.000000
mdy	5.492556	-1.642332	0.002980
ea	68.813562	-1.646472	0.000000
if	43.388363	-1.647015	0.000061
CG1718	4.080975	-1.649549	0.000000
Gel	53.721454	-1.650221	0.000000
CG3505	30.342080	-1.653089	0.000000
mino	9.922143	-1.654228	0.000000
CG10444	9.767251	-1.654531	0.000000
Efr	27.033660	-1.655711	0.000032
Phk-3	875.726305	-1.656137	0.000007
Pxd	90.785024	-1.658670	0.000065
bdg	5.802164	-1.660901	0.000000
msb1l	10.349111	-1.662062	0.000081
Sox15	6.216426	-1.664221	0.000000
CG15343	6.257203	-1.664235	0.034476
SERCA	130.679323	-1.665559	0.000010
l(2)03659	5.241011	-1.666054	0.000000
CG42238	4.261679	-1.668739	0.000029
CG4914	12.431059	-1.670603	0.000229
mim	3.462744	-1.670924	0.000000
spz	11.214265	-1.671902	0.000000
CG11555	31.055263	-1.672482	0.000000
Skeletor	64.269527	-1.673808	0.000065
CG10232	5.975912	-1.674704	0.001162
qless	94.660418	-1.675561	0.000059
CG42237	10.592436	-1.675996	0.000525
jp	4.393557	-1.677561	0.000045
Gpdh	39.746909	-1.678331	0.000001
CG6006	7.579494	-1.679100	0.000000
Exn	15.455099	-1.679248	0.000000
Lsp1gamma	565.116362	-1.679413	0.001494
CG13907	1.225474	-1.681273	0.030708
foxo	14.394705	-1.684974	0.000000

CG6145	15.259439	-1.685456	0.000024
CG5577	3.269978	-1.688377	0.007272
Nplp2	294.036864	-1.688968	0.000394
CG3967	9.620433	-1.690757	0.000000
agt	5.709039	-1.691287	0.011332
CG5863	12.208013	-1.694047	0.000000
lbm	5.592034	-1.694430	0.015951
caix	3635.864092	-1.695068	0.000000
CG9775	36.272491	-1.695074	0.000001
CG7402	59.839851	-1.695306	0.000000
sals	6.403599	-1.695366	0.000067
Pdp1	4.427082	-1.695702	0.000029
CG17029	193.240291	-1.699301	0.000000
CG43861	2.619419	-1.699421	0.000710
CG10184	12.461120	-1.703905	0.002307
CG7720	21.173811	-1.706645	0.000000
CG42514	6.771116	-1.707363	0.000018
cnn	3.220572	-1.713026	0.000000
neo	5.681246	-1.713263	0.000132
Dyrk2	6.333908	-1.716394	0.000000
CG12868	19.352739	-1.720876	0.000025
CG8112	18.323053	-1.721424	0.000282
Snoo	8.787569	-1.721837	0.000000
SLIRP2	13.939479	-1.722096	0.022392
Atet	9.182729	-1.723955	0.000000
Cht7	58.384468	-1.727873	0.000003
Tg	30.785952	-1.728002	0.000004
CG8177	6.423159	-1.728206	0.000000
spri	8.736179	-1.728921	0.000002
Pif1B	15.363737	-1.729602	0.000000
CG7470	1.711245	-1.730866	0.012074
CG14401	12.675222	-1.732327	0.000001
CG43313	4.419374	-1.734498	0.000000
CG14629	22.155045	-1.735569	0.000044
CG9008	13.896646	-1.736386	0.000000
Lsd-2	19.694048	-1.737753	0.000000
MYPT-75D	2.927798	-1.739406	0.000069
CG31324	2.866880	-1.744889	0.010522
DOR	74.344032	-1.746598	0.000000
Mp	9.295440	-1.748941	0.000000
CG13239	17.130732	-1.749525	0.000201
CG5928	14.194068	-1.750465	0.000001
CG9331	62.369956	-1.753932	0.000000
CG2765	58.346828	-1.754018	0.000000
CG7466	8.920699	-1.756739	0.000000
Sp212	6.965807	-1.758195	0.000234
AMPdeam	13.651901	-1.758359	0.000000
Cpr47Eb	2875.274824	-1.761689	0.000000
CG8157	16.113384	-1.764199	0.000008
CG12512	7.636352	-1.766635	0.000010
inv	1.930804	-1.767559	0.000336
CG5397	300.550005	-1.767592	0.000000
Cyp6d4	16.401004	-1.770291	0.000000
tsl	28.911794	-1.773041	0.000000
AOX1	19.556512	-1.774918	0.000000
Frq2	1.349505	-1.777098	0.007642
P5cr-2	2.661949	-1.777650	0.042591
Lcp4	7030.366023	-1.778705	0.000575
Elal	5.327743	-1.779204	0.000078
CG7054	16.468054	-1.782471	0.000009
Best1	13.358834	-1.783208	0.000000
CG5731	15.628777	-1.787545	0.000000
CG9452	3.634831	-1.791077	0.009087
Cyp6w1	3.878656	-1.791547	0.000342
Gclc	15.800816	-1.792493	0.000000
Tps1	3.114790	-1.793386	0.027467
CG30456	8.394304	-1.793538	0.000000
Acox57D-d	4.914444	-1.794054	0.000045
CG30460	12.680309	-1.796496	0.000000
CG17027	22.717769	-1.796703	0.000001
CG4847	134.845206	-1.797434	0.002629
Slc45-1	4.346653	-1.799127	0.000011
PGRP-LA	22.877848	-1.801401	0.000000
dve	1.101988	-1.802868	0.023569
Ccp84Ag	2470.931915	-1.805399	0.000000
NKCC	2.618473	-1.806418	0.001073
CG3880	6.459680	-1.807427	0.000266
CG14984	142.731496	-1.813060	0.000000
CG40006	34.271529	-1.814368	0.000000
Npc1a	49.057976	-1.817061	0.000000
SCAP	5.644007	-1.818889	0.000000
Spn	1.230621	-1.819001	0.001777
Cyp6a13	4.990877	-1.821112	0.000616
CG9005	6.771220	-1.825054	0.000000
CG10650	8.891528	-1.825470	0.000002
CG11158	11.405373	-1.825496	0.000000
scaf	228.906733	-1.826841	0.000000
nab	3.797328	-1.828210	0.000708
uzip	29.633782	-1.828813	0.000000
Wnt6	12.945829	-1.829714	0.000000
CG4928	37.066855	-1.830114	0.000000
CG9123	2.761112	-1.836412	0.026927
CG4302	2.784669	-1.839058	0.019817
Cht5	46.736124	-1.839270	0.041539
mbl	3.921956	-1.841072	0.000000
CG9471	84.097960	-1.841832	0.000000
ImpE3	2.321566	-1.843167	0.037502
Ttc19	7.951892	-1.844386	0.000032
Cpr49Ah	227.593356	-1.846348	0.000000
hbs	4.054285	-1.847878	0.000000
CG7900	57.833756	-1.860899	0.000000
CG7328	5.115272	-1.861606	0.001071
Ugt86Da	55.873289	-1.862023	0.000000
cpx	0.412823	-1.864409	0.028248
CG7365	12.757435	-1.864417	0.000083
Mal-A5	5.269616	-1.864467	0.000135
Nek2	3.442028	-1.865694	0.000156
Hn	7.192970	-1.866500	0.000830
GILT3	10.718770	-1.867063	0.000081
pre-lola-G	5.495122	-1.870658	0.000000
CG13784	24.209840	-1.872237	0.000000
fbp	36.145817	-1.876551	0.000000
KCNQ	3.780275	-1.876574	0.000001
Mmp1	48.346295	-1.876582	0.000000
wtrw	1.322350	-1.876627	0.009352
CG6231	10.321517	-1.877869	0.000000
Cpr49Ag	1400.543477	-1.878474	0.000000
CG3164	133.669425	-1.879677	0.000001
CG6321	3.106645	-1.879689	0.015862
CG13659	5.590881	-1.882766	0.000549
nec	6.516723	-1.883839	0.000038
CG34165	19.421084	-1.884379	0.000002
nSyb	0.569571	-1.884674	0.049493
CG42795	1.141160	-1.887616	0.000015
ap	6.953211	-1.889270	0.000000
Cpr97Ea	161.108521	-1.891818	0.000000
CG13196	4.414885	-1.893104	0.000025
CG16713	14.610843	-1.895605	0.040052
CG34291	25.158552	-1.897098	0.037063
tutl	1.510789	-1.897207	0.000001
CG6415	4.332764	-1.900013	0.036178
CG9689	9.799741	-1.900032	0.000002
Cpr66Cb	3.311303	-1.901004	0.033392
CG11883	6.716044	-1.901917	0.000000
fau	84.309424	-1.902968	0.000001
CG13283	2.092434	-1.908304	0.028229
CG34382	3.463044	-1.908339	0.000020
CG31538	3.239429	-1.908417	0.000564

CG42542	17.426571	-1.910342	0.000000
CG11897	3.512183	-1.910657	0.000000
CG14257	2.479731	-1.915229	0.001975
CG6125	23.584357	-1.916795	0.000000
tsh	7.396529	-1.916992	0.000000
Acer	4.818266	-1.926162	0.000003
pre-mod(mdg4)-W	2.047119	-1.926814	0.000060
sqa	1.052758	-1.932603	0.000901
CG14933	10.136012	-1.932818	0.000006
Cad88C	0.421471	-1.933514	0.025080
cv-d	4.042776	-1.935298	0.000000
CG10737	34.979443	-1.935331	0.000000
CG10345	10.745742	-1.935675	0.000020
CG9279	0.704956	-1.937998	0.015296
CG12003	1.360452	-1.941984	0.032491
CG5758	177.168815	-1.943373	0.000000
CG11852	804.255209	-1.947410	0.000000
ppk	1.417520	-1.949187	0.022101
Ctr1A	72.798314	-1.951747	0.000000
St3	5.635132	-1.954909	0.000000
Nep3	0.479333	-1.955842	0.032949
CG8915	3.200567	-1.956820	0.000001
GMF	19.882336	-1.956841	0.000000
CG31125	2.883171	-1.958339	0.014003
Tom	12.529511	-1.959317	0.000009
CG13920	2.993094	-1.959541	0.027041
CG9427	100.937833	-1.959547	0.000000
CG8586	1.656328	-1.960272	0.021478
CG11378	1.482374	-1.960364	0.033739
CG11905	2.586581	-1.961920	0.000019
CG31785	3.320965	-1.962184	0.010355
CG17026	87.844546	-1.963240	0.000000
grk	5.127730	-1.963460	0.000071
twz	1.676643	-1.965439	0.018536
KFase	10.685892	-1.968531	0.000000
CG5687	1.479724	-1.968691	0.019135
nompA	0.681395	-1.968694	0.018788
hh	2.066056	-1.969181	0.010385
CG13679	724.562404	-1.971537	0.000651
Cpr49Af	75.138508	-1.973200	0.014973
CG17572	4.363015	-1.974033	0.004267
PK1-R	7.492956	-1.977112	0.000000
CG3630	6.064079	-1.978950	0.000003
cpo	1.221870	-1.979366	0.000000
ple	27.450405	-1.981523	0.000000
gce	9.371784	-1.985713	0.000000
Ca-beta	0.298477	-1.988924	0.036968
spel1	6.746574	-1.990436	0.000000
CG13606	12.065970	-1.992986	0.000000
Cpr100A	505.259776	-1.995723	0.000000
CG5002	0.990762	-1.998645	0.047415
nub	3.806417	-2.001968	0.000000
b	11.838624	-2.010148	0.000000
CG15046	4.457481	-2.011105	0.000033
tok	6.045400	-2.016306	0.000000
Ugt36Ba	4.632745	-2.017321	0.000007
CG13124	85.343879	-2.017378	0.000000
Gnmt	5.793577	-2.017823	0.042724
Cys	654.947293	-2.020551	0.000000
Octbeta2R	1.857655	-2.021411	0.000012
TwdlE	2.052025	-2.021724	0.030442
CG5023	84.960990	-2.021890	0.000000
CDase	22.355704	-2.022228	0.000000
Jabba	40.922077	-2.025062	0.000000
CG14526	2.382544	-2.030614	0.009607
CG14636	9.535777	-2.031103	0.000000
CG42390	5.712404	-2.032935	0.000000
CG31826	19.363265	-2.033470	0.000000
Cda4	122.669452	-2.033723	0.000000
Hk	0.239855	-2.037504	0.041383
futsch	0.200721	-2.038366	0.008281
Eglp2	5.141696	-2.038468	0.000834
CG42240	5.701508	-2.040039	0.000000
htl	1.497545	-2.041581	0.001428
CG11438	3.527053	-2.042979	0.000004
CG31321	43.442926	-2.043055	0.000000
CG34115	7.070105	-2.045805	0.011743
Ugt35a	17.406595	-2.046926	0.000000
CG9593	3.825240	-2.047181	0.008913
Cyp12e1	43.659414	-2.047966	0.000000
Pde9	1.054551	-2.048741	0.000438
CG15701	0.832462	-2.051551	0.010191
FASN1	46.170500	-2.053218	0.000000
Cyp312a1	16.155522	-2.057587	0.000000
amon	0.747558	-2.059040	0.011341
CG42486	11.123117	-2.059100	0.000000
Adh	120.297137	-2.059281	0.000000
Obp56d	1421.894913	-2.060687	0.000000
Sp7	26.947506	-2.065158	0.000000
CG10175	2.414465	-2.065826	0.000021
CG2233	22.941380	-2.068521	0.000052
CG4239	13.997751	-2.068788	0.000000
f	0.420595	-2.069202	0.009831
Nfl	0.829503	-2.069835	0.015566
ckd	53.265516	-2.072095	0.000000
CG11400	9.391924	-2.072472	0.000001
CG9877	171.794927	-2.073425	0.000056
CG31918	21.305050	-2.073492	0.000000
CG7458	2.626529	-2.077270	0.001530
Hr38	2.260307	-2.078980	0.000000
CG31689	6.322501	-2.080375	0.000000
CG4757	1.938010	-2.081324	0.005120
CG8128	7.140304	-2.084179	0.000001
CG30377	4.071158	-2.085585	0.000000
CG14995	7.741735	-2.088830	0.000000
Cyp6a14	2.937332	-2.088992	0.000008
nonA-l	4.306162	-2.089041	0.000000
kcc	5.072430	-2.090799	0.000000
CG10137	3.471484	-2.091885	0.000000
Pal2	2.403909	-2.092146	0.001864
CG3568	2.020080	-2.093564	0.037984
so	1.055987	-2.097923	0.011400
CAH2	172.564215	-2.098343	0.000000
Spn77Bb	2.495585	-2.099320	0.007507
CG15414	35.891278	-2.100450	0.000002
Clect27	779.981061	-2.105849	0.000000
CG34452	2.868222	-2.108128	0.007531
CG7497	269.630228	-2.108468	0.000000
CG9265	44.684957	-2.113558	0.000000
shf	6.987318	-2.117658	0.000002
smp-30	2.168410	-2.118701	0.011344
CG9386	17.178004	-2.119595	0.000000
CG3097	44.805580	-2.120624	0.000000
CG8012	1016.980796	-2.126045	0.000000
CG8925	13.351166	-2.128201	0.000000
bmm	3.625229	-2.129830	0.000036
Gabat	2.498523	-2.131199	0.000660
CG17325	19.585876	-2.132546	0.000000
CG4982	10.325533	-2.133661	0.017648
vg	3.862611	-2.138857	0.000000
CG10710	1.681177	-2.138968	0.010369
CG13024	22.826202	-2.140337	0.000000
dmGlut	31.856655	-2.143957	0.000000
Proc	11.801325	-2.144863	0.000000
Ance-4	2.113663	-2.145489	0.033495
Glycogenin	56.877621	-2.145608	0.000000
obst-A	375.178479	-2.149360	0.000000

CG34396	1.166748	-2.151988	0.002970
CG32694	70.027861	-2.152065	0.000000
CG7772	20.864742	-2.153837	0.000000
CG3168	2.297094	-2.155938	0.000133
SmydA-9	4.333206	-2.157943	0.000095
CG9782	143.137344	-2.158873	0.000000
CG17109	13.780900	-2.163780	0.000000
CG8369	200.093440	-2.164567	0.000000
CG31313	260.905601	-2.165065	0.000000
Pkcdelta	0.614281	-2.168223	0.008152
SclB	106.015219	-2.170434	0.000000
Adat1	8.643247	-2.172781	0.000000
CG17323	2.303304	-2.173596	0.009619
Cyp317a1	4.428629	-2.175707	0.000000
CG2556	4.132114	-2.178557	0.000007
CG33970	10.245224	-2.179267	0.000000
PPO3	0.820088	-2.181179	0.029072
Cpr67B	104.326954	-2.185924	0.000001
CG14285	7.737469	-2.185949	0.000011
CG8785	3.149364	-2.187658	0.001525
CG14866	1.251320	-2.191581	0.019378
CG2781	15.152232	-2.192609	0.000000
CG17646	48.013081	-2.193970	0.000000
Sh	0.093833	-2.194065	0.023366
St1	15.444179	-2.196871	0.000000
CG45076	36.124816	-2.202471	0.000000
mspo	0.774743	-2.203206	0.012947
beat-IIIc	0.602481	-2.204504	0.011221
CG45078	19.159210	-2.206406	0.000013
yellow-e3	2.596305	-2.208676	0.009349
hwt	0.352114	-2.209238	0.005950
CG34301	19.430915	-2.212432	0.000298
tld	2.715659	-2.213672	0.000020
CG6044	2.665326	-2.214110	0.003884
Cpr60D	128.941949	-2.215398	0.000025
Ccp84Ad	262.376376	-2.215763	0.000000
sr	0.251697	-2.217290	0.031457
CG2003	6.485062	-2.218750	0.000000
CG8641	0.646155	-2.227064	0.027252
Shab	0.227610	-2.227145	0.011151
GstZ2	1.896279	-2.228931	0.012841
tau	0.896004	-2.230946	0.000670
mamo	2.091527	-2.238043	0.000000
Nna1	1.558031	-2.238169	0.000000
CG11409	31.351095	-2.238967	0.000000
NimB2	36.525991	-2.241812	0.000000
CAH1	3043.728825	-2.242660	0.000000
AstA-R2	2.226357	-2.242670	0.001157
CG10738	4.931098	-2.242855	0.000000
CG15784	217.276315	-2.243571	0.000000
Vha68-1	2.733292	-2.245265	0.000021
Spn88Eb	2.490994	-2.245713	0.003612
CG6218	4.759625	-2.245729	0.000000
GstE7	7.614222	-2.254017	0.000317
GstE3	89.376051	-2.255439	0.000000
CG4300	18.349730	-2.259184	0.000000
Adgf-C	60.867166	-2.259199	0.000000
CG18622	5.746735	-2.262385	0.000009
igl	0.579464	-2.268546	0.043031
Ugt86Di	1.865105	-2.269766	0.003261
Tsf1	3290.727503	-2.272554	0.000000
Tsp42Eg	9.798494	-2.273701	0.000001
yellow-f	2.347356	-2.278050	0.005380
CG10031	6.778599	-2.279436	0.002136
ab	6.953885	-2.283127	0.000000
CG44085	4.010576	-2.290409	0.000000
Act87E	147.164033	-2.291062	0.000000
CRMP	9.642353	-2.295037	0.000000
sosie	0.905226	-2.296284	0.048578
Cyp12a5	1.674304	-2.297148	0.007087
CG4945	1.003251	-2.297263	0.011400
CG34120	19.007333	-2.301207	0.000000
Zasp52	14.591815	-2.301877	0.000000
CG46309	4.672609	-2.301902	0.000021
Mlp84B	53.969071	-2.304261	0.000000
hid	2.220411	-2.306064	0.000004
bol	0.520095	-2.307692	0.002155
Lsd-1	14.090994	-2.310243	0.000000
CG4733	4.695818	-2.310287	0.000000
CG43897	23.244614	-2.310721	0.000000
Eglp4	20.769416	-2.314971	0.000000
MFS9	12.114660	-2.315374	0.000000
CG14132	77.311423	-2.316606	0.000000
CG13937	2.397117	-2.317160	0.000714
Fmo-2	3.957566	-2.317723	0.000183
CG9449	68.161816	-2.319216	0.000000
brp	0.126136	-2.319879	0.026686
Cpr65Ay	37.487998	-2.321228	0.000000
apolpp	26.587067	-2.323387	0.000000
rn	3.734313	-2.323887	0.000000
EbpIII	407.428211	-2.324626	0.000000
Tret1-1	5.640018	-2.328827	0.000000
CG14615	1.011043	-2.331931	0.018433
Men	75.685693	-2.332328	0.000000
Sirup	97.387146	-2.333516	0.000000
Dll	2.626176	-2.333759	0.000000
CG4962	4755.174592	-2.334380	0.000000
CG31760	0.320173	-2.339173	0.043445
CG32241	389.945784	-2.341042	0.000003
Est-Q	1.862062	-2.345198	0.003582
Epac	0.370524	-2.350501	0.002151
PK2-R2	0.584615	-2.358380	0.033581
CG43386	40.359643	-2.361120	0.000000
Itgbn	0.818069	-2.361880	0.003836
CG13607	1.943291	-2.362191	0.006548
Cyp318a1	154.243846	-2.366127	0.000000
Adk3	22.349159	-2.366525	0.000000
AcCoAS	19.357661	-2.370013	0.000000
CG13639	19.325567	-2.370354	0.001135
CHKov2	37.531101	-2.371444	0.000000
Tsp42Eo	3.297491	-2.378926	0.002839
fd96Cb	1.186672	-2.387976	0.048893
CG8086	13.397213	-2.390167	0.000000
Zasp66	52.249959	-2.394037	0.000000
alpha-Est2	2.251475	-2.396368	0.001458
CG9413	4.186059	-2.397582	0.000000
CG33181	24.921017	-2.404184	0.000000
CG3726	1.054852	-2.405703	0.001861
CG13230	106.453464	-2.407352	0.000219
CG1265	33.044266	-2.408577	0.000000
CG13875	2.529216	-2.409307	0.000355
CG9743	4.927166	-2.409949	0.000003
obst-E	198.770943	-2.414054	0.000000
comt	2.566716	-2.418054	0.000021
disco	0.424603	-2.419440	0.036737
CG5612	3.309227	-2.419738	0.001644
Mrp4	15.125253	-2.421380	0.000000
C15	0.653068	-2.428418	0.041383
Tsp42Eh	2.578947	-2.430876	0.003380
Gpo-1	16.023703	-2.434606	0.000000
CG5783	3.215076	-2.435161	0.001036
CG8353	4.964524	-2.435369	0.000465
CG3842	7.832384	-2.437666	0.000000
CG5597	15.926010	-2.445686	0.000000
CG30411	0.927891	-2.445845	0.045741
CG14968	41.563328	-2.449702	0.000000
Sr-CIV	1.748962	-2.451704	0.003261
CG31262	1.123019	-2.454390	0.015621

CG31140	0.349995	-2.454489	0.003526
amd	5.187400	-2.457521	0.000000
CG14642	5.965578	-2.457624	0.000003
CG14439	27.607127	-2.462735	0.000000
CG30197	83.787818	-2.464300	0.000000
CG9701	38.428171	-2.469909	0.000000
Shal	0.685512	-2.473526	0.000721
Odc1	1.181693	-2.476931	0.048877
CG15117	1.856225	-2.478050	0.000049
CG34232	56.887259	-2.479137	0.000000
Achl	0.703471	-2.483809	0.001923
inaD	0.532503	-2.493194	0.044375
pros	0.059485	-2.497386	0.033281
CG42305	20.396274	-2.500177	0.000000
CG44245	100.310064	-2.502479	0.000000
Cyp28d1	1.496390	-2.512119	0.006223
Mdr49	3.504556	-2.512190	0.000000
GluRIID	2.867648	-2.513843	0.000004
SK	0.198350	-2.514691	0.006833
alpha-Est9	25.749706	-2.515969	0.000000
CG9297	44.970207	-2.518629	0.000000
dac	0.389500	-2.519146	0.005273
CG31248	16.203223	-2.521184	0.011422
fon	50.524590	-2.523087	0.000000
CG11345	17.374172	-2.523148	0.015404
CG2070	42.143584	-2.526791	0.000000
CG8008	10.059134	-2.527782	0.000000
Wnt2	0.747279	-2.528620	0.011713
CG9512	5.041516	-2.528787	0.000001
CG13043	1631.794850	-2.529347	0.000000
ImpE1	0.859054	-2.534509	0.000510
CG33521	11.437197	-2.537538	0.000000
Dat	6.980569	-2.540380	0.000000
nord	1.844467	-2.541953	0.000120
CG4839	1.049778	-2.545341	0.000015
Ac76E	5.420203	-2.547919	0.000000
CG42264	0.606345	-2.553797	0.032612
CG40298	2.487541	-2.558303	0.000560
CG30148	1.666687	-2.559631	0.011861
CG4213	1.354085	-2.562628	0.000092
RpS19b	1.289089	-2.565350	0.048946
CG12164	8.392081	-2.572246	0.000000
CG34454	6.143305	-2.580162	0.001438
VAChT	0.115579	-2.584387	0.048578
Dbi	157.964022	-2.588291	0.000000
Mp20	408.304808	-2.596122	0.000000
CG9626	0.598994	-2.602701	0.002149
CG13641	5.338521	-2.603615	0.002413
CG32333	0.209134	-2.604564	0.031476
Jhl-26	69.788507	-2.615646	0.000000
Srpk79D	1.038392	-2.617660	0.000021
Sox102F	0.756383	-2.621779	0.000413
CG15247	1.326680	-2.631157	0.002712
CG6830	49.150205	-2.636365	0.000000
CG16959	4.788198	-2.636497	0.000000
CG31183	1.635926	-2.646760	0.000000
betaTub97EF	45.434575	-2.649295	0.000000
disco-r	0.447033	-2.652996	0.000322
Obp56a	1416.589579	-2.656734	0.000000
CG33307	3.702235	-2.670889	0.000084
rpr	7.002549	-2.672168	0.000330
CG32485	4.994915	-2.673208	0.000029
ppk26	1.680507	-2.675015	0.000637
CG5867	424.312913	-2.676012	0.000000
CG14964	2.078356	-2.676886	0.000000
CG31287	1.324536	-2.682942	0.004038
CG1674	30.154595	-2.683584	0.000000
CG32214	24.036013	-2.684097	0.034578
CG4666	4.359843	-2.685054	0.000085
l(3)mbn	32.445980	-2.685920	0.000000
CG43078	4.711081	-2.687738	0.000000
wun2	1.820126	-2.692983	0.000825
mwh	1.255444	-2.709806	0.000026
CG42331	0.155958	-2.711880	0.048007
loh	1.012094	-2.717056	0.005882
GstE9	4.683003	-2.717444	0.000340
CG42749	10.936999	-2.722350	0.000011
CG7299	206.654213	-2.731395	0.000001
sv	0.340470	-2.736226	0.005269
CG4984	7.488629	-2.741113	0.000000
CG13699	0.307363	-2.741888	0.024950
shd	2.111423	-2.743140	0.000004
CG4301	0.385996	-2.745150	0.003124
reb	62.024822	-2.746396	0.000000
RluA-1	1.183910	-2.748660	0.000172
CG8539	1.157809	-2.760377	0.006408
bdl	1.814035	-2.762942	0.000028
Traf-like	0.531896	-2.763105	0.035029
Lcp3	1054.871473	-2.768167	0.000205
CG2736	4.458208	-2.775853	0.000047
CG7227	4.007178	-2.778307	0.000000
Kif3C	0.381732	-2.779842	0.008683
CG8105	0.674243	-2.780598	0.033332
CG4872	8.909942	-2.780822	0.000000
Cyp4p3	3.540615	-2.782024	0.000167
Actn	77.930088	-2.782156	0.000000
CG1909	0.664430	-2.784069	0.006968
CG13318	7.952984	-2.786300	0.000000
CG42326	14.585820	-2.788230	0.000000
CG14762	0.285950	-2.789099	0.033691
kn	0.391363	-2.789102	0.011840
Ank2	0.205805	-2.792587	0.000000
Ant2	2.008765	-2.806233	0.000961
CG14186	0.615192	-2.806651	0.004719
Cpr47Ec	13028.646000	-2.809657	0.000000
ringer	36.003129	-2.813400	0.000000
CG10962	19.694807	-2.813515	0.000000
Argk	327.248073	-2.815967	0.000000
GstE6	86.615679	-2.817099	0.000000
CG3108	0.332515	-2.817852	0.021647
shakB	0.146271	-2.820710	0.001459
CG15203	4.673510	-2.820835	0.000370
Jheh1	74.995109	-2.827866	0.000000
CG32392	0.274597	-2.830638	0.043824
CG7214	3096.940250	-2.833683	0.000000
7B2	11.893765	-2.838388	0.000000
CG9876	2.124535	-2.841006	0.000099
Antp	23.192480	-2.843361	0.000000
IM33	94.304330	-2.843943	0.000000
CG42404	0.125598	-2.848128	0.041270
slo	0.250113	-2.849443	0.000700
CG6908	4.412590	-2.850146	0.000013
dsb	0.762111	-2.850654	0.000211
CG45263	0.099266	-2.856086	0.014857
cert	83.887498	-2.857967	0.000000
CG13360	16.288722	-2.861260	0.000000
CG43693	1.542309	-2.864714	0.000365
LManVI	0.381348	-2.868306	0.048809
CG31029	0.604370	-2.876540	0.005476
tn	6.494010	-2.877749	0.000000
CG14304	5.942114	-2.878707	0.000000
Mf	83.155147	-2.881594	0.000000
cDIP	0.796033	-2.882194	0.012757
CG15431	0.696483	-2.884334	0.000029
CG9919	0.556050	-2.885941	0.019789
CG14109	3.582831	-2.888205	0.000109
pigs	6.127152	-2.889206	0.000000
CG16798	5.143203	-2.896378	0.000001

CG11951	0.563386	-2.899164	0.008500
CG13912	1.403840	-2.909457	0.026637
AOX2	47.695260	-2.912279	0.000000
CG10339	1.071131	-2.919326	0.000776
TpnC73F	311.146907	-2.922599	0.000000
CG14695	4.383827	-2.928591	0.000010
Cpr65Ec	7.670854	-2.932893	0.001053
CG14456	24.303482	-2.937969	0.000000
CG13012	4.215287	-2.938217	0.000626
Apoltp	1.157818	-2.943023	0.000000
Kaz1-ORFB	43.987996	-2.944296	0.000000
CG13065	1.327186	-2.948074	0.036468
Mdr65	1.446131	-2.949265	0.000002
CG13067	49792.672982	-2.951919	0.000000
Cda5	22.996196	-2.953118	0.000000
CG31345	2.267643	-2.953350	0.000901
GluRIIA	1.233046	-2.955396	0.000094
bgm	3.117121	-2.955798	0.000000
CG2993	0.172681	-2.963402	0.043445
CG7058	0.149509	-2.963593	0.038463
CG17278	38.517927	-2.965839	0.000000
metro	1.097317	-2.978209	0.000038
CG5326	65.673770	-2.978221	0.000000
Rgk3	0.688763	-2.979847	0.000307
CG3556	0.379508	-2.983805	0.006217
Asph	14.396626	-3.004538	0.000000
RpS5b	0.631833	-3.004842	0.049090
CG5177	241.228983	-3.007123	0.000000
sls	4.502536	-3.007992	0.000000
CG3348	41.930863	-3.008225	0.000000
CG30062	2.258371	-3.008255	0.013434
CG17108	53.855504	-3.009553	0.000000
CG14795	15.686972	-3.020689	0.000003
CG12105	0.365610	-3.023788	0.001580
CG16743	2.903191	-3.024205	0.000177
CG13731	257.033513	-3.027918	0.000000
NimC2	0.580273	-3.028870	0.026946
GstD10	14.204502	-3.030754	0.000000
Hsp68	14.903383	-3.034333	0.000000
CG6225	1.134534	-3.040160	0.000051
CG9498	4.070962	-3.040446	0.000001
CG10361	3.042706	-3.042076	0.000404
RIC-3	9.867252	-3.054902	0.000000
Glut4EF	3.040379	-3.058730	0.000000
Lst	31.902208	-3.066006	0.000000
yellow-f2	1.428125	-3.066025	0.000389
nrm	4.669047	-3.070436	0.000000
Cyp311a1	0.606791	-3.071630	0.027252
CG10132	1.738553	-3.074462	0.000000
ClC-a	14.050949	-3.076952	0.000000
CG1441	21.915727	-3.078599	0.000000
CG4335	1.079532	-3.094679	0.021174
Cyp6a21	3.573432	-3.096090	0.000004
LUBEL	0.972327	-3.098380	0.000000
CG10205	46.997039	-3.100323	0.000000
alpha-Est10	24.937641	-3.101641	0.000000
Schip1	0.951627	-3.105163	0.000608
CG34448	1.677335	-3.106144	0.005413
Cyp4e3	3.109072	-3.113185	0.000003
CG13293	0.883647	-3.128439	0.000019
wupA	263.830884	-3.129129	0.000000
TpnC47D	54.387025	-3.133337	0.000000
Calx	0.357296	-3.133821	0.000032
repo	0.302579	-3.136590	0.020091
Lcp65Ab1	10968.569110	-3.148033	0.000000
CG15199	1.563957	-3.149739	0.025166
CG33110	6.372270	-3.149830	0.000000
CG3823	33.149495	-3.150667	0.000000
Mpcp1	22.449974	-3.153692	0.000000
CG11221	1.493661	-3.162413	0.000113
CG1461	4.619540	-3.164946	0.000020
TwdlN	19.320840	-3.165384	0.000017
Kua	0.252530	-3.165516	0.037698
psh	5.104173	-3.166101	0.000000
CG34141	1.326029	-3.182058	0.000047
CG15756	3.640557	-3.184312	0.000004
CG3301	11.211689	-3.191259	0.000000
Cpr62Bc	2388.833948	-3.196972	0.000000
CG18294	56.842066	-3.197214	0.000568
CG15021	1.894715	-3.200300	0.004885
dtr	0.410956	-3.215873	0.001960
Lcp65Ab2	7.765903	-3.223198	0.000112
CG30154	716.784819	-3.223416	0.000000
Cpr78Cc	99.168986	-3.223573	0.000016
ham	0.638540	-3.228396	0.000005
CG42846	6.562257	-3.230246	0.000126
CG7378	5.072936	-3.236163	0.000000
up	386.829084	-3.237586	0.000000
CG8736	660.871880	-3.239937	0.000000
CG42565	0.361732	-3.244749	0.012297
NLaz	7.218714	-3.245547	0.000000
CG15731	0.508771	-3.247596	0.038631
CG8888	49.408790	-3.255392	0.000000
ImpL3	66.927091	-3.264118	0.000000
Pkd2	0.497399	-3.266460	0.003143
CG12910	0.706683	-3.277640	0.001975
CG16779	0.083544	-3.288421	0.007768
CG12911	5.180973	-3.295658	0.000000
Tm2	204.462886	-3.297902	0.000000
Ude	93.463367	-3.299235	0.000000
alphaTub85E	23.892162	-3.303494	0.000000
Act57B	2275.228487	-3.304804	0.000000
Cpr66D	7.738523	-3.321438	0.000000
Spn31A	1.231870	-3.325474	0.003404
CG7695	7.440695	-3.328170	0.000032
Kr	0.324941	-3.328209	0.010038
CG7997	21.210759	-3.340713	0.000000
Ntl	0.259952	-3.344177	0.039002
prc	1.237608	-3.350853	0.000177
Ca-alpha1D	0.551242	-3.353589	0.000001
CG14688	8.386546	-3.379063	0.000000
CG15553	8.423189	-3.381172	0.000000
tilB	0.568424	-3.383116	0.014857
CG10226	0.827833	-3.402268	0.000004
CG11370	29731.223949	-3.404871	0.000000
TfAP-2	0.382651	-3.405316	0.009135
sns	0.419666	-3.410740	0.000003
Prm	122.464633	-3.410793	0.000000
CG42562	16.264338	-3.414568	0.000000
Mlp60A	61.753031	-3.416047	0.000000
CG5225	1.945772	-3.430853	0.000002
CG46317	4.350793	-3.439228	0.000003
CNMa	1.607149	-3.445787	0.000017
CG14661	99.053667	-3.447012	0.000000
dpr12	0.377729	-3.452322	0.000691
CG3999	1.864435	-3.457073	0.000097
tnc	1.179701	-3.458078	0.000000
tyn	7.665699	-3.466511	0.000000
AQP	2.182771	-3.466804	0.000097
CG13063	1771.397825	-3.474971	0.000000
Acp1	1569.180106	-3.476442	0.000000
CG2065	29.654875	-3.490848	0.000000
CG12290	2.672887	-3.500649	0.000000
CG11843	2.373126	-3.501100	0.000015
CG6329	0.419174	-3.505734	0.002192
CG13223	0.926114	-3.507657	0.001018
DopEcR	0.384933	-3.508084	0.001710
SclA	83.005916	-3.508606	0.000000

Unc-89	8.250194	-3.525477	0.000000
CG6739	47.630248	-3.527352	0.000000
Ugt86Dd	4.036763	-3.534038	0.000000
CG42561	8.534944	-3.536132	0.000001
ninaC	0.510642	-3.538473	0.000011
Mlc2	984.991406	-3.543337	0.000000
CG8192	68.086622	-3.548229	0.000000
CG42337	0.506655	-3.550062	0.000523
CG33099	3.259169	-3.553873	0.000001
CG42817	1.729328	-3.558553	0.000000
bt	17.972719	-3.574683	0.000000
CG1124	96.758544	-3.574743	0.000000
CG2016	43.200051	-3.581947	0.000000
CG5756	0.213747	-3.583430	0.009729
CG15282	66.734301	-3.584394	0.000000
CG15563	1.101410	-3.587345	0.024398
CG14395	0.324027	-3.595515	0.001561
CG42269	2.877683	-3.598168	0.000000
e	10.546009	-3.609116	0.000000
Sur	0.309237	-3.611143	0.000060
CanA1	3.398649	-3.617025	0.000000
Lim1	0.649184	-3.620044	0.000051
CG9509	1.164095	-3.629204	0.000004
Mlc1	511.848759	-3.631534	0.000000
CG45095	4.984062	-3.633772	0.000000
CG9269	3.261945	-3.636899	0.003787
CG10237	20.093429	-3.649574	0.000000
snk	2.265775	-3.663479	0.000001
CG6106	0.931863	-3.674667	0.000060
CG6330	13.325602	-3.676581	0.000000
CG6293	3.258298	-3.693812	0.000000
SmydA-1	3.675364	-3.699798	0.000000
Edg91	1586.252952	-3.712294	0.000000
CG43795	0.088486	-3.714060	0.039596
CG3191	61.595541	-3.715694	0.000000
Pde1c	5.403808	-3.719536	0.000000
m	2.785110	-3.721725	0.000000
CG1213	3.050321	-3.727821	0.000218
CG43191	0.843026	-3.733175	0.006520
CG6834	2.332103	-3.738496	0.000000
C901	1.468102	-3.740197	0.000010
CG15249	1.544657	-3.747613	0.000044
CG16799	8.924412	-3.749972	0.000000
CG32647	0.096118	-3.753846	0.046371
Obp83g	107.267034	-3.754616	0.000000
CG7016	24.995296	-3.763027	0.000000
Osi19	7.339566	-3.764456	0.000000
CG33226	1.170754	-3.767338	0.005073
CG10953	263.357446	-3.767352	0.000000
CG18304	1.154101	-3.770139	0.000000
CG4630	5.067287	-3.770371	0.000000
l(2)01289	15.806768	-3.801087	0.000000
CG17036	5.292501	-3.804037	0.000000
CG4991	7.454903	-3.804643	0.000000
Vha36-3	25.941342	-3.843000	0.000000
Cyp18a1	119.392394	-3.861483	0.000000
CG40198	83.554672	-3.863940	0.000000
CG8852	1.746735	-3.866861	0.000006
SLC22A	3.524679	-3.881451	0.000000
Cyp12a4	6.308021	-3.892516	0.000000
D	0.182833	-3.915786	0.048163
qvr	0.430089	-3.923695	0.000023
SmydA-5	0.922651	-3.931004	0.000405
CG11670	4.448201	-3.931651	0.000000
CG31516	0.223251	-3.943405	0.049133
CG8219	0.197297	-3.943410	0.022953
CG5849	0.410907	-3.963893	0.003261
rpk	0.988109	-3.964098	0.000025
Mhc	276.555495	-3.967118	0.000000
Vmat	0.316770	-3.968401	0.000015
frac	7.265007	-3.974628	0.000000
Ndg	7.441252	-3.980087	0.000000
CG30457	645.860334	-3.982398	0.000000
CG3649	1.075330	-3.987959	0.000664
Rh50	3.428869	-3.990810	0.000000
Cyp12b2	3.567504	-3.991710	0.000000
CG6296	0.891673	-4.009434	0.000838
CG8249	2.388549	-4.017513	0.000000
ST6Gal	0.249187	-4.036553	0.044443
CG3104	0.591382	-4.038869	0.000536
CG7409	2.742088	-4.047896	0.000035
CG13068	3446.312181	-4.049452	0.000000
gammaSnap2	0.563146	-4.057786	0.020350
Oamb	1.101197	-4.091241	0.000000
CG42329	1.575425	-4.095136	0.000000
Tsp42En	2.178902	-4.107597	0.000013
CG14856	0.312762	-4.110890	0.034706
CG13285	0.970895	-4.127971	0.002050
CG33469	1.927145	-4.135353	0.001223
CG13954	0.332918	-4.162400	0.000005
CG11835	8.112775	-4.165979	0.000000
Neurochondrin	26.545001	-4.170490	0.000000
Cpr47Ee	1.518429	-4.201344	0.000540
CG9289	0.393238	-4.210828	0.003554
CG14147	2.747867	-4.211307	0.000112
CG31954	2.197471	-4.211944	0.000541
su(r)	15.324535	-4.213342	0.000000
CG6688	0.900080	-4.215028	0.000779
CG5376	5.132351	-4.221131	0.000000
CG2010	4.070891	-4.241031	0.000000
Smyd4-3	1.527954	-4.241801	0.000000
Cyp4p1	3.287493	-4.260656	0.000000
Nep1	2.854451	-4.273741	0.000000
CG14770	8.696327	-4.285596	0.000000
CG4607	10.481289	-4.304974	0.000000
lectin-24A	1.074371	-4.306254	0.002419
TwdlG	2.251460	-4.306548	0.000000
Gs1	8.188865	-4.330804	0.000000
GstD6	4.386581	-4.357994	0.000000
Cpr11A	146.871459	-4.390539	0.000000
CG33626	2.017348	-4.432265	0.000807
nol	2.620579	-4.441265	0.000244
CG43291	0.195379	-4.449745	0.031640
CG12655	14.258462	-4.466576	0.000000
CG17974	16.035842	-4.507205	0.000000
CG10064	0.266511	-4.516949	0.008446
GstD7	23.260850	-4.518388	0.000000
CG11760	1.234102	-4.542941	0.002018
CG6867	3.770578	-4.546278	0.000000
FMRFaR	0.409064	-4.550861	0.000109
Faa	10.946766	-4.555261	0.000000
CG10348	2.542341	-4.560878	0.000000
pyd3	14.960948	-4.581021	0.000000
dao	0.460352	-4.615215	0.000073
CG9194	1.617135	-4.621183	0.000000
pre-mod(mdg4)-AD	2.386423	-4.635479	0.000001
Cln3	1.750675	-4.685213	0.000000
CG12998	2.417141	-4.692316	0.000002
Muc30E	0.176788	-4.692855	0.001521
CG32248	37.044237	-4.697684	0.000000
CG15096	10.884317	-4.703981	0.000000
Cpr73D	1.059760	-4.706036	0.000000
CG32793	0.379145	-4.741042	0.001257
Alp4	12.173146	-4.745488	0.000000
Cyp4d21	7.981220	-4.775909	0.000000
CG3604	125.629094	-4.785363	0.000001

CG33178	42.079893	-4.790889	0.000000
SmydA-2	1.027444	-4.826431	0.000018
CG6083	0.741832	-4.845157	0.002084
CG5895	0.432998	-4.860433	0.006435
CG14573	19.699230	-4.863783	0.000097
CG34357	0.212093	-4.871987	0.000056
Hsc70-1	0.357686	-4.896974	0.002754
CG9360	158.928098	-4.903698	0.000000
CG13059	15.189680	-4.904627	0.000000
CG14082	0.195599	-4.911297	0.009800
Ucp4B	1.290808	-4.929230	0.000143
CG12116	12.258703	-4.940093	0.000000
CG14598	28.330040	-4.949017	0.000000
ppk17	0.244778	-4.955226	0.018410
CG6733	3.673401	-4.957566	0.000000
RyR	2.477778	-4.965077	0.000000
CG14854	2.629303	-4.985372	0.000086
MsR1	2.809774	-5.007413	0.000000
Gfrl	0.056224	-5.012377	0.012226
NT1	2.106950	-5.013121	0.000000
CG15597	630.382454	-5.021213	0.000000
CG13862	2.362907	-5.042905	0.001040
CG31371	0.361283	-5.056046	0.005007
jef	0.142594	-5.056441	0.006763
CG43134	221.097097	-5.082845	0.000000
CG3940	16.121816	-5.139765	0.000000
CG5955	2.193888	-5.141128	0.000001
CG42822	69.757352	-5.145512	0.000000
CG14568	22.234335	-5.153438	0.000144
CG31445	0.296310	-5.159875	0.001169
Sp1	0.844404	-5.212542	0.000000
SmydA-8	1.471172	-5.213235	0.000000
CG13721	3.432174	-5.236523	0.000002
Yp3	1.492682	-5.247133	0.000007
CG16885	2195.874850	-5.250095	0.000000
CG32847	0.464743	-5.255180	0.043892
CG32603	669.773882	-5.261909	0.000000
CG30458	2.620430	-5.276533	0.000322
Cpr50Cb	1.482170	-5.279367	0.001587
SmydA-4	1.631412	-5.280646	0.000000
CG14445	5.251990	-5.304655	0.000000
Jon99Fii	0.727127	-5.307146	0.033215
CG32808	13.781771	-5.309085	0.000000
CG7888	2.872403	-5.311858	0.000001
pirk	0.956350	-5.314955	0.000038
CG13793	0.929773	-5.351536	0.000049
CG31288	1.186274	-5.379047	0.000046
CG44008	2.949825	-5.423445	0.000000
Sln	0.090622	-5.500860	0.030576
CG5945	14.784153	-5.580642	0.000000
CG43175	1.630413	-5.583927	0.000337
CG33995	0.668677	-5.587208	0.000828
CG31769	5.677843	-5.593827	0.000000
CG40472	47.091444	-5.596757	0.000000
Cpr49Ae	28.528877	-5.600878	0.000000
Cyp6a2	34.944788	-5.628361	0.000000
Cyp4e1	2.345210	-5.643299	0.000000
CG32091	13.306919	-5.662722	0.000000
Smyd4-2	1.301845	-5.669790	0.000000
CG11044	0.895288	-5.703154	0.000006
Cyp9h1	2.129756	-5.708620	0.000000
CG18067	25.693789	-5.730903	0.000000
CG31871	2.819691	-5.745786	0.000010
stnB	0.044395	-5.746434	0.023118
CG5386	0.435617	-5.746672	0.026138
MtnE	0.613274	-5.761783	0.032808
CG33301	1.340222	-5.809750	0.000021
Ugt37c1	1.935744	-5.841865	0.000083
Obp44a	2.717611	-5.843301	0.000000
Scp2	0.628969	-5.847902	0.002440
Lip1	0.641880	-5.853591	0.000159
Ccp84Aa	484.245722	-6.035277	0.000000
CG15564	0.513537	-6.051157	0.000663
CG12607	98.647797	-6.090247	0.000000
CG16884	1722.310304	-6.173087	0.000000
Kif19A	0.115019	-6.175679	0.036487
TwdlT	15.241313	-6.179898	0.000000
Cpr78Cb	0.933736	-6.188628	0.000014
CG13315	5.571929	-6.204160	0.000000
Cyp6a8	0.866858	-6.264415	0.002307
CG4998	2.523482	-6.269984	0.000000
CG1368	721.995815	-6.277284	0.000000
CG11891	27.566267	-6.291312	0.000000
CG9083	0.426985	-6.326074	0.017674
Cpr62Bb	3.026953	-6.331888	0.000000
Scgdelta	1.904119	-6.354010	0.000000
CG6472	4.211565	-6.382162	0.000000
cyr	0.607523	-6.404098	0.000018
CG10560	0.437485	-6.404490	0.017080
CG30101	2.873567	-6.421083	0.000000
CG32036	0.714826	-6.421519	0.010036
CG43742	0.649662	-6.452712	0.001260
Cp36	0.463955	-6.478223	0.005499
CG4702	8.166534	-6.550895	0.000000
CG3339	0.082605	-6.581619	0.000112
Loxl2	1.584564	-6.585007	0.000005
CG16758	9.811079	-6.597484	0.000000
Pdfr	0.113782	-6.686689	0.007562
Ppi1	0.217557	-6.707372	0.001960
IFT52	0.292312	-6.729062	0.011976
Muc4B	0.635237	-6.773619	0.000314
CG13722	63.148736	-6.832790	0.000000
Spn100A	2.963347	-6.841569	0.000000
CG6999	0.632418	-6.874033	0.007943
CG32266	1324.487278	-7.043486	0.000000
CG31198	0.251345	-7.091469	0.009352
CG15545	4.390911	-7.100610	0.000000
CG5724	0.206781	-7.131006	0.032808
Cpr67Fa1	1521.665431	-7.153569	0.000000
CG9822	0.401020	-7.157909	0.030738
CG11841	0.434772	-7.221123	0.007114
CG32237	0.157227	-7.255902	0.024200
CG14564	179.111941	-7.257183	0.000044
TwdlM	1.609884	-7.272456	0.000014
CG5070	1.664611	-7.307977	0.001295
CG9649	0.472306	-7.346433	0.000436
CG11585	49.920650	-7.449184	0.000000
CG14369	1.229229	-7.456084	0.000123
CG11796	15.080514	-7.469388	0.000000
CG6972	4.376009	-7.570554	0.000000
Rh6	0.518092	-7.654957	0.000689
CG14105	1.587740	-7.676220	0.000282
TwdlH	1.404446	-7.749887	0.001316
CG15740	0.119664	-7.769975	0.014308
CG14820	0.435787	-7.808165	0.003379
CG11425	1.079281	-7.820712	0.000305
CG14292	3.346157	-7.899855	0.001420
Npc2h	3.225408	-7.906635	0.000000
CG9400	2.425185	-7.977370	0.000000
GstD2	26.062559	-7.994239	0.000000
TwdlP	39.077486	-8.019339	0.000000
Cyp313a4	120.506874	-8.175328	0.000000
GstD5	1.060527	-8.175763	0.000869
Cralbp	4.532859	-8.187003	0.000000
Ccp84Ab	424.007275	-8.213491	0.000000
CG34281	5.447272	-8.354603	0.000004
PH4alphaNE1	10.007829	-8.360599	0.000000
salt	0.322699	-8.745846	0.011177

CG13051	1959.888069	-8.759385	0.000000
CG14419	19.050147	-8.760053	0.000000
MsR2	0.106102	-8.778081	0.028622
CG34267	0.834891	-8.835790	0.038275
sand	0.957100	-8.863022	0.000001
CG10598	5.091543	-8.917175	0.000000
Lcp65Ag2	416.238340	-8.936812	0.000000
CG32284	1.269331	-8.942735	0.001975
CG14880	3.363094	-9.143312	0.000000
CG42821	38.066484	-9.180407	0.000000
CG3264	1.024547	-9.206562	0.000305
CG13640	401.296966	-9.552297	0.000000
SmydA-3	0.504746	-9.801877	0.000013
Jon99Fi	0.682438	-9.846432	0.024852
CG13744	0.429972	-9.877353	0.000295
atk	0.152800	-9.879428	0.000211
Cpr67Fa2	425.633350	-9.914027	0.000000
CG31219	0.568336	-9.925707	0.000964
CG10814	0.871702	-10.197916	0.000011
sit	12.144828	-10.229998	0.000000
CG34305	266.852444	-10.314493	0.000000
Act88F	2.459598	-10.344365	0.000000
CG13905	2.006615	-10.396172	0.008058
CG15515	212.517748	-10.521421	0.000000
CG34327	47.736312	-10.807000	0.000000
CG15221	0.215965	-10.824219	0.003951
mei-217	0.311497	-10.852251	0.000093
CG15894	0.273301	-10.980588	0.000000
CG14569	92.441361	-11.057732	0.000048
Jon99Ciii	1.242820	-11.085955	0.005413
CG14096	14.289660	-11.186828	0.000242
CG40485	0.907130	-11.394902	0.000001
Cpr49Aa	0.993264	-11.592834	0.001390
CG18557	0.543408	-11.594938	0.001587
Vml	0.295796	-11.760270	0.007514
CG11350	651.692824	-11.798447	0.000000
CG12480	2.061776	-12.129567	0.000000
CG13047	1031.327050	-12.320656	0.000000
CG30334	44.175018	-12.585479	0.000000
CG13069	1096.550521	-12.602491	0.000000
CG14457	0.780704	-12.716799	0.000005
CG15554	5.069354	-12.774194	0.000000
Acp65Aa	11.874998	-13.008542	0.000000
CG13705	557.066422	-13.219056	0.000000
CG31559	14.850510	-13.285062	0.000000
Jon25Biii	2.004619	-13.426941	0.000634
CG13618	25.483088	-13.433717	0.000000
CG15213	7.283018	-13.526729	0.000000
Lcp65Ae	544.991078	-13.533592	0.000000
CG14191	9.556007	-13.557063	0.000000
ato	0.221559	-13.602511	0.034309
TwdlO	96.714539	-13.916368	0.000000
CG13157	5.198984	-13.941213	0.000000
CG13297	10.382897	-14.063906	0.000000
CG13674	376.659606	-14.158366	0.000000
brv3	0.732966	-14.283197	0.000000
CG43666	21.614895	-14.437076	0.000000
Lcp65Ac	676.994523	-14.587510	0.000000
CG13226	0.308811	-14.690620	0.038180
CG17290	2.639293	-14.865828	0.000000
CG13841	1.424316	-14.879748	0.000004
CG34447	0.960799	-14.907207	0.000001
CG31606	0.450896	-15.371006	0.033056
Cpr65Ax2	1906.288457	-15.444082	0.000000
CG14565	65.471599	-15.676070	0.000000
Cpr65Ax1	273.825247	-16.652867	0.000000
Lcp65Ag1	2012.350222	-16.695126	0.000000
CG17560	0.199547	-16.790102	0.035443
Cpr49Ad	9.640839	-16.939293	0.000000
CG17404	0.376116	-16.993383	0.029310
CG15023	0.423398	-17.126711	0.032789
CG14153	0.857993	-17.412384	0.000099
CG13041	21.934091	-17.797634	0.000000
CG13983	0.414557	-17.949764	0.022518
CG32719	2.110052	-18.193426	0.000000
Cpr92A	0.327607	-18.274165	0.015566
CG43149	0.425387	-18.528097	0.019494
AstC	0.339052	-19.993712	0.011705
Jon66Ci	1.592175	-20.740714	0.000322
CG12256	1.128055	-21.422196	0.000898
CG8160	1.632552	-21.924137	0.000000
TwdlY	3.602309	-22.021531	0.000000
CG18180	1.935870	-22.066954	0.000007
Cp7Fc	4.618252	-22.904084	0.000000
CG15225	28.924725	-23.021458	0.000000
Twdlalpha	1.892761	-23.217768	0.000000
CG10581	19.946670	-23.399207	0.000000
Ag5r2	0.550656	-23.816803	0.017272
CG8534	0.483884	-24.122562	0.016386
CG31668	1.546991	-24.393645	0.000000
Peritrophin-15b	2.080904	-25.085868	0.000103
Lcp65Ag3	917.800304	-25.205271	0.000000
CG11581	0.331150	-25.374312	0.007166
CG34208	63.285092	-26.578917	0.000000
Cpr47Eg	1374.792583	-26.868170	0.000000
CG31821	0.409536	-29.822672	0.010399
Obp99d	13.097596	-32.554772	0.000000
CG42819	2.815869	-34.741085	0.000024
LManV	0.237721	-35.835037	0.004275
lectin-37Db	1.320875	-36.448925	0.001257
CG43711	1.247606	-43.708339	0.000004
Cpr64Ad	475.664562	-43.903456	0.000000
CG13060	6.962906	-46.512529	0.000000
Jon99Cii	3.652246	-48.311684	0.000000
CG17633	0.850769	-56.551678	0.000238
CG11131	0.881057	-59.982681	0.000384
CG13066	162.769552	-65.467892	0.000000
Lcp65Af	345.204645	-90.139345	0.000000
CG31343	0.165615	-90.673060	0.045631
pre-mod(mdg4)-Y	0.210503	-101.879516	0.035744
CG14324	1.623867	-138.319747	0.031004
pre-mod(mdg4)-K	0.550936	-376.153760	0.007811